BioMed Research International

Brain Computer Interface Systems for Neurorobotics: Methods and Applications

Lead Guest Editor: Victor H. C. De Albuquerque
Guest Editors: Robertas Damaševičius, Nuno M. Garcia, Plácido R. Pinheiro, and Pedro P. R. Filho

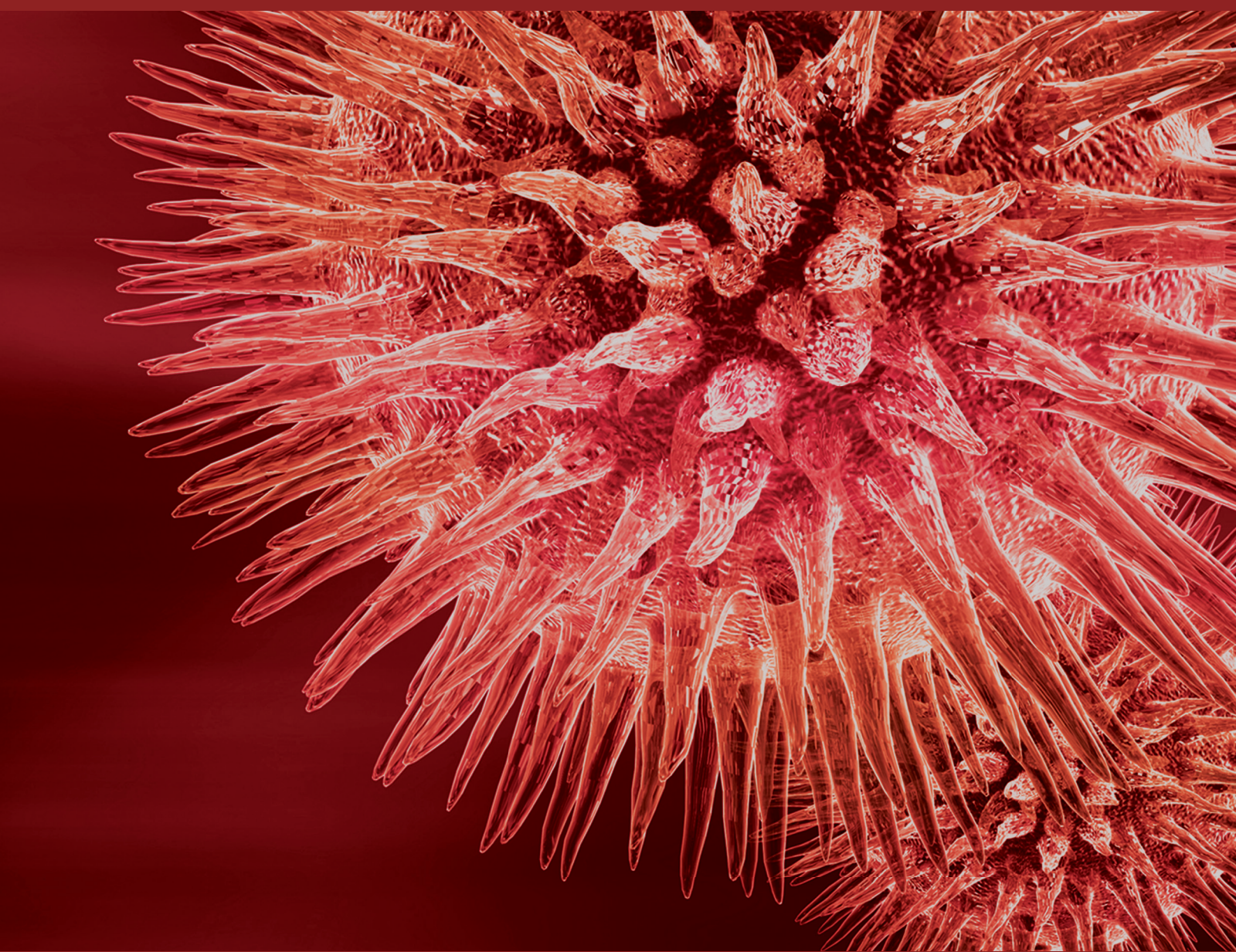

Brain Computer Interface Systems for Neurorobotics: Methods and Applications

BioMed Research International

Brain Computer Interface Systems for Neurorobotics: Methods and Applications

Lead Guest Editor: Victor H. C. De Albuquerque
Guest Editors: Robertas Damaševicius, Nuno M. Garcia, Plácido R. Pinheiro, and Pedro P. R. Filho

Contents

Hindawi
BioMed Research International
Volume 2017, Article ID 2505493, 2 pages
https://doi.org/10.1155/2017/2505493

Editorial

Brain Computer Interface Systems for Neurorobotics: Methods and Applications

Victor Hugo C. de Albuquerque,[1] Robertas Damaševičius,[2] Nuno M. Garcia,[3] Plácido Rogério Pinheiro,[1] and Pedro P. Rebouças Filho[4]

[1] *Programa de Pós Graduação em Informática Aplicada, Laboratório de Bioinformática, Universidade de Fortaleza, Fortaleza, CE, Brazil*
[2] *Department of Software Engineering, Kaunas University of Technology, Kaunas, Lithuania*
[3] *Department of Informatics, Instituto de Telecomunicações and ALLab Assisted Living Computing and Telecommunications Laboratory, Universidade da Beira Interior, Covilhã, Portugal*
[4] *Laboratório de Processamento de Imagens e Simulação Computacional, Instituto Federal de Educação, Ciência e Tecnologia do Ceará, Maracanaú, CE, Brazil*

Correspondence should be addressed to Victor Hugo C. de Albuquerque; victor.albuquerque@unifor.br

Received 7 August 2017; Accepted 7 August 2017; Published 30 October 2017

Brain computer interface (BCI) systems establish a direct communication between the brain and an external device. These systems can be used for entertainment, to improve the quality of life of patients and to control virtual and augmented reality applications, industrial machines, and robots. In the neuroscience field such as in neurorehabilitation, BCIs are integrated into controlled virtual environments used for the treatment of disability or cognitive development of subjects, for example, in case of cerebral palsy, Down syndrome, and depression. Its aim is to promote a recovery of brain function lost due to a lesion through noninvasive brain stimulation (brain modulation) in a more accurate and faster manner than the traditional techniques. Neurorobotics combines BCIs with robotics aiming to develop artificial limbs, which can act as real members of human body being controlled from a brain-machine interface. With the advancement of a better understanding of how our brain works, new realistic computational algorithms are being considered, making it possible to simulate and model specific brain functions for the development of new Computational Intelligence algorithms and, finally, BCI for mobile devices/apps.

As an augmentative communication channel, BCI has already attracted considerable research interest thanks to recent advances in neurosciences, wearable biosensors, and data mining. However, to overcome numerous challenges the BCI technology still requires research in high-performance and robust signal processing and machine learning algorithms to produce a reliable and stable control signal from nonstationary brain signals to allow development of real-life BCI systems usable across many individuals. Further improvements to BCI systems are necessary to ensure that they can meet the needs of specific user groups such as disabled or impaired people as well as common users.

The main objective of this special issue is to promote a discussion on the recent advances related to BCI systems for neurorobotics from novel methods and/or applications in order to identify innovative, current, and great contribution works to the field of neuroscience. This special issue contains 09 published original works selected from 13 submitted articles, addressing new trends in the area from several novel methods and techniques used in different applications. For example, Q. Gao et al. presented a novel hybrid BCI using EEG signal, which consists of a motor imagery-based online interactive brain-controlled switch, aka "Teeth Clenching" state detector, and a SSVEP-based BCI was proposed to provide multidimensional BCI control. N. Yu et al. proposed a novel method for extracting the single-trial evoked potential (EP) based on multiple-input single-output autoregressive

modeling with exogenous input (MISO-ARX). F. A. Araújo et al. proposed the Auris System, based on a noninvasive brain activity recording using a electroencephalographic device, conceived to provide the musical experimentation for people who have some type of hearing loss, being able to extract musical information from audio and create a representation for music using different stimuli, a new media format to be interpreted by other senses than the hearing. A. M. Batula et al. used, for the first time, four-class motor imagery-based online functional near infrared spectroscopy BCIs adopted to control a robot with upper- and lower-limb movement imagery mapped to four high-level commands to control the navigation of a simulated or real robot in a room. A significant improvement in classification accuracy was found between the control of virtual robot-based BCI and the real robot BCI. L. Carelli et al. accomplished the systematic review of BCI for cognitive assessment and training, describing some preliminary attempts to develop verbal-motor free BCI-based tests for evaluating specific or multiple cognitive domains in patients with Amyotrophic Lateral Sclerosis (ALS), disorders of consciousness, and other neurological diseases, presenting the more heterogeneous and advanced field of BCI-based cognitive training, which has its roots in the context of neurofeedback therapy and addresses patients with autism spectrum disorder (ASD) and attention deficit hyperactivity disorder, stroke patients, and elderly subjects. Z. Lin et al. proposed a triple-rapid serial visual presentation (RSVP) paradigm with three types of image retrieval simultaneously and a target image appearing three times to improve the detection accuracy of the multitrial P300-based classification methods. C. A. D. R. Paula et al.'s research aims to evidence quantitative differences in the frequency spectrum pattern between EEG signals of children with and without ASD during analysis of human facial expression, such as neutral, happy, and angry. A. Athanasiou et al. proposed an off-the-shelf BCI-controlled anthropomorphic robotic arms involving, mainly, social Human-Robot Interaction for assistive technologies and rehabilitation. N. Zhuang et al. perform emotion recognition based on the empirical mode decomposition (EMD) of EEG signals.

Acknowledgments

The (lead) guest editors wish to thank all the authors and reviewers for helping to improve the works published.

Victor Hugo C. de Albuquerque
Robertas Damaševičius
Nuno M. Garcia
Plácido Rogério Pinheiro
Pedro P. Rebouças Filho

Hindawi
BioMed Research International
Volume 2017, Article ID 2181380, 9 pages
https://doi.org/10.1155/2017/2181380

Research Article

Auris System: Providing Vibrotactile Feedback for Hearing Impaired Population

Felipe Alves Araujo,[1] Fabricio Lima Brasil,[2] Allison Candido Lima Santos,[1] Luzenildo de Sousa Batista Junior,[1] Savio Pereira Fonseca Dutra,[1] and Carlos Eduardo Coelho Freire Batista[1]

[1]*Digital Video Applications Lab, Universidade Federal da Paraíba, R. dos Escoteiros s/n, Mangabeira, 58055-000 João Pessoa, PB, Brazil*
[2]*Santos Dumont Institute, Edmond and Lily Safra International Institute of Neuroscience, Rod. RN 160, Km 03, No. 3003, 59280-000 Macaiba, RN, Brazil*

Correspondence should be addressed to Felipe Alves Araujo; felipealves@lavid.ufpb.br

Received 1 May 2017; Accepted 3 July 2017; Published 12 September 2017

Academic Editor: Victor H. C. de Albuquerque

Deafness, an issue that affects millions of people around the globe, is manifested in different intensities and related to many causes. This impairment negatively affects different aspects of the social life of the deaf people, and music-centered situations (concerts, religious events, etc.) are obviously not inviting for them. The Auris System was conceived to provide the musical experimentation for people who have some type of hearing loss. This system is able to extract musical information from audio and create a representation for music pieces using different stimuli, a new media format to be interpreted by other senses than the hearing. In addition, the system defines a testing methodology based on a noninvasive brain activity recording using an electroencephalographic (EEG) device. The results of the tests are being used to better understand the human musical cognition, in order to improve the accuracy of the Auris musical representation.

1. Introduction

Deafness is an issue that affects a significant part of the population in all countries, but the incidence increases especially in the developing ones, like Brazil, in which deafness is defined as bilateral hearing loss of forty-one decibels [1]. According to the Brazilian Institute of Geography and Statistics (IBGE) census, 5.10% of Brazilian population have some type of hearing impairment [2]. On a worldwide scale, according to the World Health Organization (WHO) [3], the number of people who have disabling hearing loss is around 360 million, and 1.1 billion young people (aged between 12 and 35 years) are at risk of hearing loss due to exposure to noise in recreational settings. It is important to point out that hearing loss impacts not only leisure's problems, but also all kinds of daily activities. These data reinforce the need for solutions to reintegrate this group in activities which are centered in auditory stimuli, such as musical events.

Different solutions are being developed in order to help people with hearing disabilities to consume music. The Model Human Cochlea [4] is an example of device for musical accessibility, which uses a musical representation in a vibrotactile display. The vibration is expressed through eight voice coils embedded in the back of a chair and distributed in a four by two matrix. Each voice row is associated with a different channel and represents a specific element of the music.

Another project uses a similar approach, but using different tools to represent vibrations. The Haptic Chair [5] is responsible for vibrations transmissions through contact speakers (transducers). The main concept used in this device is to enhance music vibration without any artificial effect; in other words, it amplifies the pure audio signal. Such approach allows the subjects with partial deafness to hear the audio transmitted through transducers vibrations. In addition, a visual display is used to expose visual sequences created based on the music, allowing the subjects to follow information

through elements such as shapes, with different brightness and colors. The system displays visual effects that match the current note duration, pitch, and also loudness, timbre, and key changes. Different configurations were tested using music, visual display, and the Haptic Chair— the test results, obtained through the conduction of usability questionnaires, indicated that the difference between the Flow State Scale score of the music with Haptic Chair and music with visual display and Haptic Chair configurations was not significant. When the participants were asked about the configuration that represents a first choice, 54% preferred consuming music with Haptic Chair only and 46% preferred consuming music with the visual interface and the Haptic Chair.

The use of visual interfaces for deaf people is shown to be important, because it enhances the possibility of immersion and, together with the haptics information, increases the amount of information for the music representation. A study using fMRI [6] indicated that some visual stimuli are able to activate the auditory cortex in deaf people, in the same way it happens when people with no hearing impairment listen to sound. This study suggests the relevance of visual information for the comprehension of interaction of deaf people with different forms of musical representation, which means that video may be used to help deaf people to understand and consume music.

Brain-machine interfaces (BMI) allow direct translation of electric or metabolic brain activity into control signals of external devices or computers bypassing the peripheral nervous and muscular system. The neural or metabolic brain activity can be recorded from sensors outside the brain such as using electro- or magnetoencephalography (EEG/MEG), functional magnetic resonance imaging (fMRI), or near-infrared spectroscopy (NIRS) [7].

The aim of the current study is to translate audio stimuli to a new media composed of filtered audio and tactile vibrations, in order to verify whether this combination can be used to overcome deafness for the perception of music and also understand how the brain interprets these new tactile information. The testing is based on information captured from the subjects using inexpensive commercially available EEG electrodes. The system named Auris [8] is responsible for reproducing the new media created from the original audio. The reproduction is done through two different devices, one named Auris Chair and another named Auris Bracelet. The union of these two devices is responsible for reproducing musical elements, such as melody, rhythm, and harmony.

2. Materials and Methods

The initial discussions for the Auris System development arose from the restrictions faced by the VLibras project [9], which developed solutions aiming at people with hearing impairment. Musical information was not studied by this project, and this gap motivated the development of the Auris System. While researching the state of the art, we understood that most of the previously presented approaches were trying to translate audio into some other media that could be perceived by people with hearing impairment, but most of their results and analysis were guided by subjective information, which could lead to imprecise conclusions.

The following subsections, thus, aims to explain how the Auris System was conceived, how it works, the methodology to evaluate how effective the system is, and how similar, from a neurological standpoint, is hearing music, compared to the experience provided by Auris System.

2.1. Auris System. The Auris System was designed to foster the possibility of a better musical experience for the hearing impaired population. The system brings a set of tools that converts audio to a new media (consisting in a filtered audio synchronized with tactile impulses) in order to be played through loudspeakers and special haptic interfaces, improving the musical experience for deaf people, or anyone with hear deficits. The system is currently composed of the Auris Chair, the Auris Bracelet, and two integrated software components: (a) the Auris Core and (b) the Auris Controller, whose development was deeper described in a previous study [8]. Some software components were further improved and are explained in this work.

The Auris Chair is composed of four six-inch speakers positioned on the back of the Auris Chair and a subwoofer positioned on the seat, both acoustically insulated. This is the component responsible for playing back the filtered audio (Auris Audio). The Auris Bracelet consists of a series of vibration motors attached to small plastic plates disposed in an 1×6 matrix. The Auris Bracelet function is to represent harmonic or melodic information present in the songs through different vibration patterns and can act with different configurations in relation to the combination of motors vibration and represented musical tones.

The System architecture is depicted in Figure 1 describing the following components: Auris Controller; Auris Core, Midi Melody Generator, Auris Stream, Auris Filter, Auris Drivers, Auris Chair, and Auris Bracelet.

The Auris Controller (1) is responsible for managing the functioning of the other components, in order to provide the conversion between regular audio in a media that is perceivable by deaf people. The Auris Controller starts the process by receiving two inputs: an audio file (*.wav* or *.mp3*) and a configuration file. The Auris Core (2) receives the audio and configuration files, processes them with its subcomponents (Midi Melody Generator, Auris Stream, and Auris Filter), and returns the generated artifacts. The audio process for generating the Auris Stream and Auris Audio artifacts, consists, respectively, in extraction of the melodic information from the original audio file using the implementation made by [10], which provides a MIDI representation of it through MELODIA algorithm developed by [11]; after that, the extraction of specific information from MIDI file, used to compose the Auris Stream file, can be executed; for the Auris Audio, the required process consists in generating a filtered version of the audio, in order to amplify the low level frequencies that can also be perceived by the tactile system. Those two processes are required for generating the artifacts, which will be forwarded to the Auris Controller, responsible for commands of the Auris Chair (3.1) and the Auris Bracelet (3.2) (via its drivers) to play filtered audio and

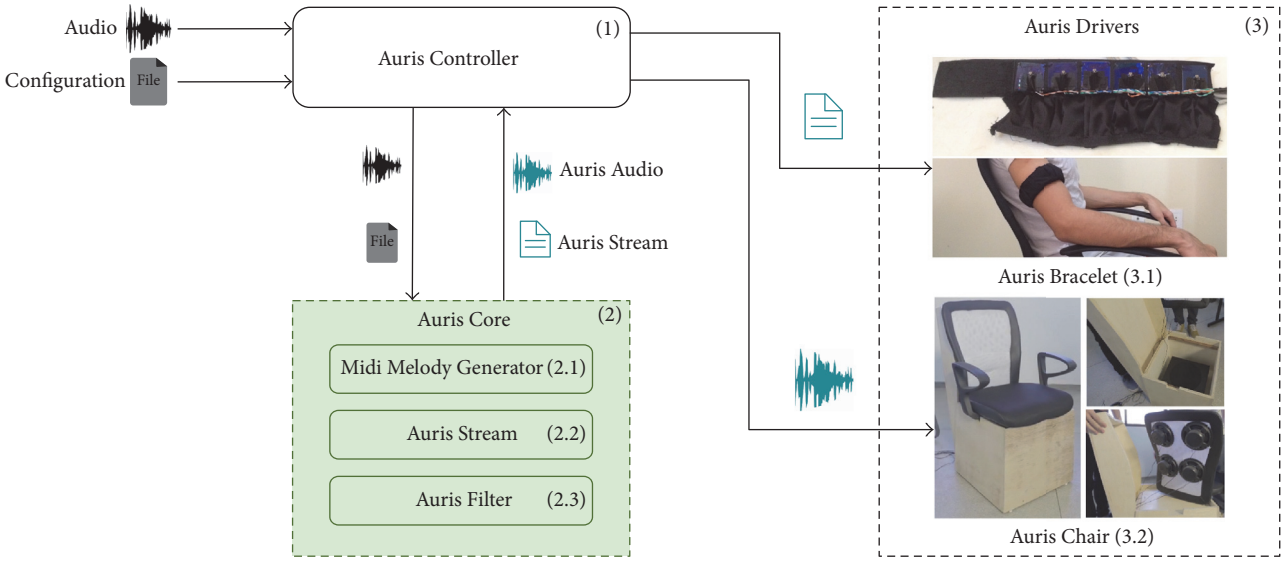

Figure 1: Schematic overview of the Auris System.

the extracted melody information, according to the defined configuration.

The methodology used for the melodic musical information extraction was developed by [11] and divided into four steps. In the first one, the experimenter utilizes a sinusoidal extraction process to obtain the spectral peaks, which serve as input for the salience function. In the second step, he gets the possible melody candidates on fundamental frequency. The third step creates the pitch salience, and then verifies which pitch belongs to the original melody. In the last step, from the pitches belonging to the melody, a selection occurs generating the melody in fundamental frequency.

After the extraction step previously explained, it is possible to access information regarding the notes distribution in time (moment that a note starts and ends) from the melody in the audio and then describe it based on our configuration file. The configuration file is responsible for specifying and providing the motors and the notes represented by them; the vibration range of each motor; the notes distribution in bracelet; and the method of representation. Finally the Auris Stream file can be built as an archive which contains the information of the extracted music and instructions of how we are going to transmit melody though the Auris Bracelet. The Auris Stream file enables the visualization of which motor will vibrate by using his own Identifier (ID), the start/end time of vibration which is measured in milliseconds, and the intensity which can range from 0 to 255, where 0 is the minimum and 255 is the maximum range.

2.1.1. Musical Representation. This section aims to clarify relevant aspects regarding the way Auris presents music to its users. As previously mentioned, the Auris System converts regular audio containing music to a filtered version, which is combined with a MIDI file, in order to be reproduced by the loudspeakers attached to the chair and also by the haptics interface.

More intense and strong vibrations are more relevant to the users perception than weak ones. The purpose of Auris Filter is to enhance weak vibrations using an application to increase the gain of interest frequencies. The vibration frequencies are sensible to touch and vary from 10 Hz to 1000 Hz [12]. Vibration frequencies above this range are very difficult to be perceptible to touch and the range from 200 Hz to 300 Hz is the best touch sensitive frequencies [13].

These frequencies ranges are not adequate considering the fact that music will be carried by the audio to be filtered. In other words, it can not represent most of the music timbres, rhythm variations, and other different musical elements. This representation problem can be easily noticed through the violin scale spectrogram generated by Sonic Visualiser [14] application and presented in Figure 2.

In Figure 2, we have a crescent and decrescent violin notes scale sequence. The red, yellow, and blue colors represent, respectively, the high, moderate, and weak intensity of the signal, in that spectral region. It is noticeable that notes above 3 kHz are more present.

For this task, we used the Essentia library [15] and Pure Data Platform [16]. Essentia is used when audio filter and gain configuration are the same for the whole song and when it is desired to use the maximum processing speed. Pure Data is used when it is necessary to process the song in real time, allowing the experimenter to change the parameters such as filter configuration, cutting frequency, gain, or bandwidth (Bandpass filter) also in real time while the audio is processed. This approach allows the use of Pure Data not only for music, but also for ambient sound if a microphone is connected into the computer.

According to the hardware configuration used to build the Auris Chair, the capacity of frequency representation ranges from 70 Hz to 20 kHz on speakers, and 20 Hz to 200 Hz on Subwoofer. The song "Cleanin' Out My Closet" by Eminem was arbitrarily chosen and used during our tests

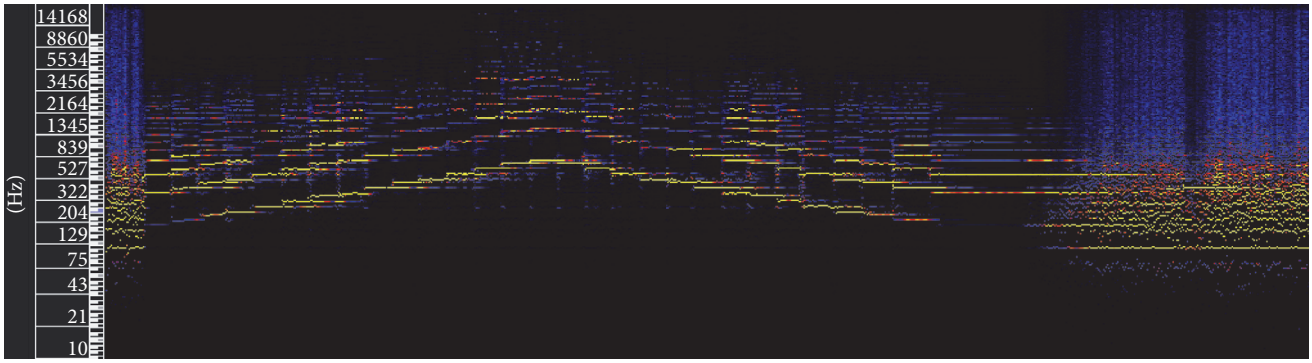

Figure 2: Violin notes scale, generated by Sonic Visualiser.

and will be taken as an example in order to highlight our decisions regarding complementing the audio with a haptics interface. This particular song has a very strong presence of frequencies below 5000 Hz, since Hip hop is a genre that commonly provides music with low frequencies. The limit for vibration frequencies sensible to touch ranges from 10 Hz to 1000 Hz. For this song, in this context, if we do not use the Auris Bracelet and use only the filtered sound representation, the range from 1 kHz to 5 kHz would not be well represented. Since the Auris Bracelet makes a translation from musical frequencies into tactile vibrations, including frequencies that would not be perceivable through the filtered audio, it facilitates the process of identifying a larger part of the musical elements from what is playing, even if the frequencies are above 1 kHz.

2.2. Methods. Different approaches were used in order to evaluate subject perceptions. In order to obtain the most expressive feedback from the subjects involved, among deaf and hearing persons, two different processes were used during the development of the Auris System. The first approach has been through the usability questionnaires, but with drawback of subjective answers by the participants. In the second one, we used an electroencephalogram (EEG) test to obtain a measured feedback from participants. To acquire the electrical activity data in this test, we used an Emotiv EPOC® [17]. This device was used for recording brain signals from the participants during the system experimentation. Deaf and hearing participants had their data collected during part of the experiments.

In all experiments, the participants were informed about the process that would happen and had the freedom to choose the music volume that would be played. In the first test approach, the participants were not isolated and could watch the other participants' experiments. In the second, with the acquisition of EEG signals, participants were isolated in an enclosed environment in order to avoid interfering variables.

Both groups of participants, between deaf and hearing persons, had just had contact with the test evaluator, but, in the deaf group, the participation of a professional interpreter of the Brazilian sign language was necessary. Distinct artifacts were chosen for integrating the test scenarios, and they were used in different configurations, depending on the group which the test was being applied to. These artifacts were the Auris Chair, Auris Bracelet, a video monitor, and an in-ear headphone.

2.2.1. The Auris System and the Visual Stimuli Comprehension. In order to understand the results presented by the author [5], where the visual interface was not significant together with the Haptic Chair, we decided to use a visual element in the first step on our system evaluation. This visual interface has the role of displaying the public video used in our tests. The video contents are composed of a classical dance, more precisely a waltz, where two persons dance according to this music style. The objective here was to evaluate the comprehension by the deaf participants between the audio vibrations and the displayed video content. For this purpose, the video was combined with three different music pieces from different genders.

The songs chosen were

(i) Eminem, Cleanin' Out My Closet

(ii) System Of A Down, B.Y.O.B.

(iii) Tchaikovsky, Waltz of the Flowers.

The experiment was applied at the institution Fundação Centro Integrado de Apoio à Pessoa com Deficiência (FUNAD). The deaf participants were invited to sit on the Auris Chair and feel, or experience, the three different music pieces. Each music piece was played separately but combined with the same video. The participant was informed about every music change, and only after the three executions were they asked about which song most matches the video presented.

2.2.2. The Auris System and Electroencephalogram Tests. The second approach was ran with acquisition of EEG signals. In this way, deaf and hearing participants had their electrical brain activity recorded using an Emotiv device. The acquired data were captured during four music types' executions. Each participant listened to or felt one musical sample of each tag used in the experiment, according to Table 1.

Different music pieces were chosen for composing this part of tests, more specifically eight. These songs were classified into four different types, defined according to emotional

Table 1: Table of the music and tags used on tests.

Music type *(tags)*	Artist, title
Calm positive	Mike Oldfield, Harmonia Mundi
	Pink Martini, White Christmas
Energetic positive	George Benson, All Of Me
	Jennifer Lopez, Let's Get Loud
Dark calm	David Sylvian, Bringing Down The Light
	Matanza, Clube dos Canalhas
Dark energetic	Celine Dion, Regarde moi
	Placebo, Meds

tags, informed by different users around the world in a crowdsourcing technique, as proposed by [18]. After that, the eight different music pieces could be separated in pairs, according to the different tags. These songs and types can be better observed in Table 1.

Brain activity data acquisition from participants was ran at Universidade Federal da Paraíba (UFPB). The Auris System was used as well as the tactile devices, and the deaf subjects were invited to sit in an Auris Chair and/or use the Auris Bracelet to feel the music vibrations. In the case of hearing persons, they used an in-ear headphone for listening to the music pieces.

2.2.3. Experiment Setup. In the two sessions of experiments, we had a total of 13 participants (deaf or hearing person); their ages and devices used on each test can be found on Table 2.

The pure audio signal was used in both tests, although the Auris Filter provides different configurations of gain and filters; it was necessary to evaluate the feedbacks provided by the participants, before applying any modification on audio signal. In addition, participants that used the Auris Bracelet had just had contact with one configuration of the Auris Bracelet (the most simple), in which each motor vibrates on the same frequency and alternates the vibrating motor for melody representation.

Participants that used the Emotiv device had their data recorded using the Test Bench version 1.0.0.0 software provided by Emotiv SDK. For offline analysis we used EEGLAB version 13.5.4b, importing the.edf file containing the data acquired from each volunteer, using a BIOSIG load option. Channels presented in the Emotiv interface were defined, as well as their specific scalp locations. Before plotting the data, the baseline from the sample was removed and the Independent Component Analysis (ICA) decomposition was executed.

After preprocessing the data, it was possible to plot the graph spectra and maps, for analyzing a component contribution at one specific channel and power. In our case, the channel F3 and the frequency 12 Hz were specified to reproduce the graphs from 100 percent of the acquired data.

Previous work has shown that mental imagination of sound generally elicits an increase of alpha band activity (8–12 Hz) in the electroencephalogram (EEG) [19]. Based on that, we chose 12 Hz in our data analysis.

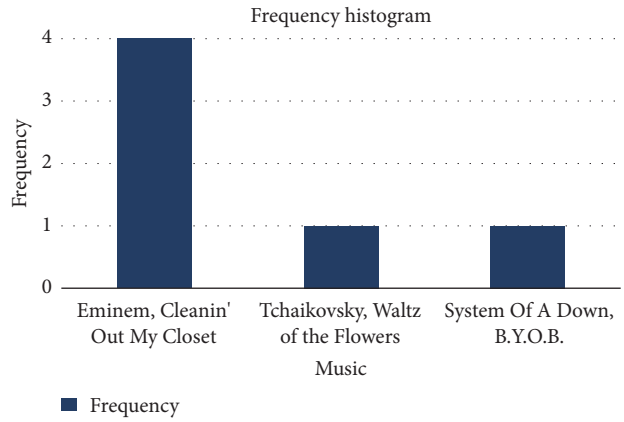

Figure 3: Association between music and video by deaf participants.

3. Results

Experiments were conducted in order to evaluate the Auris System. In the first session of experiments we evaluated the audio-video correlation by the deaf participants, using the Auris System. The evaluation consisted of usability questionnaires. Afterwards we conducted experiments that analyzed the deaf and hearing patients feedback, through the EEG signals acquired with the Emotiv device; the experiment aims to evaluate the participants experience with quantitative data, providing basis for establishing the differences between deaf and listeners perception.

3.1. Questionnaire Results. The first session of experiment evaluated the Auris System with the support of visual stimuli, in order to facilitate the comprehension of music. The users were exposed to three different songs as soundtrack to a single video instance. The participants were asked which of the songs was best related to the video. We were able to produce a frequency histogram analyzing the participants answers, which are represented in Figure 3. The graphic expresses on the x-axis the songs listened to by the participants and the y-axis expresses the number of participants that chose that song with the video.

The original audio from the video content was the classical song by *Tchaikovsky, Waltz of the Flowers*. According to the graphic it is possible to observe that most participants have chosen the song by *Eminem, Cleanin' Out My Closet*. Despite the fact that these two songs have different styles, they have similar tempo information. This common characteristic was evidenced through hardware configurations of the Auris Chair, which, for the test, was composed of speakers and a loudspeaker component (subwoofer), that emitted filtered audio, so the rhythmic information had a significant presence in the music translation reproduced through the Auris Chair.

Two different musical software programs were used to extract specific musical aspects such as tempo, energy, and key results from the used music. The software programs used were Ableton Live 9 [20] and Mixed in Key 8 [21]. After this extraction, we were able to construct Table 3.

Table 2: Table of participants information and characteristics of the tests.

Test	Participant	Type	Age	Used devices		
				Auris Chair	Auris Bracelet	EEG
FUNAD	1	Deaf	15	X		
	2	Deaf	27	X		
	3	Deaf	28	X		
	4	Deaf	31	X		
	5	Deaf	46	X		
	6	Deaf	62	X		
UFPB	2	Deaf	27	X		X
	7	Deaf	16	X		X
	8	Deaf	26	X		X
	9	Deaf	28	X	X	X
	10	Deaf	29	X	X	X
	11	Hearing person	20			X
	12	Hearing person	23			X
	13	Hearing person	23			X

Table 3: Table of musical analysis.

Music	Tempo (bpm)	Energy	Key result
Tchaikovsky, Waltz of the Flowers	141.88	3	D
Eminem, Cleanin' Out My Closet	147.99	4	Am
System Of A Down, B.Y.O.B.	97.23	7	G#m

Analyzing Table 3 we can perceive the similarity present between *Eminem, Cleanin' Out My Closet,* and *Tchaikovsky, Waltz of the Flowers,* songs. Both songs express a similar tempo and energy information, indicating that the Auris Chair improves the rhythmical, dynamic, and volume information from the audio input, according to the FUNAD test participant's answers.

Based on this scenario, we are able to foresee that the possibility of audio-video association for deaf participants can be enhanced by the use of the Auris System. Four different profoundly deaf participants (born deaf) were able to associate the song with the same tempo ("Cleaning out my closet") with the video. The most precise association between audio and video was made by one subject that was not deaf from birth, choosing *Tchaikovsky, Waltz of the Flowers*. One participant, which is profoundly deaf from birth, associated the *System Of A Down, B.Y.O.B.,* music correctly.

The contact with the subjects and the stories and experiences that they brought to our attention were as rich as the data produced by these experiments. Most of those experiences were regarding their relationship with situations that were audio centered or in which audio played an important role (such as attending music concerts and playing video games) and their workarounds to improve such experiences (getting closer to the loudspeakers, using headphones and/or loudspeakers touching the neck or palms of the feet). Many different rounds and questionnaire test versions were conducted until we were able to have sufficient amount of data to analyze.

From those experiments we could empirically detect that some subjects became more sensible to music through the usage of the Auris System, and considering subjects with the same profoundness of deafness, the distinguishing factor was related to the subjects past activities and relationship with audio centered situations. One particular subject highlighted such suspicion: although he was born with profound deafness, he was able to distinguish most musical characteristics, even being able to relate genres and similar bands—during the interviews he stated that, during his whole life, he enjoyed attending music concerts and standing close to the loudspeakers. The other subjects, with the same level of deafness and which did not demonstrate a high level of musical sensitivity, all expressed in the interviews that they did not have a history of attending audio centered events. Some even mentioned that they felt socially excluded of such events.

In order to better understand the experience provided by the Auris System and attenuate the amount of subjectivity on the data that we were considering for our analysis and in order to have more precise directions to identify which elements of the system should be modified to produce a better musical representation using other media than audio (e.g., what parameters shall be considered for the audio filtering and what tactile representation suits better this type of harmony or melody), the next subsection discusses our efforts in such direction, where EEG data collection was used for the experiments.

3.2. EEG Results. For ease of presentation and hence understanding, all analyses were focused on data from the frontal site in the left hemisphere, on channel F3. This channel was selected because it is usually used in studies involving auditory responses [22] and it is also included in vibrotactile

Table 4: Table of relative topographic distribution of power, from representative deaf (1a and 2a), and hearing participants (1b and 2b) for 12 Hz at channel F3. Each colored line represents the spectrum activity of one single data channel.

Nr.	a	b
1	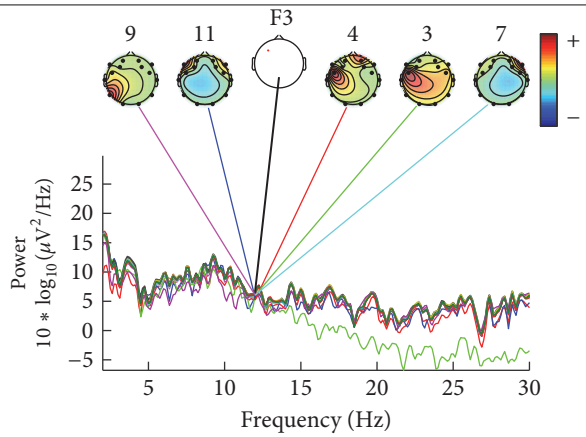	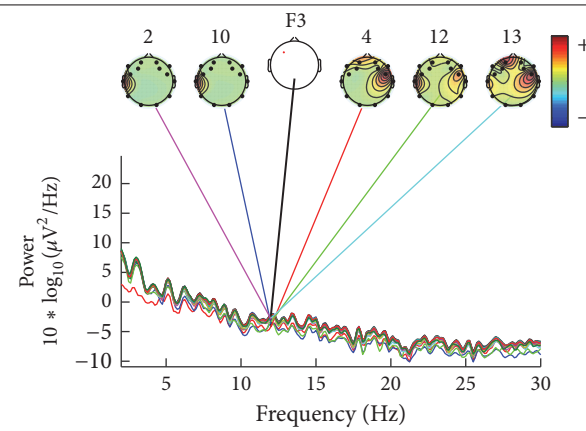
2	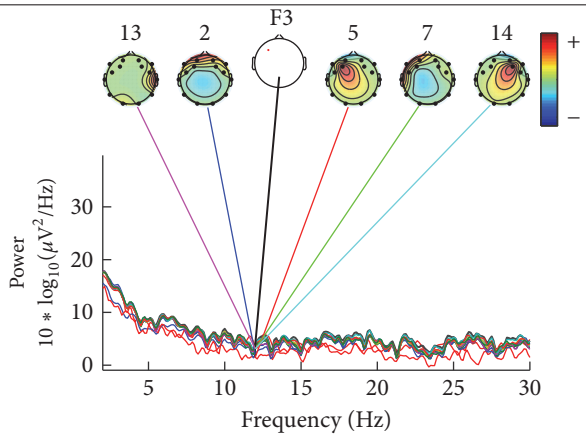	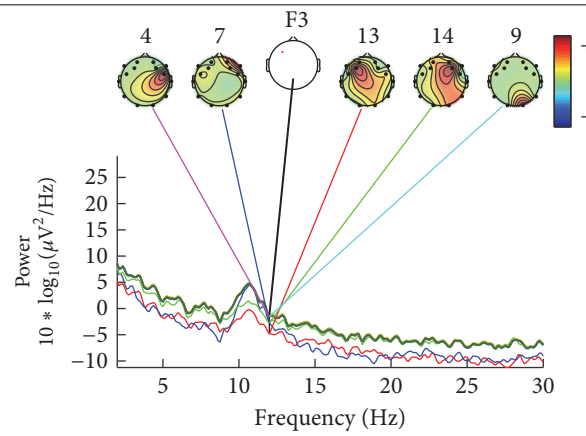

discrimination loop [23]. In order to know which components contribute most strongly to which frequencies in the data, we plotted the mean log spectrum of a set of data epochs at all channels as a bundle of traces. For 12 Hz we plotted the relative topographic distribution of power (Table 4).

For construction of Table 4 the EEG data collected by the deaf and hearing volunteers was used, which have listened to/felt the same music tag, defined as energetic and positive, according to Table 1.

Table 4 shows that similar components contribute strongly to deaf participants, and other similar components contribute strongly do hearing persons. Deaf participants showed also a higher power for lower frequencies, what was not seen in the hearing participants.

4. Discussion

This study evaluated the functioning and translation of audio stimulus from music pieces to a different representation using low frequency sound and tactile vibration in deaf and hearing volunteers. The evaluation considered the recording of brain signal with noninvasive EEG electrodes (using the Emotiv device) while participants consumed music; the deaf participants used the Auris System, composed of the drivers Auris Chair and the Auris Bracelet.

The first results suggest that deaf patients that never had a similar experience related to music were capable of identifying and associating musical information concerning the rhythm and energy present in the music, associating them accordingly with a video presented to them, with the exception of one participant that was not deaf from birth. The audio-video association made by the deaf participants was possible through the use of the Auris System and the Auris Chair hardware.

Based on the previous findings and relating them to the results presented by [5], in which deaf participants express an nonsignificant effect after addition of the visuals element combined with the Haptic Chair, we realized that the problem is probably not related to the visual and tactile feedback association, suggesting the necessity of more depth studies related to visual representation for music aimed at deaf people.

During the period of research development and survey of the related works, we noticed that the previous findings [4, 5] associated with our context presented their results based on less objective evaluation mechanisms—the type of information that can be obtained through EEG may express

more. The state of the art presents findings in which the participants provided the data through usability questionnaires, expressing the strength of emotions and perceptions and explaining such information to a professional interpreter. These evaluation methodologies were used in the first step of our analysis, but a discomfort was perceived in the participants, in addition to a difficulty in describing their perceptions. Based on this and in other previous findings, which use EEG signals as part of the evaluation [11, 24], the necessity and the possibility for a more expressive feedback are perceivable, exposed in the second session's results.

With use of EEG, recent studies [25] recorded the mismatch negativity of the auditory event-related potential to changes in musical features in adolescent cochlear implants users and in normal-hearing age mates. They reported that behavioral discrimination of rhythm and melodic contour may be significantly improved, even from short term training, whereas detection of changes in pitch was poor and unaffected by music training.

Music interpretation was a hard task for some deaf participants. We believe that, despite the translation of music elements (rhythm, harmony, melody, and timbres), patients had no previous experience to these vibrations patterns and, even though they maybe perceiving, they could not differentiate important elements of the songs. We believe that continuous musical stimulation using different media other than audio during daily life activities would support a natural learning curve for a pattern recognition that enhances music experimentation.

Further studies are necessary to clarify brain dynamics associated with vibrotactile and bass-sound impact in deaf people. Such understanding will guide the development of a better musical representation that is not any translation, but one that might lead to experiences similar to those experimented by hearing people.

5. Conclusion

The presented results are encouraging, but there is still a long way to develop a system that significantly helps people with some degree of deafness to achieve a satisfactory level of musical perception. Nevertheless, the learning resulting from conducting the tests exceeded our expectations. Several reports and empirical conclusions from the tested subjects were also primordial for the accomplishment of this work. The need to improve the representation system is evident and urgent, so users can easily identify the different elements involved in music (rhythm, harmony, melody, and timbres) and offer better ways of representing and expressing these elements (visual stimuli, more levels of tactile stimuli, etc.); it is clear that the methodology evaluation has also to consider a broader universe of subjects and particularities involved in musical perception, such as cultural context (e.g., different cultures use different musical scales and focus on different elements and thus people from different places may perceive music differently).

The evaluation methodology was based mainly on the interpretation of EEG data; thus a more in-depth interpretation of the new data generated on the forthcoming tests is required and also a bigger universe of test to analyze. Those data should be used to better understand how the musical cognition happens by hearing persons and to produce a better understanding of what the Auris System's users are experimenting, so we will have better possibilities to bring one experience closest to the other.

The Auris representation system (currently consolidated in the chair) is being redesigned in two versions: one with miniaturized components such as mobile/wearable option and another to coexist in environments where sound is consumed by hearing people. An integration with the VLibras system [9] is under development, which will make VLibras able to represent musical information by offering a visual representation of musical elements—when used with the Auris system, the avatar of the VLibras system presents the lyrics of the song in LIBRAS (Brazilian sign language), moving the trunk according to the rhythm and emphasizing moments of apex. Other visual references representing musical elements are being studied to be used along with the VLibras avatar.

Our preliminary results reinforce findings of [26], where vibrotactile channel functions as a valuable feedback modality in a BMI-controlled setting. With improvements of stimulation paradigm, training protocol, and device functioning we believe that people with different levels of hearing impairment will be able to use this music translation device in their daily life activities in the future.

Conflicts of Interest

The authors declare that there are no conflicts of interest regarding the publication of this article.

Acknowledgments

The authors would like to thank the entire VLibras project team for the support offered since the beginning of the project development, especially the deaf Tamara, Alexandre, and Klícia. They thank the deaf volunteers of all tests and Fundação Centro Integrado de Apoio à Pessoa com Deficiência (FUNAD), for giving space for the first test of the Auris System. Thanks are due to the contributing musicians, Daniel Jesi and Guilherme Alves, and Professor Edneia Alves, for all the support offered, including the performance of several tests.

References

[1] BRASIL decree no. 5.296,http://www.planalto.gov.br/ccivil_03/_ato2004-2006/2004/decreto/D5296.htm.

[2] I. C. Demográfico, "Caractersticas gerais da populaτπo, religiπo e pessoas com deficiΩncia," *Rio de Janeiro: Instituto Brasileiro de Geografia e Estatstica*, 2010.

[3] World Health Organization Deafness and Hearing Loss, http://www.who.int/mediacentre/factsheets/fs300/en/.

[4] M. Karam, G. Nespoli, F. Russo, and D. I. Fels, "Modelling perceptual elements of music in a vibrotactile display for deaf users: a field study," in *Proceedings of the 2nd International Conferences on Advances in Computer-Human Interactions, ACHI 2009*, pp. 249–254, IEEE, Washington, D.C., USA, February 2009.

[5] S. Nanayakkara, E. Taylor, L. Wyse, and S. H. Ong, "An enhanced musical experience for the deaf: design and evaluation of a music display and a haptic chair," in *Proceedings of the 27th International Conference Extended Abstracts on Human Factors in Computing Systems, CHI 2009*, pp. 337–346, ACM, New York, NY, USA, April 2009.

[6] E. M. Finney, I. Fine, and K. R. Dobkins, "Visual stimuli activate auditory cortex in the deaf," *Nature Neuroscience*, vol. 4, no. 12, pp. 1171–1173, 2001.

[7] P. R. De Almeida Ribeiro, F. Lima Brasil, M. Witkowski et al., "Controlling assistive machines in paralysis using brain waves and other biosignals," *Advances in Human-Computer Interaction*, vol. 2013, Article ID 369425, 2013.

[8] F. A. Araújo and C. E. Batista, "Auris: system for facilitating the musical perception for the hearing impaired," in *Proceedings of the 22nd Brazilian Symposium on Multimedia and the Web*, pp. 135–142, WebMedia, Teresina, PI, Brazil, November 2016.

[9] VLibras, http://vlibras.gov.br.

[10] J. Salamon, "Melody Extraction," http://www.justinsalamon.com/melody-extraction.

[11] J. Salamon and E. Gómez, "Melody extraction from polyphonic music signals using pitch contour characteristics," *IEEE Transactions on Audio, Speech and Language Processing*, vol. 20, no. 6, pp. 1759–1770, 2012.

[12] C. Stumpf, *Tonpsychologie*, Cambridge University Press, Leipzig, Germany, 1883.

[13] I. R. Summers and M. C. Martin, "A tactile sound level monitor for the profoundly deaf," *British Journal of Audiology*, vol. 14, no. 1, pp. 33–36, 1980.

[14] C. Cannam, C. Landone, and M. Sandler, "Sonic visualiser: an open source application for viewing, analysing, and annotating music audio files," in *Proceedings of the 18th ACM international conference on Multimedia*, pp. 1467-1468, ACM, Firenze, Italy, October 2010.

[15] D. Bogdanov, "Essentia: an audio analysis library for music information retrieval," in *Proceedings of the International Society of Music Information Retrieval*, pp. 493–498, Citeseer, 2013.

[16] M. Puckette, "Pure data: another integrated computer music environment," in *Proceedings of the Second Intercollege Computer Music Concerts*, pp. 37–41, 1996.

[17] E. Inc, Emotiv epoc, http://emotiv.com/epoc/.

[18] J. Li, H. Lin, and L. Zhou, "Emotion tag based music retrieval algorithm," in *Information Retrieval Technology*, pp. 599–609, Springer, Beijing, China, 2010.

[19] R. S. Schaefer, R. J. Vlek, and P. Desain, "Music perception and imagery in EEG: Alpha band effects of task and stimulus," *International Journal of Psychophysiology*, vol. 82, no. 3, pp. 254–259, 2011.

[20] Ableton live 9, https://www.ableton.com.

[21] Mixed in key 8.0, https://mixedinkey.com.

[22] N. A. Badcock, P. Mousikou, Y. Mahajan, P. de Lissa, J. Thie, and G. McArthur, "Validation of the Emotiv EPOC® EEG gaming system for measuring research quality auditory ERPs," *PeerJ*, vol. 1, no. e38, 2013.

[23] A. A. González-Garrido, V. D. Ruiz-Stovel, F. R. Gómez-Velázquez et al., "Vibrotactile sound discrimination training affects brain connectivity in profoundly deaf individuals," *International Journal of Psychophysiology*, vol. 108, p. 156, 2016.

[24] J. Eaton, D. Williams, and E. Miranda, *Affective jukebox: a confirmatory study of EEG emotional correlates in response to musical stimuli*, Michigan Publishing, University of Michigan Library, Ann Arbor, MI, USA, 2014.

[25] B. Petersen, E. Weed, P. Sandmann et al., "Brain responses to musical feature changes in adolescent cochlear implant users," *Frontiers in Human Neuroscience*, vol. 9, article no. 7, 2015.

[26] F. Cincotti, L. Kauhanen, F. Aloise et al., "Vibrotactile feedback for brain-computer interface operation," *Computational Intelligence and Neuroscience*, vol. 2007, Article ID 48937, 12 pages, 2007.

Hindawi
BioMed Research International
Volume 2017, Article ID 3591914, 11 pages
https://doi.org/10.1155/2017/3591914

Research Article

High-Frequency EEG Variations in Children with Autism Spectrum Disorder during Human Faces Visualization

Celina A. Reis Paula,[1,2] Camille Reategui,[1] Bruna Karen de Sousa Costa,[3] Caio Queiroz da Fonseca,[3] Luana da Silva,[4] Edgard Morya,[1] and Fabricio Lima Brasil[1]

[1]*Edmond and Lily Safra International Institute of Neuroscience, Santos Dumont Institute, Rod. RN 160, Km 03, No. 3003, 59280-000 Macaiba, RN, Brazil*
[2]*Anita Garibaldi Center for Education and Research in Health, Santos Dumont Institute, Rod. RN 160, Km 02, No. 2010, 59280-970 Macaiba, RN, Brazil*
[3]*Electrical Engineering Department, Federal University of Campina Grande (UFCG), 882 Aprígio Veloso St, 58429-900 Campina Grande, PB, Brazil*
[4]*Electrical Engineering Department, Federal University of Santa Maria (UFSM), 1000 Roraima Av., 97105-900 Santa Maria, RS, Brazil*

Correspondence should be addressed to Celina A. Reis Paula; larissaangelia2010@gmail.com and Fabricio Lima Brasil; brasil@isd.org.br

Received 1 May 2017; Revised 27 June 2017; Accepted 27 July 2017; Published 6 September 2017

Academic Editor: Victor H. C. de Albuquerque

Autism spectrum disorder (ASD) is a neuropsychiatric disorder characterized by the impairment in the social reciprocity, interaction/language, and behavior, with stereotypes and signs of sensory function deficits. Electroencephalography (EEG) is a well-established and noninvasive tool for neurophysiological characterization and monitoring of the brain electrical activity, able to identify abnormalities related to frequency range, connectivity, and lateralization of brain functions. This research aims to evidence quantitative differences in the frequency spectrum pattern between EEG signals of children with and without ASD during visualization of human faces in three different expressions: neutral, happy, and angry. Quantitative clinical evaluations, neuropsychological evaluation, and EEG of children with and without ASD were analyzed paired by age and gender. The results showed stronger activation in higher frequencies (above 30 Hz) in frontal, central, parietal, and occipital regions in the ASD group. This pattern of activation may correlate with developmental characteristics in the children with ASD.

1. Introduction

Autism spectrum disorder is a neurodevelopmental disorder with well-defined diagnostic criteria such as communications/social interaction and behavior deficits, with restricted and repetitive interests and activities [1, 2]. These social communication disturbances present a complex and heterogeneous pattern and for that reason fit in a spectrum and may present various patterns of severity in symptoms or evolution profile. The initial publications about the autism spectrum disorder were only in the form of case reports [3, 4]. In 1966, the first epidemiological study suggested the occurrence of 4.5 children with ASD per 10,000 inhabitants in the age range of 8 to 10 [5]. However, further studies realized in Europe, United States, Canada, and Japan suggest an increase in this incidence, with values of 10, 30, or even 60 cases per 10,000 inhabitants [6]. Nowadays, the ASD seems to affect approximately 1 in 68 children, most common among boys [7]. There is a suggestion of increased incidence and prevalence of ASD worldwide [8]. This increase is probably due to the changes in the diagnostic criteria [9], emergence and development of diagnostics, early intervention services, and more direct approaches related to the diagnosis of the disorder [10].

Table 1: Participants demographics.

	Experimental group (ASD)				Control group			
	Age(yrs)	Gender	Language structure	Age at diagnosis (yrs)		Age	Gender	Language structure
Subject 1	10	Male	Sentences	5	Subject 9	10	Male	Verbal fluency
Subject 2	12	Female	Phrases	5	Subject 10	12	Female	Verbal fluency
Subject 3	6	Male	Word	2	Subject 11	6	Male	Verbal fluency
Subject 4	7	Male	Sentences	3	Subject 12	7	Male	Verbal fluency
Subject 5	8	Male	Sentences	4	Subject 13	8	Male	Verbal fluency
Subject 6	9	Male	Word	4	Subject 14	9	Male	Verbal fluency
Subject 7	5	Male	Sentences	3	Subject 15	5	Male	Verbal fluency
Subject 8	11	Male	Sentences	4	Subject 16	11	Male	Verbal fluency

The ASD diagnostics are realized according to the observation of initial symptoms in early childhood with impairments in their daily functionality [2], neurodevelopment, children's behavioral characteristics, and objective clinical analysis. The clinical signs should fulfill the diagnostic criteria described in the Diagnostic and Statistical Manual for Autism (DSM-V). Questionnaires, checklists, and diagnostic scales support the evaluation and confirm the diagnosis [11]. Children with ASD can present a heterogeneous clinical picture, in which the behavioral symptoms prevail. Such facts boost a search for biological markers of the disorder using different tools, for example, the electroencephalogram (EEG), the Eye-Tracker, the Functional and Structural Magnetic Resonance Imaging (fMRI or MRI), Positron Emission Tomography (PET), and Computerized Tomography (CT) based on emission of single photon (SPECT) [12]. These tools have been increasingly exploited in scientific research.

Abnormal EEG activity of the epileptic type occurs in 30% of the cases of ASD, even without epileptic seizures [13]. Paroxysmal discharges and slow focal activity were registered in the temporal region in EEG of patients with the disorder, especially those with developmental regression [14]. Although EEG can provide important information about brain function during resting and stimulation, the qualitative visual signal analysis of time domain seems to be insufficient to consider a pathognomonic pattern for the ASD [15]. Techniques for quantitative analysis, such as the Fourier Transform, favor a more detailed frequency analysis by bandwidth and its characteristics. EEG analysis of children with ASD shows differences in brain electrical signals compared to children without ASD [5, 16]. A reduction in the power spectrum in the alpha bandwidth (4–8 Hz) was previously observed in EEGs of children with ASD during rest [14]. Also, hemispheric asymmetry of activity has been shown, such as greater activity in the left frontal lobe when observing happy facial expressions with smiles [17] and decreased activity in the same region when observing facial expressions of fear [18]. It was also observed that a theta power spectrum in the frontal midline (Fm) is related to emotional states. Sammler and colleagues proposed that pleasant emotions (opposed to unpleasant) are related to the increase in the theta power density in the Fm [19]. Thus, in light of previous studies and considering the behavioral component in the diagnosis of ASD, it is expected that the use of the EEG to access neural activities elicited by social stimuli has the potential of providing a quantitative analysis of impairment in social interaction activities of this group [20].

Neuropsychological patterns verified in ASD might suggest the involvement of other brain regions. The difficulty in maintaining attentional focus or the behavior of paying attention to a face or object details instead of the whole picture might be related to difficulty in shared attention and in the executive function, capabilities that involve the frontal region.

The current study aims to show quantitative differences in the frequency spectrum pattern between the EEG of children with and without ASD before and during the observation of human faces. We believe that finding these differences can lead to a better understanding of how these children could potentially be better stimulated and taught using their respective preference of human faces or figure faces. We hypothesize that social interaction impairment present in children with ASD, when compared with children without ASD, can occur due to a deficit in the visual processing of human faces. In addition, we also hypothesize that the brain's electrical activity presents a different quantitative pattern in the power spectrum in the bandwidths during the observation of stimulus such as human faces with different emotion expressions.

2. Materials and Methods

2.1. Participants. This research was authorized by the Ethics Committee of the Federal University of Rio Grande do Norte (CAAE 46207015.0.0000.5537). The consent form was read and explained to the parents, and after their agreement, they signed the consent form. EEG data were recorded at the Anita Garibaldi Center for Education and Research in Health (CEPS). Sixteen children participated in the study: eight with ASD and 8 without ASD. All of them were from the same metropolitan region and were paired by age (Table 1). The age of the participants varied from 5 to 12 years

Figure 1: Images showing human faces with neutral, happy, and angry expressions.

(M = 8.44, SD = 2.24), and only two (one of each group) were female. The inclusion criteria for the group with ASD were the presence of the diagnostics realized by a neuropediatrician after neuropsychological evaluation. For the children of the control group, it was necessary to test for intellectual disability with the ASD diagnostics, also by the same team. Children with epileptic seizures in the last 3 years did not participate in the research. Subjects who did not cooperate to perform the exam also were excluded and respective data were not included in the analysis.

The ASD diagnostics were realized by a neuropediatric physician, considering the fulfillment of the diagnostics criteria of the DSM-V, the neuropsychological evaluation with the childhood autism rating scale (CARS), an IQ test, and language evaluation.

2.2. Experimental Setup

2.2.1. EEG. EEG-1200 (Neurofax, Nihon Kohden, Tokyo, Japan) was used for noninvasive brain electrophysiological signal acquisition (sampling rate 1.000 Hz) with 22 electrodes (Ag/AgCl disk electrode, 10/20 distribution with ear lobes ground) positioned with previous scalp preparation (cleaned with neutral soap, dry and no hair creams or hair products, and impedance lower than 5 kΩ). EEG data were recorded and synchronized (StimTracker ST-100, Cedrus, USA) with visual stimulation and eye-tracking.

2.2.2. Visual Stimuli. Visual stimuli with 30 human faces were presented on a grey background (Figure 1). The faces were paired by expression and classified into three groups: 10 neutral, 10 happy, and 10 angry.

All stimuli were size dimensioned and standardized to keep equivalent distances between the eyes, mouth, and nose in a central square area of the 17″ LCD screen (100 Hz, Samsung) 60 cm from the participant's eyes. E-Prime® 2.0 software (Psychology Software Tools, Inc., USA) presented in a sequence (happy-neutral-angry faces), interspersed by a fixation point in the center of the screen. Each face was presented for 3 seconds with 0.5 to 1.0 s of interval controlled by Mangold Vision 3.9 (Mangold International GmbH, Germany) software in programmed sequence and time.

2.2.3. Eye-Tracking. An Eye-Tracker (Eye-Tech TM3 60 Hz, Mesa, USA) was positioned under the screen to ensure the participants were looking at fixation point and visual stimuli during the task.

2.2.4. Task. Participants sat comfortably in a quiet dimmed room 60 cm from the LCD screen with EEG electrodes. They were instructed to keep the eyes at the fixation point and look at the image during the presentation. After eye-tracking calibration, EEG recording started two minutes before the visual stimulation.

2.3. Data Preprocessing. EEG data underwent preprocessing with a custom MATLAB (Mathworks, USA) script, EDF Browser (© Copyright 2017 Teunis van Beelen), and Python (Python Software Foundation).

2.3.1. EDF Browser. EDF Browser converted raw EEG data to ASCII format compatible with Python and MATLAB. The epochs to be analyzed were correctly separated according to the stimuli marker registered during the experiment in order to organize files. Thus, for each subject, three files were generated containing, respectively, all epochs of happy, neutral, and angry faces, for all EEG channels. These files were then processed by Python Programming Language.

2.3.2. Python Programming Language. Python libraries for data manipulation and analysis were used to organize sets of trials with all subjects of each group and separate channels. This resulted in.csv files with raw EEG data of subjects for each type of stimuli and for each channel. Thereafter, these files were processed by MATLAB.

2.3.3. MATLAB. A MATLAB code designed a 6th-order bandpass Butterworth filter with a lower cutoff frequency of 1 Hz and a higher cutoff frequency of 100 Hz. A Notch filter removed the frequency component of the electrical grid (58–62 Hz). Moreover, a technique for detecting spectral perturbation related to the event (ERSP) was implemented. The ERSP consists of a tool to observe the variations on local field potentials related to the event by calculating the mean and the standard deviation of the EEG signal in order to normalize the signal prior to the event. Each epoch has −500 ms before stimulus presentation and +3.500 ms. Spectral features related to the event were calculated for this time window. After that, the same procedure was done in the event epochs, where they were analyzed with the ERSP tool

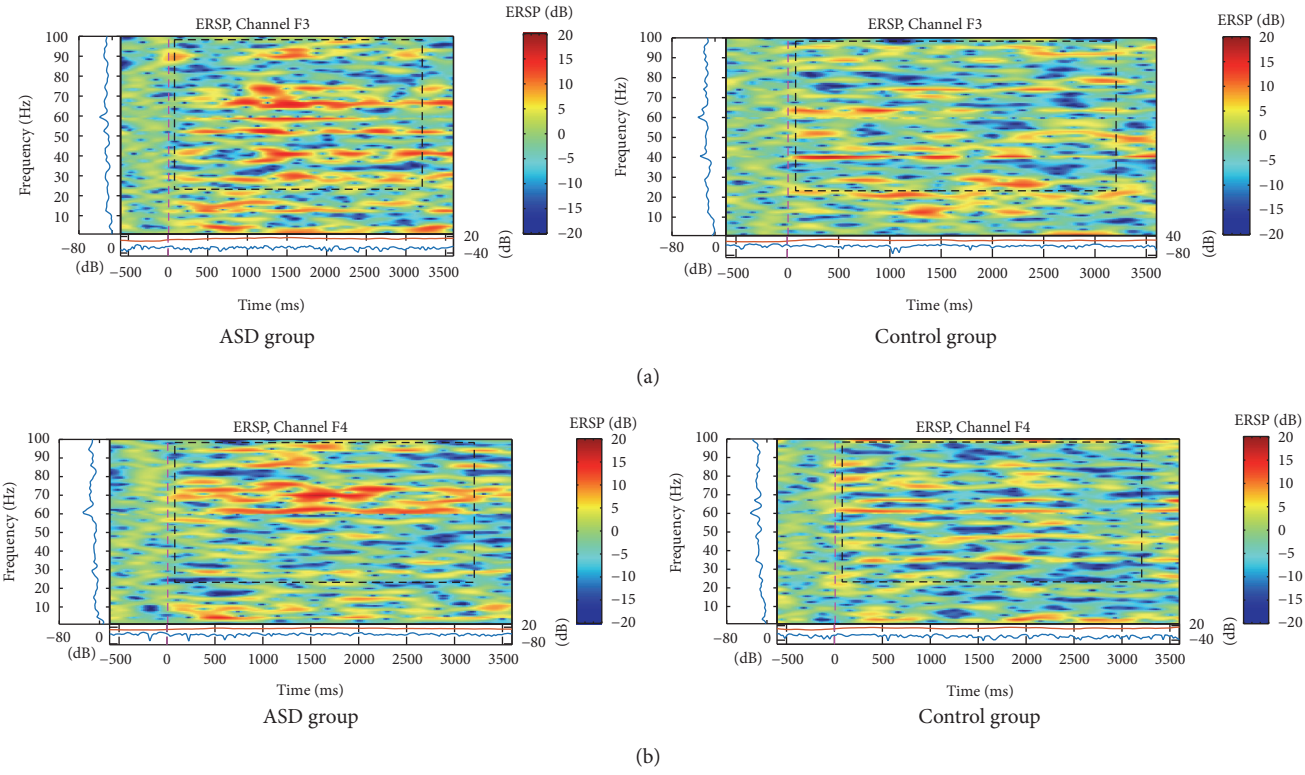

Figure 2: ERSP of (a) F3 and (b) F4 electrodes for the total mean of samples for angry expression signal in an interval of 3 seconds (plus a basal activity of 500 ms before and after an event) for ASD and control groups that showed significant variations or spectral perturbations. The ERSP image in the upper panel presents the ERSP (Event-Related Spectral Perturbation) data in dB, with mean baseline spectral power subtracted at each time in the epoch. The upper left marginal panel presents mean spectral power during the baseline period (blue). The marginal panel under the ERSP image shows the maximum (red) and minimum (blue) ERSP values relative to baseline power for each frequency.

in order to calculate the variation or spectral perturbation related to the event occurrence.

3. Data Analysis and Results

3.1. Clinical Results. Group ASD presented verbal patterns, with 37.5% able to speak few words and sentences, but not enough to maintain a dialogue. Control group also presented verbal patterns, with 100% able to speak few words, sentences, and adequate conversation. All children were attending school, 50% of group ASD were literate, and 50% were in the presyllabic stage. In the control group, only one subject (4 years old) was in the presyllabic stage and the others (87%) were literate.

The ASD's diagnostic age was 4.77 years (SD = 2.30). The ASD parents' age was 40.37 ± 4.59 years and the control group parent's age was 34.62 ± 8.17 years. The predominant parent's education level was college (43.8%) for the ASD group and high-school (56.3%) for the control group. The average income for both groups was between 1 and 5 minimum salaries (75%).

3.2. EEG Power Spectral Density. EEG Power Density Spectrograms were generated using MATLAB for the mean of ASD and control group. Differences between ASD and control groups were observed in power spectrum parameters, with stronger activation for Gamma band (above 30 Hz), and along frontal, central, parietal, and occipital electrodes.

For the ASD group, the major activation was verified in the Fp and F electrodes for frequencies above 20 Hz, in the parietal and central electrodes for frequencies between 40 and 50 Hz, and in the occipital electrodes for frequencies above 40 Hz. In a lower incidence, there was also an increase of slow activity (below 8 Hz) in the frontal, parietal, and occipital regions. In general, the major activation occurred in the left brain hemisphere for the ASD group.

Graphics were generated with the mean of each group according to the type of stimulus (neutral, happy, and angry expressions) and only graphics that showed differences between the ASD and control groups were presented. In this case, the distinctness of the evaluation responses was confirmed in the F3/F4, C3/C4, P3/P4, and O1/O2 electrodes. In frontal electrodes, the activation was bigger in the ASD group and mainly in higher frequencies (above 30 Hz), but it was also increased in the theta and delta bands for angry faces, as shown in Figures 2(a) and 2(b).

In parietal electrodes, the differences between the groups were also verified. ASD group presented more activation in

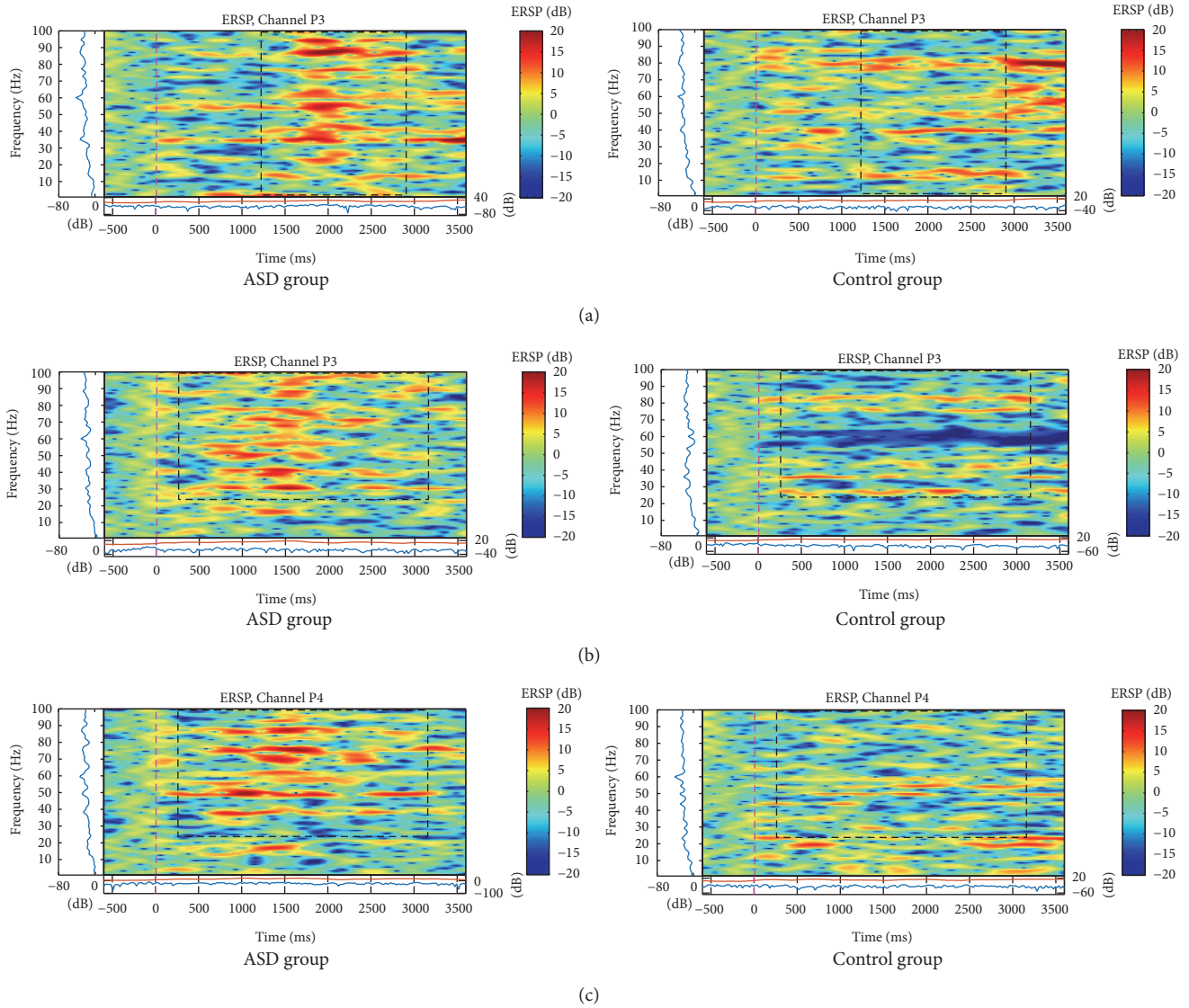

Figure 3: ERSP of P3 (a, b) and P4 (c) electrodes for total mean of samples of the neutral (a), and angry (b), and (c) faces signals in interval of 3 seconds (plus a baseline activity of 500 ms before the event) for ASD and control groups that showed significant spectral perturbations. In ERSP image, the upper panel presents the ERSP (Event-Related Spectral Perturbation) data in dB, with mean baseline spectral power (in dB) subtracted at each time in the epoch. Upper left marginal panel presents the mean spectral power during the baseline period (blue). Marginal panel under the ERSP image shows the maximum (red) and minimum (blue) ERSP values relative to baseline power at each frequency.

slow frequencies (below 5 Hz) for neutral faces on electrode P3 and higher frequencies (above 30 Hz) for neutral faces as well as for angry faces, having a symmetric pattern only for the latter (Figure 3). Analysis of variance showed a main effect for Gamma band on electrodes P3, $F(1, 1118) = 9.55$, $p < .000$, and P4, $F(1, 1118) = 6.20$, $p < .000$. Post hoc independent-samples t-test indicated that scores for electrode P3 were significantly higher for the ASD group ($M = .255$, SD = .341) than for the control group ($M = .071$, SD .200), $t(1118) = 11.1$, $p < .001$.

The C3 and C4 electrodes showed higher bilateral activation in all frequency bands in the ASD group to the stimulus of neutral (Figure 4) and angry (Figure 5) faces. Analysis of variance showed a main effect for Gamma band on electrodes C3, $F(1, 1118) = 8.36$, $p < .000$, and C4, $F(1, 1118) = 75.1$, $p < .000$. Post hoc independent-samples t-test indicated that scores for electrode C3 were significantly higher for the ASD group ($M = .287$, SD = .340) than for the control group ($M = .114$, SD .266), $t(1118) = 9.47$, $p < .001$, and the same pattern was found for electrode C4, where the ASD group were higher ($M = .255$, SD .327) than for the control group ($M = .103$, SD = .253), $t(1118) = 8.67$, $p < .001$.

The activation was similar for parietal and central regions on neutral faces (similarity just on the left side) and mainly

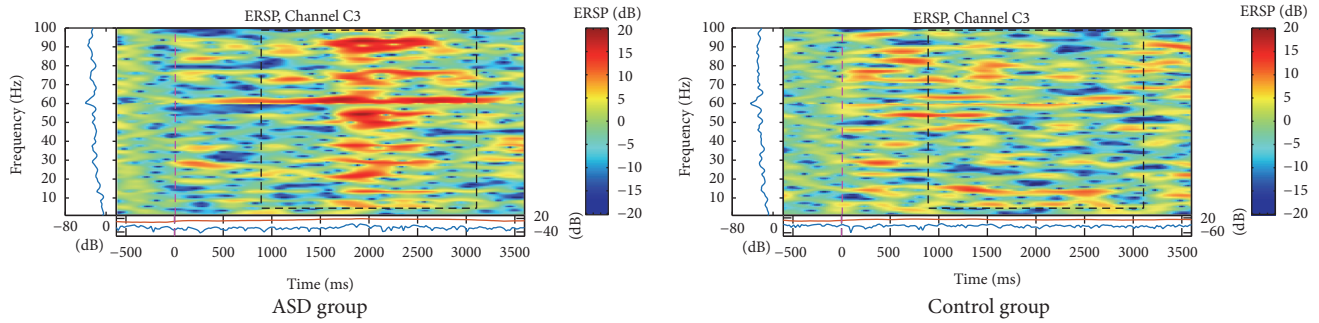

(a)

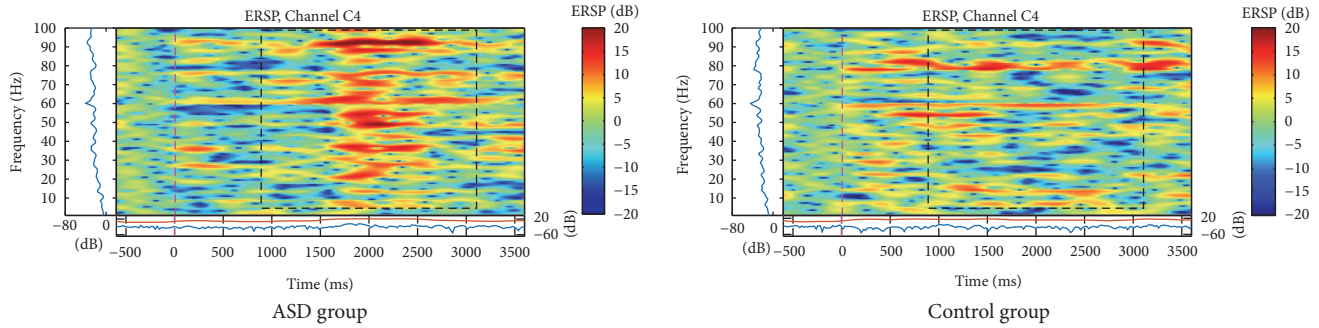

(b)

Figure 4: ERSP of (a) C3 and (b) C4 electrodes for the total mean of samples of the neutral faces signals in the interval of 3 seconds (plus a basal activity of 500 ms before the event) for the ASD and control groups that showed significant spectral perturbations. In the ERSP image, the upper panel presents the ERSP (Event-Related Spectral Perturbation) data in dB, with mean baseline spectral power (in dB) subtracted at each time in the epoch. The upper left marginal panel presents the mean spectral power during the baseline period (blue). The marginal panel under the ERSP image shows the maximum (red) and minimum (blue) ERSP values relative to baseline power at each frequency.

for angry faces (bilateral similarity). Neutral faces showed an increase of spectral power between 10 and 100 Hz, mostly at 2 seconds, in C3, C4 (Figure 4), and P3 channels (Figure 3(a)), but only for ASD group.

For angry face stimulus, spectral power was higher in higher frequencies (between 20 and 50 Hz), on C3 and C4 channels, at 1.5 seconds (Figure 5). The P3 (Figure 3(b)) and P4 (Figure 3(c)) channels similarly showed higher power in higher bands (above 60 Hz).

For the happy face stimulus, the C3 and C4 channels of the control group presented activation in frequencies under 8 Hz from the beginning of the stimuli till 2 seconds later (Figure 6). Simultaneously, there was an activation in higher frequencies (above 30 Hz). However, in ASD group, there was desynchronization mainly in higher frequencies (above 30 Hz) until the end of the stimulus.

Differences occurred in occipital electrodes in the ASD group for the three types of faces, and there was a bilateral desynchronization, but mainly in the left hemisphere for neutral faces (Figure 7(c)). Also, on the left hemisphere, there were differences between happy and angry faces due to a significant increase in spectral power in all frequency bands, mainly the higher bands right after the happy pattern stimulus (Figures 7(a) and 7(b)) and during the angry pattern stimulus (Figure 8). In this case, significant activation occurred to the right hemisphere also in the ASD group before happy faces and there was no asymmetry in the control group (Figures 7 and 8).

4. Discussion

In this study, EEG analyses in children with ASD diagnostics paired with children without ASD were compared during the observation of faces with neutral, happy, and angry expression. Children with ASD presented stronger power spectrum in higher frequencies than the control group for some brain areas. Differences were more evident in occipital and center-parietal regions. Central regions showed a similar pattern to parietal, with same power activation in the same time that the stimulus was presented. Given the clinical evidence of an emotional, cognitive, and behavioral deregulation [21], one of the possible explanations is a perturbation in brain function with stronger or weaker connectivity between areas like the amygdala and prefrontal ventrolateral cortex and orbitofrontal cortex [21].

Developmental psychology suggests that children imitate facial gestures from an early age. This premature imitation might be related to a direct connection from a visual input

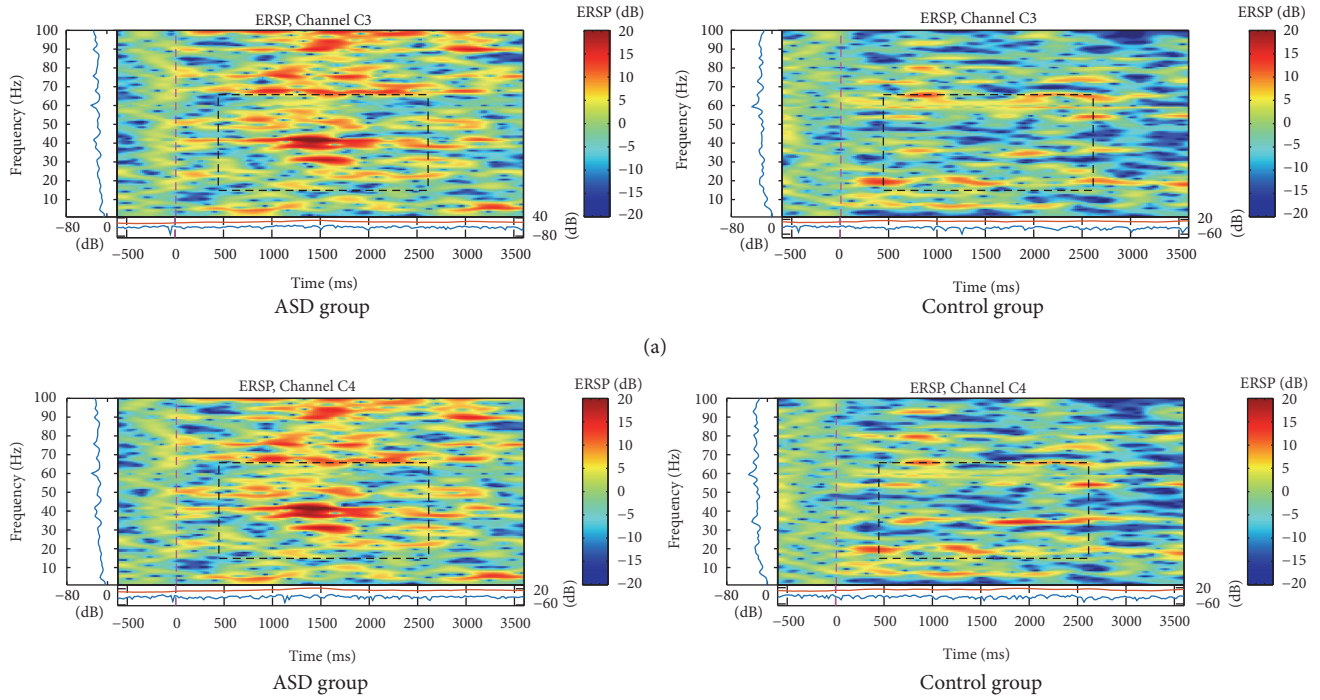

Figure 5: ERSP of (a) C3 and (b) C4 electrodes for the total mean of samples of the angry faces signals in the interval of 3 seconds (plus a basal activity of 500 ms before the event) for the ASD and control groups that showed significant variations or spectral perturbations. In the ERSP image, the upper panel presents the ERSP (Event-Related Spectral Perturbation) data in dB, with mean baseline spectral power (in dB) subtracted at each time in the epoch. The upper left marginal panel presents the mean spectral power during the baseline period (blue). The marginal panel under the ERSP image shows the maximum (red) and minimum (blue) ERSP values relative to baseline power at each frequency.

to a specific motor output [22]. This function is related to the systems of mirror neurons [23]. Failures in this system may be related to the social cognition deficits of ASD. This system suggests a strong relationship between action and intention recognition with social cognition, since it seems to regulate premotor cortex during observation action [24].

It is believed that mirror neurons form a system localized in the inferior parietal lobe, inferior frontal gyrus, superior temporal sulcus, and parietal-frontal lobe. Mirror neurons can be activated by visual stimulus. It was observed that, for visual stimuli indicating action, children with ASD present stronger activation of primary motor areas when compared to activation in the supplementary motor area [25].

Formation of the local network is needed for typical development in childhood and, after that, distribution of neural network in the teenage years and adult phase [26]. ASD children seem to have an atypical organization of the primary motor cortex, resulting in a subconnectivity with weak and short functional reach [26]. These subnetworks might generate execution loss of gestures linked to communication with consequent influence on social behavior [26].

Children with ASD can present differences in brain activities in visual-spatial processing related to object recognition (occipital, temporal, and ventral) and localization of objects in space (parietal, temporal, and dorsal). Communication failures between the dorsal and ventral pathways can harm the visual processing [27] and a lesion in these areas can lead to visual negligence and spatial distortions of body movements [27]. Various neurophysiological studies [7, 28–30] have tried to correlate these clinical symptoms through the demonstration of deficiencies or functional abnormalities of neural networks.

The findings of this study can be correlated to the clinical signs of children with ASD. The hypothesis is that, in ASD children, a deficit in facial expression processing will occur, with consequent failure in the storage for posterior access. The primary visual and primary motor areas are well activated, with some influence of decoding of the parietal lobe. Because of that, a bigger power spectrum might have occurred practically of the same pattern of central and parietal regions. It is believed that, in C3 and C4 electrodes during the stimuli of neutral and angry face, the presence of excessive fast rhythm in the ASD group when compared to the control group is probably due to the bottom-up activation. These failures of connectivity promote a mirror neurons system behavior similarly to the imitation of immature children that presents the direct conversion of the stimulus input (primary visual cortex) and motor output (motor cortex). In contrast,

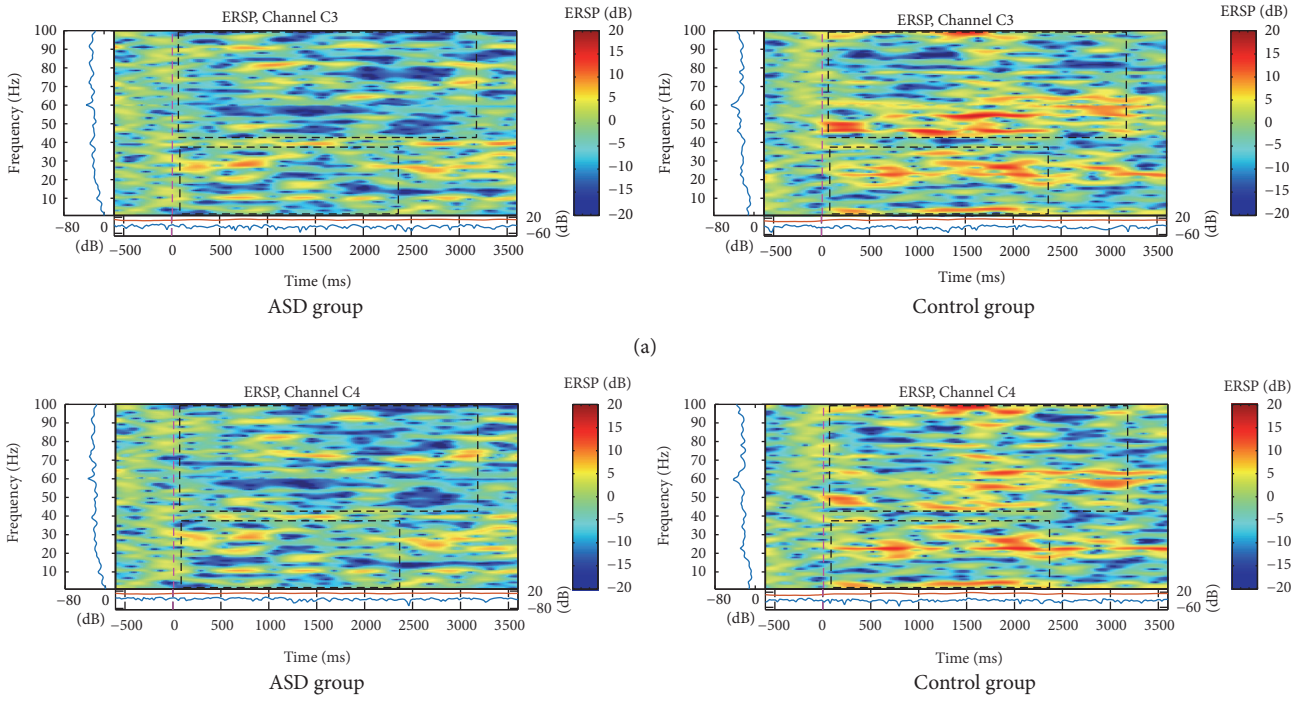

Figure 6: ERSP of (a) C3 and (b) C4 electrodes for the total mean of samples of the happy faces signals in the interval of 3 seconds (plus a basal activity of 500 ms before the event) for the ASD and control groups that showed significant variations or spectral perturbations. In the ERSP image the upper panel presents the ERSP (Event-Related Spectral Perturbation) data in dB, with mean baseline spectral power (in dB) subtracted at each time in the epoch. The upper left marginal panel presents the mean spectral power during the baseline period (blue). The marginal panel under the ERSP image shows the maximum (red) and minimum (blue) ERSP values relative to baseline power at each frequency.

children with ASD have visual tracking patterns with greater fixation in regions important for emotional expressiveness (such as eyes and mouth) when exposed to happy face stimuli [28]. This behavior may help a more emotional maturity processing and therefore, a cerebral hypoactivation in C3 and C4 for fast frequency bands in this group in relation to the control was observed in this study. Similarly, there is a flaw in the rendering of faces with emotion mainly for neutral and angry expressions.

Another explanation for the motor deficits of child with ASD is the failure in visual and motor circuitry. Stereotyped and repetitive behaviors are reported in 64% of the ASD cases and the child realizes the inadequate movements mainly in the attempt of sensory regulation as a mechanism of an organization [31]. In ASD, proprioceptive prejudice associated with reception failure and visual stimuli processing harms motor learning and contributes to the motor behavior and social inappropriateness [32], facilitating the presence of the stereotyped and repetitive behavior. The sensory processing disorder (hypo- or hyperresponsive) may be related to the origin of the functional limitations of the child [33]. Also, there might be some prejudice in motor planning because of the inappropriate visual processing in the ASD. Knowing that the motor and sensory systems cooperate with each other [34], the joint failure of these systems can cause motor dysfunction. A second possible explanation for this study having verified more activation of fast frequencies in the center region is neural plasticity. In children with ASD, failure in sensory/visual processing and in planning together can promote differentiated motor behavior that might occur due to the activation of groups of neurons of primary function without regulation. ASD children might have a failure in the visual processing because of a modification in the communication between dorsal and ventral pathways, which are mediated by connections with the frontal cortex [27]. The failure of the visual processing can promote more activation in the primary visual area.

In this study, a high activation in the occipital areas was found. Bigger activation in O1 and O2 that occurred when happy and angry face group were presented might be due to stronger activation of the primary visual cortex relative to the control group. It is known that in ASD there are failures in visual perception and that it seems to cause more fixation to parts of the stimulus relative to the whole, and also there are erratic visualization patterns [35]. This more intense focal fixation and probable prejudice of face processing can justify the observed pattern. Maybe in the neutral face, the pattern did not occur because there were no "distractors" such as the

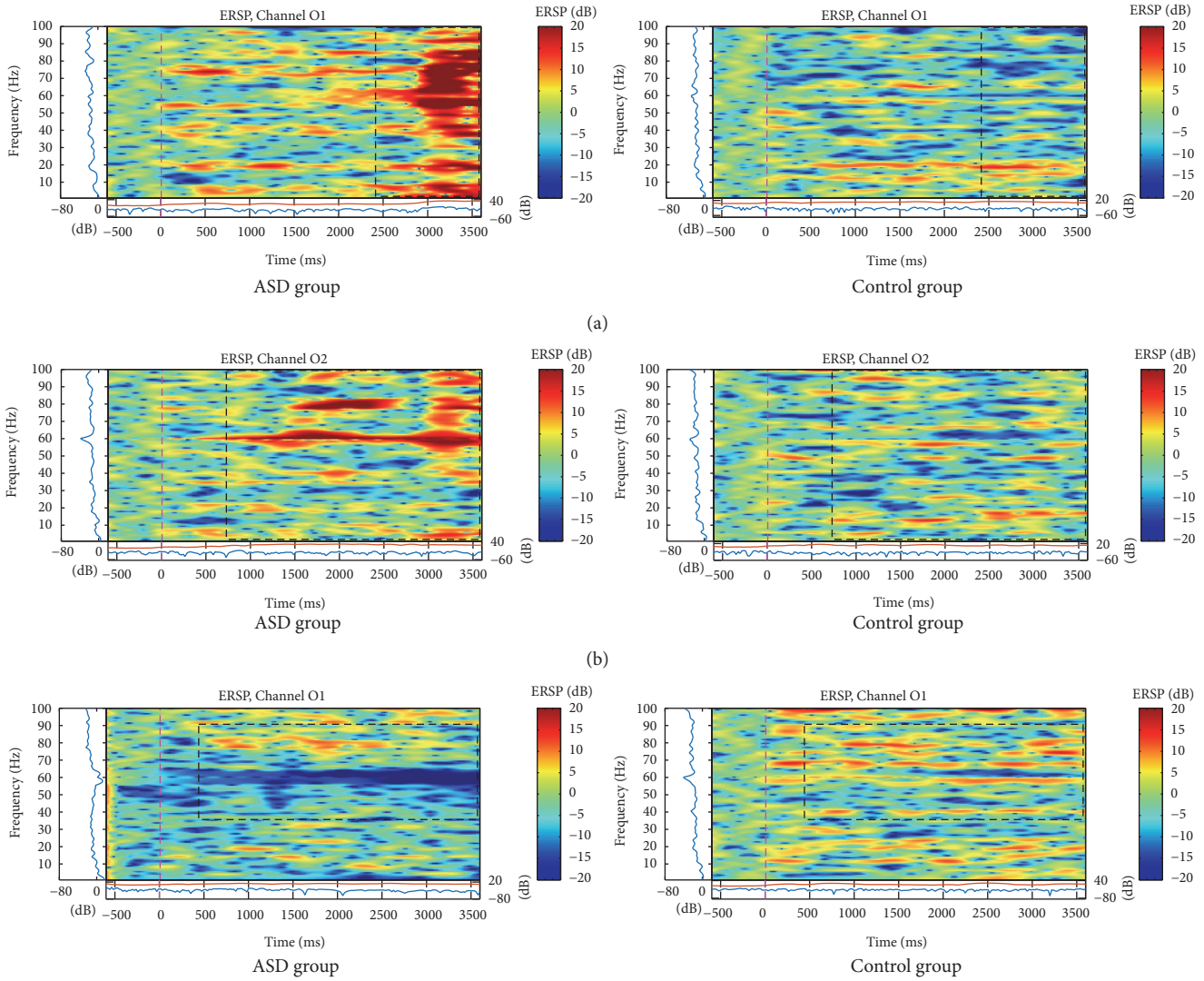

FIGURE 7: ERSP of (a) and (c) O1 and (b) O2 electrodes for the total mean of the samples of the happy (a) and (b) and neutral (c) faces signals in the interval of 3 seconds (plus a basal activity of 500 ms before the event) for the ASD and control groups that showed significant spectral perturbations. In the ERSP image, the upper panel presents the ERSP (Event-Related Spectral Perturbation) data in dB, with mean baseline spectral power (in dB) subtracted at each time in the epoch. The upper left marginal panel presents the mean spectral power during the baseline period (blue). The marginal panel under the ERSP image shows the maximum (red) and minimum (blue) ERSP values relative to baseline power at each frequency.

muscular contraction that occurs in other expressions which attract more focal attention.

5. Conclusion

The analysis of the power spectrum in children with ASD during visual stimulus of happy, neutral, and angry faces demonstrated an increase of power in higher frequencies (above 30 Hz) in the ASD group in frontal, occipital, and center-parietal areas when compared to control group. More studies are needed to better understand these differences.

Conflicts of Interest

The authors declare that they have no conflicts of interest.

Acknowledgments

The authors would like to thank the parents and kids from both groups: ASD and control, who were volunteers for this study, the technician Luciana de Morais Batista Silva who helped in data acquisition, the neuropsychologist Samantha Santos de Albuquerque Maranhão who evaluated the children and participated in the discussions, the CEPS, Jackson

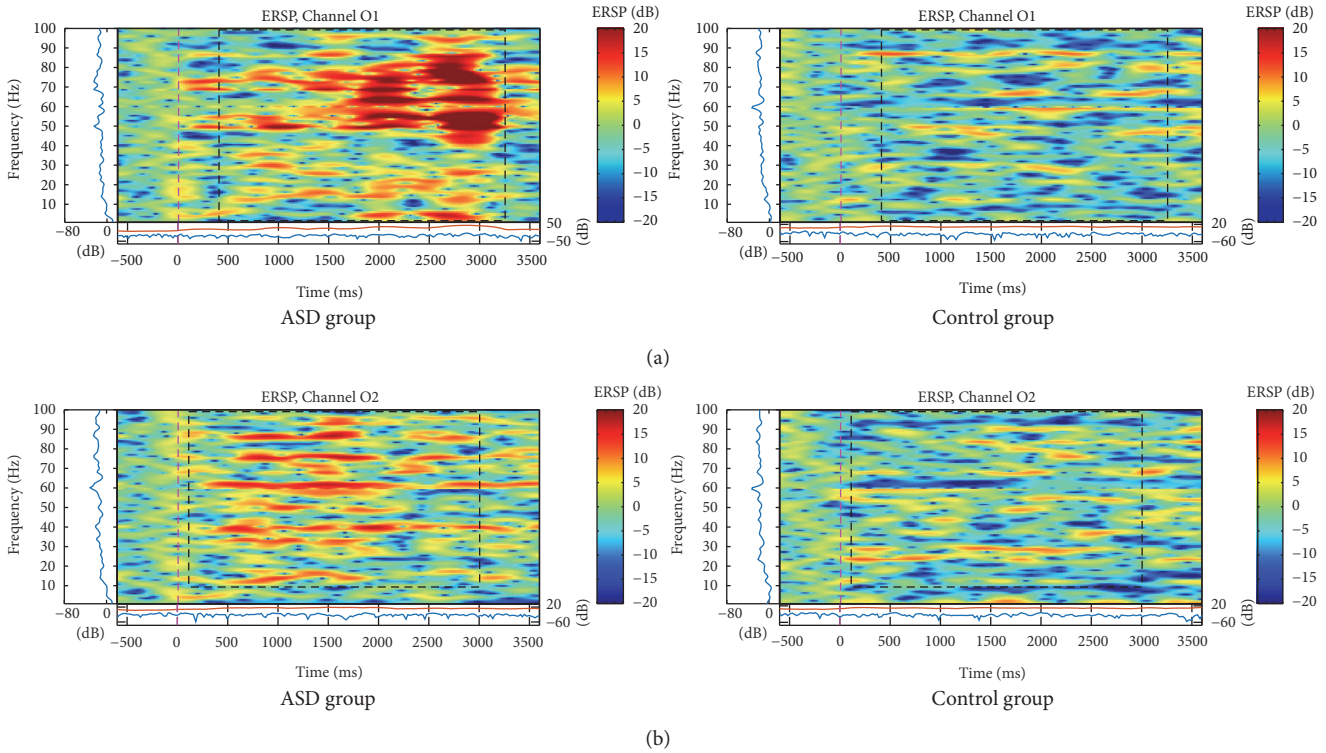

Figure 8: ERSP of (a) O1 and (b) O2 electrodes for the total mean of the samples of the angry faces signals in the interval of 3 seconds (plus a basal activity of 500 ms before the event) for the ASD and control groups that showed significant variations or spectral perturbations. In the ERSP image, the upper panel presents the ERSP (Event-Related Spectral Perturbation) data in dB, with mean baseline spectral power (in dB) subtracted at each time in the epoch. The upper left marginal panel presents the mean spectral power during the baseline period (blue). The marginal panel under the ERSP image shows the maximum (red) and minimum (blue) ERSP values relative to baseline power at each frequency.

Cionek from Brain Support for the eye-tracking system support, Professors Sanjay Joshi and Kenneth Lyons from UC Davis RASCAL Lab for the final review, and Brazilian Ministry of Education (MEC).

References

[1] American Psychiatric Association, *Diagnostic and Statistical Manual of Mental Disorders: DSM IV*, American Psychiatric Association, Washington, Wash, USA, 4th edition, 1994.

[2] American Psychiatric Association, *Diagnostic and Statistical Manual of Mental Disorders*, text rev- DSM IV-TR, American Psychiatric Press, Washington, Wash, USA, 4th edition, 2000.

[3] L. Kanner, "Autistic disturbances of affective contact," *Nervous Child*, vol. 2, pp. 217–250, 1943.

[4] L. Y. Tsai, M. C. Tsai, and G. J. August, "Brief report: Implication of EEG diagnoses in the subclassification of infantile autism," *Journal of Autism and Developmental Disorders*, vol. 15, no. 3, pp. 339–344, 1985.

[5] J. S. Schwartzman and C. A. Araújo, *Transtorno do Espectro do Autismo*, MEMNON Edições Científicas, São Paulo, Brazil, 2011.

[6] M. T. Roelfsema, R. A. Hoekstra, C. Allison et al., "Are autism spectrum conditions more prevalent in an information-technology region? A school-based study of three regions in the Netherlands," *Journal of Autism and Developmental Disorders*, vol. 42, no. 5, pp. 734–739, 2012.

[7] J. Wang, J. Barstein, L. E. Ethridge, M. W. Mosconi, Y. Takarae, and J. A. Sweeney, "Resting state EEG abnormalities in autism spectrum disorders," *Journal of Neurodevelopmental Disorders*, vol. 5, no. 1, article 24, 2013.

[8] E. Fombonne, "Epidemiology of pervasive developmental disorders," *Pediatric Research*, vol. 65, no. 6, pp. 591–598, 2009.

[9] H. I. Kaplan and B. J. Sadock, *Compêndio de Psiquiatria*, Artes Médicas, Porto Alegre, Brazil, 1990.

[10] M. C. Christina, "Early Intervention in autismo," *Infants and Young Children*, vol. 18, no. 2, pp. 74–85, 2005.

[11] A. M. Pereira, *Autismo infantil: tradução e validação da CARS (childhood autismo ratinh scale) para uso no Brasil*, Dissertação de Mestrado, Porto Alegre, Brazil, 2007.

[12] S. Bölte, K. D. Bartl-Pokorny, U. Jonsson et al., "How can clinicians detect and treat autism early? Methodological trends of technology use in research," *Acta Paediatrica, International Journal of Paediatrics*, vol. 105, no. 2, pp. 137–144, 2016.

[13] S. J. Spence and M. T. Schneider, "The role of epilepsy and epileptiform eegs in autism spectrum disorders," *Pediatric Research*, vol. 65, no. 6, pp. 599–606, 2009.

[14] N. N. Boutros, R. Lajiness-O'Neill, A. Zillgitt, A. E. Richard, and S. M. Bowyer, "EEG changes associated with autistic spectrum disorders," *Neuropsychiatric Electrophysiology*, vol. 1, no. 1, 2015.

[15] H. Sheikhania, B. M. R. Behnam, C. Mohammadi, and D. M. Noroozian, "Analysis of EEG background activity in Autism

disease patients with bispectrum and STFT measure," in *Proceedings of the 11th WSEAS International Conference on COMMUNICATIONS*, Agios Nikolaos, Crete Island, Greece, July 2007.

[16] M. Hashemian and H. Pourghassem, "Diagnosing autism spectrum disorders based on EEG analysis: A survey," *Neurophysiology*, vol. 46, no. 2, pp. 183–195, 2014.

[17] M. M. Ravicz, K. L. Perdue, A. Westerlund, R. E. Vanderwert, and C. A. Nelson, "Infants' neural responses to facial emotion in the prefrontal cortex are correlated with temperament: a functional near-infrared spectroscopy study," *Frontiers in Psychology*, vol. 6, article 922, 2015.

[18] A. L. Tierney, L. Gabard-Durnam, V. Vogel-Farley, H. Tager-Flusberg, and C. A. Nelson, "Developmental trajectories of resting eeg power: an endophenotype of autism spectrum disorder," *PLoS ONE*, vol. 7, no. 6, Article ID e39127, 2012.

[19] J. N. Saby and P. J. Marshall, "The utility of EEG band power analysis in the study of infancy and early childhood," *Developmental Neuropsychology*, vol. 37, no. 3, pp. 253–273, 2012.

[20] C. Akasari and S. Pattersom, "Interventions Addressing Social Impairment in Autism," *Current Psychiatry Reports*, vol. 14, no. 6, pp. 713–725, 2012.

[21] N. B. Pitskel, D. Z. Bolling, M. D. Kaiser, K. A. Pelphrey, and M. J. Crowley, "Sistemas neurais de reavaliação cognitiva em crianças e adolescentes com transtorno do espectro do autismo," *Developmental Cognitive Neuroscience*, vol. 10, pp. 117–128, 2014.

[22] A. N. Meltzoff and M. K. Moore, "Explaining facial imitation: a theoretical model," *Early Development and Parenting*, p. 179, 1997.

[23] S. Hanawa, M. Sugiura, T. Nozawa et al., "The neural basis of the imitation drive," *Social Cognitive and Affective Neuroscience*, vol. 11, no. 1, Article ID nsv089, pp. 66–77, 2015.

[24] I. Puzzo, N. R. Cooper, P. Vetter, R. Russo, and P. B. Fitzgerald, "Reduced cortico-motor facilitation in a normal sample with high traits of autism," *Neuroscience Letters*, vol. 467, no. 2, pp. 173–177, 2009.

[25] I. Puzzo, N. R. cooper, P. Vetter, and R. Russo, "EEG diferenças de ativação no córtex pré- motor e área motora suplementar entre indivíduos normais com traços altos e baixos de autismo," *Brain Research*, vol. 1342, pp. 104–110, 2010.

[26] D. L. Floris, A. D. Barber, M. B. Nebel et al., "Atypical lateralization of motor circuit functional connectivity in children with autism is associated with motor deficits," *Molecular Autism*, vol. 7, no. 1, article no. 35, 2016.

[27] T. P. Deramus, B. S. Black, M. R. Pennick, and R. K. Kana, "Enhanced parietal cortex activation during location detection in children with autism," *Journal of Neurodevelopmental Disorders*, vol. 6, no. 1, article no. 37, 2014.

[28] J. B. Wagner, S. B. Hirsch, V. K. Vogel-Farley, E. Redcay, and C. A. Nelson, "Eye-tracking, autonomic, and electrophysiological correlates of emotional face processing in adolescents with autism spectrum disorder," *Journal of Autism and Developmental Disorders*, vol. 43, no. 1, pp. 188–199, 2013.

[29] K. Pierce, S. Marinero, R. Hazin, B. McKenna, C. C. Barnes, and A. Malige, "Eye tracking reveals abnormal visual preference for geometric images as an early biomarker of an autism spectrum disorder subtype associated with increased symptom severity," *Biological Psychiatry*, vol. 79, no. 8, pp. 657–666, 2016.

[30] L. A. Kimberly, C. D. Gilman, J. Meinzen-Derr et al., "Multi-frequency localization of aberrant brain activity in autism spectrum disorder," *Brain and Development*, vol. 38, no. 1, pp. 82–90, 2015.

[31] A. M. Amiri, N. Peltier, C. Goldberg et al., "WearSense: detecting autism stereotypic behaviors through smartwatches," *Saúde*, vol. 5, no. 1, p. 11, 2017.

[32] M. B. Nebel, S. E. Joel, J. Muschelli et al., "Disruption of functional organization within the primary motor cortex in children with autism," *Human Brain Mapping*, vol. 35, no. 2, pp. 567–580, 2014.

[33] E. Gal, M. J. Dyck, and A. Passmore, "Relationships between Stereotyped Movements and sensory processing disorders in children with and without developmental or sensory disorders," *American Journal of Occupational Therapy*, vol. 64, no. 3, pp. 453–461, 2010.

[34] A. Tomassini, D. Spinelli, M. Jacono, G. Sandini, and M. C. Morrone, "Rhythmic oscillations of visual contrast sensitivity synchronized with action," *Journal of Neuroscience*, vol. 35, no. 18, pp. 7019–7029, 2015.

[35] G. Golarai, K. Grill-Spector, and A. L. Reiss, "Autism and the development of face processing," *Clinical Neuroscience Research*, vol. 6, no. 3-4, pp. 145–160, 2006.

Hindawi
BioMed Research International
Volume 2017, Article ID 5708937, 17 pages
https://doi.org/10.1155/2017/5708937

Research Article

Towards Rehabilitation Robotics: Off-the-Shelf BCI Control of Anthropomorphic Robotic Arms

Alkinoos Athanasiou,[1,2] Ioannis Xygonakis,[1] Niki Pandria,[1] Panagiotis Kartsidis,[1] George Arfaras,[1] Kyriaki Rafailia Kavazidi,[1] Nicolas Foroglou,[2] Alexander Astaras,[1,3] and Panagiotis D. Bamidis[1]

[1]*Biomedical Electronics Robotics & Devices (BERD) Group, Lab of Medical Physics, Faculty of Medicine, School of Health Sciences, Aristotle University of Thessaloniki (AUTH), 54124 Thessaloniki, Greece*
[2]*1st Department of Neurosurgery, "AHEPA" University General Hospital, Aristotle University of Thessaloniki (AUTH), 54636 Thessaloniki, Greece*
[3]*Robotics Laboratory, Computer Science Department, American College of Thessaloniki (ACT), 55535 Thessaloniki, Greece*

Correspondence should be addressed to Alkinoos Athanasiou; athalkinoos@auth.gr

Received 22 April 2017; Accepted 5 July 2017; Published 29 August 2017

Academic Editor: Victor H. C. de Albuquerque

Advances in neural interfaces have demonstrated remarkable results in the direction of replacing and restoring lost sensorimotor function in human patients. Noninvasive brain-computer interfaces (BCIs) are popular due to considerable advantages including simplicity, safety, and low cost, while recent advances aim at improving past technological and neurophysiological limitations. Taking into account the neurophysiological alterations of disabled individuals, investigating brain connectivity features for implementation of BCI control holds special importance. Off-the-shelf BCI systems are based on fast, reproducible detection of mental activity and can be implemented in neurorobotic applications. Moreover, social Human-Robot Interaction (HRI) is increasingly important in rehabilitation robotics development. In this paper, we present our progress and goals towards developing off-the-shelf BCI-controlled anthropomorphic robotic arms for assistive technologies and rehabilitation applications. We account for robotics development, BCI implementation, and qualitative assessment of HRI characteristics of the system. Furthermore, we present two illustrative experimental applications of the BCI-controlled arms, a study of motor imagery modalities on healthy individuals' BCI performance, and a pilot investigation on spinal cord injured patients' BCI control and brain connectivity. We discuss strengths and limitations of our design and propose further steps on development and neurophysiological study, including implementation of connectivity features as BCI modality.

1. Introduction

Advances in neural interfaces including implantable neural prosthetics and brain-computer interfaces (BCIs) have recently demonstrated remarkable results in the direction of replacing [1, 2] or even restoring [3, 4] long-lost sensorimotor function in human patients. Pathological conditions like spinal cord injury (SCI), amyotrophic lateral sclerosis, and stroke, among others, compromise an individual's physical and psychological well-being and result in social seclusion due to the severance between volition and the ability to act [5]. SCI in particular results in disconnection of afferent and efferent neural pathways and can cause permanent sensorimotor disability, often without any cognitive alteration, which negatively impacts the lives of the victims and their families [6]. BCIs aim to bridge this disconnection by detecting and decoding brain activity, thus allowing patients to control external devices, robotics, and exoskeletons [1–5]. Nonetheless, chronic SCI has been demonstrated to induce neurophysiological changes in brain structure [7] and function, both at resting state [8] and during sensorimotor process [9]. These neurophysiological changes could negatively affect

the design and development of robust and durable BCIs for motor restoration [4, 10]; hence they should be systematically investigated further [11].

Despite recent technological breakthroughs in BCI research, in terms of reliability, accuracy, and speed, the best results in robotics and neural prosthesis control have been demonstrated by invasive technology (neural implants) [1, 2, 12, 13]. Noninvasive BCIs, on the other hand, are far more widespread and hold many relative advantages, including simplicity, safety, lower cost, and range of applications [14, 15]. Moreover, novel paradigms and recent advances in noninvasive BCI protocols also aim at progressively improving past technological and neurophysiological limitations to levels comparable to invasive BCIs [16, 17]. Such a paradigm, taking into consideration the aforementioned neurophysiological alterations that disabled individuals demonstrate compared to healthy users [11], lies with investigating brain connectivity features for implementation of BCI control [17–19]. Commercial electroencephalography (EEG) BCI systems, as another approach, are based on fast, reproducible detection of a low number of mental states and have taken the spotlight in consumer applications. They are even increasingly considered for robotics control [20, 21], often employing the detection of motor imagery (MI) states. The mental execution of an action, MI, displays similarities in brain activation [22, 23] with physical execution and as such has also been deployed in rehabilitation and BCI applications for disabled individuals [5, 14]. MI consists of a visual and a kinesthetic component, corresponding to two task-dependent and distinct neural contributing systems [24–26]. Visual motor imagery (VMI) implies that a representation of the motor task is provided (e.g., video or avatar), while kinesthetic motor imagery (KMI) is based on internal simulation or rehearsal of the task. While networks formed during VMI and KMI both involve motor related cortical areas, VMI also involves the occipital and superior parietal cortical areas while KMI involves the inferior parietal cortex [24, 26].

Even past the challenges and limitations of BCI systems, the design of a robotic arm for medical engineering applications, such as rehabilitation and assistive technologies for disabled individuals, constitutes a challenge on multiple fronts, including engineering problems, design requirements, and budget cost issues [27]. Designing a custom-made robotic arm allows for greater flexibility and negates the need to purchase expensive research-level robotics. It also raises several issues: reduced accessibility to directly comparable experimental findings by other research groups [28], lack of standardization, harder validation of experimental results, and increased difficulty in assessing suitability to nonspecific applications [29] compared to similar commercially available robotic products.

While programmable automation design can be traced back to Ancient Greece [30], modern transistor-based electronics during the latter half of the 20th century have allowed for complex electromechanical devices (mechatronics) of unprecedented programmability, precision, speed, strength, and durability. Subsequent integration of sensors and powerful digital microprocessors has increased the versatility of modern robots and medical applications (surgical applications, mechatronic prosthesis, and rehabilitation) are developing fast. Currently robotic systems are constantly under direct human control, but semiautonomous algorithms are also under development [31]. Constant advances in artificial intelligence algorithms mean that robots with medical decision support capabilities may be a likely next technological step [32]; however careful planning and public debate are required to ensure a human operator remains in the loop at all times to assume legal and ethical responsibility [33].

To that end, social robotics and Human-Robot Interaction (HRI) are considered important—yet sometimes overlooked—aspects of robotics development [34, 35]. User perception, satisfaction, and overall experience are of equal importance to hardware/software performance and quality standards [36]. Especially in fields such as rehabilitation that depends on human psychology, the success of a robot cannot be meaningfully assessed using technological performance and industrial integration criteria alone [36]. The accommodation of registering an external machine as a part of one's own body schema, which significantly affects the rehabilitation process, should also be taken into account [37]. HRI psychological and social characteristics can be investigated with questionnaires, carefully correlating psychological perception measurements with the characteristics of the robotic system used [34, 37]. The Godspeed questionnaire was selected for our purposes due to providing reproducible and comparable subjective measurements and sufficient coverage of HRI-related psychological states [36]. Such tools can prove invaluable in developing improved medical robotics particularly for prosthesis and rehabilitation applications [38].

In our previous work we have already presented the conceptual design and development of the Mercury robotic arm for biomedical applications and dealt with construction standards and validation tests [21]. We implemented a Body-Machine Interface (BMI) control module and conducted a pilot end-user assessment experimental study [39], focusing on both the technical characteristics and performance, as well as on HRI [36]. Our research team has since further improved the robotic arms in terms of anthropomorphism and allowing for movement along more Degrees-of-Freedom (DoFs) through the addition of a gripper resembling a human hand. We also improved the electronics and integrated a second symmetric Mercury arm into the system [40].

In the remainder of this paper we present our progress and goals towards developing off-the-shelf BCI-controlled robotic arms for assistive technologies and rehabilitation applications. In Materials and Methods, we first account for further development of the robotic arms and electronics, including a qualitative assessment study of the BMI module. We subsequently report on the implementation of the BCI control module using an off-the-shelf EEG-BCI system and the development of BCI-robotics communication; then we present two illustrative experimental applications of the BCI-controlled robotic arms. The first experiment is a study on healthy individuals to compare MI modalities for optimal BCI performance. The second experiment regards a comparative pilot investigation on SCI patients and healthy individuals for noninvasive control of multiple robotic arm motions

and functional connectivity [41]. In Results and Discussion we first report the results of these two illustrative experiments regarding training, performance, and qualitative assessment, as well as briefly presenting pilot findings regarding brain networks. We then discuss the strengths and limitations of our experimental design and propose further steps on robotic development and neurophysiological study.

2. Materials and Methods

2.1. Mercury: Short Account on Development Milestones of the Robotics

2.1.1. The Robotic Arms Platform. The Mercury robotic arm system has been developed as a customized design by our team for two technological generations so far [39, 40]. Design requirements focused on biomedical engineering applications, specifically intuitive remote robotic control, HRI research, and medical robotics for rehabilitation. Emphasis was placed primarily on fluid, anthropomorphic motion, fast response times to control triggers, and low fabrication cost. At a lower priority we regarded precision of movement and heavy lifting capability. Since the development of the robotic system has been presented elsewhere [39, 40], hereby we briefly report the technological characteristics of the system used in our current experimentation.

The Mercury robotic platform comprises a robotic arm currently capable of movement along 8 DoFs (at shoulder, elbow, wrist, hand gripper, and thumb joints), as well as a choice between two control modules [42]: (a) a custom-designed BMI capable of sensing the movement of a human operator's arm and (b) a commercially available BCI (EPOC, Emotiv, USA) which was integrated into the system. The system uses commercially available DC motors to provide movement: (a) along Cartesian vectors for the robotic shoulder joint (2 DoFs: "right-left" and "up-down"), the elbow joint (1 DoF: "up-down"), and the wrist joint (1 DoF: "up-down") and (b) 2 DoFs along rotation axis between the "shoulder/elbow" and "elbow/wrist" parts. Two servomotors complement the robotic arm's movement capabilities, allowing for gripping small objects with a 3D printed, anthropomorphic gripper: 1 DoF is used for the thumb and 1 DoF for the rest of the fingers (Figure 1).

2.1.2. The Body-Machine Interface. The BMI control module for the Mercury robotic arm has been described in previous work in terms of design, construction, cost, and features [39]. In the current section we provide a synopsis of the BMI module simply to facilitate comprehension of the technological evolution of our overall experimental robotic setup. The Mercury BMI comprises an exoskeletal position sensing harness (EPSN), which is worn by the user around their arm. It uses analogue resistance sensors to capture the movements of the shoulder, elbow, and wrist, as well as the gripping movement of the human hand. Movement is captured along 6 DoFs, a subset of the actual capabilities of the real human arm but enough to provide a realistic reproduction of the movement of the aforementioned joints.

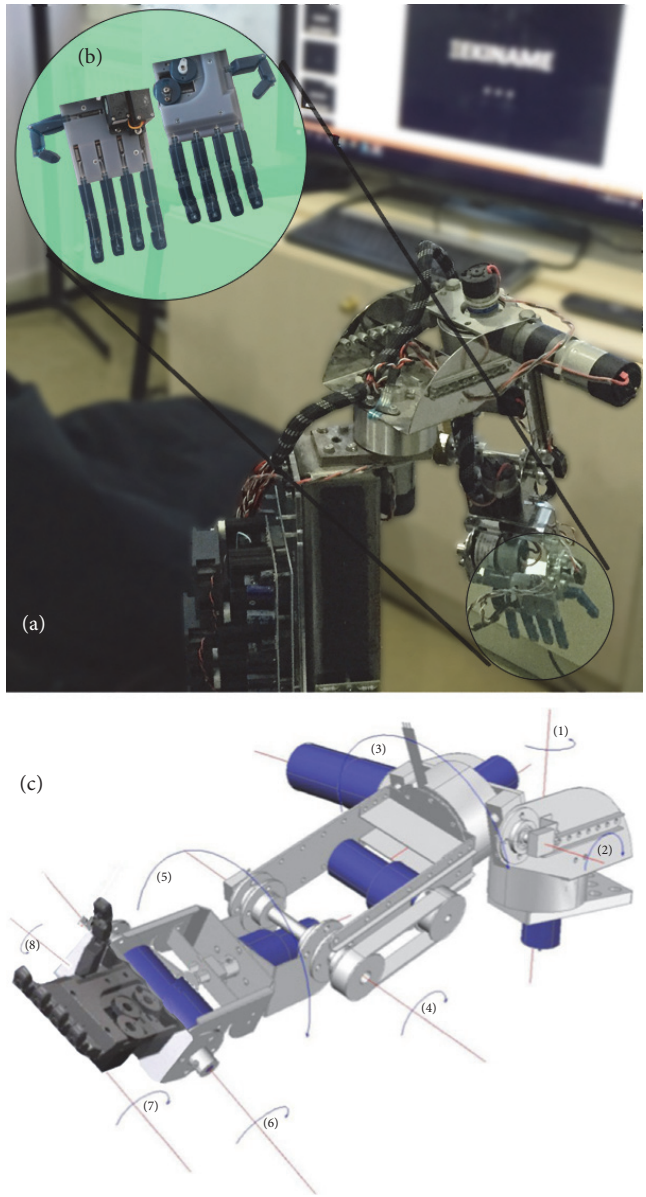

Figure 1: Current generation of Mercury robotic arm: (a) the robotic arm in position during an illustrative experiment, (b) the 3D-printed gripper (in focus circle), and (c) schematic of the 8 DoFs of the robotic arm. Mercury arms are house-built, of low cost, and anthropomorphic.

During the design process of the EPSN, emphasis was placed on rapid capture and transfer of control signals to the Mercury robotic arm, allowing it to replicate the movement of the human operator's arm in a fluid, anthropomorphic fashion. For this purpose analogue classical automation control circuits were used to calculate analogue control signals subsequently fed to an Atmel ATmega2560 microprocessor. The microprocessor handled digitization, interface to a PC, and generation of the control signals for the Mercury robotic arm. Initial experiments using the EPSN focused on HRI, specifically the time required for first-time human operators to develop the skills to control the Mercury robotic arm

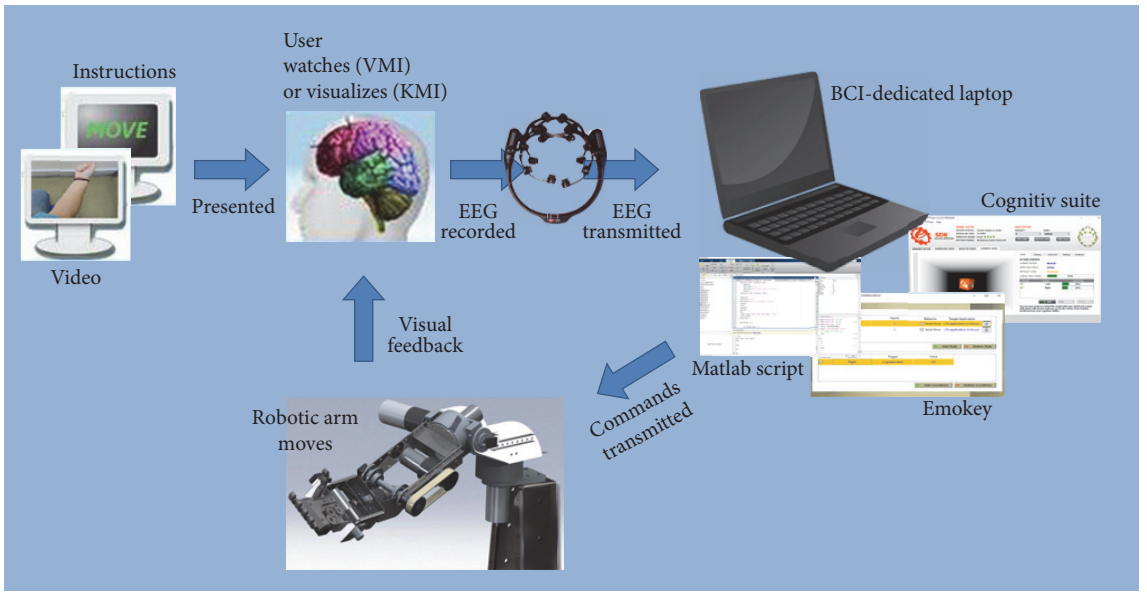

Figure 2: Schematic of Brain-Computer Interface loop: using off-the-shelf EEG-BCI for control of house-built robotic arms.

and perform basic tasks such as knocking, gripping, lifting, and placing small objects [39]. Those initial experiments also gathered perceived psychometric characteristics from pilot testers, classified by age, sex, level of education, and familiarization with electronics and robotics technology [43, 44]. These comparisons revealed not only a tendency of female pilot testers and those unfamiliar with robotics to perceive the Mercury robotic arm as being more humanlike, but also a disillusionment effect being induced to all participants after the pilot testing.

2.2. Brain-Computer Interface Module Development

2.2.1. Off-the-Shelf Brain-Computer Interface. Advances in both hardware and software technologies rendered real-time EEG processing a possibility, including detection and identification of brain activity features for use in BCIs. Currently there are several BCI systems available commercially, one of which is the Emotiv EPOC (USA), sold around $300, which is significantly lower than most medical EEG devices. It is a portable, wireless EEG recording device that has 14 dry electrodes arranged according to the international 10–20 System and can be easily mounted to the user's head. The device operates at an internal sampling rate of 2048 Hz and the data are transmitted wirelessly at 2.4 GHz to a USB dongle with a sampling rate of 128 Hz. The BCI capabilities of the device are accessed by the Cognitiv suite and rely on Event Related Desynchronization (ERD). The user initially needs to record a resting state EEG after which he is able to train up to four mental commands, using a machine-learning pipeline to teach the BCI how he visualizes. The pipeline operates along the stages of preprocessing, feature extraction, reduction of dimensionality, and classifier training. Following the training, the suite will continually attempt to identify the trained commands by analyzing the user's EEG. During this process, the suite presents a floating box that will execute any mental command that it identifies, and the action power, corresponding to the level of confidence of each classification.

2.2.2. Communication between BCI and Robotics. In order to achieve online communication between the commercial BCI application and the robotic arms, the trained BCI classes are mapped in real-time to computer controls, using a combination of the BCI's native Emokey application (Emotiv, USA) and an in-house script, developed in Matlab environment (Mathworks, USA). In our implementation, the BCI is trained in only three classes: one for resting state and two for general "left" or "right" directions, using either visual or kinesthetic motor imagery. Each BCI class is linked to a specific key button, which is enabled when the detected mental state corresponds to that class. Then the script accepts the corresponding command as input and transmits it through a serial port, with Baud Rate 9600, to the on-board microcontroller unit for each Mercury robotic arm (Figure 2). The arms' units translate that input to specific positional coordinates for each of the 8 DoFs' motor. Using this approach, we achieve a move reaction time of the system that approximates 0.2 seconds.

2.3. Current Experimental Setup. The Bioethics & Ethics Committee of Faculty of Medicine, Aristotle University of Thessaloniki, approved the experimental protocol. All experiments were conducted after the participants providing informed consent and no remuneration was given. To facilitate the integration of the robotic arms (or the limb presentation during EEG recording) into the participants' own body schema, their arms and body were covered with a black curtain [37] during all experimental procedures. Wherever visual cues were used (video of arms or legs moving) the presented limbs were always matched with regard to the participant's sex. Furthermore, none of the

Figure 3: Overview of the experimental setup in the Thess-AHALL Living Lab. The figure is modified with authors' permission [46].

participants in any experiment reported prior experience with MI practices or BCI experiments (characterized as BCI-naïve [45]). Finally, the participants reported on their user experience, rating the HRI characteristics of the system by answering the Godspeed questionnaire [36], translated in the Greek language [44].

All experimental parts that involved the use of the robotic arms were conducted in the Thessaloniki Active and Healthy Ageing Living Lab technology showcase room (Thess-AHALL, member of ENoLL, http://www.aha-livinglabs.com, http://medphys.med.auth.gr) [46, 47] that is equipped with accelerometers for fall detection and observation cameras [48]. Participants comfortably sat on a chair, while disabled individuals sat on a wheelchair, docked between the two robotic arms and facing a 42″ TV/computer monitor located a meter away (Figure 3). EEG recordings were taken from an Emotiv EPOC headset with a sampling rate of 128 Hz and wirelessly transmitted to the BCI-dedicated laptop that was mounted on the frame and operated by the investigator, situated behind the participant.

The experimental parts that involved the use of high-resolution EEG recording were conducted in a specially designed magnetic shielded room for recordings with presentation capabilities and audiovisual monitoring. The participants sat on an inclined armchair inside the room, while facing a 21″ computer monitor located a meter away. Recordings were obtained using the 10-5 international electrode system for high-resolution EEG [49] with a sampling rate of 1000 Hz and impedance threshold set at 10 kOhm. An active electrodes cap was used (Brain Products, Germany) connected to a 128-channel EEG (Nihon-Kohden, Japan).

2.4. Qualitative Assessment Experiment: Comparison of MI Modalities. The first of the two illustrative experimental applications was a qualitative assessment study, comparing MI modalities for control of the BCI-controlled robotic arms by healthy individuals with regard to BCI training and optimal performance [50]. The participants were trained to use visual and kinesthetic cues to control simple motor tasks of the two robotic arms and we assessed their skill training and success rates.

2.4.1. Subjects and Training Procedure. In total thirty healthy participants were included in the study, 18 male (60%) and 12 female (40%), ranging from 19 to 46 years (median age 24 years). All 12 female and 14 of the male participants declared that they were right-handed. From the rest of the male participants, 2 declared being left-handed and 2 being ambidextrous.

Kinesthetic motor imagery (KMI) modality was trained first. The participants were asked to relax and resting state EEG with eyes-open was first trained as the neutral BCI class. All participants were then asked to strongly imagine a commonly performed (daily routine) movement for each

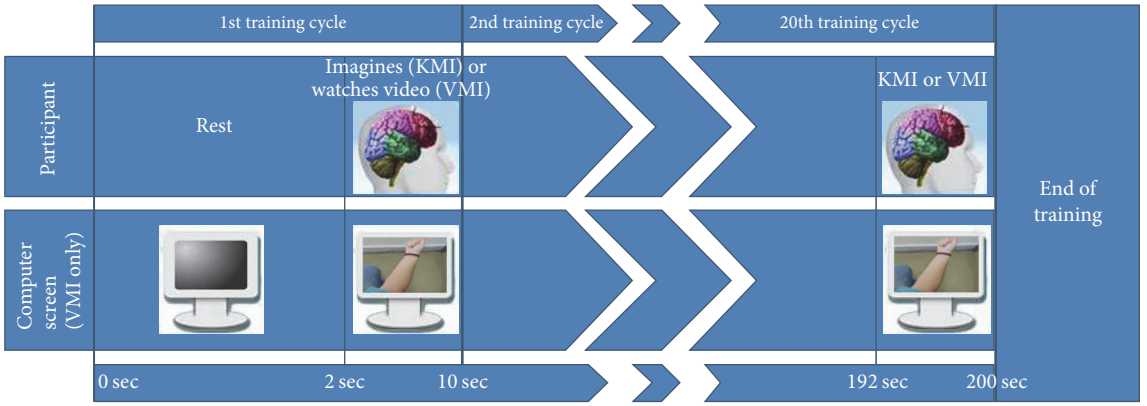

Figure 4: The training procedure of the qualitative assessment experiment.

hand (left and right) without actually moving their limbs. A "left" and "right" BCI class was trained accordingly, 20 times each. Always the "left" class was trained first and training was conducted in blocks of five training cycles. Each cycle consisted of 8 seconds of continuous recording of the mental state ("training") and 2 seconds of rest (Figure 4), while the achieved training skill percentage and the action power of each cycle were recorded (action power threshold was set at 50%). When the KMI training was concluded (Figure 4), the participants rested for 2 minutes before attempting to control the robotic arms (control trials are described in Section 2.4.2).

The participants rested for 10 minutes after the KMI control trials and then the VMI modality was trained. The training procedure was the same but instead of imagining a movement, during the "training" cycle, a video played on the TV monitor (left or right forearm pronation). Again when the VMI training was concluded, 2-minute rest intervened before the participants attempted to control the robotic arms.

2.4.2. Robotic Arm Control Trials and Success Rates. The participants attempted to control the "elbow/wrist" rotational DoF of each robotic arm. First they attempted to move the right robotic arm 10 times with the "right" BCI class and then the left robotic arm 10 times with the "left" BCI class. Each trial cycle lasted 10 seconds with a 2-second rest between them and a successful trial was marked by any detection of the correct BCI class during the 10-second period. When the correct class was detected the relevant DoF moved (corresponding to pronation), while it remained idle otherwise.

For the control trials using KMI, only a command was given to the participants to attempt to control the robotic during the trial cycle. For the control trials using VMI, during the trial cycle, on the TV monitor the same video that the participants were trained to played and no command was given (Figure 5). Success rate was recorded for each robotic arm and imagery modality (successful trials in 10 consecutive trial cycles of right or left robotic arm control in either KMI or VMI). Success rates for each imagery modality were also calculated (successful trials in 20 trial cycles of both robotic arms control).

2.4.3. Statistical Analysis

(1) Demographics. Six participants who did not succeed in passing action power threshold during skill training (50%) were excluded from further analysis. All further comparisons regarding demographics (as well as skill training, success scores, and Godspeed questionnaire, as presented in next sections) were made on the remaining participants ($n = 24$). Planned comparisons explored the age differences across the remaining participants using as grouping factor the gender/sex (female, male). The age was tested for normality following Shapiro-Wilk Test [51, 52] after controlling for sex. However, age did not meet the normality assumption when controlled for sex. Therefore, age differences between sexes were explored using Mann–Whitney (U) Test. We did not control for hand dominance as grouping factor because the majority of the remaining participants were right-handed. Significant age differences between female and male participants were not found ($U = 68$; $p = 0.816$).

(2) Kinesthetic against Visual Motor Imagery Skill Training. KMI skill training scores were compared against VMI skill training scores (a) for all remaining participants and (b) for participants grouped by gender. For all participants, scores were compared for both hands (left and right hand separately) and also across training blocks after those being tested for normality assumption. The differences between Kinesthetic and Visual Skill scores were normally distributed across training blocks for both hands. Therefore, Paired t-tests were planned for each training block and for both hands separately. After grouping by gender, we compared again KMI and VMI skill training scores across training blocks and for both hands separately. For the aforementioned statistical analyses Paired t-tests were used since differences (Kinesthetic-Visual Skill scores) were still normally distributed after controlling for sex.

(3) Kinesthetic against Visual Motor Imagery Success Scores in Robotic Arm Control. Planned comparisons regarding the KMI and VMI success scores of BCI robotic arms (both right and left) control were performed. The number of successful trials in ten consecutive trials was defined as success scores.

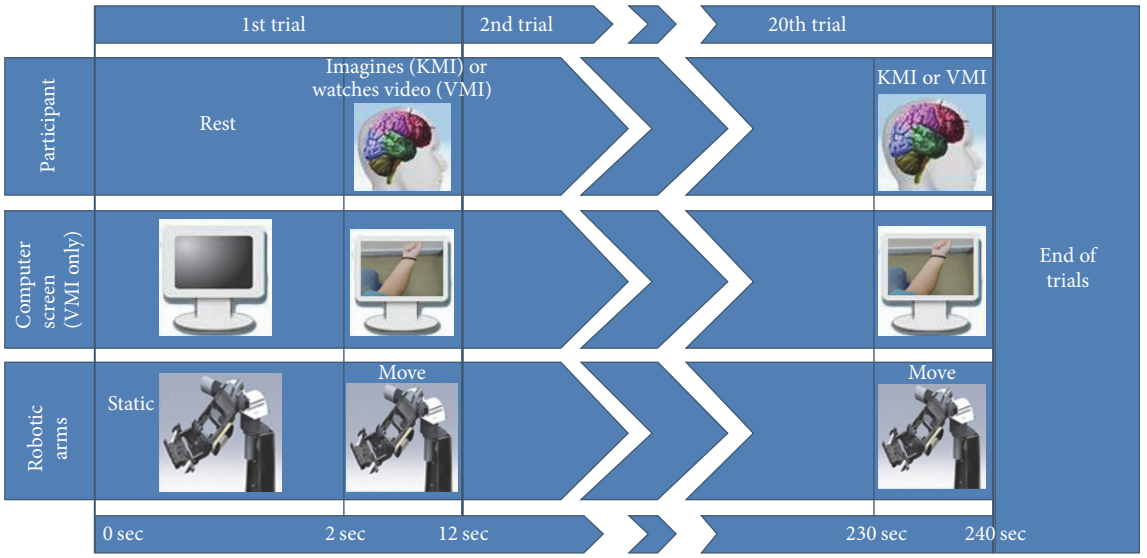

Figure 5: Overview of robotic arm control trials during the qualitative assessment experiment.

Statistical analysis was performed using Wilcoxon Signed Ranks test as KMI and VMI success scores were obtained by the same participant.

(4) Godspeed. Godspeed scores of each key concept (Anthropomorphism, Animosity, Likeability, Perceived Intelligence, and total Godspeed) score were analyzed as interval variables (for more information see Section 2.6.). Therefore, we tested for normality assumption grouping by sex (female, male) and used Shapiro-Wilk Test. Likeability, Perceived Intelligence, Perceived Safety, and total Godspeed score were found to be normally distributed and t-tests were performed between female and male participants. Anthropomorphism and Animosity were analyzed between two groups following Mann–Whitney (U) test.

2.5. Pilot Patient Investigation: BCI Control and Functional Brain Connectivity. The second of the two illustrative experimental applications is an ongoing pilot study that involves SCI patients and healthy individuals controlling multiple DoFs of the robotic arms, as well as an investigation of their brain connectivity [53]. The participants are trained with visual cues of various arm movements or walking and then use kinesthetic cues for BCI control of the robotic arms. Apart from assessing their performance, we moreover perform a pilot analysis of the functional brain networks formed for each different movement.

Three SCI patients were already recruited for participation in the pilot study, one female (28 years old) and two male (52 and 47 years old), as well as three age and sex matched healthy individuals as control group. The patients' neurological level of injury was C4, C4, and T7, respectively and their Asia Impairment Scale classification was D, C (incomplete injuries), and A (complete injury), respectively. The protocol involves a full neurological examination using the International Standards for Classification of Spinal Cord Injury [54] and assessment of their functional status using the Spinal Cord Independence Measure III [55] in the Greek language (g-SCIM-III) [56]. Moreover, the protocol also involves healthy and patient participants both answering Vividness of Visual Imagery Questionnaire (VVIQ) [57], Beck Depression Inventory (BDI) [58, 59], and Rosenberg Self-esteem Questionnaire (RSQ) [60, 61]. Since the investigation is ongoing and more patients are expected to be recruited, our focus hereby will be on presenting an overview of the methodological aspects of the study, as well as provisional results regarding functional connectivity from one subject and healthy control.

2.5.1. High-Resolution EEG Recording during Multiple Movements. While under high-resolution EEG recording (as described in Section 2.3) the participants watched random video recordings of upper limbs performing movements of all DoFs or lower limbs walking. The participants attempted to register these movements as being their own [37], without moving their own limbs (VMI) (Figure 6). The presentation followed an oddball paradigm, displaying randomly 9 repetitions of 34 videos, divided into 3 sets with 10-minute rest between them. For each of 8 possible DoFs of the arms, both directions of movement were displayed, for both left and right arm, totaling 32 videos of upper limbs. The remaining 2 videos were walking (from walker's perspective) and an oddball wildlife video. All videos had duration of 5 seconds, followed by 4 seconds of black screen.

2.5.2. BCI Control of Robotic Arms. In the second part of the experiment, the participants used the commercial EEG-BCI to control the robotic arms. Three BCI classes were trained: resting state, left, and right. The participants were asked to visualize the videos they were presented during the previous part during the training of left and right. Each direction was trained 20 times, each cycle lasting 8 seconds, followed by 2 seconds of rest.

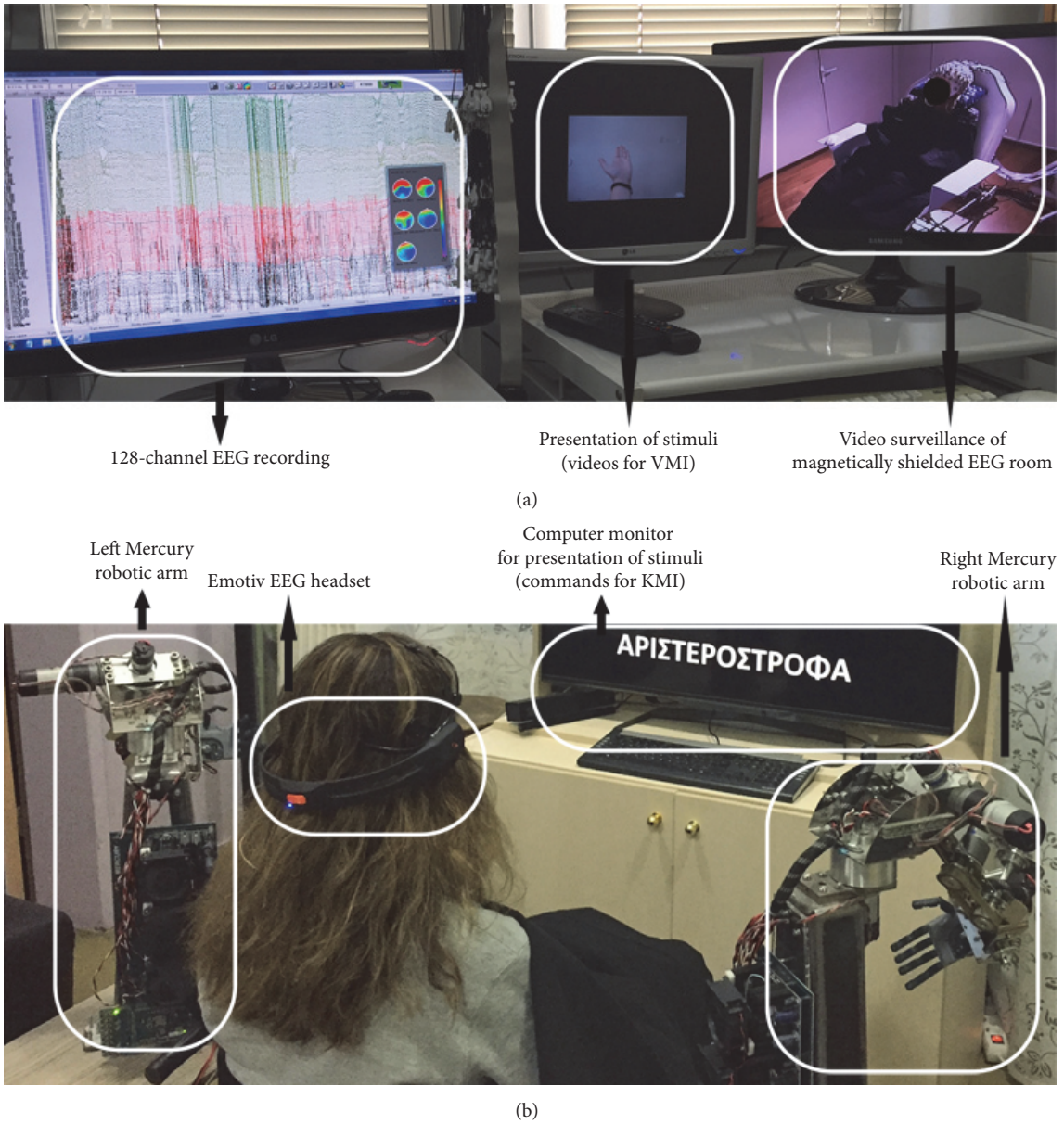

Figure 6: 28-year-old female SCI patient participating in the pilot investigation: (a) 1st part of the experiment, 128-channel EEG recording during oddball presentation of multiple limb movements (visual imagery); (b) 2nd part of the experiment, control of robotic arms using a commercial EEG-BCI headset, employing mental rehearsal of movements (kinesthetic imagery).

After the system's training to each participant's brainwaves, they were asked to follow presented instructions, corresponding to specific DoFs of the robotic arms and to specific direction of movement. The participants attempted to visualize the same movements to achieve control (KMI), without moving their limbs, while the BCI detected one of the three aforementioned classes. The presentation followed a pseudorandom routine that included an instruction to perform each of 32 possible arm movements once. Each instruction lasted 30 seconds, followed by 5 seconds of rest period. The participants' performance in each movement was rated on a 0–5 scale and an overall percentage score was calculated to denote overall BCI performance.

2.5.3. Signal Analysis and Brain Networks

(1) Preprocessing. The acquired high-resolution raw EEG signals were band-pass filtered between 2 and 50 Hz using a zero-phase finite impulse response filter, downsampled at 100 Hz, and rereferenced to the common average reference (CAR) [62]. Triggers were set at the onset of each visual stimulus, using the signal from an optic diode, and epochs were extracted from −2000 msec prestimulus to 4000 post-stimulus. Epochs were visually inspected and the heavily artifactual contaminated ones (due to subject movements, spasticity, and electrode disconnection) were rejected. The remaining epochs were averaged according to the event type

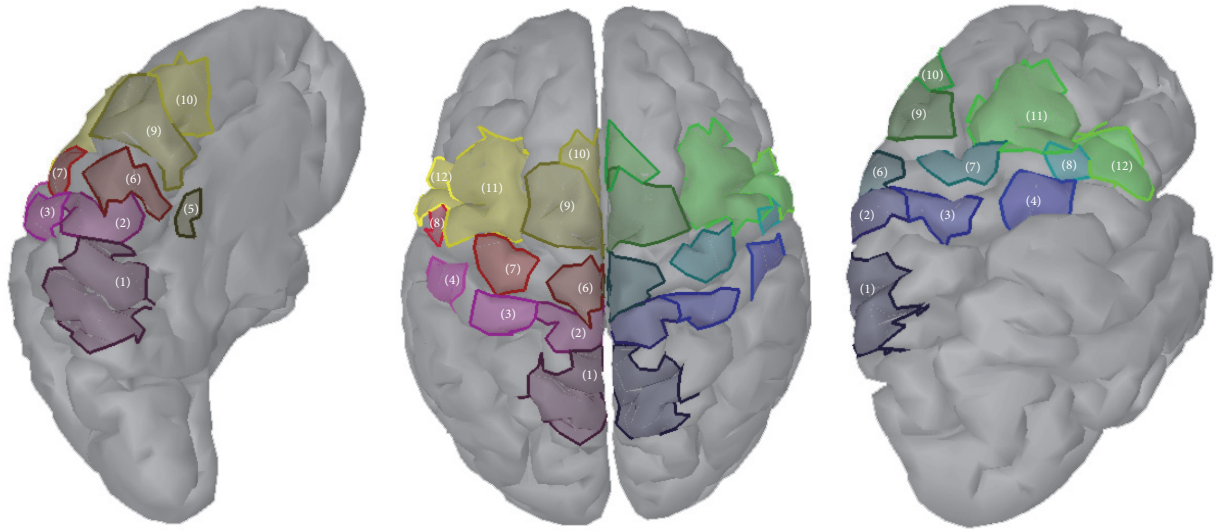

(a) (b) (c)

Figure 7: Regions of interest (ROIs) for connectivity analysis at the cortical level: (a) midline surface, left hemisphere, (b) top view, both hemispheres, and (c) lateral view, right hemisphere. (1): SAC, (2): S1F, (3): S1H, (4): S2, (5): CMA, (6): M1F, (7): M1H, (8): M1L, (9): SMA, (10): pSMA, (11): PMd, and (12): PMv.

(motor imagery of different movements), resulting in 34 average epochs per subject.

(2) Cortical Current Density Estimation. In order to improve spatial resolution of the data and counter smearing caused by the volume conduction effect we deployed cortical current density estimation (CCD) [62] using the Brainstorm [63] toolbox for Matlab. CCD essentially maps the sensor potentials to dipole current distribution that are assumed in fixed positions over the cortex. Dipoles also are referred to as sources, model electrical activity of neuronal groups that fire synchronously [64]. CCD requires first a model of the head conveying information about the electrical properties and geometry of different parts of the head (e.g., scalp, skull, and cortex), electrode position, and source space dipole positions [65]. The Montreal Neurological Institute (MNI) COLIN 27 MRI [66, 67] was used as default subject anatomy to compute a three-shell (scalp, skull, and cortex) head model with boundary element method (BEM) using OpenMEEG [68] via Brainstorm. The cortical surface is assumed as source space. Having the head model and sensor data, CCD estimation was performed using standardized LORETA (sLORETA) method [69] with dipole orientation (5023) constrained normally to the cortex [70]. Noise covariance matrix was estimated on resting state data that take place at the start of each session and was regularized.

(3) Functional Connectivity. After solving the inverse problem of the average trials functional connectivity was performed on the source domain, analyzing the connectivity between 24 cortical regions of interest (ROIs), 12 in each hemisphere (Figure 7): Somatosensory Association Cortex (SAC), Primary Foot Somatosensory Area (S1F), Primary Hand Somatosensory Area (S1H), Secondary Somatosensory Area (S2), Cingulate Motor Area (CMA), Primary Foot Motor Area (M1F), Primary Hand Motor Area (M1H), Primary Lip Motor Area (M1L), Supplementary Motor Area (SMA), pre-Supplementary Motor Area (pSMA), Dorsal Premotor Cortex (PMd), and Ventral Premotor Cortex (PMv). Scouts were defined as ROIs, in the same manner as in our previous study based on neuroanatomical landmarks and Brodmann areas [71], locating scouts on the MNI cortical surface. Connectivity between those areas was calculated for the time period of −1000 msec prestimulus to 2000 msec poststimulus on each of the 34 averaged epochs, using Granger causality [72], for each subject. Networks were calculated for delta (1–4 Hz), theta (4–7 Hz), alpha (8–13 Hz), and beta (13–30 Hz) brainwave bands. Then the functional networks were comparatively assessed, displaying connections with power of at least 60% of the connection with highest power for each network.

2.6. Godspeed Questionnaire Translation and Statistical Manipulation. The Godspeed questionnaire consists of five semantic differential scales, equipped with Likert type scaling evaluating the attitude towards robots in the subcategories of Anthropomorphism, Animacy, Likeability, Perceived Intelligence, and Perceived Safety [36]. Our team performed a double-blind forward and backward translation and adaptation to the Greek language [44]. Accuracy of the procedure was evaluated by a third independent researcher and concepts that needed further resolution were pinpointed and put to the same procedure again, in order to produce an accurate adaptation. The Greek version of the questionnaire (Godspeed-g) was used both in the BMI validation study [43] and the current experimental applications and has also been made available through the original questionnaire's official webpage [73]. Despite the criticism that the original questionnaire has attracted in terms of redundancy and suitability [74],

it remains the most widely applied tool in studying user perception of robots [75].

As with the original one, in the translated version, each semantic differential scale represents a key concept enclosing a short questionnaire. Each short questionnaire results in a score adding the ratings of the respondent. However, in the last two questions of Perceived Safety subcategory reversed rating was used, to associate the lower scores to the negative assessment, as is the case with the other items of the questionnaire [76]. Finally, a total Godspeed score could be calculated adding the scores of each key concept. Semantic differential data can be analyzed as any other rating data, as both Likert scales and semantic differential scales are rating scales and the distributions of the responses are not forced [77]. The analysis of Godspeed data was performed using the guidelines of H. N. J. Boone and D. A. Boone (2012) [78].

3. Results and Discussion

3.1. Qualitative Assessment Experiment

3.1.1. Kinesthetic against Visual Motor Imagery Skill Training. Participants achieved higher median skill training percentage using KMI. That for the left arm was 26.5% (1st training block), 56.5% (2nd), 75.5% (3rd), and 72.5% (4th) for KMI and 20,5%, 54.5%, 71.5%, and 73%, respectively, for VMI. For the right arm it was 14.5%, 26%, 36%, and 24.5% for KMI and 8.5%, 17%, 17,5%, and 14.5% for VMI. There was a fatigue effect, median skill training percentage dropping from 3rd training block to 4th in all settings but left arm VMI.

Statistical testing resulted in significant difference between KMI and VMI skill training score only for the right hand extracted by training block 1 ($t(23) = 2.151$; $p = 0.042$) and block 2 ($t(23) = 2.181$; $p = 0.040$) indicating that KMI skill training scores are higher than those of VMI in training blocks 1 and 2. Statistically significant findings were found neither at training blocks 3 and 4 nor for the left hand across any training block. When discriminating participants by sex, marginally significant difference between KMI and VMI skill scores was found for female participants in training block 2 ($t(11) = 2.136$; $p = 0.056$) favoring KMI training against VMI. Male participants' scores between KMI and VMI training did not reach significance across training blocks. Following the same analysis for the left hand did not yield any significant outcome.

3.1.2. Success Scores in Robotic Arm Control and Godspeed Questionnaire. Median success score was 7 for both left and right arm VMI, 5.5 for left arm KMI, and 5 for right arm KMI (Figure 8). Comparing success scores between KMI and VMI for right and left hand separately, the differences were not found statistically significant (right hand: $Z = -0.945$; $p = 0.344$; left hand: $Z = -1.476$; $p = 0.140$). Differences between female and male respondents to Godspeed questionnaire did not reach statistical significance (Anthropomorphism: $U = 64$, $p = 0.643$; Animosity: $U = 70.5$, $p = 0.931$; Likeability: $t(16.226) = 0.483$, $p = 0.636$; Perceived Intelligence: $t(22) = 0.121$, $p = 0.905$; Perceived Safety: $t(22) = -0.861$, $p = 0.399$) and total Godspeed score ($t(22) = -0.085$, $p = 0.933$).

3.1.3. Discussion. While participants appeared to perform better using VMI rather than KMI as an imagery modality for BCI control, our analysis did not prove a statistically significant correlation [50]. Individual differences could play a role, since some participants performed better with KMI; it is worthwhile to explore this difference, as BCI control should be tailored to the needs of each individual [50]. Perception of the robot did not correlate to either performance or the sex of the operator. This qualitative assessment experiment provided us with important field insight on the operation of the robotic arms and the BCI control modality. Further comparisons, using this design, could include different users groups to perform either imagery type, in order to determine specific characteristics for each. Studying disabled users could also provide answers on the effect of neurological disability on imagery capacity and an ability to perform with BCI.

3.2. Pilot Patient Investigation

3.2.1. Results and Discussion. Our experimental paradigm allows control of multiple DoFs of two robotic arms using a 3-class BCI implementation along with VMI training and the use of AI algorithms. As we have also shown in the proof-of-concept [53], disabled and healthy operators (Figure 9(a)) can achieve comparable, above-chance, performance levels in BCI control of the robotic arms (56.88%, 43.13%, and 55.00% by healthy participants and 52.00%, 46.25%, and 19.38% by SCI patients). While, after only a training session, for some movements only minimal control is achieved, further training sessions are suggested in order to improve performance. Nonetheless, in certain movements excellent performance was achieved (arms were moving towards the desired direction for the most part) and this finding was not correlated to intrinsic difficulty of any movement [53].

As this is an ongoing investigation and subject recruitment continues, we hereby only provisionally present results from connectivity analysis, while a comprehensive assessment of performance, psychometric evaluation, and functional connectivity will be performed with the conclusion of the study. Healthy participants scored 77, 75, and 56 (out of max 80) in the VVIQ questionnaire, while SCI patients scored 54, 69, and 72 (Figure 9(b)). Moreover, healthy participants evaluated the robotic arms with 77, 87, and 68 (out of max 120) in total Godspeed score and SCI patients gave 88, 76, and 96 (Figure 9(c)). The Godspeed subcategories whose scoring by healthy and SCI participants seems to differ are Perceived Safety and Perceived Intelligence (Figure 9(d)), although that is a trend that needs to be tested for statistical significance in data from more participants. In the categories of Anthropomorphism, Animacy, and Likeability, both groups gave almost identical answers (Figure 9(d)).

In Figure 10, functional connectivity networks over the ROIs that we defined at the cortical level (seen in Figure 7) are presented for different motor tasks, performed by a female SCI patient and a healthy control.

Functional connectivity holds promise in classifying imagery of multiple classes (multiple different movements) or complex motions, based on imagery modalities. A possible

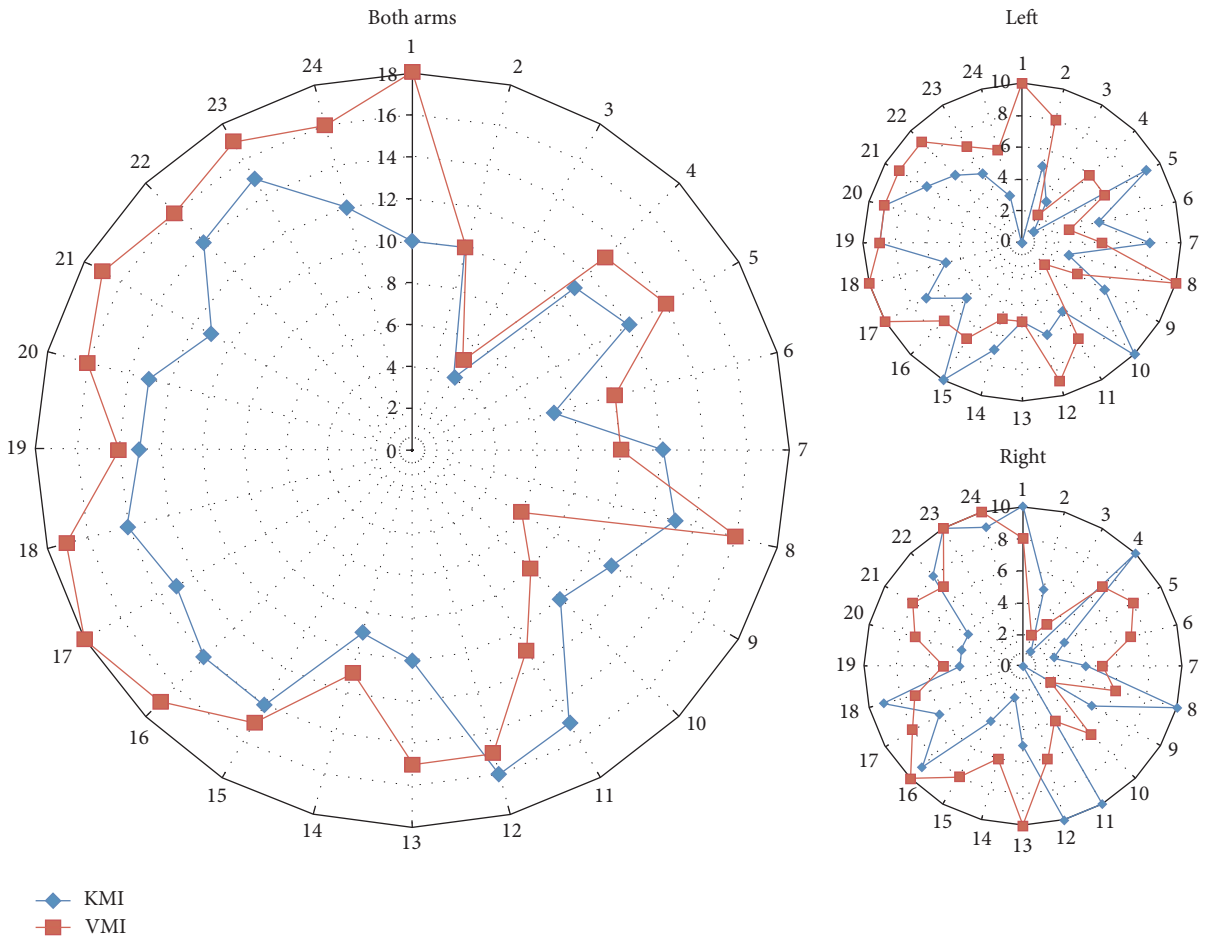

Figure 8: KMI against VMI success scores for 24 participants above action power threshold. Most participants performed better with VMI but the difference was not statistically significant.

automated approach would be to identify significant connections for each task using Network-Based Statistics (NBS). In our opinion, semiautonomous algorithms and AI should be part of a strategy to control multiple DoFs of robotic arms. Our BCI approach uses a 3-class implementation to achieve control of many (32 possible) DoFs but currently relies on research intervention. The low-class approach employed could be feasible both for BCI training and neurophysiological investigation. While training and functional connectivity study is performed using high-resolution EEG, it is highly impractical to use such systems for everyday BCI applications. Therefore, we aim to downscale the findings from high-resolution EEG regarding functional connectivity to control features for commercial low-resolution EEG-BCI headset. Moreover, other investigations could include trauma-induced brain reorganization with a focus on possible rehabilitation opportunities.

3.3. Future Steps

3.3.1. Further Robotics Development. A natural milestone for future development is the integration of the BCI and robotic arms system into the operator's perceived body mental image [37]. From the user's point of view, this requires rapid, fluid, accurate, and predictable system performance. Furthermore, this necessity consequently corresponds to rapid processing of analogue BCI input: filtering and extraction of relevant brainwave information into the relevant robotic control signals in near-real-time (<100 ms). Maintaining time lag to a minimum is particularly important in order to avoid confusing the human brain's natural visual and tactile feedback loops. Determining the upper limit in response time lag is likely to depend on both the task and the user; we believe it will be meaningful to investigate this limit and the gradual deterioration of user control past it, across different types of tasks. Furthermore, we plan to investigate the operator's perception (from the HRI perspective) as response time lag varies across the aforementioned time limit.

Another important aspect of perceived body mental image that needs to be taken into account in further development is anthropomorphism. In our current technological generation, user perception of the robotic arm, as measured by Godspeed, did not correlate with performance [50]. As further robotics development would also focus on improving anthropomorphic characteristics of the system, as well as the users' perception, it would be interesting to identify possible correlations between advancements in that direction and

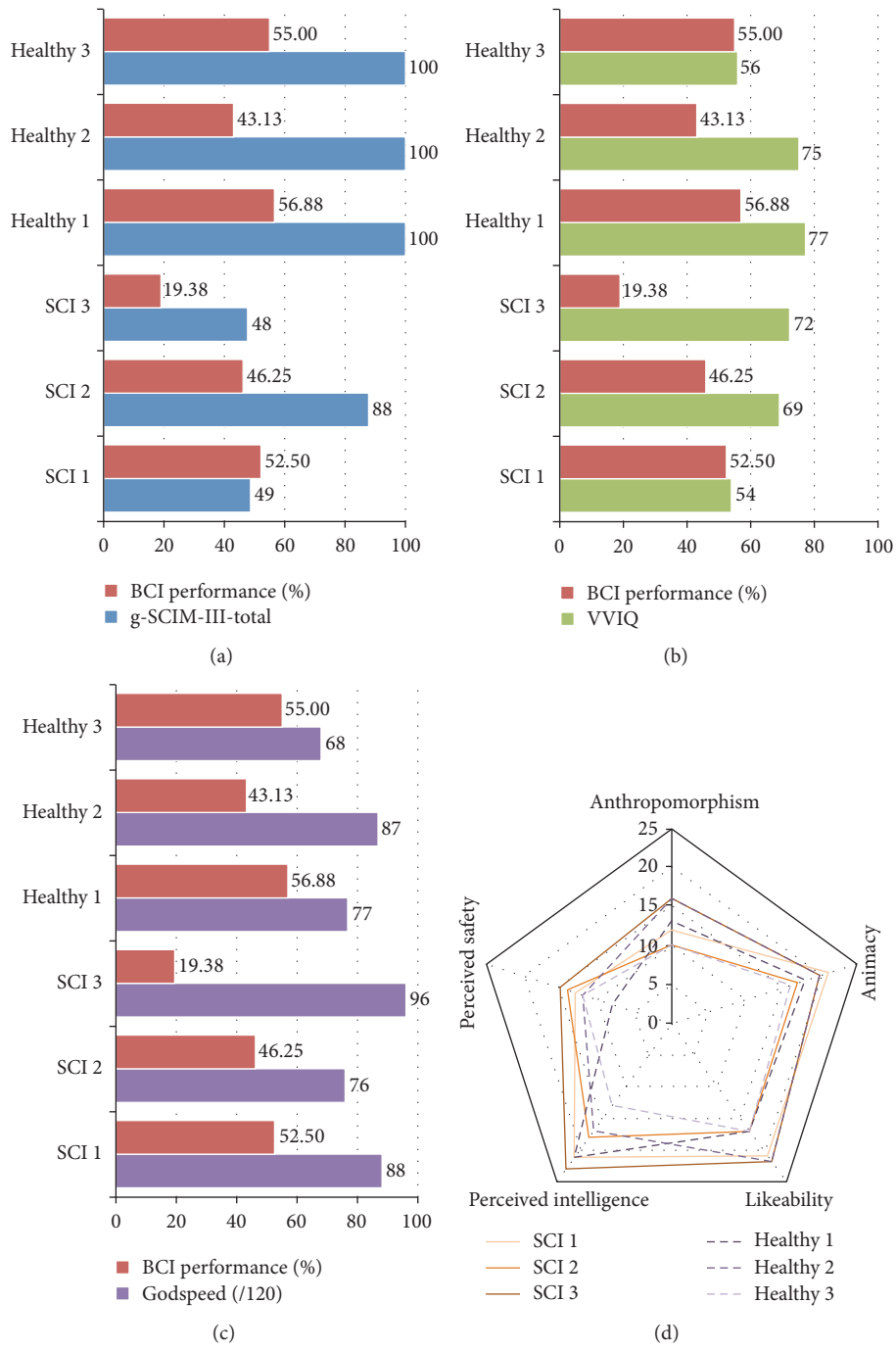

Figure 9: Performance in BCI control of patient and healthy participants in comparison to (a) their g-SCIM-III total score, (b) VVIQ score, and (c) Godspeed total score. Also (d) evaluation of the robotic arms in each separate Godspeed subcategory by participant.

performance, as well as to identify possible "uncanny valley"-like phenomena [74]. An important question, also with regard to real-time response of BCI-robotics systems, would be to investigate whether operators would expect more natural and fluid response from a near humanlike robotics system than from a more mechanical-looking one, and whether not meeting such expectations would affect either user perception or performance. Furthermore, as subject recruitment progresses through the ongoing study [53], we also aim to investigate correlations between operators' emotional state, perception of the robotics, and performance. Finally, further robotics development and associated experiments should focus on naturalistic scenarios and real-life applications, designed for both disabled and healthy end-users.

3.3.2. Further Neurophysiological Investigation. There are several paradigms for sensorimotor BCI implementation that vary from machine learning to signal processing perspective.

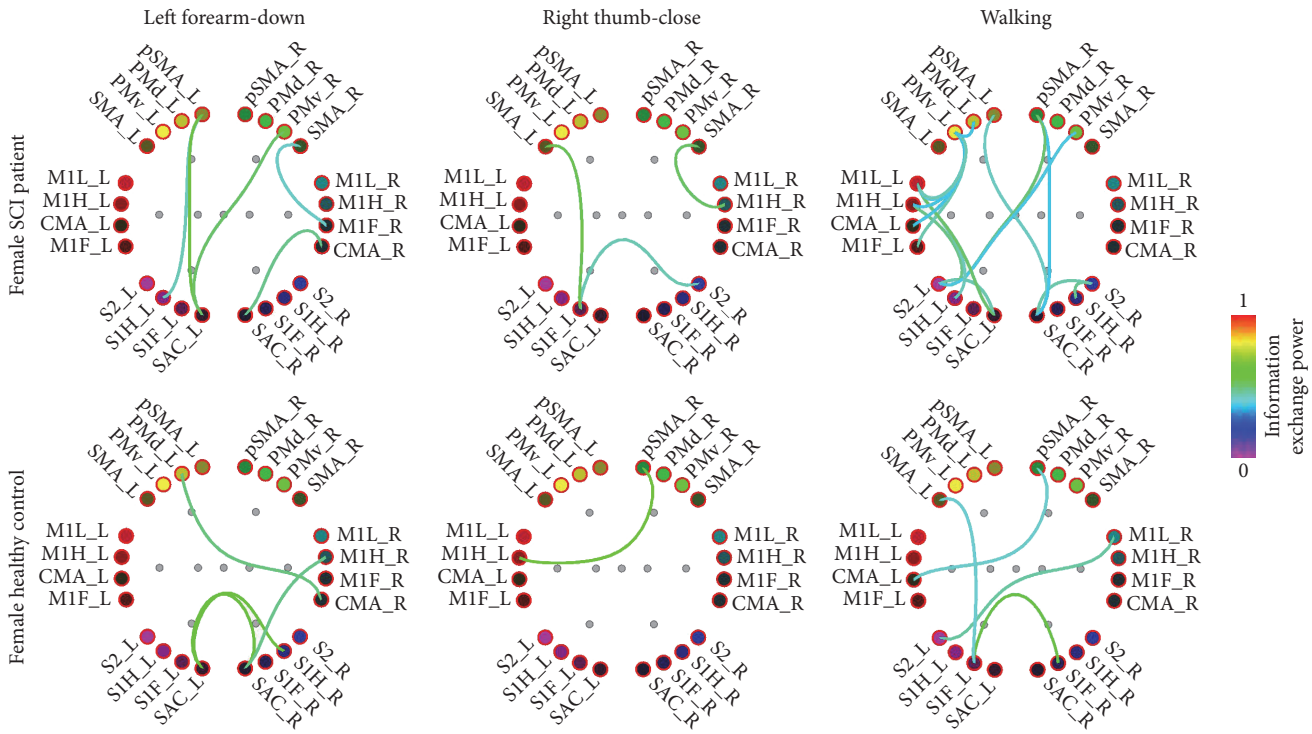

Figure 10: Functional connectivity networks formed in alpha brainwave band during different visual motor imagery tasks performed by an SCI patient and a sex and age matched healthy control participant (connections > 60% max power displayed).

Current BCIs are capable of easily recognizing two classes, which translates to control of 1 DoF but usually fails to work with more classes. One of the biggest challenges of noninvasive motor imagery BCIs is the low spatial resolution of EEG, due to volume conduction effect [79]; hence spatial features extracted directly from EEG are poorly discriminative.

Cortical current density estimation methods can be deployed to compensate for the low spatial resolution of EEG, by reconstructing activation of cortical sources using EEG data and realistic head model, so essentially transforming sensor data to a higher dimension space, where spatial resolution is higher. Several studies concluded that features extracted from source space are superior over sensor based [70], and a recent published study has achieved sufficient discrimination of complex movements of the same limb, utilizing source imaging techniques [70].

One of the strongest requirements of Mercury BCI algorithm is natural control of a multi-DoF robotic arm, corresponding to multiclass in terms of decoding. Decoding brain activity is still an open challenge especially when it turns to multiple classes [80], although implementation of functional connectivity features for BCI class classification [71] is expected to provide applicable solutions [17]. A foreseeable future direction of BCI algorithms is to extract almost solely features from source space. Data driven ROI specification for each subject based on ICA could be used, instead of static ROIs for all subjects. Features extraction scheme will be based on a combination of spectral, spatial, and connectivity features to improve robustness. For classification, hierarchical approach seems appealing for the multiclass problem.

Such a processing pipeline is highly computational demanding, and at this stage of its development we work with offline analysis until the results are encouraging to proceed to real-time implementation. Recent advancements in Graphic Processing Units (GPUs) and Field-Programmable Gate Arrays (FPGAs), which have proven to be effective in rendering computationally demanding applications in real-time, could be employed for an online implementation of our paradigm.

High-resolution EEG data and its analysis for functional connectivity from multiple motor imageries are expected to provide insight in brain network adaptive and maladaptive reorganization that occurs after SCI [11]. Most published studies have focused on resting state connectivity and those that have used MI have not yet discriminated between different motor tasks. On the other hand, low-density EEG data recorded through KMI-BCI operation can be further studied for functional connectivity networks and compared to data gathered from high-resolution EEG recordings during VMI. Such an approach could possibly facilitate the downscaling of a network-based BCI in the future for multiple DoFs and control of complex movement sequences. This should also point towards whether this network classification is possible with affordable, off-the-shelf, noninvasive BCI devices and low-resolution EEG.

3.3.3. Limitations. In the context of our design and experiments, we encountered several limitations. First of all, although demands for portability, ease of use, low cost, and availability made the selection of a commercial dry electrode

EEG headset necessary, the accompanying commercial (and undisclosed) BCI algorithm did not meet the needs of our neurophysiological experimentation [21, 81]. Current BCI technology has not demonstrated autonomous control of multiple classes and this constitutes a challenging implementation that necessitates BCI algorithms tailored to the need of the specific task (multi-DoF control). Possible solutions could lie in the source space and connectivity-based BCIs [17]. The group's next steps include developing own, true online, algorithms to be tested for the control of the 8 DoFs of the robotic arms, making use of AI to support classification. Nonetheless, combining a commercial EEG headset with elaborate homemade BCI and real-time computational approaches to the source space is also a challenge to meet.

4. Conclusions

Advances in BCIs have demonstrated remarkable results in the direction of replacing and restoring lost sensorimotor function in human patients. Novel paradigms and recent advances in noninvasive BCI protocols aim at progressively improving past technological and neurophysiological limitations. Neurophysiological changes in the brain network level, induced by SCI, could prove critical in designing and developing robust and durable noninvasive BCIs for motor restoration and rehabilitation. Moreover, successful rehabilitation strategies should take into account user perception, satisfaction, and overall experience, alongside performance. We presented our implementation of BCI-controlled 8-DoF anthropomorphic robotic arms, using noninvasive off-the-shelf BCI technology. Moreover we presented two illustrative experimental applications on healthy individuals and SCI patients. Current, state-of-the-art, BCI technology is unable to control multiple DoFs but semiautonomous AI algorithms and connectivity-based BCIs could provide solutions towards that direction. Individual differences appear to play a role in motor imagery based BCIs and multiple training sessions are always encouraged in order to improve performance in robotic arm control. Functional connectivity holds promise in classifying imagery of multiple classes (multiple different movements) or complex motions, based on imagery modalities. Future development aims at facilitating the integration of BCI and robotic arm system into the operator's perceived body mental image, thus requiring rapid, fluid, accurate, predictable system performance and improved anthropomorphism. Online implementation of connectivity-based classifiers, although currently too computationally demanding, is expected to be soon feasible. High-resolution EEG data and its analysis for functional connectivity from multiple motor imageries are expected to provide insight in brain network adaptive and maladaptive reorganization that occurs after SCI and, subsequently, into promoting or preventing it accordingly [11].

Ethical Approval

This study was conducted in accordance with the Declaration of Helsinki (1964) and its following amendments. The institutional Ethical Committee approved the study.

Consent

All experiments were conducted with the subjects' understanding and written informed consent.

Disclosure

The Cervical Spine Research Society-European Section (CSRS-ES) had no involvement in the study design, writing, or decision for the submission of this paper.

Conflicts of Interest

The authors declare that there are no conflicts of interest regarding the publication of this article.

Acknowledgments

This study was conducted as part of the development of the project CSI:Brainwave, which was partially supported by a "Mario Boni" Research Grant, awarded by Cervical Spine Research Society-European Section (CSRS-ES). The project continues by funding of the Lab of Medical Physics through the LLM care self-funding initiative (http://www.llmcare.gr).

References

[1] L. R. Hochberg, D. Bacher, B. Jarosiewicz et al., "Reach and grasp by people with tetraplegia using a neurally controlled robotic arm," *Nature*, vol. 485, no. 7398, pp. 372–375, 2012.

[2] J. L. Collinger, B. Wodlinger, J. E. Downey et al., "High-performance neuroprosthetic control by an individual with tetraplegia," *The Lancet*, vol. 381, no. 9866, pp. 557–564, 2013.

[3] A. R. C. Donati, S. Shokur, E. Morya et al., "Long-term training with a brain-machine interface-based gait protocol induces partial neurological recovery in paraplegic patients," *Scientific Reports*, vol. 6, no. 1, p. 30383, 2016.

[4] M. Alam, W. Rodrigues, B. N. Pham, and N. V. Thakor, "Brain-machine interface facilitated neurorehabilitation via spinal stimulation after spinal cord injury: Recent progress and future perspectives," *Brain Research*, vol. 1646, pp. 25–33, 2016.

[5] J. J. Daly and J. R. Wolpaw, "Brain-computer interfaces in neurological rehabilitation," *The Lancet Neurology*, vol. 7, no. 11, pp. 1032–1043, 2008.

[6] K. D. Anderson, M. E. Acuff, B. G. Arp et al., "United States (US) multi-center study to assess the validity and reliability of the Spinal Cord Independence Measure (SCIM III)," *Spinal Cord*, vol. 49, no. 8, pp. 880–885, 2011.

[7] R. Nardone, Y. Höller, F. Brigo et al., "Functional brain reorganization after spinal cord injury: Systematic review of animal and human studies," *Brain Research*, vol. 1504, pp. 58–73, 2013.

[8] M. Kaushal, A. Oni-Orisan, G. Chen et al., "Evaluation of whole-brain resting-state functional connectivity in spinal cord injury: a large-scale network analysis using network-based statistic," *Journal of Neurotrauma*, vol. 34, no. 6, pp. 1278–1282, 2017.

[9] F. De Vico Fallani, F. A. Rodrigues, L. Da Fontoura Costa et al., "Multiple pathways analysis of brain functional networks from EEG signals: an application to real data," *Brain Topography*, vol. 23, no. 4, pp. 344–354, 2011.

[10] B. Lee, C. Y. Liu, and M. L. J. Apuzzo, "A primer on brain-machine interfaces, concepts, and technology: A key element in the future of functional neurorestoration," *World Neurosurgery*, vol. 79, no. 3-4, pp. 457–471, 2013.

[11] A. Athanasiou, M. A. Klados, N. Foroglou, K. R. Kavazidi, K. Polyzoidis, and P. D. Bamidis, "Reorganization of brain networks after spinal cord injury: a qualitative synthesis of the literature," in *Front. Hum. Neurosci. Conference Abstract: SAN2016 Meeting*, 2016.

[12] J.-H. Lee, J. Ryu, F. A. Jolesz, Z.-H. Cho, and S.-S. Yoo, "Brain-machine interface via real-time fMRI: Preliminary study on thought-controlled robotic arm," *Neuroscience Letters*, vol. 450, no. 1, pp. 1–6, 2009.

[13] T. Yanagisawa, M. Hirata, Y. Saitoh et al., "Real-time control of a prosthetic hand using human electrocorticography signals: Technical note," *Journal of Neurosurgery*, vol. 114, no. 6, pp. 1715–1722, 2011.

[14] L. F. Nicolas-Alonso and J. Gomez-Gil, "Brain computer interfaces, a review," *Sensors*, vol. 12, no. 2, pp. 1211–1279, 2012.

[15] F. Galán, M. Nuttin, E. Lew et al., "A brain-actuated wheelchair: asynchronous and non-invasive Brain-computer interfaces for continuous control of robots," *Clinical Neurophysiology*, vol. 119, no. 9, pp. 2159–2169, 2008.

[16] J. Meng, S. Zhang, A. Bekyo, J. Olsoe, B. Baxter, and B. He, "Noninvasive electroencephalogram based control of a robotic arm for reach and grasp tasks," *Scientific Reports*, vol. 6, no. 1, article 38565, 2016.

[17] M. Hamedi, S.-H. Salleh, and A. M. Noor, "Electroencephalographic motor imagery brain connectivity analysis for BCI: a review," *Neural Computation*, vol. 28, no. 6, pp. 999–1041, 2016.

[18] H. L. Benz, H. Zhang, A. Bezerianos et al., "Connectivity analysis as a novel approach to motor decoding for prosthesis control," *IEEE Transactions on Neural Systems and Rehabilitation Engineering*, vol. 20, no. 2, pp. 143–152, 2012.

[19] H. Zhang, R. Chavarriaga, and J. D. R. Millán, "Towards Implementation of motor imagery using brain connectivity features," pp. 1–4, 2014.

[20] G. N. Ranky and S. Adamovich, "Analysis of a commercial EEG device for the control of a robot arm," in *Proceedings of the 2010 IEEE 36th Annual Northeast Bioengineering Conference (NEBEC)*, pp. 1-2, New York, NY, USA, 2010.

[21] A. Astaras, N. Moustakas, A. Athanasiou, and A. Gogoussis, "Towards brain-computer interface control of a 6-degree-of-freedom robotic arm using dry EEG electrodes," *Advances in Human-Computer Interaction*, vol. 2013, Article ID 641074, 6 pages, 2013.

[22] L. Xu, H. Zhang, M. Hui et al., "Motor execution and motor imagery: A comparison of functional connectivity patterns based on graph theory," *Neuroscience*, vol. 261, pp. 184–194, 2014.

[23] S. Hétu, M. Grégoire, A. Saimpont et al., "The neural network of motor imagery: an ALE meta-analysis," *Neuroscience and Biobehavioral Reviews*, vol. 37, no. 5, pp. 930–949, 2013.

[24] A. Guillot, C. Collet, V. A. Nguyen, F. Malouin, C. Richards, and J. Doyon, "Brain activity during visual versus kinesthetic imagery: an fMRI study," *Human Brain Mapping*, vol. 30, no. 7, pp. 2157–2172, 2009.

[25] A. Saimpont, M. F. Lafleur, F. Malouin, C. L. Richards, J. Doyon, and P. L. Jackson, "The comparison between motor imagery and verbal rehearsal on the learning of sequential movements," *Frontiers in Human Neuroscience*, vol. 7, 2013.

[26] N. Mizuguchi, M. Nakamura, and K. Kanosue, "Task-dependent engagements of the primary visual cortex during kinesthetic and visual motor imagery," *Neuroscience Letters*, vol. 636, pp. 108–112, 2017.

[27] W. S. Harwin, T. Rahman, and R. A. Foulds, "A Review of design issues in rehabilitation robotics with reference to north american research," *IEEE Transactions on Rehabilitation Engineering*, vol. 3, no. 1, pp. 3–13, 1995.

[28] P. Kubben and N. Pouratian, "An open-source and cross-platform framework for brain computer interface-guided robotic arm control," *Surgical Neurology International*, vol. 3, no. 1, p. 149, 2012.

[29] P. H. Chang and H. S. Park, "Development of a robotic arm for handicapped people: A task-oriented design approach," *Autonomous Robots*, vol. 15, no. 1, pp. 81–92, 2003.

[30] N. Sharkey, "The programmable robot of ancient Greece," 2007, https://www.newscientist.com/article/mg19526111-600-the-programmable-robot-of-ancient-greece/.

[31] F. Nageotte, P. Zanne, C. Doignon, and M. De Mathelin, "Stitching planning in laparoscopic surgery: towards robot-assisted suturing," *International Journal of Robotics Research*, vol. 28, no. 10, pp. 1303–1321, 2009.

[32] Y. Kassahun, B. Yu, A. T. Tibebu et al., "Surgical robotics beyond enhanced dexterity instrumentation: a survey of machine learning techniques and their role in intelligent and autonomous surgical actions," *International Journal of Computer Assisted Radiology and Surgery*, vol. 11, no. 4, pp. 553–568, 2016.

[33] R. Siqueira-Batista, C. R. Souza, P. M. Maia, and S. L. Siqueira, "Robotic surgery: bioethical aspects," *ABCD. Arquivos Brasileiros de Cirurgia Digestiva (São Paulo)*, vol. 29, no. 4, pp. 287–290, 2016.

[34] T. Fong, I. Nourbakhsh, and K. Dautenhahn, "A survey of socially interactive robots," *Robotics and Autonomous Systems*, vol. 42, no. 3-4, pp. 143–166, 2003.

[35] K. Dautenhahn, "Methodology & themes of human-robot interaction: a growing research field," *International Journal of Advanced Robotic Systems*, vol. 4, no. 1, pp. 103–108, 2007.

[36] C. Bartneck, D. Kulić, E. Croft, and S. Zoghbi, "Measurement instruments for the anthropomorphism, animacy, likeability, perceived intelligence, and perceived safety of robots," *International Journal of Social Robotics*, vol. 1, no. 1, pp. 71–81, 2009.

[37] O. Christ and M. Reiner, "Perspectives and possible applications of the rubber hand and virtual hand illusion in non-invasive rehabilitation: Technological improvements and their consequences," *Neuroscience and Biobehavioral Reviews*, vol. 44, pp. 33–44, 2014.

[38] T. Kooijmans, T. Kanda, C. Bartneck, H. Ishiguro, and N. Hagita, "Accelerating robot development through integral analysis of human-robot interaction," *IEEE Transactions on Robotics*, vol. 23, no. 5, pp. 1001–1012, 2007.

[39] N. Moustakas, A. Athanasiou, P. Kartsidis, P. D. Bamidis, and A. Astaras, "Development and user assessment of a body-machine interface for a hybrid-controlled 6-degree of freedom robotic arm (MERCURY)," in *Proceedings of the 13th Mediterranean Conference on Medical and Biological Engineering and Computing 2013, MEDICON 2013*, pp. 65–68, September 2013.

[40] N. Moustakas, P. Kartsidis, A. Athanasiou, A. Astaras, and P. D. Bamidis, "Development of MERCURY version 2.0 robotic arms for rehabilitation applications," in *Proceedings of the 8th ACM International Conference on PErvasive Technologies Related to Assistive Environments (PETRA '15)*, July 2015.

[41] "Brainwave control of a wearable robotic arm for rehabilitation and neurophysiological study in cervical spine injury (CSI:Brainwave)," https://clinicaltrials.gov/ct2/.

[42] N. Moustakas, A. Athanasiou, P. Bamidis, A. Kalfas, A. Astaras, and A. Gogoussis, "A Hybrid body-machine and brain-computer interface for a 6-degree of freedom robotic arm (Mercury)," in *Proceedings of the 5th Panhellenic Conference on Biomedical Technology Conference*, p. 108, 2013.

[43] P. Kartsidis, N. Moustakas, A. Athanasiou, A. Astaras, P. D. Bamidis, and M. Carlo, "Comparative analysis of perceived psychometric characteristics : pilot study of the "Mercury" 6-degree of freedom robotic arm," in *Proceedings of the 7th Electrical and Computer Engineering Student Conference*, pp. 179–181, 2014.

[44] A. Astaras, A. Athanasiou, A. Alexandrou, P. Kartsidis, N. Moustakas, and P. D. Bamidis, "Double-blind greek translation and online implementation of the Godspeed robotics questionnaire," in *Proceedings of the 6th Panhellenic Conference on Biomedical Technology Conference*, p. 34, 2015.

[45] S. Perdikis, R. Leeb, and J. D. R. Millan, "Subject-oriented training for motor imagery brain-computer interfaces," in *Proceedings of the 2014 36th Annual International Conference of the IEEE Engineering in Medicine and Biology Society, EMBC 2014*, pp. 1259–1262, August 2014.

[46] E. I. Konstantinidis and P. D. Bamidis, "Density based clustering on indoor kinect location tracking: A new way to exploit active and healthy aging living lab datasets," in *Proceedings of the 2015 IEEE 15th International Conference on Bioinformatics and Bioengineering (BIBE)*, pp. 1–6, November 2015.

[47] E. I. Konstantinidis, A. Billis, C. Bratsas, A. Siountas, and P. D. Bamidis, "Thessaloniki active and healthy ageing living lab: The roadmap from a specific project to a living lab towards openness," in *Proceedings of the 9th ACM International Conference on PErvasive Technologies Related to Assistive Environments (PETRA '2016)*, pp. 1–4, July 2016.

[48] E. I. Konstantinidis, P. E. Antoniou, G. Bamparopoulos, and P. D. Bamidis, "A lightweight framework for transparent cross platform communication of controller data in ambient assisted living environments," *Information Sciences*, vol. 300, no. 1, pp. 124–139, 2015.

[49] R. Oostenveld and P. Praamstra, "The five percent electrode system for high-resolution EEG and ERP measurements," *Clinical Neurophysiology*, vol. 112, no. 4, pp. 713–719, 2001.

[50] G. Arfaras, A. Athanasiou, N. Pandria et al., "Visual versus kinesthetic motor imagery for BCI control of robotic arms (Mercury 2.0)," in *Proceedings of the 30th IEEE International Symposium on Computer-Based Medical Systems*, vol. 2.0, pp. 440–445, 2017.

[51] S. S. Shapiro and M. B. Wilk, "An analysis of variance test for normality: Complete samples," *Biometrika*, vol. 52, no. 3-4, pp. 591–611, 1965.

[52] D. Öztuna, A. H. Elhan, and E. Tüccar, "Investigation of four different normality tests in terms of type 1 error rate and power under different distributions," *Turkish Journal of Medical Sciences*, vol. 36, no. 3, pp. 171–176, 2006.

[53] A. Athanasiou, G. Arfaras, I. Xygonakis et al., "Commercial BCI Control and functional brain networks in spinal cord injury: a proof-of-concept," in *Proceedings of the 30th IEEE International Symposium on Computer-Based Medical Systems*, pp. 262–267, 2017.

[54] S. C. Kirshblum, S. P. Burns, F. Biering-Sorensen et al., "International standards for neurological classification of spinal cord injury (revised 2011)," *Journal of Spinal Cord Medicine*, vol. 34, no. 6, pp. 535–546, 2011.

[55] M. Itzkovich, I. Gelernter, F. Biering-Sorensen et al., "The Spinal Cord Independence Measure (SCIM) version III: Reliability and validity in a multi-center international study," *Disability and Rehabilitation*, vol. 29, no. 24, pp. 1926–1933, 2007.

[56] A. Athanasiou, A. Alexandrou, E. Paraskevopoulos, N. Foroglou, A. Prassas, and P. D. Bamidis, "Towards a Greek adaptation of the Spinal Cord Independence Measure (SCIM)," in *Proceedings of the 15th European Congress of Neurosurgery (EANS 14)*, pp. 181–184, 2015.

[57] D. F. Marks, "Visual imagery differences in the recall of pictures," *British Journal of Psychology*, vol. 64, no. 1, pp. 17–24, 1973.

[58] A. T. Beck, R. A. Steer, and M. G. Garbin, "Psychometric properties of the Beck Depression Inventory: twenty-five years of evaluation," *Clinical Psychology Review*, vol. 8, no. 1, pp. 77–100, 1988.

[59] M. Giannakou, P. Roussi, M.-E. Kosmides, G. Kiosseoglou, A. Adamopoulou, and G. Garyfallos, "Adaptation of the beck depression inventory-II to greek population," *Hellenic Journal of Psychology*, vol. 10, no. 2, pp. 120–146, 2013.

[60] W. Petersen, "Society and the Adolescent Self-Image. Morris Rosenberg. Princeton University Press, Princeton, N.J., 1965. xii + 326 pp. $6.50," *Science*, vol. 148, no. 3671, p. 804, 1965.

[61] C. Galanou, M. Galanakis, E. Alexopoulos, and C. Darviri, "Rosenberg Self-Esteem Scale Greek Validation on Student Sample," *Psychology*, vol. 05, no. 08, pp. 819–827, 2014.

[62] K. A. Ludwig, R. M. Miriani, N. B. Langhals, M. D. Joseph, D. J. Anderson, and D. R. Kipke, "Using a common average reference to improve cortical neuron recordings from microelectrode arrays," *Journal of Neurophysiology*, vol. 101, no. 3, pp. 1679–1689, 2009.

[63] F. Tadel, S. Baillet, J. C. Mosher, D. Pantazis, and R. M. Leahy, "Brainstorm: a user-friendly application for MEG/EEG analysis," *Computational Intelligence and Neuroscience*, vol. 2011, Article ID 879716, 13 pages, 2011.

[64] H. Hallez, B. Vanrumste, R. Grech et al., "Review on solving the forward problem in EEG source analysis," *Journal of NeuroEngineering and Rehabilitation*, vol. 4, no. 1, p. 46, 2007.

[65] R. Grech, T. Cassar, J. Muscat et al., "Review on solving the inverse problem in EEG source analysis," *Journal of NeuroEngineering and Rehabilitation*, vol. 5, no. 1, p. 25, 2008.

[66] C. J. Holmes, R. Hoge, L. Collins, R. Woods, A. W. Toga, and A. C. Evans, "Enhancement of MR images using registration for signal averaging," *Journal of Computer Assisted Tomography*, vol. 22, no. 2, pp. 324–333, 1998.

[67] A. Evans, D. Collins, S. Mills, E. Brown, R. Kelly, and T. Peters, "3D statistical neuroanatomical models from 305 MRI volumes," in *Proceedings of the 1993 IEEE Conference Record Nuclear Science Symposium and Medical Imaging Conference*, pp. 1813–1817, San Francisco, CA, USA, 1993.

[68] A. Gramfort, T. Papadopoulo, E. Olivi, and M. Clerc, "OpenMEEG: Opensource software for quasistatic bioelectromagnetics," *BioMedical Engineering Online*, vol. 9, no. 1, p. 45, 2010.

[69] R. D. Pascual-Marqui, "Standardized low-resolution brain electromagnetic tomography (sLORETA): technical details," *Methods and Findings in Experimental and Clinical Pharmacology*, vol. 24, Supplement D, pp. 5–12, 2002.

[70] B. J. Edelman, B. Baxter, and B. He, "EEG source imaging enhances the decoding of complex right-hand motor imagery

tasks," *IEEE Transactions on Biomedical Engineering*, vol. 63, no. 1, pp. 4–14, 2016.

[71] A. Athanasiou, M. A. Klados, C. Styliadis, N. Foroglou, K. Polyzoidis, and P. D. Bamidis, "Investigating the role of alpha and beta rhythms in functional motor networks," *Neuroscience*, 2016.

[72] D. Chicharro, "On the spectral formulation of Granger causality," *Biological Cybernetics*, vol. 105, no. 5-6, pp. 331–347, 2011.

[73] "Greek version of the Godspeed Questionnaire Series Available," http://www.bartneck.de/2013/04/17/greek-version-of-the-godspeed-questionnaire-series-available.

[74] M. Destephe, M. Brandao, T. Kishi, M. Zecca, K. Hashimoto, and A. Takanishi, "Walking in the uncanny valley: Importance of the attractiveness on the acceptance of a robot as a working partner," *Frontiers in Psychology*, vol. 6, article no. 204, 2015.

[75] A. Weiss and C. Bartneck, "Meta analysis of the usage of the Godspeed Questionnaire Series," in *Proceedings of the 2015 24th IEEE International Symposium on Robot and Human Interactive Communication (RO-MAN)*, pp. 381–388, September 2015.

[76] M. Giuliani, R. P. A. Petrick, M. E. Foster et al., "Comparing task-based and socially intelligent behaviour in a robot bartender," in *Proceedings of the 2013 15th ACM International Conference on Multimodal Interaction (ICMI '13)*, pp. 263–270, December 2013.

[77] R. V. Dawis, "Scale Construction," *Journal of Counseling Psychology*, vol. 34, no. 4, pp. 481–489, 1987.

[78] H. N. J. Boone and D. A. Boone, "Analyzing Likert data," *Journal of Extension*, vol. 50, no. 2, p. 30, 2012.

[79] S. P. Van Den Broek, F. Reinders, M. Donderwinkel, and M. J. Peters, "Volume conduction effects in EEG and MEG," *Electroencephalography and Clinical Neurophysiology*, vol. 106, no. 6, pp. 522–534, 1998.

[80] S. S. M. Salehi, M. Moghadamfalahi, F. Quivira, A. Piers, H. Nezamfar, and D. Erdogmus, "Decoding Complex Imagery Hand Gestures," 2017, https://arxiv.org/abs/1703.02929.

[81] M. Spüler, "A high-speed brain-computer interface (BCI) using dry EEG electrodes," *PLOS One*, 2017.

Hindawi
BioMed Research International
Volume 2017, Article ID 1695290, 11 pages
https://doi.org/10.1155/2017/1695290

Review Article

Brain-Computer Interface for Clinical Purposes: Cognitive Assessment and Rehabilitation

Laura Carelli,[1] Federica Solca,[1] Andrea Faini,[2] Paolo Meriggi,[3] Davide Sangalli,[1] Pietro Cipresso,[4,5] Giuseppe Riva,[4,5] Nicola Ticozzi,[1,6] Andrea Ciammola,[1] Vincenzo Silani,[1,6] and Barbara Poletti[1]

[1]*Department of Neurology and Laboratory of Neuroscience, IRCCS Istituto Auxologico Italiano, P.le Brescia 20, 20149 Milan, Italy*
[2]*Department of Cardiovascular, Neural and Metabolic Sciences, IRCCS Istituto Auxologico Italiano, P.le Brescia 20, 20149 Milan, Italy*
[3]*ICT & Biomedical Technology Integration Unit, Centre for Innovation and Technology Transfer (CITT), Fondazione Don Carlo Gnocchi Onlus, Via Capecelatro 66, 20148 Milan, Italy*
[4]*Applied Technology for Neuro-Psychology Lab, IRCCS Istituto Auxologico Italiano, P.le Brescia 20, 20149 Milan, Italy*
[5]*Department of Psychology, Catholic University of Milan, Largo A. Gemelli 1, 20123 Milan, Italy*
[6]*Department of Pathophysiology and Transplantation, "Dino Ferrari" Center, Università degli Studi di Milano, Via Francesco Sforza 35, 20122 Milan, Italy*

Correspondence should be addressed to Barbara Poletti; b.poletti@auxologico.it

Received 30 March 2017; Revised 13 June 2017; Accepted 3 July 2017; Published 23 August 2017

Academic Editor: Plácido R. Pinheiro

Alongside the best-known applications of brain-computer interface (BCI) technology for restoring communication abilities and controlling external devices, we present the state of the art of BCI use for cognitive assessment and training purposes. We first describe some preliminary attempts to develop verbal-motor free BCI-based tests for evaluating specific or multiple cognitive domains in patients with Amyotrophic Lateral Sclerosis, disorders of consciousness, and other neurological diseases. Then we present the more heterogeneous and advanced field of BCI-based cognitive training, which has its roots in the context of neurofeedback therapy and addresses patients with neurological developmental disorders (autism spectrum disorder and attention-deficit/hyperactivity disorder), stroke patients, and elderly subjects. We discuss some advantages of BCI for both assessment and training purposes, the former concerning the possibility of longitudinally and reliably evaluating cognitive functions in patients with severe motor disabilities, the latter regarding the possibility of enhancing patients' motivation and engagement for improving neural plasticity. Finally, we discuss some present and future challenges in the BCI use for the described purposes.

1. Introduction

BCIs have been studied with the primary motivation of providing assistive technologies for people with severe motor disabilities, particularly locked-in syndrome (LIS) caused by neurodegenerative disease such as Amyotrophic Lateral Sclerosis (ALS) or by stroke [1]. Such approach involves the use of suitable cortical signals as input to control external devices or for Augmentative and Alternative Communication purposes in patients suffering from central nervous system injury. BCI has been studied for more than 25 years and has been extensively validated, even if with still heterogeneous results according to both the method employed and the populations involved [2, 3]. A review of BCI studies is not within the objective of the present work [4].

A newly emerging field of research concerns the use of BCIs to enhance motor and cognitive recovery within neurorehabilitation settings. In fact, most of common rehabilitation tools require a minimal level of motor control to perform the therapeutic tasks; therefore, patients with severe motor deficits are not allowed to accomplish traditional rehabilitation training. Some recent reviews have presented and discussed main advances in the use of BCIs for rehabilitation purposes [5–7]. A further work has discussed the current status of BCI as a rehabilitation strategy in stroke patients [8]. In addition to the use of BCI to restore motor function

or provide feedback to patients (i.e., during motor imagery), the authors underlie further advantages of brain activation monitoring during rehabilitation, in particular, the possibility of monitoring the global level of attention concerning the task and the level of interhemispheric balance.

Within the neurorehabilitation setting, the assessment and training of cognitive impairments represent a more innovative and less explored area. The evaluation of cognitive abilities in patients at advanced stages of paralysis represents a challenge, since standard assessment tools for both verbal and nonverbal cognitive abilities typically involve a motor response. In ALS, evidence suggests the need for some task modifications in order to make the standard neuropsychological assessment suitable for patients with verbal and motor impairment [9]. Also the *Edinburgh Cognitive and Behavioural ALS Screen* (ECAS), recently designed by Abrahams and colleagues [10] for ALS patients, cannot be performed in moderate-severe stages of the disease. Besides, even tests relying on some form of rudimentary motor function such as blinking, nodding, or pointing [11] are not administrable to totally locked-in patients where even the presence of minimal motor functions could be prevented.

Recently, some attempts have been made in order to obtain verbal-motor free indicators of executive functions changes in ALS. In particular, event-related potentials (ERP) have been employed to assess cognitive dysfunctions with minimal motor demands [12–14]. Such approach, even if valuable, provides quantitative and qualitative data not comparable with scores obtained from standard cognitive testing, therefore not allowing a reliable and longitudinal evaluation of neuropsychological functions.

The evaluation of cognitive capacities in patients with severe motor disabilities has also relevant implication for BCI systems usability aspects. Among the physiological and psychological factors that influence or affect BCI use, several studies have showed an effect of both general mental load and more specific cognitive functions on BCI performance. For example, the P300 ERP signals, employed in the frequently adopted P300 BCI systems, depend on attention and working memory processes; in such approach, reduced level of attention or higher levels of working memory load are associated with lower amplitudes and prolonged latencies [15]. Recent studies confirmed the role of working memory, together with general intelligence [16] and attention [17], on P300 BCI performance. Some approaches have attempted to manage such aspects by employing different interfaces [18] or stimulation modes [19], in order to reduce mental load. In addition to the need for technical adaptations, the described findings suggest the potential benefit of working memory training to improve BCI usability and performance.

The use of BCIs for cognitive training is another emerging field of study within neurorehabilitation settings and could improve both patients' clinical conditions and BCIs' usability. In particular, the possibility of enhancing neural plasticity by providing real-time feedbacks in an engaging setting could improve the treatment efficacy and transferability to real-life contexts.

We present the current state of art about BCI applications addressing cognitive aspects, with regard to approaches targeting both assessment and rehabilitation of cognitive functions. As below described, such approaches involve patients with severe motor deficits, in order to overcome verbal-motor limitations, together with other clinical populations without physical disability, according to the advantages provided by the use of BCI with respect to traditional cognitive training methods.

2. Material and Methods

Between January and February 2017 we performed a search on the PubMed, Web of Science, and Scopus databases. We searched the terms "BCI" or "brain-computer interface" or "brain machine interface" in combination with the following terms: "neurofeedback," "cognitive," "rehabilitation," "training," "assessment," and "neuropsychological." Other definitions of BCI (i.e., Mind-Machine Interface (MMI)) were included; however no relevant results were obtained, according to the topic of the present review. We searched the reference list of retrieved papers to identify additional relevant articles. Only studies in English were considered for the present systematic review. Other reviews of literature dealing with the topic of our work have been considered within this work. A total number of 1701 items have been found with PubMed, 2950 items with Web of Science, and 3977 items with Scopus.

Studies where NF was described without referring to a BCI system were excluded. Moreover, studies were cognitive tasks/abilities were included in the BCI protocols with aims other than assessment or rehabilitation of cognitive abilities (i.e., monitoring of cognitive state during motor rehabilitation, means to perform motor tasks; study of brain functions not aimed at clinical purposes) were not considered.

The systematic search resulted in 9 records for cognitive assessment and 15 records for cognitive training, consisting of experimental studies that were included in Tables 1 and 2. Studies presenting design or development of BCI-based protocols without reporting experimental data on healthy controls or clinical populations were considered within the manuscript, but not reported in the Tables. Other results concerning NF and BCI studies or reviews have been considered and reported within introduction and discussion for enhancing and supporting considerations about the described results. Actually, to the best of our knowledge, no other review concerning BCI use for cognitive assessment or rehabilitation is available.

3. Results and Discussion

3.1. Cognitive Assessment through BCI-Based Systems. The application of BCI systems in order to develop new neuropsychological assessment tools mainly employed EEG-based BCIs (see Table 1). These types of BCI are included in noninvasive BCIs; that is, they do not require surgical implantation to acquire signals; surface EEG is the most widely used noninvasive technique for BCI studies in neurological patients [20]. The main EEG-based paradigms detected and used are sensorimotor rhythms (SMRs), slow cortical potentials

Table 1: BCI applications to cognitive assessment.

Study (year)	Signals/EEG-based paradigms	Sample	Measure (test)	Tested Variables	Patients' training required (yes/no)
Iversen & coll. (2008a)	SCPs	2 late-stage ALS patients	Delayed matching-to-sample task	Accuracy (% of correct responses)	Yes
Iversen & coll. (2008b)	SCPs	1 late-stage ALS patient	Conditional-associative learning task	Accuracy (% of correct responses)	Yes
Perego & coll. (2011)	SSVEP	19 healthy subjects	RCPM, CFIT	Total scores and total execution time for tests; total moves and bit-rate for BCI performance	Yes
Perego & coll. (2011)	SSVEP	26 patients with different neurological diseases (cerebral palsy, dystrophies and paresis)	RCPM	Total scores and total execution time for tests; bit-rate for BCI performance	Yes
Cipresso & coll. (2012)	P300 ERP	8 healthy subjects	Phonemic and Semantic VF test (modified version); psychological and usability questionnaire	BCI classification accuracy; execution time and errors at VF test; questionnaires' scores	No
Cipresso & coll. (2013)	P300 ERP	8 healthy subjects and one ALS patient	Phonemic and Semantic Verbal Fluency test (modified version), psychological and usability questionnaire	BCI classification accuracy; execution time and errors at VF test; questionnaires' scores	No
Li & coll. (2015)	SSVEP + P300 ERP	11 brain-injured patients (6 VS, 3 MCS, 2 EMCS)	Number recognition, number comparison, mental calculation	Accuracy rate and number of trials for each test	No
Westergren & coll. (2016)	SSVEP	11 healthy subjects	Four cognitive tests resembling WAIS test battery	BCI classification accuracy, ITR and tests' score	No
Poletti & coll. (2016)	P300 ERP	15 moderate-stage ALS patients and 15 healthy controls	Token Test, RCPM, d2 test, MCST	Tests' total scores and execution times	No

SCPs: slow cortical potentials; SSVEP: steady state visually evoked potentials; ERP: event-related potentials; ALS: amyotrophic lateral sclerosis; VS: vegetative state; MCS: minimally conscious state; EMCS: emerged from MCS; RCPM: Raven's colored progressive matrices test; CFIT: Culture Fair Intelligence Test; VF: Verbal Fluency test; WAIS: Wechsler adult intelligence scale; MCST: modified card sorting test; ITR: information transfer rate.

Table 2: BCI applications to cognitive rehabilitation.

Study (year)	Signals/paradigms	Sample	Method	Outcome measures
Lim & coll. (2010)	Frontal (Fp1 and Fp2) and parietal (Pz) EEG signals, covering theta, alpha, beta 1, and beta 2 EEG waves	20 ADHD children	Mathematics and English comprehension questions, with the BCI system monitoring attention level	ADHD Rating Scale-IV
Lim & coll. (2012)	Frontal EEG signals (Fp1 and Fp2)	20 ADHD children	Colour Stroop Task during Calibration. Training game (Cogoland). Mathematics and English worksheet	ADHD Rating Scale-IV
Lee & coll. (2013)	Frontal EEG signals (Fp1 and Fp2)	31 healthy elderly	Colour Stroop Task during Calibration. BCI system based on a card-pairing memory game	RBANS. Usability and acceptability questionnaire
Toppi & coll. (2014)	SMRs	2 stroke patients	NF training based on 10 sessions on SMRs	EEG data while performing the Sternberg memory task. Behavioral performance at the Sternberg task. Scores at RAVLT and CBTT
Gomez-Pilar & coll. (2014)	SMR-EEG	40 healthy elderly	NF training consists in imagery motor exercises combined with memory and logical relation tasks	Luria–AND test
Burke & coll. (2015)	iEEG theta and alpha oscillations	14 neurosurgical patients with medication-resistant epilepsy	Individual prestimulus electrode fluctuations used to modulate memory performance	BCI and standard free recall episodic memory task
Lee & coll. (2015)	Frontal EEG signals (Fp1 and Fp2)	39 healthy Chinese-speaking elderly	Colour Stroop Task during Calibration. BCI system based on a card-pairing memory game	Repeatable Battery for the Assessment of Neuropsychological Status (RBANS). Usability and acceptability questionnaire
Rohani & Puthusserypady (2015)	P300 ERP	6 healthy young participants (24–32 years)	Two oddball attention tasks, targeting visual attention and discrimination, performed within a 3D Virtual Classroom	Average error rate in detecting P300 by the classifier
Salisbury & coll. (2015)	EEG (not further specified)	A 25-year-old man with spinal cord injury	Training session with cube rotation and manipulation paradigm presented on a laptop computer, followed by BCI trial (Emotive EEG gaming system)	Screening measures related to cognition, psychological disposition and pain
Salisbury & coll. (2016)	EEG (not further specified)	25 participants (18–64 years) with traumatic or nontraumatic spinal cord injury	Training session with cube rotation and manipulation paradigm presented on a laptop computer, followed by BCI trial (Emotive EEG gaming system)	Screening measures related to cognition, psychological disposition and pain

Table 2: Continued.

Study (year)	Signals/paradigms	Sample	Method	Outcome measures
Gomez-Pilar & coll. (2016)	SMR-EEG	63 healthy elderly	NF training designed for training motor imagery that implies ERS/ERD of alpha and beta frequency bands in the EEG	Luria-AND test
Kim & Lee (2016)	SMR and mid-beta waves of Fp1 and Fp2	20 children with cerebral palsy	BCI-FES group versus FES control group	Sensorimotor rhythms (SMR) and middle beta waves (M-beta)
Kleih & coll. (2016)	P300 ERP	5 stroke patients with aphasia	Visual P300 speller paradigm. TAP to predict spelling success	BCI usability (visual analog scale) and spelling performance (accuracy)
Rana & coll. (2016)	fMRI bold response	8 healthy adults (age > 61 years old)	rtfMRI approach to train participants to upregulate anterior insula during a facial emotion recognition task	Average percentage change in the BOLD signal and DCCS scores
Musso & coll. (2017)	Auditory ERP	20 healthy subjects and 1 aphasic stroke patient	Word ERP responses to 6 bisyllabic words recorded with an auditory BCI	Average target and nontarget ERP responses

EEG: electroencephalogram; SMRs: sensory motor rhythm; iEEG: intracranial EEG; ERP: event-related potentials; SMR: sensorimotor rhythms; FES: functional electrical stimulation; fMRI: functional magnetic resonance imaging; ADHD: attention-deficit/hyperactivity disorder; ASD: autism spectrum disorder; RBANS: repeatable battery for the assessment of neuropsychological status; TAP: attention performance test; Luria–AND test: Luria adult neuropsychological diagnosis (AND) test; DDCS: dimensional change card sort; rtfMRI: real-time fMRI; RAVLT: Rey auditory verbal learning test; CBTT: Corsi block tapping test; NF: neurofeedback.

(SCPs), event-related potentials (ERPs), and visually evoked potentials (VEPs).

Iversen et al. [21, 22] aimed at assessing some cognitive functions in completely paralyzed ALS patients by developing a SCPs EEG-BCI. In a first study [21], training was applied to two severely paralyzed ALS patients, during which they could learn to control certain components of their EEG in order to direct the movement of a visual symbol on a monitor. Next, a series of two-choice cognitive task was administered, such as odd/even number and larger/smaller numbers discrimination. Performance was also assessed using a matching-to-sample paradigm, which was used to examine the ability to discriminate numbers, letters, colors, and to perform simple calculations. In a successive study, Iversen et al. [22] employed the same SCP-EEG control in order to administrate a conditional-associative learning task to a late-stage ALS patient, testing the ability to learn arbitrary associations among visual stimuli. In both studies, a good level of accuracy was observed in detecting patients' performances, according to a within subjects experimental design. Patients were also able to understand the verbal instructions and to respond accordingly in the successive tasks. However, such method requires an extensive pretraining in order to learn to control EEG, which can take some weeks; moreover, it cannot be used for tasks based on recall or where a choice must be made among more than two stimuli.

Perego and coll. [23] applied a steady state visually evoked potentials (SSVEP) based BCI system to develop a psychometric assessment based on a widely used clinical test (Raven Colored Progressive Matrices (RCPM)). The protocol has been validated on 19 healthy subjects and compared to a paper-based administration: results showed congruent performances obtained with the two methods. A successive study by the authors [24] tested the SSVEP BCI cognitive protocol on a sample of patients with physical disabilities due to different neurological disease and confirmed its reliability in a clinical population; however, 11 out of 26 participants were excluded from the protocol according to involuntary movements and poor cooperation or because they did not elicit SSVEP response. Westergren et al. [25] applied a SSVEP-based BCI to develop four cognitive tests based on the Wechsler Adult Intelligence Scale (WAIS) matrix tests; they administered the short battery to a group of 11 healthy subjects, obtaining findings that supported the accuracy and usability of the developed system. Even if promising, this protocol should be validated on a clinical population.

Overall, the described approaches present some limitations, such as important rearrangement of the original cognitive tests, possibly producing biased results and extensive pretraining; furthermore, the adaptation of single cognitive tests does not match the clinical need for a comprehensive neuropsychological evaluation.

Differently from other BCIs approaches, P300-based ones do not require learning of self-regulation of the brain response and feedback. A possible reduction in training time represents an important chance in order to extend the use of Augmented and Alternative Communication (AAC) to cognitive assessment purposes [26]. On the other side, the use of P300 requires, as a precondition, an intact visual system, at least for the visual modality, which has been proved

to be more reliable than the auditory one and preserved ability to pay attention; this may represent a problem in some patients. Recently, we presented a new verbal-motor free neuropsychological battery, by adapting some traditional neuropsychological tests (i.e., Token Test, Modified Card Sorting Test (MCST), Raven Colored Progressive Matrices (RCPM), and d2 Test) to the P300-BCI administration, according to a reasonable adherence to the original validated tests [27]. Usability components, relationship to clinical and psychological variables, and convergent validity of the developed battery in a sample of ALS patients and healthy controls were investigated. In ALS patients, the proposed P300-BCI-based assessment showed a high rate of calibration accuracy, together with satisfactory levels of usability and sensitivity, independently from clinical aspects, such as disease progression (ALFRS-R) and disease onset, or psychological factors such as anxiety and depression. Even if the described protocol satisfies the need for a comprehensive evaluation of cognitive abilities, some issues arise from performing several tests with BCI; in particular, prolonged time for administration and cognitive effort could involve fatigue effects and reduce the reliability of the assessment. This study was included within an extended project, evaluating P300-BCI use for neuropsychological assessment with a particular attention to usability, pleasantness, fatigue, and emotional aspects [28, 29]. Within such project, preliminary attempts to adapt another widely used traditional neuropsychological test, that is, Verbal Fluency, have been performed as a proof of concept which needs further investigations.

Recently, an hybrid brain-computer interface combining P300 and SSVEP has been used to detect number processing and mental calculation in patients with disorder of consciousness (DOC) [30]. Results were obtained on eleven patients: five of them achieved accuracy rates that were significantly higher than the chance level and demonstrated preserved ability to follow commands, in addition to number processing and calculation abilities. However, patients were easily fatigued, thus leading to insufficient training data, and their level of object-selective attention was much lower than for healthy subjects. Moreover, gaze-dependent BCIs can provide unreliable data in DOC patients, since they often lose their ability to fixate their gaze; therefore, visual abilities should be accurately evaluated when employing gaze-dependent BCIs that should eventually be replaced by gaze-independent systems.

Then, the field of research about the development of cognitive tasks based on BCI for patients with motor disabilities is still at dawn and represents a promising area to be developed.

3.2. Cognitive Training in Neurological Patients and Healthy Subjects by Means of BCI. BCI has been used to enhance attention and other cognitive abilities (see Table 2), based on the principle of neurofeedback (NF) therapy (T). In particular, a largely employed NFT is that based on surface EEG, as it is relatively cheap, usable, and portable. EEG-NFT involves that neural signals can be measured and used to improve neural functions: patients observe a suitable graphical representation of their actual brain activity, usually processed through a computer, and learn to self-regulate this activity in order to bring it to a desired state. This approach has been used for treating several conditions, including both neurological and psychological disorders, such as attention-deficit hyperactivity disorder (ADHD), anxiety, epilepsy, and addictive disorders [31]. Moreover, NF has also been applied for cognitive enhancement [32–34]. Typically, tasks involved in NFT are repetitive and standardized and respond to the need to indicate to participants when they have reached the required brainwave pattern. Some of results obtained employing such approach with ADHD patients are controversial; for example, a recent systematic review and an experimental study [35] concluded that literature fails to support any benefit of NF on neurocognitive functioning in ADHD, possibly due to study limitations. An extensive review on NF approaches is beyond the scope of this article.

Recently, EEG-BCI systems have been employed in order to improve cognitive functions in patients with ADHD. Munoz and colleagues [36] designed and presented a BCI-based videogame for training sustained attention in ADHD patients, to be implemented by means of low-cost BCI systems. However, such system has not been validated in a clinical population. Lim and colleagues [37, 38] developed a series of training games, where users' attentional levels measured by EEG signals can be used to perform exercise. Such approach proved to be useful to enhance attention abilities in children with ADHD, by improving parent-rated inattentive scores on the ADHD Rating Scale.

Lee and colleagues then modified their training program in a successive study, introducing a new game with a memory training component addressing elderly population [39]. The BCI training was showed to improve both attention and visuospatial and memory components; moreover, usability and acceptability rates were satisfying for the target population. The same authors then replicated the study on a sample of healthy, predominantly Chinese-speaking elderly, in order to determine the generalizability of the developed system and training task to a different linguistic population [40]. They confirmed the BCI training potential in improving cognition in both English- and Chinese-speaking elderly, showing its usability and acceptability in the latter population.

Another application of BCI for cognitive enhancement in the elderly has been developed by Gomez-Pilar and colleagues [41, 42]. The authors developed a motor-imagery-based BCI system to perform NF in healthy elderly, which was realized by means of five different tasks of increasing difficulty levels. In such tasks, subjects were trained in learning and practice motor imagery and performing logical and memory exercises. Feedback consisted of an item moving on the screen, controlled by motor imagery tasks. Results from cognitive tests and EEG changes showed an improvement after five sessions. In particular, cognitive changes concerned visuospatial, language, memory, and conceptual domains.

Such studies are of particular interest, because only few application of NFT previously addressed cognitive enhancement in the elderly [31, 43, 44].

Pineda et al. [45] also hypothesized that BCI-based NF using specific EEG frequency bands should induce neuroplastic changes of the mirror neuron system in autism

spectrum disorder (ASD). According to these suggestions, Friedrich and colleagues [46] developed a BCI game application for combined NF and biofeedback treatment of children with ASD. The proposed system requires children to modulate their brain activity and peripheral physiological activation in social games, with feedback consisting in emotional imitation behavior within social interactions. Such approach entails the value of maintaining player interest and realizing ecological situations in order to maximize learning and transferability to real-life contexts.

Kim & Lee [47] employed a BCI-based functional electrical stimulation (FES) training on children affected by spastic cerebral palsy, with EEG patterns during concentration used to trigger FES: FES was applied as patients concentrated on finger extension, wrist extension, wrist abduction, and wrist circumduction while holding a wrist bar. SMRs and middle beta waves (M-beta) were recorded prior and after the training as outcome measures. Results showed an increase of such indexes that are associated with logical thinking, problem solving, and attentiveness to external stimuli, suggesting an effect of the performed training also on nonmotor functions. Salisbury and colleagues [48] presented a single-case feasibility study on a patient with spinal cord injury (SCI), where EEG-BCI was employed for reducing pain and improving nonmotor functions such as mood and cognition, as part of inpatient rehabilitation treatment. Even if no data are presented about the described therapeutic goals, the study supported the feasibility and tolerability of this approach in the patient. A successive study on an extended sample of SCI patients [49] did not show any effect of the BCI training on measures related to cognition, psychological disposition, and pain.

Another application of BCI to recovery cognitive functions regards aphasia rehabilitation in stroke patients [50, 51]. Kleih and colleagues [50] supported the feasibility of a P300-BCI speller communication system with aphasic patients, after implementation of individualized adaptations and some training. According to the authors, further application of the developed approach could involve improvement of neural plasticity by activating language circuits, promoting aphasia recovery. Musso and colleagues [51] preliminary investigated the presence of neuronal markers of auditory attention and acoustic processing as prerequisite for auditory BCI application in a stroke patient and concluded that BCI training could be feasible for him. Such promising findings should be supported by further investigations on the target sample, but could be preliminary to BCI applications for rehabilitation of speech production deficits in aphasic patients. Additionally, also memory functions have been addressed in stroke patients with BCI-based NF interventions [52]. The authors employed a set of relevant neurophysiological indexes that revealed sensitive to training intervention outcomes, therefore useful to be integrated to standard neuropsychological assessment results to evaluate and quantify the changes induced by the BCI-based cognitive rehabilitative intervention.

Burke and colleagues [53] used intracranial EEG (iEEG) in neurosurgical patients to detect theta and alpha oscillations which correlate with optimal memory encoding, thus using them to trigger item presentation in a free recall task. This is the first application of iEEG in a BCI to enhance memory functions.

Besides EEG, NF studies based on functional magnetic resonance (MRI) have been shown to produce behavioral changes in schizophrenia and in substance addiction disorders. Several studies investigated the effect of volitional brain regulation of specific areas, such as amygdala and anterior cingulate, on cognition and behavior. Based on this findings, Rana and colleagues [54] investigated the feasibility of applying real-time feedback MRI NF in aging research. In a sample of healthy elderly, they showed that volitionally control of anterior insula during a facial emotion recognition task is associated with increased cognitive flexibility, supporting the efficacy of this approach for cognitive enhancement and training.

Another interesting field of work concerns the use of virtual reality as a therapeutic intervention for neurorehabilitation and its integration with BCI systems [55]. An interesting application of such model is that of Rohani and Puthusserypady [56], who realized a P300 based VR (virtual classroom) system for training attention abilities in ADHD patients. This study is also the first attempt to develop a BCI system for attention training that is based on P300 potential, according to its direct link to attentional and voluntary cognitive activity. The developed system, tested in healthy participants, revealed to be promising, as supported by usability and motivational aspects.

Overall, the presented studies involve increasing levels of complexity and sophistication with respect to traditional NF models: the integration of multidimensional indexes (i.e., neuropsychological, neurophysiological, and behavioral), the realization of engaging and realistic settings for training of cognitive functions, and the use of innovative BCI systems.

4. Conclusions

We presented an overview of studies employing different BCI systems with the aim of realizing cognitive assessment or rehabilitation protocols. Main measures and procedures adopted for the described purposes are summarized as follows. With regard to cognitive assessment, the studies presented mainly employed ad hoc designed cognitive tasks, realized according to the characteristics and restrictions of the BCI paradigm adopted [21, 22, 25, 30]. Cipresso et al. [28, 29] used a widely known cognitive test, that is, Verbal Fluency, even if with relevant modifications in administration and scoring methods with respect to the traditional "paper and pencil" version, in order to adapt to the BCI system. Differently, a few authors [23, 24, 27] realized a BCI-based version of a validated and standardized neuropsychological measure of fluid intelligence, that is, the RCPM, with particular attention at maintaining a reasonable adherence to the original test. Both authors highlighted convergent validity of the adapted test with other related paper and pencil measures. Poletti et al. [27] also realized adaptations of other traditional validated neuropsychological tests, by extending the purposes toward the realization of a verbal-motor free

comprehensive neuropsychological battery similar to that employed in clinical settings.

According to cognitive rehabilitation, the methods seem more heterogeneous, according both to the different clinical populations involved (i.e., ADHD, healthy elderly, stroke patients, and spinal cord injury) and to the specific target of cognitive interventions (attention, memory, language, and visuospatial abilities). Typically, cognitive rehabilitation relies on a set of tasks and procedures that are more flexible and adaptable than those used for cognitive evaluation purposes, since it is tailored on patients' specific needs and residual capacities. Moreover, the realization of engaging settings for cognitive training, sometimes involving gaming systems, entails the realization of more realistic and interactive protocols that needs to be consistently adopted across several studies for standardization.

With regard to clinical populations recruited, despite BCI application for cognitive assessment mainly addressed clinical populations with physical disabilities up to locked-in conditions (i.e., ALS and MCS), for whom BCI and other assistive technologies were firstly developed, cognitive rehabilitation has been mainly used with target patients of NFT (ADHD, ASD, and cognitive enhancement in the elderly). An emerging field of study concerns BCI application for rehabilitation of language deficit in stroke patients, even if few and heterogeneous findings have been collected as yet.

An interesting finding arising from the present review concerns the limited number of studies addressing the use of BCI for cognitive assessment of patients with physical limitations, despite the clinical and ethical relevance of longitudinal neuropsychological evaluation in neurological disorder, especially in neurodegenerative conditions. Perhaps, the need for an expensive equipment and specific competencies in order to use the system and analyze data is one of the main obstacles in the use of BCI in clinical settings. At present, a widely used BCI paradigm is the visual P300 BCI: even if it requires patients to perform ocular movements and fixation to some extent, several studies demonstrated that it can be employed also with ALS patients in the late stage of the disease where oculomotor abilities are often altered [57, 58]. However, several studies have proposed gaze-independent P300 or SSVEP-based BCIs for patients with DOC who often lose the ability to fixate their gaze in order to overwhelm such clinical and methodological issue [30].

With regard to the use of BCI alongside more traditional NF applications, feedback visualizations in NFT (and biofeedback) paradigms range from controlling a simple bar graph to more complex and realistic visual stimuli. In typical application of NFT, the feedback is not related to the specific meaning of the signals being trained or the expected behavioral outcomes. However, a specific feedback for certain signals being trained might be more effective in promoting behavioral changes by activating specific brain areas. Moreover, the level of motivation involved in performing the task is increased by the sense of agency that the user perceive, that is, its capacity of making something relevant happen. For these purposes, the introduction of new ways of providing feedback and reward within BCI-based NFT, such as virtual reality environments, appears promising to improve efficacy and transferability of learnings to real-life contexts.

Another issue concerning the use of BCI for both cognitive assessment and, more specifically, rehabilitation purposes is that of slow learners, particularly applicable to older adults [54]. The possibility of integrating expensive modalities targeting deep brain region, such as fMRI-based NF, with less cost-intensive NF training methods, that is, EEG, could help in providing a longer training period to such population. An emerging technology, useful for these purposes, is represented by real-time fMRI (rtfMRI) [59]. Even if this approach has been poorly investigated with randomized clinical studies, its potential application in combination with other technologies deserves further consideration.

To conclude, some emerging challenges arise from the present review and represent possible relevant targets of future investigation within the field of BCI use for clinical purposes. In particular:

(1) the possibility of bringing BCI-based training into patient's home, by developing low-cost and portable systems, in order to provide more intensive, effective, and long-term treatments of cognitive functions;

(2) in relation to the previous point, the improvement of usability (simplification of procedures) and customizability of BCIs to users' characteristics and cognitive capacities; in particular, the issue of usability investigation has not been detailed in the present review, but represents a relevant aspect when dealing with clinical populations and their families [7];

(3) the investigation about outcomes of BCI-based cognitive interventions, with respect to brain functional changes and reorganization; in particular, the use of quantitative measures, such as fMRI and EEG, to be integrated with behavioral and neuropsychological findings, will help to better clarify the efficacy and impact of training protocols, as also suggested by recent reviews [60, 61];

(4) the improvement in realization of BCI-based neuropsychological tests, to be validated in clinical populations against gold standard measures; in particular, such approach should take into consideration the simplification of procedures for tests' administration and a limited number of items composing each test, in order to reduce cognitive effort and interference in the detection of patients' cognitive profiles; according to these increased usability and reliability components, several aspects of cognition should be involved in BCI-based assessment protocols, in order to meet clinical and ethical needs involved in neurodegenerative disorders.

Overall, even with some limitations due to technical and methodological issues, literature on BCI highlights promising findings in both cognitive assessment and training contexts, thus promoting innovative BCI-based applications for neurorehabilitation settings and aging research.

Conflicts of Interest

The authors declare that there are no conflicts of interest regarding the publication of this article.

References

[1] D. de Massari, C. A. Ruf, A. Furdea et al., "Brain communication in the locked-in state," *Brain*, vol. 136, no. 6, pp. 1989–2000, 2013.

[2] M. Marchetti and K. Priftis, "Brain-computer interfaces in amyotrophic lateral sclerosis: a metanalysis," *Clinical Neurophysiology*, vol. 126, no. 6, pp. 1255–1263, 2015.

[3] R. M. Gibson, A. M. Owen, and D. Cruse, "Brain–computer interfaces for patients with disorders of consciousness," *Progress in Brain Research*, vol. 228, pp. 241–291, 2016.

[4] N. Birbaumer, A. Ramos Murguialday, C. Weber, and P. Montoya, "Neurofeedback and Brain-Computer Interface. Clinical Applications," *International Review of Neurobiology*, vol. 86, pp. 107–117, 2009.

[5] U. Chaudhary, N. Birbaumer, and A. Ramos-Murguialday, "Brain-computer interfaces for communication and rehabilitation," *Nature Reviews Neurology*, vol. 12, no. 9, pp. 513–525, 2016.

[6] J. J. Daly and J. E. Huggins, "Brain-computer interface: current and emerging rehabilitation applications," *Archives of Physical Medicine and Rehabilitation*, vol. 96, no. 3, pp. S1–S7, 2015.

[7] A. Riccio, F. Pichiorri, F. Schettini et al., "Interfacing brain with computer to improve communication and rehabilitation after brain damage," *Progress in Brain Research*, vol. 228, pp. 357–387, 2016.

[8] L. E. van Dokkum, T. Ward, and I. Laffont, "Brain computer interfaces for neurorehabilitation—its current status as a rehabilitation strategy post-stroke," *Annals of Physical and Rehabilitation Medicine*, vol. 58, no. 1, pp. 3–8, 2015.

[9] L. H. Goldstein and S. Abrahams, "Changes in cognition and behaviour in amyotrophic lateral sclerosis: nature of impairment and implications for assessment," *The Lancet Neurology*, vol. 12, no. 4, pp. 368–380, 2013.

[10] S. Abrahams, J. Newton, E. Niven, J. Foley, and T. H. Bak, "Screening for cognition and behaviour changes in ALS," *Amyotrophic Lateral Sclerosis and Frontotemporal Degeneration*, vol. 15, no. 1-2, pp. 9–14, 2014.

[11] A. Anastasia and S. Urbina, *Psychological Testing*, Prentice Hall, Upper Saddle River, NJ, USA, 7th edition, 1997.

[12] C. Seer, S. Fürkötter, M.-B. Vogts et al., "Executive dysfunctions and event-related brain potentials in patients with amyotrophic lateral sclerosis," *Frontiers in Aging Neuroscience*, vol. 7, article 225, 2015.

[13] B. Kotchoubey, S. Lang, S. Winter, and N. Birbaumer, "Cognitive processing in completely paralyzed patients with amyotrophic lateral sclerosis," *European Journal of Neurology*, vol. 10, no. 5, pp. 551–558, 2003.

[14] N. Neumann and B. Kotchoubey, "Assessment of cognitive functions in severely paralysed and severely brain-damaged patients: neuropsychological and electrophysiological methods," *Brain Research Protocols*, vol. 14, no. 1, pp. 25–36, 2004.

[15] J. Polich, "Updating P300: an integrative theory of P3a and P3b," *Clinical Neurophysiology*, vol. 118, no. 10, pp. 2128–2148, 2007.

[16] S. A. Sprague, M. T. McBee, and E. W. Sellers, "The effects of working memory on brain-computer interface performance," *Clinical Neurophysiology*, vol. 127, no. 2, pp. 1331–1341, 2016.

[17] A. Riccio, L. Simione, F. Schettini et al., "Attention and P300-based BCI performance in people with amyotrophic lateral sclerosis," *Frontiers in Human Neuroscience*, vol. 7, article 732, 2013.

[18] L. da Silva-Sauer, L. Valero-Aguayo, A. de la Torre-Luque, R. Ron-Angevin, and S. Varona-Moya, "Concentration on performance with P300-based BCI systems: a matter of interface features," *Applied Ergonomics*, vol. 52, article 2090, pp. 325–332, 2016.

[19] J. Xie, G. Xu, J. Wang, M. Li, C. Han, and Y. Jia, "Effects of mental load and fatigue on steady-state evoked potential based brain computer interface tasks: a comparison of periodic flickering and motion-reversal based visual attention," *PLoS ONE*, vol. 11, no. 9, Article ID e0163426, 2016.

[20] A. Burns, H. Adeli, and J. A. Buford, "Brain-computer interface after nervous system injury," *Neuroscientist*, vol. 20, no. 6, pp. 639–651, 2014.

[21] I. H. Iversen, N. Ghanayim, A. Kübler, N. Neumann, N. Birbaumer, and J. Kaiser, "A brain-computer interface tool to assess cognitive functions in completely paralyzed patients with amyotrophic lateral sclerosis," *Clinical Neurophysiology*, vol. 119, no. 10, pp. 2214–2223, 2008.

[22] I. H. Iversen, N. Ghanayim, A. Kübler, N. Neumann, N. Birbaumer, and J. Kaiser, "Conditional associative learning examined in a paralyzed patient with amyotrophic lateral sclerosis using brain-computer interface technology," *Behavioral and Brain Functions*, vol. 4, article 53, 2008.

[23] P. Perego, A. C. Turconi, G. Andreoni et al., "Cognitive ability assessment by brain-computer interface validation of a new assessment method for cognitive abilities," *Journal of Neuroscience Methods*, vol. 201, no. 1, pp. 239–250, 2011.

[24] P. Perego, A. C. Turconi, C. Gagliardi, and G. Andreoni, "Psychometric evaluation with brain-computer interface," in *Human-Computer Interaction*, J. A. Jacko, Ed., vol. 6761 of *Lecture Notes in Computer Science (including subseries Lecture Notes in Artificial Intelligence and Lecture Notes in Bioinformatics)*, pp. 406–413, 2011.

[25] N. Westergren, R. L. Bendtsen, T. W. Kjaer, C. E. Thomsen, S. Puthusserypady, and H. B. Sorensen, "Steady state visual evoked potential based brain-computer interface for cognitive assessment," in *Proceedings of the 2016 38th Annual International Conference of the IEEE Engineering in Medicine and Biology Society (EMBC '16)*, pp. 1508–1511, Orlando, FL, USA, August 2016.

[26] P. Cipresso, L. Carelli, F. Solca et al., "The use of P300-based BCIs in amyotrophic lateral sclerosis: From augmentative and alternative communication to cognitive assessment," *Brain and Behavior*, vol. 2, no. 4, pp. 479–498, 2012.

[27] B. Poletti, L. Carelli, F. Solca et al., "Cognitive assessment in Amyotrophic Lateral Sclerosis by means of P300-Brain Computer Interface: a preliminary study," *Amyotrophic Lateral Sclerosis and Frontotemporal Degeneration*, vol. 17, no. 7-8, pp. 473–481, 2016.

[28] P. Cipresso, P. Meriggi, L. Carelli et al., "Brain computer interface and eye-tracking for neuropsychological assessment of executive functions: a pilot study," in *Proceedings of the 2nd International Workshop on Computing Paradigms for Mental Health (MindCare '12)*, pp. 79–88, February 2012.

[29] P. Cipresso, P. Meriggi, L. Carelli et al., "Cognitive assessment of executive functions using brain computer interface and eye-tracking," *ICST Transactions on Ambient Systems*, vol. 13, no. 01–06, p. e4, 2013.

[30] Y. Li, J. Pan, Y. He et al., "Detecting number processing and mental calculation in patients with disorders of consciousness using a hybrid brain-computer interface system," *BMC Neurology*, vol. 15, no. 1, article no. 259, 2015.

[31] E. Angelakis, S. Stathopoulou, J. L. Frymiare, D. L. Green, J. F. Lubar, and J. Kounios, "EEG neurofeedback: a brief overview and an example of peak alpha frequency training for cognitive enhancement in the elderly," *The Clinical Neuropsychologist*, vol. 21, no. 1, pp. 110–129, 2007.

[32] A. W. Keizer, R. S. Verment, and B. Hommel, "Enhancing cognitive control through neurofeedback: A role of gamma-band activity in managing episodic retrieval," *NeuroImage*, vol. 49, no. 4, pp. 3404–3413, 2010.

[33] D. Vernon, T. Egner, N. Cooper et al., "The effect of training distinct neurofeedback protocols on aspects of cognitive performance," *International Journal of Psychophysiology*, vol. 47, no. 1, pp. 75–85, 2003.

[34] D. J. Vernon, "Can neurofeedback training enhance performance? An evaluation of the evidence with implications for future research," *Applied Psychophysiology Biofeedback*, vol. 30, no. 4, pp. 347–364, 2005.

[35] M. A. Vollebregt, M. Van Dongen-Boomsma, J. K. Buitelaar, and D. Slaats-Willemse, "Does EEG-neurofeedback improve neurocognitive functioning in children with attention-deficit/hyperactivity disorder? A systematic review and a double-blind placebo-controlled study," *Journal of Child Psychology and Psychiatry and Allied Disciplines*, vol. 55, no. 5, pp. 460–472, 2014.

[36] J. E. Munoz, D. S. Lopez, J. F. Lopez, and A. Lopez, "Design and creation of a BCI videogame to train sustained attention in children with ADHD," in *Proceedings of the 10th Colombian Computing Conference (10CCC '15)*, pp. 194–199, September 2015.

[37] C. G. Lim, T. S. Lee, and C. Guan, "Effectiveness of a brain-computer interface based program for the treatment of ADHD: a pilot study," *Psychopharmacol Bull*, vol. 43, no. 1, pp. 73–82, 2010.

[38] C. G. Lim, T. S. Lee, C. Guan et al., "A brain-computer interface based attention training program for treating attention deficit hyperactivity disorder," *PLoS ONE*, vol. 7, no. 10, Article ID e46692, 2012.

[39] T.-S. Lee, S. J. A. Goh, S. Y. Quek et al., "A brain-computer interface based cognitive training system for healthy elderly: a randomized control pilot study for usability and preliminary efficacy," *PLoS ONE*, vol. 8, no. 11, Article ID e79419, 2013.

[40] T.-S. Lee, S. Y. Quek, S. J. A. Goh et al., "A pilot randomized controlled trial using EEG-based brain–computer interface training for a Chinese-speaking group of healthy elderly," *Clinical Interventions in Aging*, vol. 10, pp. 217–227, 2015.

[41] J. Gomez-Pilar, R. Corralejo, L. F. Nicolas-Alonso, D. Álvarez, and R. Hornero, "Assessment of neurofeedback training by means of motor imagery based-BCI for cognitive rehabilitation," in *Proceedings of the Annual International Conference of the IEEE Engineering in Medicine and Biology Society*, vol. 2014, pp. 3630–3633.

[42] J. Gomez-Pilar, R. Corralejo, L. F. Nicolas-Alonso, D. Álvarez, and R. Hornero, "Neurofeedback training with a motor imagery-based BCI: neurocognitive improvements and EEG changes in the elderly," *Medical and Biological Engineering and Computing*, vol. 54, no. 11, pp. 1655–1666, 2016.

[43] G. Lecomte and J. Juhel, "The effects of neurofeedback training on memory performance in elderly subjects," *Psychology*, vol. 2, no. 8, pp. 846–852, 2011.

[44] J. Reis, A. M. Portugal, L. Fernandes et al., "An alpha and theta intensive and short neurofeedback protocol for healthy aging working-memory training," *Frontiers in Aging Neuroscience*, vol. 8, article 157, 2016.

[45] J. A. Pineda, A. Juavinett, and M. Datko, "Self-regulation of brain oscillations as a treatment for aberrant brain connections in children with autism," *Medical Hypotheses*, vol. 79, no. 6, pp. 790–798, 2012.

[46] E. V. Friedrich, N. Suttie, A. Sivanathan, T. Lim, S. Louchart, and J. A. Pineda, "Brain-computer interface game applications for combined neurofeedback and biofeedback treatment for children on the autism spectrum," *Frontiers in Neuroengineering*, vol. 7, p. 21, 2014.

[47] T.-W. Kim and B.-H. Lee, "Clinical usefulness of brain-computer interface-controlled functional electrical stimulation for improving brain activity in children with spastic cerebral palsy: A pilot randomized controlled trial," *Journal of Physical Therapy Science*, vol. 28, no. 9, pp. 2491–2494, 2016.

[48] D. B. Salisbury, S. Driver, and T. D. Parsons, "Brain-computer interface targeting non-motor functions after spinal cord injury: a case report," *Spinal Cord*, vol. 53, supplement 1, pp. S25–S26, 2015.

[49] D. B. Salisbury, T. D. Parsons, K. R. Monden, Z. Trost, and S. J. Driver, "Brain-computer interface for individuals after spinal cord injury," *Rehabilitation Psychology*, vol. 61, no. 4, pp. 435–441, 2016.

[50] S. C. Kleih, L. Gottschalt, E. Teichlein, and F. X. Weilbach, "Toward a P300 based brain-computer interface for aphasia rehabilitation after stroke: presentation of theoretical considerations and a pilot feasibility study," *Frontiers in Human Neuroscience*, vol. 10, p. 547, 2016.

[51] M. Musso, A. Bamdadian, S. Denzer, R. Umarova, D. Hübner, and M. Tangermann, "A novel BCI based rehabilitation approach for aphasia rehabilitation," in *Proceedings of the 6th International Brain-Computer Interface Meeting*, Asilomar Conference Center, Pacific Grove, Calif., USA, May–June 2016.

[52] J. Toppi, D. Mattia, A. Anzolin et al., "Time varying effective connectivity for describing brain network changes induced by a memory rehabilitation treatment," in *Proceedings of the Annual International Conference of the IEEE Engineering in Medicine and Biology Society*, vol. 2014, pp. 6786–92014.

[53] J. F. Burke, M. B. Merkow, J. Jacobs, M. J. Kahana, and K. A. Zaghloul, "Brain computer interface to enhance episodic memory in human participants," *Frontiers in Human Neuroscience*, vol. 8, article 1055, pp. 1–10, 2015.

[54] M. Rana, A. Q. Varan, A. Davoudi, R. A. Cohen, R. Sitaram, and N. C. Ebner, "Real-time fMRI in neuroscience research and its use in studying the aging brain," *Frontiers in Aging Neuroscience*, vol. 8, article 239, 2016.

[55] W.-P. Teo, M. Muthalib, S. Yamin et al., "Does a combination of virtual reality, neuromodulation and neuroimaging provide a comprehensive platform for neurorehabilitation?—A narrative review of the literature," *Frontiers in Human Neuroscience*, vol. 10, article 284, 2016.

[56] D. A. Rohani and S. Puthusserypady, "BCI inside a virtual reality classroom: a potential training tool for attention," *EPJ Nonlinear Biomedical Physics*, vol. 3, no. 1, p. 12, 2015.

[57] A. Kübler and N. Birbaumer, "Brain-computer interfaces and communication in paralysis: extinction of goal directed thinking in completely paralysed patients?" *Clinical Neurophysiology*, vol. 119, no. 11, pp. 2658–2666, 2008.

[58] C. Donaghy, M. J. Thurtell, E. P. Pioro, J. M. Gibson, and R. J. Leigh, "Eye movements in amyotrophic lateral sclerosis and its mimics: a review with illustrative cases," *Journal of Neurology, Neurosurgery and Psychiatry*, vol. 82, no. 1, pp. 110–116, 2011.

[59] L. E. Stoeckel, K. A. Garrison, and S. Ghosh, "Optimizing real time fMRI neurofeedback for therapeutic discovery and development," *NeuroImage Clinical*, vol. 10, no. 5, pp. 245–255, 2014.

[60] M. Ordikhani-Seyedlar, M. A. Lebedev, H. B. D. Sorensen, and S. Puthusserypady, "Neurofeedback therapy for enhancing visual attention: state-of-the-art and challenges," *Frontiers in Neuroscience*, vol. 10, article 352, 2016.

[61] Y. Jiang, R. Abiri, and X. Zhao, "Tuning up the old brain with new tricks: attention training via neurofeedback," *Frontiers in Aging Neuroscience*, vol. 9, no. 52, 2017.

Hindawi
BioMed Research International
Volume 2017, Article ID 8317357, 9 pages
https://doi.org/10.1155/2017/8317357

Research Article

Emotion Recognition from EEG Signals Using Multidimensional Information in EMD Domain

Ning Zhuang,[1] Ying Zeng,[1,2] Li Tong,[1] Chi Zhang,[1] Hanming Zhang,[1] and Bin Yan[1]

[1]*China National Digital Switching System Engineering and Technological Research Center, Zhengzhou 450002, China*
[2]*Key Laboratory for NeuroInformation of Ministry of Education, School of Life Science and Technology, University of Electronic Science and Technology of China, Chengdu, China*

Correspondence should be addressed to Bin Yan; ybspace@hotmail.com

Received 27 March 2017; Revised 21 June 2017; Accepted 16 July 2017; Published 16 August 2017

Academic Editor: Robertas Damaševičius

This paper introduces a method for feature extraction and emotion recognition based on empirical mode decomposition (EMD). By using EMD, EEG signals are decomposed into Intrinsic Mode Functions (IMFs) automatically. Multidimensional information of IMF is utilized as features, the first difference of time series, the first difference of phase, and the normalized energy. The performance of the proposed method is verified on a publicly available emotional database. The results show that the three features are effective for emotion recognition. The role of each IMF is inquired and we find that high frequency component IMF1 has significant effect on different emotional states detection. The informative electrodes based on EMD strategy are analyzed. In addition, the classification accuracy of the proposed method is compared with several classical techniques, including fractal dimension (FD), sample entropy, differential entropy, and discrete wavelet transform (DWT). Experiment results on DEAP datasets demonstrate that our method can improve emotion recognition performance.

1. Introduction

Emotion plays an important role in our daily life and work. Real-time assessment and regulation of emotion will improve people's life and make it better. For example, in the communication of human-machine-interaction, emotion recognition will make the process more easy and natural. Another example, in the treatment of patients, especially those with expression problems, the real emotion state of patients will help doctors to provide more appropriate medical care. In recent years, emotion recognition from EEG has gained mass attention. Also it is a very important factor in brain computer interface (BCI) systems, which will effectively improve the communication between human and machines [1].

Various features and extraction methods have been proposed for emotion recognition from EEG signals, including time domain techniques, frequency domain techniques, joint time-frequency analysis techniques, and other strategies.

Statistics of EEG series, that is, first and second difference, mean value, and power are usually used in time domain [2]. Nonlinear features, including fractal dimension (FD) [3, 4], sample entropy [5], and nonstationary index [6], are utilized for emotion recognition. Hjorth features [7] had also been used in EEG studies [8, 9]. Petrantonakis and Hadjileontiadis introduced higher order crossings (HOC) features to capture the oscillatory pattern of EEG [10]. Wang et al. extracted frequency domain features for classification [11]. Time-frequency analysis is based on the spectrum of EEG signals; then the energy, power, power spectral density (PSD), and differential entropy [12] of certain subband are usually utilized as features. Short-time Fourier transform (STFT) [13, 14], Hilbert-Huang transform (HHT) [15, 16], and discrete wavelet transform (DWT) [17–19] are the most commonly used techniques for spectrum calculating. It has been commonly tested and verified that higher frequency subband such as Beta (16–32 Hz) and Gamma (32–64 Hz) bands outperforms lower subband for emotion recognition [20, 21].

Other features extracted from combination of electrode are utilized too, such as coherence and asymmetry of electrodes in different brain regions [22–24] and graph-theoretic features [25]. Jenke et al. had done a research comparing the

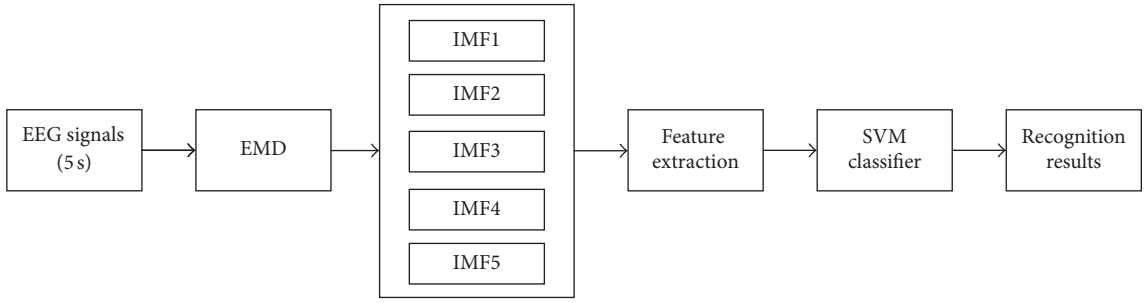

Figure 1: Block diagram of the proposed method.

performance of different features mentioned above and got a guiding rule for feature extraction and selection [26].

Some other strategies such as utilizing deep network to improve the classification performance have also been researched. Zheng and Lu used deep neural network to investigate critical frequency bands and channels for emotion recognition [27]. Yang et al. used hierarchical network with subnetwork nodes for emotion recognition [28].

EMD is proposed by Huang et al. in 1998 [29]. Unlike DWT, which needs to predetermine transform base function and decomposition level, EMD can decompose signals into IMF automatically. These IMFs represent different frequency components of original signals, with band-limited characteristic. By applying Hilbert transform to IMF, we can get instantaneous phase information of IMF. So EMD is suitable for analysis of nonlinear and nonstationary sequence, such as neural signals.

EMD is a good choice for EEG signals and we utilize it for emotion recognition from EEG data. Which feature is effective for emotion recognition in EMD domain? Which IMF component is best for classification? Is the performance based on EMD strategy better compared to time domain method and time-frequency method or not? All these have not been researched yet and we investigate them in our research.

EMD has been widely used for seizure prediction and detection, but for emotion recognition based on EMD, there is not so much research. Higher order statistics of IMFs [30], geometrical properties of the decomposed IMF in complex plane [31], and the variation and fluctuation of IMF [32] are used as features for seizure prediction and detection. For emotion recognition, Mert and Akan extracted entropy, power, power spectral density, correlation, and asymmetry of IMF as features and then utilized independent component analysis (ICA) to reduce dimension of the feature set [33]. The classification accuracy is computed with all the subjects mixed together.

In this paper, we present an emotion recognition method based on EMD. We utilize the first difference of IMF time series, the first difference of the IMF's phase, and the normalized energy of IMF as features. The motivation of using these three features is that they depict the characteristics of IMF in time, frequency, and energy domain, providing multidimensional information. The first difference of time series depicts the intensity of signal change in time domain. The first difference of phase measures the change intensity in phase and normalized energy describes the weight of current oscillation component. The three features constitute a feature vector, which is fed into SVM classifier for emotional state detection.

The proposed method is studied on a publicly available emotional database DEAP [20]. The effectiveness of the three features is investigated. IMF reduction and channel reduction for feature extraction are both discussed, which aim at improving the classification accuracy with less computation complexity. The performance is compared with some other techniques, including fractal dimension (FD), sample entropy, differential entropy, and time-frequency analysis DWT.

2. Method

To realize emotional state recognition, the EEG signals are decomposed into IMFs by EMD. Three features of IMFs, the fluctuation of the phase, the fluctuation of the time series, and the normalized energy, are formed as a feature vector, which is fed into SVM for classification. The whole process of the algorithm is shown in Figure 1.

2.1. Data and Materials. DEAP is a publicly available dataset for emotion analysis, which recorded EEG and peripheral physiological signals of 32 participants as they watched 40 music videos. All the music video clips last for 1 minute, representing different emotion visual stimuli, with grade from 1 to 9. Among the 40 music videos, 20 are high valence visual stimuli and 20 are low valence visual stimuli. The situation is exactly the same for arousal dimension. After watching the music video, participants performed a self-assessment of their levels on arousal, valence, liking, dominance, and familiarity, with ratings from 1 to 9. EEG was recorded with 32 electrodes, placing according to the international 10-20 system. Each electrode recorded 63 s EEG signal, with 3 s baseline signal before the trial.

In this paper, we used the preprocessed EEG data for study, with sample rate 128 Hz and band range 4–45 Hz. EOG artefacts were removed as method in [20]. The data was segmented into 60-second trials and a 3-second pretrial baseline removed. The binary classifications of valence and arousal dimension are considered. We utilized the participants' self-assessment as label. If the participant's rating was <5, the label

of valence/arousal is low and if the rating was ≥5, the label of valence/arousal is high.

Each music video lasts for 1 minute, and 5 s EEG signals are extracted as a sample. So for each subject who watched 40 music videos, we acquire 480 labeled samples.

2.2. Empirical Mode Decomposition. EMD decomposes EEG signals into a set of IMFs by an automatic shifting process. Each IMF represents different frequency components of original signals and should satisfy two conditions: (1) during the whole data set, the number of extreme points and the number of zero crossings must be either equal or differ at most by one; (2) at each point, the mean value calculated from the upper and lower envelope must be zero [29]. For input signal $x(t)$, the process of EMD is as follows:

(1) Set $h(t) = x(t)$ and $h_{\text{old}}(t) = h(t)$.

(2) Get local maximum and minimum of $h_{\text{old}}(t)$.

(3) Interpolate the local maximum and minimum with cubic spline function and get the upper envelope $e_{\max}(t)$ and lower envelope $e_{\min}(t)$.

(4) Calculate the mean value of the upper and lower envelope as

$$m(t) = \frac{\left(e_{\min}(t) + e_{\max}(t)\right)}{2}. \tag{1}$$

(5) Subtract $h_{\text{old}}(t)$ with $m(t)$:

$$h_{\text{new}}(t) = h_{\text{old}}(t) - m(t). \tag{2}$$

If $h_{\text{new}}(t)$ satisfies the two conditions of IMF, then the first IMF component imf_1 is gotten; otherwise, set $h_{\text{old}}(t) = h_{\text{new}}(t)$ and go to step (2), repeating steps (2)–(5) until $h_{\text{new}}(t)$ satisfies the two conditions of IMF. Finally imf_1 is gotten as

$$\text{imf}_1 = h_{\text{new}}(t). \tag{3}$$

(6) If imf_n is gotten, set $h_{\text{old}}(t)$ as

$$h_{\text{old}}(t) = h_{\text{old}}(t) - \text{imf}_n. \tag{4}$$

Go to step (2) and repeat steps (2)–(5) to get imf_{n+1}.

By the iterative process described above, $x(t)$ can be finally expressed as

$$x(t) = \sum_{n=1}^{L} \text{imf}_n + r. \tag{5}$$

It is a linear combination of IMF components and the residual part r. Figure 2 shows a segment of original EEG signals corresponding to the first five decomposed IMFs. EMD works like an adaptive high pass filter. It shifts out the fastest changing component first and as the level of IMF increases, the oscillation of IMF becomes smoother. Each component is band-limited, which can reflect the characteristic of instantaneous frequency.

2.3. Feature Extraction. In this paper, three features of IMF are utilized for emotion recognition, the first difference of time series, the first difference of phase, and the normalized energy. The first difference of time series depicts the intensity of signal change in time domain. The first difference of phase reveals the change intensity of phase, representing the physical meaning of instantaneous frequency. Normalized energy describes the weight of current oscillation component. The motivation of using these three features is that they depict the characteristics of IMF in time, frequency, and energy domain, utilizing multidimensional information.

2.3.1. First Difference of IMF Time Series. The first difference of times series D_t depicts the intensity of signal change in time domain. Previous research has revealed that the variation of EEG time series can reflect different emotion states [2]. For an IMF component with N points, $\text{IMF}\{\text{imf}_1, \text{imf}_2, \ldots, \text{imf}_N\}$, the definition of D_t is

$$D_t = \frac{1}{N-1} \sum_{n=1}^{N-1} \left|\text{imf}(n+1) - \text{imf}(n)\right|. \tag{6}$$

2.3.2. First Difference of IMF's Phase. Based on EMD, EEG is decomposed into multilevel IMFs, each IMF being band-limited and representing an oscillation component of original EEG signals. For an N-point IMF, $\text{IMF}\{\text{imf}_1, \text{imf}_2, \ldots, \text{imf}_N\}$, Hilbert transform is applied to it, obtaining an analytic signal $z(n)$

$$z(n) = x(n) + jy(n). \tag{7}$$

The analytic signal can be further expressed as follows:

$$z(n) = A(n) e^{j\varphi(n)}, \tag{8}$$

where $A(n) = \sqrt{x(n)^2 + y(n)^2}$ is the amplitude of $z(n)$ and $\varphi(n) = \arctan(y(n)/x(n))$ is the instantaneous phase.

First difference of phase D_p is defined as

$$D_p = \frac{1}{N-1} \sum_{n=1}^{N-1} \left|\varphi(n+1) - \varphi(n)\right| \tag{9}$$

which measures the change intensity in phase and represents the physical meaning of instantaneous frequency.

2.3.3. Normalized Energy of IMF. For an N-point IMF, $\text{IMF}\{\text{imf}_1, \text{imf}_2, \ldots, \text{imf}_N\}$, the normalized energy E_{norm} is defined as follows:

$$E_{\text{norm}} = \frac{\sum_{n=1}^{N} \text{imf}^2(n)}{\sum_{n=1}^{N} s^2(n)}, \tag{10}$$

where $s(n)$ is the original EEG signal points. So the numerator is the energy of IMF and the denominator represents the energy of original EEG data set. The normalized energy describes the weight of current oscillation component. When fed into the classifier, $\log(E_{\text{norm}})$ is taken as an element of the feature vector according to [26].

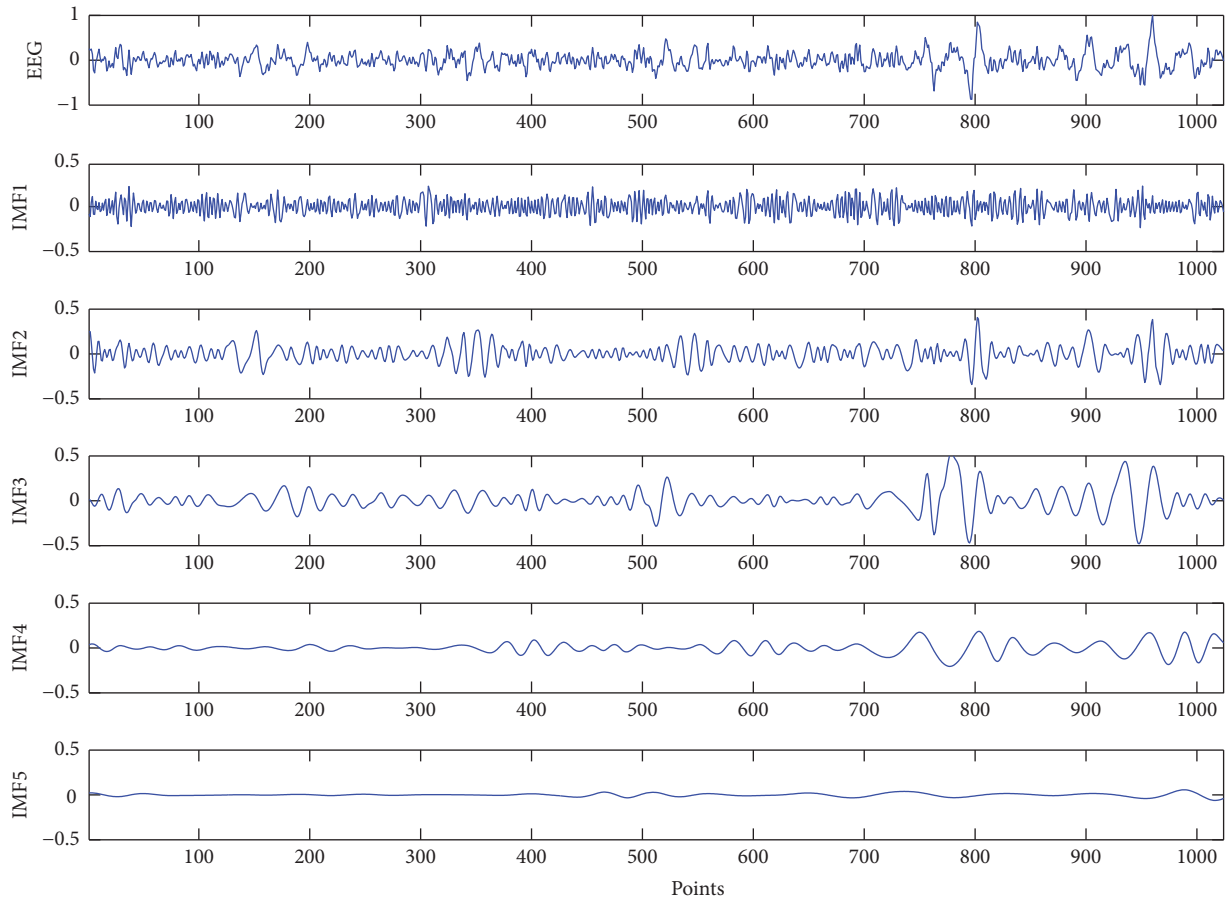

Figure 2: EEG signals and the corresponding first five IMFs.

2.4. SVM Classifier. The extracted features are fed into SVM for classification. SVM is widely used for emotion recognition [34, 35], which has promising property in many fields. In our study, LIBSVM is implemented for SVM classifier with radial basis kernel function and default parameters setting [36].

3. Performance Verification

In the following subsections, we test our method on DEAP emotional dataset. Training and classifying tasks were conducted for each subject independently and we utilized leave-one-trail-out validation to evaluate the classification performance. Each subject watched 40 music video clips, and every video clips lasted 1 minute. In our experiment, we utilized the participants' self-assessment as label. Every 5 s EEG signals are extracted as a sample, so for each subject we acquire 480 labeled samples.

In leave-one-trail-out validation, for each subject, 468 samples extracted from 39 trails were assigned to training set, and 12 samples extracted from the remaining one trail were assigned to test set. So there was no correlation between samples in the training set and the test set. Among the total 40 trails of one subject, each trail will be assigned to the test set once as the validation data. The 40 results from the 40 test trails then can be averaged to produce a general estimation for each subject. The final mean accuracy is computed among all the subjects.

3.1. Effectiveness of the Features for Emotion Recognition. In order to evaluate the effectiveness of the three features for emotion recognition, we first use only one single feature for classification each time. All the experiments in this subsection are under the condition that the first five IMF components and total 32 electrodes are utilized for feature extraction. The training and classifying for each subject were conducted, respectively, and the mean accuracy was computed among all the subjects.

The mean classification accuracies of three features are given in Figure 3. It shows that all the three features can distinguish high level from low level on both valence and arousal dimension, higher than random probability of 50%. For valence dimension, the classification accuracy yields 68.27%, 64.46%, and 61.07% with features D_t, D_p, and E_{norm}, respectively. For arousal dimension, the classification accuracy yields 69.89%, 67.56%, and 63.76% with features D_t, D_p, and E_{norm}, respectively.

3.2. IMF Reduction for Feature Extraction. In this subsection, we did two experiments to investigate the role of different IMF components in emotion recognition. In the

Table 1: Comparison of performance for different IMFs selected for feature extraction (32 channels) (standard deviation shown in parentheses).

Component	Valence		Arousal	
	Accuracy (%)	t-test (IMF1)	Accuracy (%)	t-test (IMF1)
IMF1	**70.41** (7.05)	$p = 1$	**72.10** (7.51)	$p = 1$
IMF2	63.47 (7.10)	$p = 0.0002$	66.58 (9.36)	$p = 0.0032$
IMF3	61.45 (8.57)	$p = 0$	64.56 (10.52)	$p = 0.0019$
IMF4	59.55 (8.56)	$p = 0$	63.99 (10.96)	$p = 0.0012$
IMF5	55.74 (9.20)	$p = 0$	62.38 (12.23)	$p = 0$
IMF1-2	69.02 (7.00)	$p = 0.4399$	70.47 (8.29)	$p = 0.1940$
IMF1–3	68.47 (6.69)	$p = 0.2705$	70.08 (8.10)	$p = 0.3116$
IMF1–4	67.99 (6.58)	$p = 0.1688$	69.60 (8.08)	$p = 0.2107$
IMF1–5	67.59 (6.58)	$p = 0.1086$	69.00 (8.37)	$p = 0.1293$

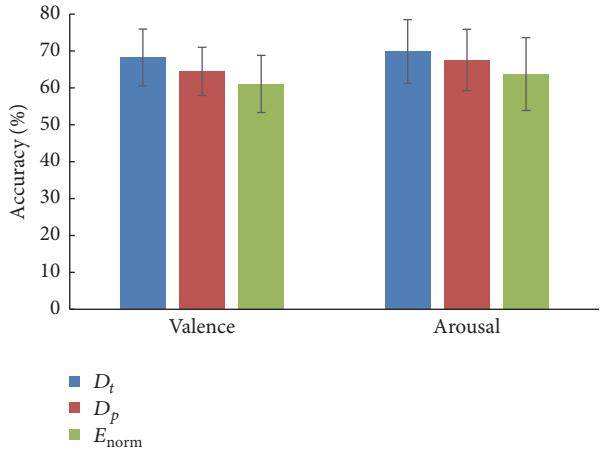

Figure 3: Classification accuracies of three single features. For each subject, one single feature was extracted from the first five IMF components. "D_t," "D_p," and "E_{norm}" in the figure are corresponding to the three single features, respectively. The mean accuracies for all circumstances were computed among all the subjects. Error bars show the standard deviation of the mean accuracies across all subjects.

Table 2: Performance of 8 channels selected for feature extraction (Fp1, Fp2, F7, F8, T7, T8, P7, and P8) (standard deviation shown in parentheses).

Predict	Label			
	Valence		Arousal	
	High	Low	High	Low
High	6664	2723	7493	2748
Low	2024	3949	1555	3564
$F1$ score	0.7374		0.7769	
Accuracy (%)	69.10 (6.95)		71.99 (7.77)	

first experiment, each time only one IMF component was utilized for feature extraction and we analyzed which IMF is effective for emotion recognition. In the second experiment, we further verified whether the combination of multi-IMFs would improve the accuracy.

Table 2 gives all the results in detail. Standard deviation of the mean accuracies across all subjects is shown in parenthesis. "IMF1," "IMF2," "IMF3," "IMF4," and "IMF5" are corresponding to single IMF component. "IMF1–3" in the table represents the first three IMFs, corresponding to IMF1, IMF2, and IMF3. Similarly, "IMF1–4" and "IMF1–5" are corresponding to the first four IMFs and the first five IMFs, respectively.

It shows that IMF1 yields the best performance, 70.41% for valence and 72.10% for arousal. As the level increases, the performance decreases sharply. The performance of IMF5 is only 55.74% for valence and 62.38% for arousal. We applied t-test ($\alpha < 0.05$) to examine the performance between only IMF1 utilized for feature extraction and other circumstances. The null hypothesis is "the performance is similar" and if p value is larger than α, the null hypothesis is accepted. The results of t-test in Table 1 show that the performance of IMF1 is more splendid than other single components, IMF2, IMF3, IM4, and IMF5, with p far less than 0.05. It also shows that performance of multi-IMF combinations is similar to only IMF1 utilized for feature extraction, with p larger than 0.05.

IMF1 represents the fastest changing component of EEG signals, with the highest frequency characteristic. As the level increases, the oscillation becomes smoother with frequency becoming lower and lower. So we infer that the valence and arousal of emotion relate more tightly to high frequency. It is also coincided with the finding in [26] that Beta (16–32 Hz) and Gamma (32–64 Hz) bands are successfully selected more often than other bands. These two bands are higher frequency subbands of EEG signals.

So combining the results of classification accuracy and t-test, in practical use, we just need to extract features from IMF1, which will save vast time and relieve computation burden because only one level of EMD decomposition needed to be done.

3.3. Channel Reduction for Feature Extraction. Form verification in Section 3.2, we know that using component IMF1 will achieve good performance. In this subsection, we will investigate which electrodes are informative based on EMD strategy.

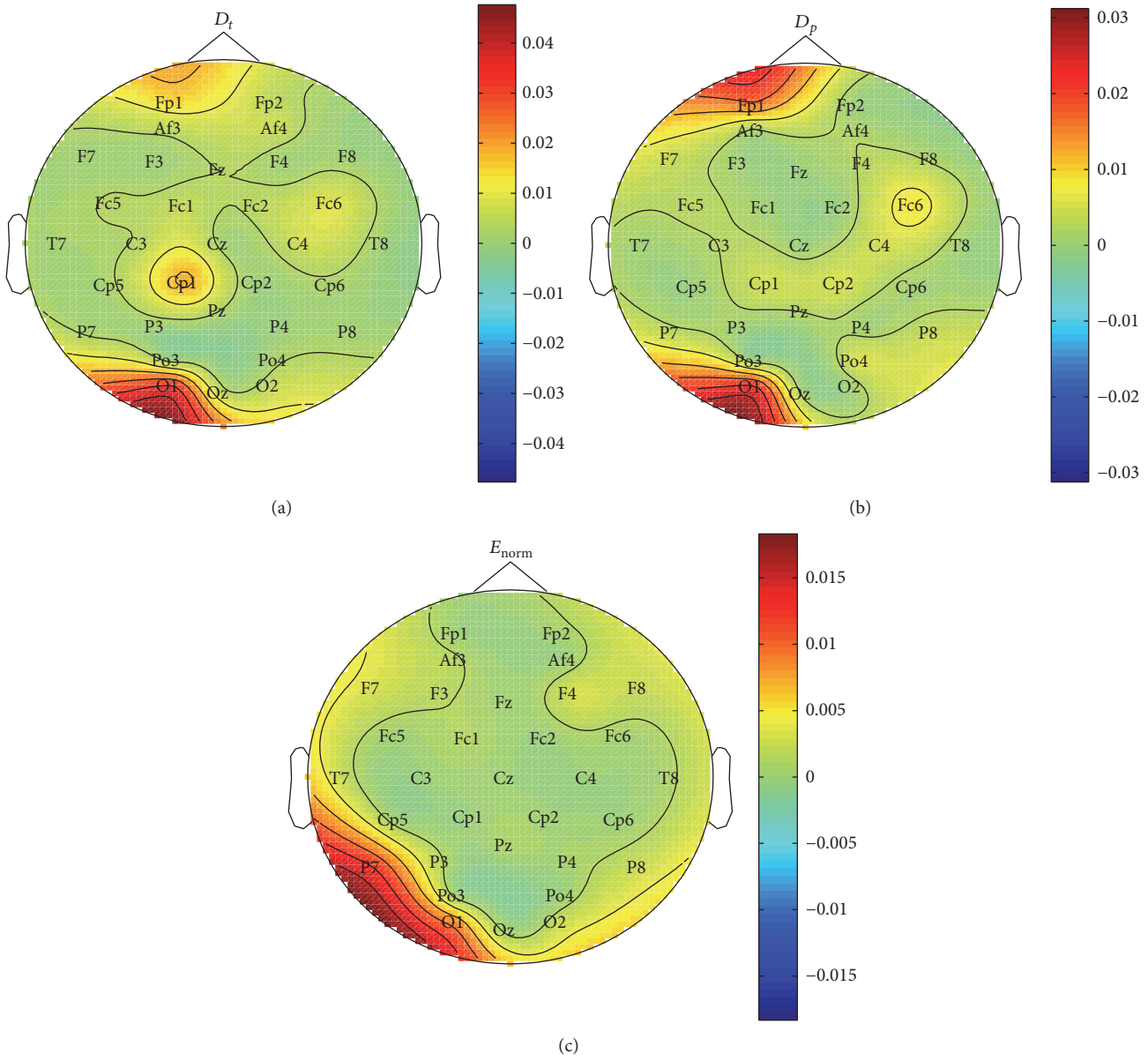

FIGURE 4: Fisher distance of different channels with subject 1. Features are extracted from component IMF1. For each channel, Fisher distance is calculated among features extracted from 480 labeled emotion samples of subject 1. (a) Fisher distance under feature D_t. (b) Fisher distance under feature D_p. (c) Fisher distance under feature E_{norm}.

Fisher distance is an efficient criterion of divisibility between two classes, which is broadly used in pattern recognition. It computes the ratio of between-class scatter degree and within-class scatter degree between two classes. Larger ratio means larger divisibility of the two classes. In our experiment, we used fisher distance to mark important electrodes under condition that IMF1 is used for feature extraction. For each channel, fisher distance is calculated among features extracted from one subject's total 480 labeled emotion samples.

Figure 4 gives fisher distance on valence dimension with subject 1. Figure 4(a) shows that, under feature D_t, electrodes Fp1, Fp2, FC6, Cp1, O1, and Oz have larger values. Figure 4(b) shows that, under feature D_p, Fp1, FC6, Cp1, Cp2, O1, Oz, P7, and P8 have larger values. Figure 4(c) shows that, under feature E_{norm}, F7, F8, T7, T8, P7, P8, O1, O2, and Oz have larger values.

Based on the analysis of all the subjects, we selected the following 8 electrodes Fp1, Fp2, F7, F8, T7, T8, P7, and P8 for channel reduction verification. Table 2 gives $F1$ score and classification accuracy with 8 channels selected for emotion recognition. We see that $F1$ score is 0.7374 for valence and 0.7769 for arousal. The classification accuracy with 8 channels is 69.10% for valence and 71.99% for arousal, slightly lower than accuracy with total 32 channels. We also applied t-test to examine whether the performance of 8 channels is similar

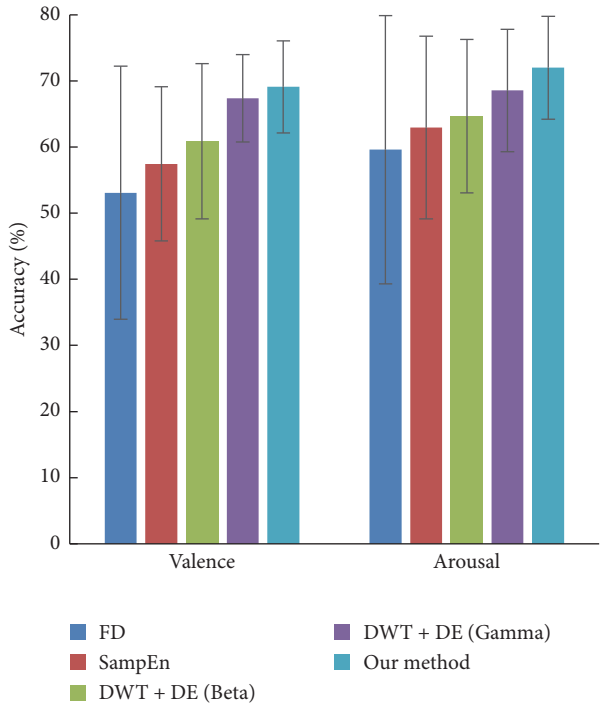

Figure 5: Classification accuracies of different methods. "FD," "SampEn," and "DE" in the figure are corresponding to fractal dimension, sample entropy, and differential entropy, respectively. The mean accuracy was computed among all the subjects. Error bars show the standard deviation of the mean accuracies across all subjects.

to total 32 channels. The null hypothesis is "the performance is similar" and if p value is larger than α, the null hypothesis is accepted. The t-test result shows that the performance under 8 channels and 32 channels is similar, with $p = 0.4194$ for valence and $p = 0.9521$ for arousal.

So in practical use, we just need to extract features from IMF1 with 8 channels. Our offline experiment used every 5 s EEG signals as a labeled emotion sample. This infers that our method may provide a new solution for real-time emotion recognition in BCI systems.

3.4. Results Comparison with Other Methods. In this subsection, we compared our proposed method with some classical methods, including fractal dimension (FD), sample entropy, differential entropy, and time-frequency analysis DWT. We used box counting for fractal dimension calculating. The parameter for sample entropy SampEn(m, r, N) was set as $r = 0.2$, $m = 2$, and $N = 128$. We used "db4" decomposition to realize DWT. Then the differential entropy of Beta (16–32 Hz) and Gamma (32–64 Hz) bands is extracted as features. Our method used IMF1 for feature extraction of D_t, D_p, and E_{norm}. For all the methods, 8 selected channels FP1, FP2, F7, F8, T7, T8, P7, and P8 are used for feature extraction.

From Figure 5 and Table 3, we see that our method yields the highest accuracy, 69.10% for valence and 71.99% for arousal. We applied t-test ($\alpha < 0.05$) to examine the performance between classical method and our method. The null hypothesis is "the performance is similar" and if p value is larger than α, the null hypothesis is accepted. The results of t-test in Table 3 show that the performance of our method is more splendid than fractal dimension, sample entropy, and differential entropy of Beta band with p far less than 0.05. It also shows that the performance of our method is similar and better than the differential entropy of Gamma band.

EMD strategy outperforms time domain method, including fractal dimension and sample entropy. This is because compared to methods in time domain, EMD has the advantage of utilizing more oscillation information. Compared to time-frequency method DWT, EMD can decompose EEG signals automatically, getting rid of selecting transform window first. The classification accuracy is also higher than DWT. So the experiment results infer that our method based on EMD strategy is suitable for emotion recognition from EEG signals.

4. Discussion

Emotion recognition from EEG signals has achieved significant progress in recent years. Previous methods are usually conducted in time domain, frequency domain, and time-frequency domain. In this paper, we propose a method of feature extraction for emotion recognition in EMD domain, a new aspect of view. By utilizing EMD, EEG signals can be decomposed into different oscillation components named IMF automatically. The characteristics of IMF are utilized as features for emotion recognition, including the first difference of time series, the first difference of phase, and the normalized energy.

Compared to methods in time domain, EMD has the advantage of utilizing more frequency information. The experiment results show that the proposed method outperforms method in time domain, such as fractal dimension in [3, 4] and sample entropy in [5]. Compared to time-frequency methods, such as STFT and DWT, EMD can decompose EEG signals automatically, getting rid of selecting transform window first. The classification accuracy is also higher than DWT in [18].

We investigate the role of each IMF in emotion classification. Features extracted from IMF1 yield the highest accuracy. IMF1 is corresponding to the fastest changing component of EEG signals, so our study confirms the deduction that emotion is more relative to high frequency component. This consists with findings in [26] that Beta (16–32 Hz) and Gamma (32–64 Hz) bands are successfully selected more often than other bands.

Finally, we selected 8 informative channels based on EMD strategy, namely, FP1, FP2, F7, F8, T7, T8, P7, and P8. Our proposed method just needs to extract features from IMF1 with 8 channels, which will save time and relieve computation burden. Also in our experiment, every 5 s EEG signals are extracted as a sample, so it may provide a new solution for real-time emotion recognition in BCI systems.

Our limitation is that now we just test it on DEAP dataset, so in the future we want to experiment it on more emotional datasets to verify the method comprehensively. Also we will

Table 3: The mean accuracy of different kinds of methods (Fp1, Fp2, F7, F8, T7, T8, P7, and P8) (standard deviation shown in parentheses; statistical analysis shown in column t-test).

Methods	Valence		Arousal	
	Accuracy (%)	t-test (our method)	Accuracy (%)	t-test (our method)
Fractal dimension	53.08 (19.14)	$p = 0$	59.61 (20.28)	$p = 0.0034$
Sample entropy	57.44 (11.66)	$p = 0$	62.96 (13.82)	$p = 0.0024$
DWT + differential entropy (Beta)	60.87 (11.74)	$p = 0.0013$	64.66 (11.59)	$p = 0.0048$
DWT + differential entropy (Gamma)	67.36 (6.61)	$p = 0.3185$	68.55 (9.28)	$p = 0.1189$
Our method	69.10 (6.95)	$p = 1$	71.99 (7.77)	$p = 1$

utilize more strategies such as feature smoothing and deep network to improve the classification accuracy.

5. Conclusion

In this paper, an emotion recognition method based on EMD using three statistics is proposed. An extensive analysis has been carried out to investigate the effectiveness of the features for emotion classification. The results show that the three features are suitable for emotion recognition. Then the effect of each IMF component is inquired. The results reveal that, among the multilevel IMFs, the first component IMF1 plays the most important role in emotion recognition. Also the informative channels based on EMD strategy are investigated and 8 channels, namely, FP1, FP2, F7, F8, T7, T8, P7, and P8, are selected for feature extraction. Finally, the proposed method is compared with some classical methods and our method yields the highest accuracy.

Conflicts of Interest

The authors declare that there are no conflicts of interest regarding the publication of this paper.

Acknowledgments

This work was supported by the grant from the National Natural Science Foundation of China (Grant no. 61701089).

References

[1] C.-H. Han, J.-H. Lim, J.-H. Lee, K. Kim, and C.-H. Im, "Data-driven user feedback: an improved neurofeedback strategy considering the interindividual variability of EEG features," *BioMed Research International*, vol. 2016, Article ID 3939815, 7 pages, 2016.

[2] K. Takahashi, "Remarks on emotion recognition from multi-modal bio-potential signals," in *Proceedings of the 2004 IEEE International Conference on Industrial Technology*, pp. 1138–1143, Hammamet, Tunisia, December 2004.

[3] O. Sourina and Y. Liu, "A fractal-based algorithm of emotion recognition from EEG using arousal-valence model," in *Proceedings of the International Conference on Bio-Inspired Systems and Signal Processing, BIOSIGNALS 2011*, pp. 209–214, Rome, Italy, January 2011.

[4] Y. Liu and O. Sourina, "Real-time subject-dependent EEG-based emotion recognition algorithm," *Lecture Notes in Computer Science (including subseries Lecture Notes in Artificial Intelligence and Lecture Notes in Bioinformatics)*, vol. 8490, pp. 199–223, 2014.

[5] X. Jie, R. Cao, and L. Li, "Emotion recognition based on the sample entropy of EEG," *Bio-Medical Marerials and Engineering*, vol. 24, no. 1, pp. 1185–1192, 2014.

[6] E. Kroupi, A. Yazdani, and T. Ebrahimi, "EEG correlates of different emotional states elicited during watching music videos," in *in Procceding of the 2011 Interntionnal Conference on Affective Computing*, pp. 457–466, Memphis, TN, USA, 2011.

[7] B. Hjorth, "EEG analysis based on time domain properties," *Electroencephalography and Clinical Neurophysiology*, vol. 29, no. 3, pp. 306–310, 1970.

[8] K. Ansari-Asl, G. Chanel, and T. Pun, "A channel selection method for EEG classification in emotion assessment based on synchronization likelihood," in *Proceedings of the 15th European Signal Processing Conference, EUSIPCO 2007*, pp. 1241–1245, Pozna, Poland, September 2007.

[9] R. Horlings, D. Datcu, and L. J. M. Rothkrantz, "Emotion recognition using brain activity," in *Proceedings of the International Conference on Computer Systems and Technology*, vol. 25, pp. 1–6, New York, NY, USA, 2008.

[10] P. C. Petrantonakis and L. J. Hadjileontiadis, "Emotion recognition from EEG using higher order crossings," *IEEE Transactions on Information Technology in Biomedicine*, vol. 14, no. 2, pp. 186–197, 2010.

[11] X. W. Wang, D. Nie, and B. L. Lu, "EEG-based emotion recognition using frequency domain features and support vector machines," in *in Procceding of the International Conference on Neural Information Processing*, pp. 734–743, Guangzhou, China, 2011.

[12] R.-N. Duan, J.-Y. Zhu, and B.-L. Lu, "Differential entropy feature for EEG-based emotion classification," in *Proceedings of the 2013 6th International IEEE EMBS Conference on Neural Engineering, NER 2013*, pp. 81–84, New Jersey, NJ, USA, November 2013.

[13] G. Chanel, K. Ansari-Asl, and T. Pun, "Valence-arousal evaluation using physiological signals in an emotion recall paradigm," in *Proceedings of the 2007 IEEE International Conference on Systems, Man, and Cybernetics, SMC 2007*, pp. 2662–2667, Halifax, NS, Canada, October 2007.

[14] Y.-P. Lin, C.-H. Wang, T.-P. Jung et al., "EEG-based emotion recognition in music listening," *IEEE Transactions on Biomedical Engineering*, vol. 57, no. 7, pp. 1798–1806, 2010.

[15] S. K. Hadjidimitriou and L. J. Hadjileontiadis, "Toward an EEG-based recognition of music liking using time-frequency analysis," *IEEE Transactions on Biomedical Engineering*, vol. 59, no. 12, pp. 3498–3510, 2012.

[16] S. S. Uzun, S. Yildirim, and E. Yildirim, "Emotion primitives estimation from EEG signals using Hilbert Huang Transform," in *Proceedings of the IEEE-EMBS International Conference on Biomedical and Health Informatics*, pp. 224–227, Hong Kong, China, January 2012.

[17] M. Murugappan, M. Rizon, R. Nagarajan, and S. Yaacob, "EEG feature extraction for classifying emotions using FCM and FKM," in *Proceedings of the International Conference on Applied Computer and Applied Computational Science*, vol. 1, pp. 21–25, Venice, Italy, 2007.

[18] Z. Mohammadi, J. Frounchi, and M. Amiri, "Wavelet-based emotion recognition system using EEG signal," *Neural Computing and Applications*, pp. 1–6, 2016.

[19] M. Murugappan, "Human emotion classification using wavelet transform and KNN," in *Proceedings of the 2011 International Conference on Pattern Analysis and Intelligent Robotics, (ICPAIR '11)*, vol. 1, pp. 148–153, Putrajaya, Malaysia, June 2011.

[20] S. Koelstra, C. Mühl, M. Soleymani et al., "DEAP: a database for emotion analysis; using physiological signals," *IEEE Transactions on Affective Computing*, vol. 3, no. 1, pp. 18–31, 2012.

[21] I. Wichakam and P. Vateekul, "An evaluation of feature extraction in EEG-based emotion prediction with support vector machines," in *Proceedings of the 2014 11th International Joint Conference on Computer Science and Software Engineering (JCSSE '14)*, pp. 106–110, Chon Buri, Thailand, May 2014.

[22] B. Reuderink, C. Mühl, and M. Poel, "Valence, arousal and dominance in the EEG during game play," *International Journal of Autonomous and Adaptive Communications Systems*, vol. 6, no. 1, pp. 45–62, 2013.

[23] L. Brown, B. Grundlehner, and J. Penders, "Towards wireless emotional valence detection from EEG," in *Proceedings of the 33rd Annual International Conference of the IEEE Engineering in Medicine and Biology Society, EMBS 2011*, pp. 2188–2191, Boston, MA, USA, September 2011.

[24] V. Rozgic, S. N. Vitaladevuni, and R. Prasad, "Robust EEG emotion classification using segment level decision fusion," in *Proceedings of the 2013 38th IEEE International Conference on Acoustics, Speech, and Signal Processing, ICASSP 2013*, pp. 1286–1290, Vancouver, BC, Canada, May 2013.

[25] R. Gupta, K. U. R. Laghari, and T. H. Falk, "Relevance vector classifier decision fusion and EEG graph-theoretic features for automatic affective state characterization," *Neurocomputing*, vol. 174, pp. 875–884, 2016.

[26] R. Jenke, A. Peer, and M. Buss, "Feature extraction and selection for emotion recognition from EEG," *IEEE Transactions on Affective Computing*, vol. 5, no. 3, pp. 327–339, 2014.

[27] W.-L. Zheng and B.-L. Lu, "Investigating critical frequency bands and channels for eeg-based emotion recognition with deep neural networks," *IEEE Transactions on Autonomous Mental Development*, vol. 7, no. 3, pp. 162–175, 2015.

[28] Y. Yang, Q. M. J. Wu, W. L. Zheng, and B. L. Lu, "EEG-based emotion recognition using hierarchical network with subnetwork nodes," *IEEE Transactions on Cognitive Developmental Systems*, vol. PP, no. 99, p. 1, 2017.

[29] N. E. Huang, Z. Shen, S. R. Long et al., "The empirical mode decomposition and the hilbert spectrum for nonlinear and non-stationary time series analysis," in *Proceedings of the Proceedings Mathematical Physical and Engineering Sciences*, vol. 454, pp. 903–995, 1998.

[30] S. M. S. Alam and M. I. H. Bhuiyan, "Detection of seizure and epilepsy using higher order statistics in the EMD domain," *IEEE Journal of Biomedical and Health Informatics*, vol. 17, no. 2, pp. 312–318, 2013.

[31] R. B. Pachori and V. Bajaj, "Analysis of normal and epileptic seizure EEG signals using empirical mode decomposition," *Computer Methods and Programs in Biomedicine*, vol. 104, no. 3, pp. 373–381, 2011.

[32] S. Li, W. Zhou, Q. Yuan, S. Geng, and D. Cai, "Feature extraction and recognition of ictal EEG using EMD and SVM," *Computers in Biology and Medicine*, vol. 43, no. 7, pp. 807–816, 2013.

[33] A. Mert and A. Akan, "Emotion recognition from EEG signals by using multivariate empirical mode decomposition," *Pattern Analysis and Applications*, pp. 1–9, 2016.

[34] K. Takahashi, "Remarks on emotion recognition from multi-modal bio-potential signals," in *Proceedings of the 2004 IEEE International Conference on Industrial Technology, 2004 (IEEE ICIT '04)*, pp. 1138–1143, Hammemet, Tunsia.

[35] G. Chanel, J. Kronegg, D. Grandjean, and T. Pun, "Emotion assessment: arousal evaluation using eegs and peripheral physiological signals," in *in procceding of the International Workshop on Multimedia Content Representation, Classification and Security*, pp. 530–537, Istanbul, Turkey, 2006.

[36] C. C. Chang and C. J. Lin, "LIBSVM: A library for support vector machines," *Acm Transactions on Intelligent Systems Technology*, vol. 2, no. 3, p. 27, 2007.

Hindawi
BioMed Research International
Volume 2017, Article ID 2049094, 12 pages
https://doi.org/10.1155/2017/2049094

Research Article

Multirapid Serial Visual Presentation Framework for EEG-Based Target Detection

Zhimin Lin,[1] Ying Zeng,[1,2] Hui Gao,[1] Li Tong,[1] Chi Zhang,[1] Xiaojuan Wang,[1] Qunjian Wu,[1] and Bin Yan[1]

[1]*China National Digital Switching System Engineering and Technological Research Center, Zhengzhou, China*
[2]*Key Laboratory for Neuroinformation of Ministry of Education, School of Life Science and Technology, University of Electronic Science and Technology of China, Chengdu, China*

Correspondence should be addressed to Bin Yan; ybspace@hotmail.com

Received 15 March 2017; Accepted 22 May 2017; Published 20 July 2017

Academic Editor: Pedro P. R. Filho

Target image detection based on a rapid serial visual presentation (RSVP) paradigm is a typical brain-computer interface system with various applications, such as image retrieval. In an RSVP paradigm, a P300 component is detected to determine target images. This strategy requires high-precision single-trial P300 detection methods. However, the performance of single-trial detection methods is relatively lower than that of multitrial P300 detection methods. Image retrieval based on multitrial P300 is a new research direction. In this paper, we propose a triple-RSVP paradigm with three images being presented simultaneously and a target image appearing three times. Thus, multitrial P300 classification methods can be used to improve detection accuracy. In this study, these mechanisms were extended and validated, and the characteristics of the multi-RSVP framework were further explored. Two different P300 detection algorithms were also utilized in multi-RSVP to demonstrate that the scheme is universally applicable. Results revealed that the detection accuracy of the multi-RSVP paradigm was higher than that of the standard RSVP paradigm. The results validate the effectiveness of the proposed method, and this method can provide a whole new idea in the field of EEG-based target detection.

1. Introduction

A brain-computer interface (BCI) is an advanced human-machine interaction technology that uses a person's electroencephalogram (EEG) and analyzes his/her intentions to interact with the external environment directly. Target image detection based on a rapid serial visual presentation (RSVP) paradigm is a typical BCI application [1, 2].

In the RSVP paradigm, a rapid sequence of images, such as four images per second, is sequentially presented to participants in the same location. As these participants see the target image, they likely induce a special P300 component. The P300 component is a common event-related potential (ERP) component that shows a peak waveform when a small probability event is observed after 300–500 ms [3]. And the P300 component also exhibits significant waveform characteristics in the time domain [4]. Single-trial P300-based systems, such as target image detection based on the RSVP paradigm [1, 5], are commonly used for various BCIs. The P300 component is also detected in the RSVP paradigm to determine the target image of a subject of interest. A P300 detection algorithm is essential because it determines the accuracy and reliability of BCI systems. Farwell and Donchin [6] proposed P300 Speller and used a stepwise linear discriminant analysis (SWLDA) algorithm to detect P300 components. Krusienski et al. [7] compared the performances of various P300 detection algorithms and concluded that SWLDA and Fisher's linear discriminant (FDA) are suitable for the P300 Speller system.

In the RSVP paradigm, the latency and amplitude of P300 components may vary with different experimental parameters [8], such as target probability and stimulus semantics. This variation is a great challenge for single-trial EEG classification in RSVP tasks. To overcome this problem, many scholars proposed effective single-trial detection algorithms. For example, a common spatial pattern is an approach used to

search for spatial filters that maximize the variance across two categories [9], such as target and nontarget. Rivet et al. [10, 11] proposed the xDawn algorithm designed to maximize the difference in the signal-to-noise ratio between target and nontarget classes. Bigdely-Shamlo et al. [12] adopted spatial independent component analysis specifically for the single-trial classification of RSVP data to extract a set of spatial weights and obtain maximally independent spatial-temporal sources. Gerson et al. [13–16] proposed the hierarchical discriminant component analysis (HDCA) algorithm to separate single-trial EEG signals into several time windows and to calculate the spatial filter for each time window. Alpert et al. [17] proposed the hierarchical discriminant principal component analysis (HDPCA) algorithm, which introduces principal component analysis for dimensionality reduction. Marathe et al. [18, 19] developed the sliding HDCA (sHDCA) algorithm, which involves standard HDCA evaluation formulated in a typical P300 interval (300–600 ms), and a standard HDCA classifier is slid on single-trial EEG to form a score signal. With this special method of dimension reduction, the imperceptible variation latency of P300 in single-trial EEG data can adapt to the different conditions of subjects. However, the sHDCA algorithm is complex, and its computing speed is relatively slower than that of HDCA. Cecotti et al. [20] developed a spatiotemporal filter that uses the map matrix of a convolutional neural network classifier input layer to a second hidden layer. These algorithms are effective single-trial detection methods, and the target image is assumed to appear only once.

The robustness and stability of multitrial-based P300 component detection are valuable compared to those of single-trial detection [21]. BCI systems based on multitrial detection have been used for extensive applications, such as P300 Speller. However, in target detection application, obtaining images repeatedly is inappropriate for the RSVP paradigm because this method is time-consuming and unconducive to real-time target detection. To solve this problem, Cecotti [22] proposed a dual-RSVP paradigm for target recognition and obtained good results from magnetoencephalography (MEG) data. In dual-RSVP paradigm, two image sequences are simultaneously presented on a screen. One of the image sequences is generated by another image sequence that is delayed for a certain time; hence, the image can appear twice. In this paper, we verified the feasibility of the dual-RSVP paradigm proposed by Cecotti in EEG data and further proposed a triple-RSVP paradigm. In the triple-RSVP paradigm, images can appear thrice in the left, right, and bottom sides of the screen.

On the basis of previously described methods and paradigms, we characterized the components of a multi-RSVP paradigm and revealed their contributions to improve P300 detection accuracy in EEG responses. In this study, the P300 response mechanism in the multi-RSVP framework was revealed and possible problems related to quadruple-RSVP or more conditions were discussed for further improvement. In our experiments, two different P300 detection algorithms were used to demonstrate that the proposed multi-RSVP framework works valuably compared to the traditional RSVP paradigm for EEG-based target detection.

The remaining parts of this paper are organized as follows. First, we present the general rationale for the target detection in the RSVP paradigm. Second, we discuss the specific visual stimulus methods used in this study. Third, we describe the experimental methods. Fourth, we show the classification methods and performance evaluation metrics. Finally, we interpret the results.

2. Methods

2.1. Visual Stimuli and Procedure. The participants were seated at 75 cm from a monitor. Images were selected from the ILSVRC15 [23], and the types of images include architecture, birds, artifacts, fruits, aquatic organisms, and natural scenes. The target image category was architecture. These images were presented to the subjects under the dual-RSVP and triple-RSVP paradigms (Figure 1).

Dual-RSVP is a novel experimental paradigm with target detection proposed by Cecotti [22]; the image sequence shown on the left side was presented again on the right side of screen after a certain delay (Figures 2(a) and 2(b)). The subjects gazed at the image stream on the left side until the target image was presented. The subjects then shifted their attention to look at the image stream on right side until the same target was presented. Finally, the subjects focused their attention back to the left side (Figure 3(a)). Cecotti applied this method in the MEG data and achieved good results. In this paper, we propose an improved form of dual-RSVP: triple-RSVP. Similarly, the triple-RSVP simultaneously presents three images (Figure 1(b)). The right images are formed by delaying the left images for a short period of time, and the bottom images are formed by delaying the right images for a period of time (delaying the left images for longer time, Figures 2(a)–2(c)). The subject first looks at the left side, then at the right side, and finally at the bottom side; when the target image is noticed, the subject finally diverts his/her attention back to the left side (Figure 3(b)). In dual-RSVP or triple-RSVP paradigm, the same target image repeatedly appears, and some images are missed in the process of diversion. The probability of the continuous appearance for some target images is small, and the missed images mainly are nontargets. Therefore, the RSVP sequence does not show this condition in our design.

The images were shown in blocks of 200 and flashed at 4 Hz. For these tasks, the RSVP sequence consists of 10 blocks (2000 images, i.e., 200 target images and 1800 nontarget images). Each block consists of 20 target images and 180 nontarget images. We set the left image sequence delay time to 750 ms (three images) and the bottom image sequence delay time to 1500 ms (six images), respectively.

2.2. Participants. In this paper, two independent experiments were performed, namely, target detections in dual-RSVP and triple-RSVP paradigms. Seven subjects participated in the dual-RSVP paradigm (two females and five males, mean age 20.6 years, standard deviation 1.3 years). Eight subjects participated in the triple-RSVP paradigm (one female and seven males, mean age 20.2, standard deviation 0.8 years); this is shown in Table 1. All of the subjects were students

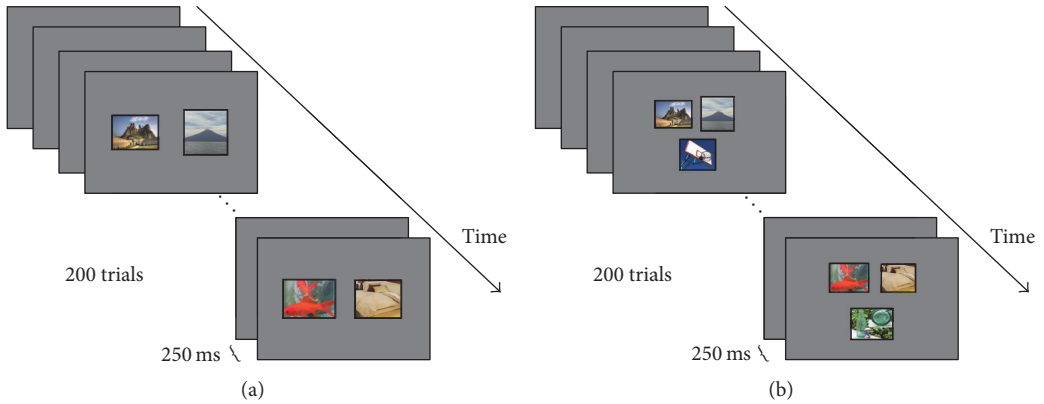

FIGURE 1: (a) Dual-RSVP: two images were simultaneously presented at the screen left side and right side. (b) Triple-RSVP: three images were simultaneously presented at the screen left, right, and bottom sides. The images were shown in blocks of 200 and flashed at 4 Hz (250 ms).

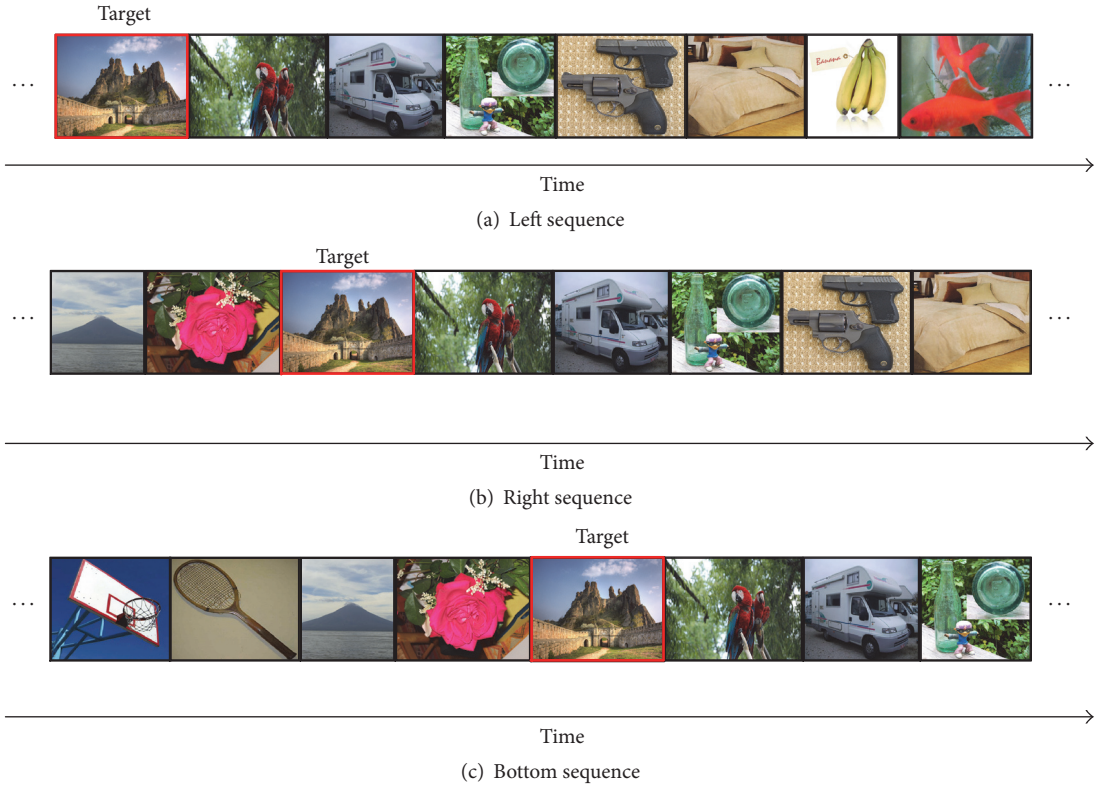

FIGURE 2: (a) Original image sequence was presented to the left side of the screen. (b) Delayed image sequence was displayed on the right side of screen. (c) Longer delayed image appeared on the bottom side of screen. The dual-RSVP includes (a) and (b). The triple-RSVP includes (a), (b), and (c).

of Zhengzhou University without previous training in the task. The subjects exhibited normal or corrected-to-normal vision with no neurological problems and were financially compensated for their participation.

2.3. EEG Acquisition and Preprocessing. EEG data were acquired by a g.USBamp system (G.Tec company) using 16 electrodes distributed in accordance with the international 10–20 system. In this experiment, the electrooculographic (EOG) will be introduced, because the subjects were asked to transfer the line of sight, when the subjects see the target. In order to ensure the accuracy of the experimental results, we need to remove the eye artifacts before analyzing the data. The EOG activity was recorded by two electrodes positioned above and below the left eye. We collected a group EOC samples before the experiment and implemented the EOC artifact removal by using the method proposed by Zhang et al. [24, 25].

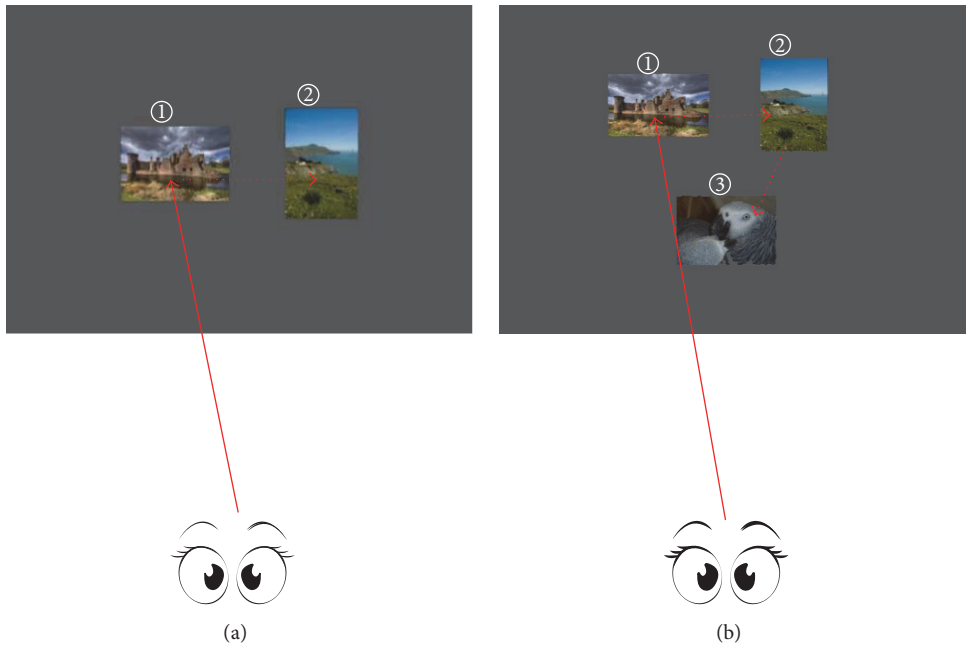

Figure 3: (a) Dual-RSVP: first, the subjects focused on the left image sequence until the target image appeared. The subjects' attention was diverted to the right image sequence until the same target image appeared on this side. Finally, the attention was diverted back to the left side. (b) Similar to (a), however, the difference is that the subjects' attention should be diverted to the bottom side.

Table 1: The human subjects information.

Experiment	Number of participants	Average age	Standard deviation
Dual-RSVP	7 (2 female and 5 male)	20.6	1.3
Triple-RSVP	8 (1 female and 7 male)	20.2	0.8

The EEG data were sampled at 2400 Hz using 200 Hz low-pass and 50 Hz notch filters. Prior to scoring the images, we preprocessed the EEG data through the following steps: band-pass filtering (0.5–60 Hz), downsampling to 600 Hz, and baseline correction. Afterwards, the EEG data were divided into epochs of 1000 ms after the stimulus onset.

2.4. EEG Analysis. To evaluate the effectiveness of the proposed method, we used the SWLDA and HDCA algorithms to analyze the EEG data. The SWLDA algorithm is a traditional and effective P300 detection algorithm. Farwell and Donchin [6] used the SWLDA algorithm to build the first P300 Speller, and Krusienski et al. [7] reported that SWLDA is the most effective early method of P300 detection. The HDCA algorithm is a new method of P300 detection in the RSVP experiment described by Gerson et al. [13–16]. Many scholars proposed various improved algorithms based on HDCA. The results for SWLDA and HDCA algorithms are a final interest score of each image. We averaged the interest score of the same image in different image sequences (left, right, and bottom sequences). We specified a threshold greater than the threshold value, that is, the target image.

2.4.1. SWLDA Algorithm. The SWLDA algorithm is a feature reduction algorithm that selects suitable features to be included in the discriminant function. The input features are weighted through least square regression to predict the target class labels. First, the most statistically significant initial feature was added to the discriminant function. After each new entry to the discriminant function, a backward stepwise analysis was performed to remove the least significant input features. This process was repeated until no remaining feature satisfies the inclusion/exclusion criteria.

In this paper, the EEG data were divided into epochs. Each epoch consists of 1000 ms EEG data. Epochs corresponding to a certain image were concatenated by each channel to construct a feature vector (14 channels and 60 sample points of each channel; a total of 840 points in a feature vector). We classified the feature vectors by SWLDA and calculated the score for each image.

2.4.2. HDCA Algorithm. The HDCA algorithm was divided into two layers. First, the HDCA algorithm was used to calculate the average data and divide the original EEG data by the time window size. The weight of each channel was then calculated in each time window to maximize the differences between the target and nontarget classes, such as in

$$y_k = \left(\frac{1}{N}\right) \sum_n \sum_i w_{ki} x_{i[(k-1)N+n]}, \quad (1)$$

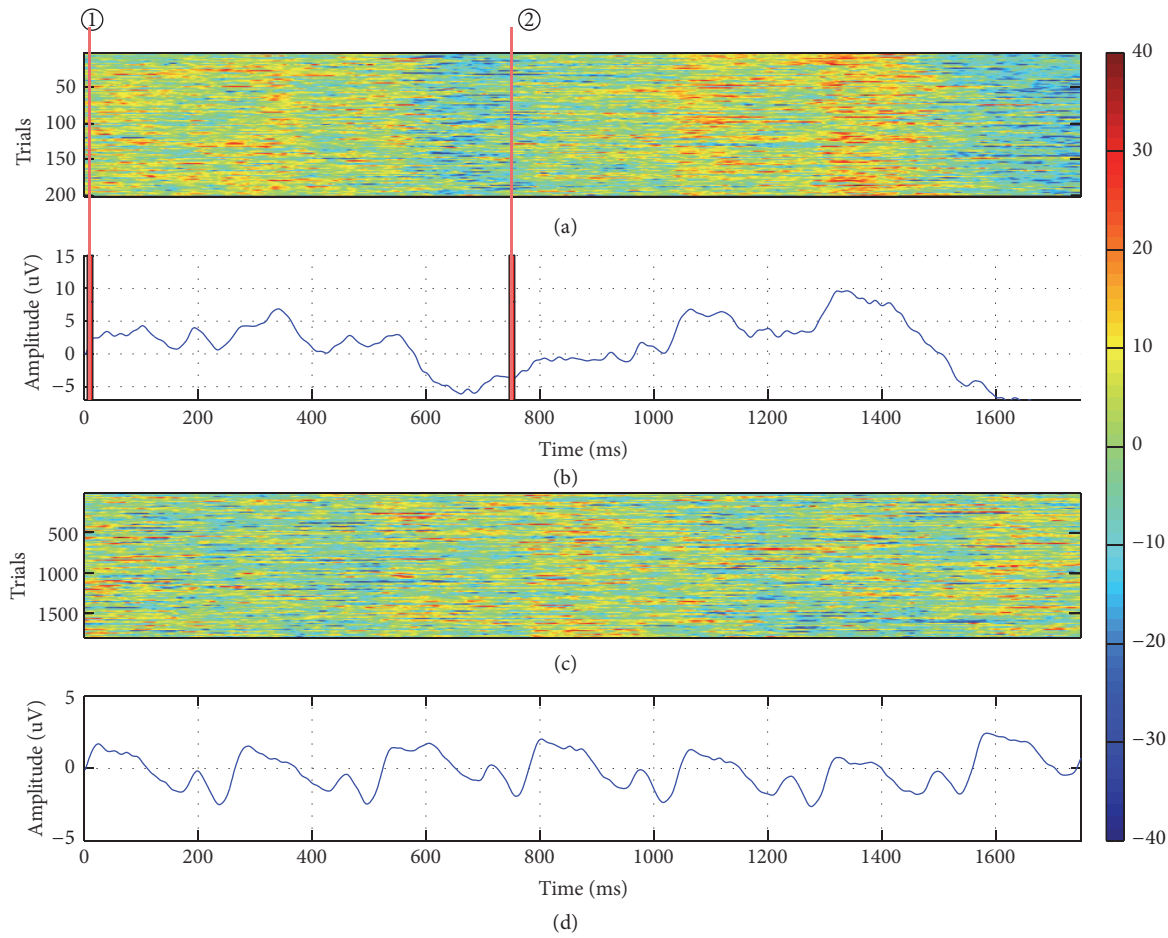

Figure 4: ERP induced by dual-RSVP. (a) All single-trial ERPs to target images at electrode Pz. (b) Grand averages across all trials of the target EEG signals at electrode Pz. (c) All single-trial ERPs to nontarget images at electrode Pz. (d) Grand averages across all trials of the nontarget EEG signals at electrode Pz. The red line ① marked on (a) and (b) is the time point of the first appearance of the target image on the left side, whereas the red line ② is the time point when the target image appeared again on the right side of the screen.

where $x_{i[(k-1)N+n]}$ represents the kth separate time window value from the single-trial data. The variable corresponds to the EEG activity at the data sample point n measured by electrode i. w is a set of spatial weights. Weight vector w_{ki} is found for the kth window and i electrode following each image presentation (T is the temporal resolution of the time window and in this paper is 0.025, N is the sampling time point of the time window, F_S is the sampling rate, K is the number of time windows, and $n = 1, 2, \ldots, N$, $N = T \times F_S$, $0 \le k \le K$). And y_k is the signal after reduced dimension in kth separate time window. In our study, the time window size cannot be determined in advance. Thus, we chose 25 ms as the time window size after numerous experimental repetitions. The weight of each channel in each time window was calculated by Fisher's linear discriminant (FLD).

$$y_{\mathrm{IS}} = \sum_k v_k y_k. \tag{2}$$

The results for the separate time windows (y_k) were then combined in a weighted y_k average to provide a final interest score (y_{IS}) for each image. FLD analysis was used to calculate the spatial coefficient w_{ki}, and logistic regression was adopted to calculate for the temporal coefficient v_k, such as in (2).

In this paper, the time window size is 25 ms, $k = 40$.

2.5. Evaluation of the Algorithm Performance. A tenfold cross-validation was conducted to determine the accuracy of all classification algorithms applied to the EEG data. Performance was evaluated based on the area under the receiver operating characteristic (ROC) curve (AUC) [26].

3. Results

3.1. Event-Related Responses. Figure 4 shows the grand mean waveform and all single-trial ERPs induced by dual-RSVP for a specific subject. The x-axis is the time of the waveform, and the selected time range is 1750 ms after the first appearance of the target. The target appears twice during this period and thus produces two P300 components. The red line marked on Figures 4(a) and 4(b) is the time point of the target image in the left and right sides of screen, respectively, with the delay of 750 ms (three images). Similarly, Figure 5 shows the grand

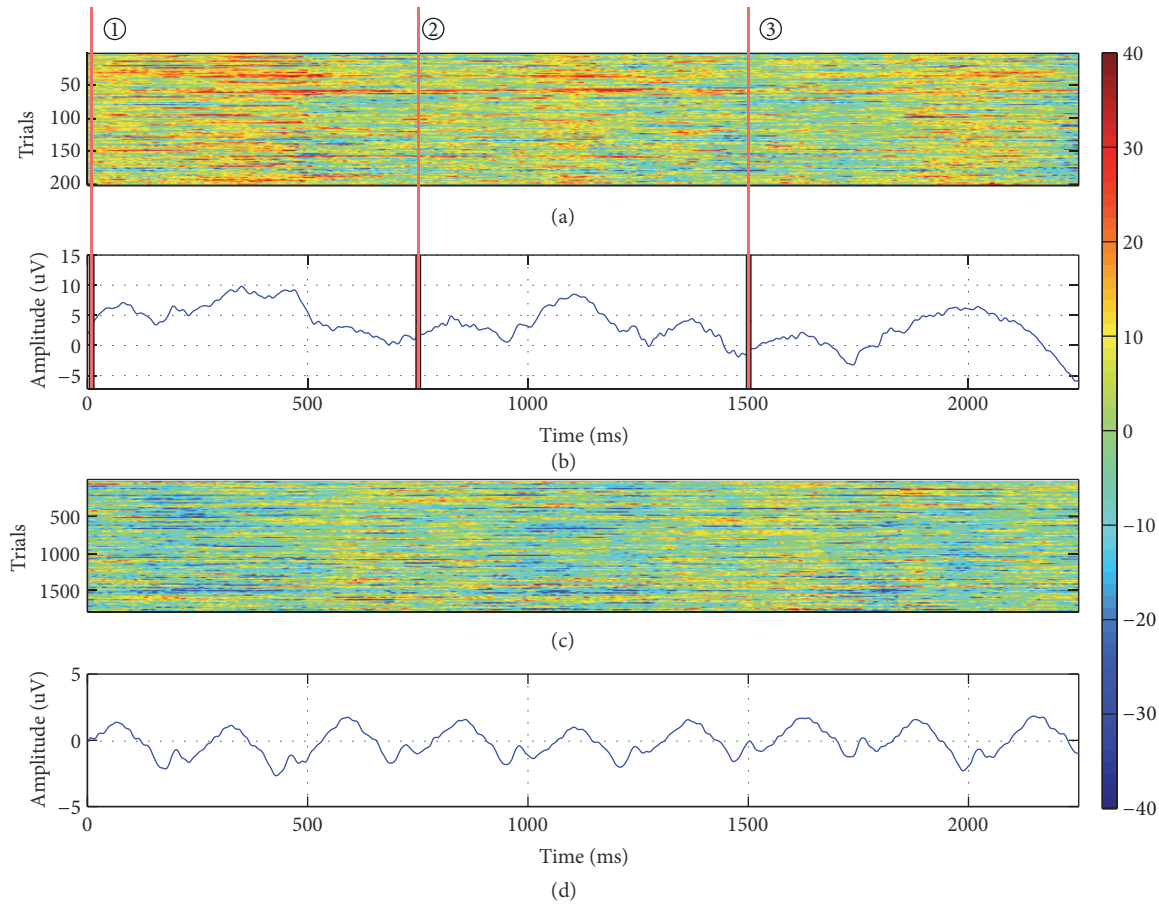

Figure 5: ERP induced by triple-RSVP. (a) All single-trial ERPs to target images at electrode Pz. (b) Grand averages across all trials of the target EEG signals at electrode Pz. (c) All single-trial ERPs to nontarget images at electrode Pz. (d) Grand averages across all trials of the nontarget EEG signals at electrode Pz. The red line ① marked on (a) and (b) is the time point of the first appearance of the target image on the left side, the red line ② is the time point when the target image appeared again on the right side, and the red line ③ is the time point when the target image finally appeared on the bottom side of the screen.

mean waveform and all single-trial ERPs induced by triple-RSVP in another subject. Three distinct P300 compositions are shown in Figure 5(b), and the x-axis time range is 2250 ms after the first appearance of the target. These findings indicate that dual-RSVP and triple-RSVP are valid for P300 and are effective in inducing P300 constituents in the EEG background.

Figure 6 further shows the observed brain topography for the target image under the dual-RSVP and triple-RSVP paradigms. Figure 6(a) shows the dual-RSVP paradigm under the brain topographic map for different time trends. The target image first appeared on the screen left side at 0 ms, followed by the second appearance at 750 ms on the screen right side. In Figure 6(a), a significant P300 activity was observed at 300 and 1050 ms (300 ms after the target occurrence). Similarly, Figure 6(b) shows the triple-RSVP paradigm under the brain topographic map for different time trends. The target image first appeared on the screen left side at 0 ms, followed by the second appearance at 750 ms on the screen right side, and lastly at 1500 ms on the screen bottom side. In Figure 6(b), a P300 component was observed at 300, 1050, and between 1800 and 1950 ms.

3.2. Dual-RSVP and Triple-RSVP Performance. We used the AUC value to evaluate the performance of the dual-RSVP and triple-RSVP paradigms. In the dual-RSVP paradigm, we compared the AUC values of the left image sequence EEG score (single-RSVP score) and the combination of the EEG scores from the left and right image sequences (dual-RSVP score) using the HDCA and SWLDA algorithms. Similarly, in the triple-RSVP paradigm, we compared the AUC values of the left image sequence EEG score (single-RSVP score), the combination of the EEG scores from the left and right image sequences (dual-RSVP score), and the combination of the EEG scores from the left, right, and bottom image sequences (triple-RSVP score) using the HDCA and SWLDA algorithms.

Table 2 shows the comparison of AUC values in dual-RSVP paradigm and used the single- and dual-RSVP scores for the seven subjects. Across the subjects, the AUC values of

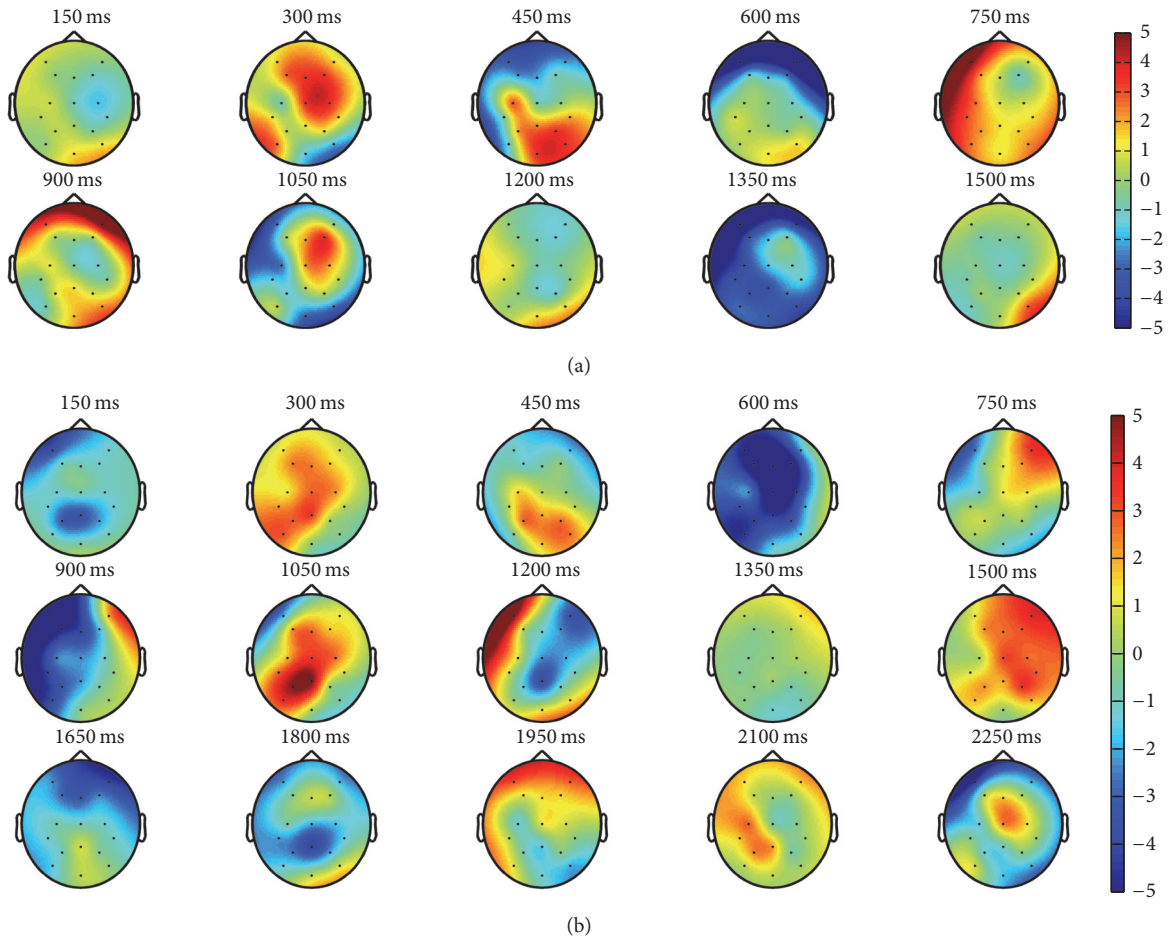

Figure 6: Brain topography induced by dual-RSVP and triple-RSVP. (a) Trend of brain topographic map changes under dual-RSVP paradigm. The target image appeared at 0 ms on the screen left side and at 750 ms on the screen right side, respectively. (b) Trend of brain topographic map changes under triple-RSVP paradigm. The target image appeared at 0 ms on the screen left side, at 750 ms on the screen right side, and at 1500 ms on the screen bottom side, respectively.

Table 2: Values of the AUC of all subjects under the dual-RSVP paradigm.

	Subjects	1	2	3	4	5	6	7	Mean	SD
Left RSVP only	HDCA	0.9294	0.7901	0.9019	0.8934	0.8813	0.8577	0.9205	0.8820	0.0471
	SWLD	0.8226	0.6917	0.7935	0.8021	0.8074	0.7615	0.8072	0.7837	0.0448
Combining with left and right RSVP	HDCA	**0.9486**	**0.8026**	**0.9409**	**0.9358**	**0.9211**	**0.8964**	**0.9583**	**0.9148**	0.0534
	SWLD	**0.8952**	**0.7293**	**0.8656**	**0.8725**	**0.8461**	**0.8268**	**0.9033**	**0.8484**	0.0588

single-RSVP score from the HDCA algorithm are in the range of 0.790–0.929 (mean: 0.882; std: 0.047). The AUC values of the dual-RSVP score from the HDCA algorithm are in the range of 0.803–0.958 (mean: 0.914; std: 0.053). The Wilcoxon signed rank test results are $p < 0.05$. The AUC values of the single-RSVP score from the SWLDA algorithm are in the range of 0.691–0.822 (mean: 0.783; std: 0.062). The AUC values of the dual-RSVP score from the SWLDA algorithm are in the range of 0.729–0.903 (mean: 0.848; std: 0.048). Wilcoxon signed rank test results are $p < 0.05$.

Table 3 shows the comparison of AUC values in triple-RSVP paradigm and the single-, dual-, and triple-RSVP scores for the eight subjects. Across the subjects, the AUC values of the single-RSVP score from the HDCA algorithm are in the range of 0.916–0.952 (mean: 0.926; std: 0.017). The AUC values of the dual-RSVP score from the HDCA algorithm are in the range of 0.935–0.965 (mean: 0.946; std: 0.009). The AUC values of the triple-RSVP score from the HDCA algorithm are in the range of 0.940–0.97 (mean: 0.952; std: 0.008). The Wilcoxon signed rank test results are $p < 0.05$. The AUC values of the single-RSVP score from the SWLDA algorithm are in the range of 0.875–0.917 (mean: 0.908; std: 0.043). The AUC values of the dual-RSVP score from the SWLDA algorithm are in the range of 0.919–0.955 (mean: 0.936; std: 0.037). The AUC values of the triple-RSVP score from the SWLDA algorithm are in the range of

Table 3: Values of the AUC of all subjects under the triple-RSVP paradigm.

	Subjects	1	2	3	4	5	6	7	8	Mean	SD
Left RSVP only	HDCA	0.9337	0.9191	0.9169	0.9306	0.9213	0.9194	0.9186	0.9512	0.9263	0.0118
	SWLD	0.9152	0.9176	0.9121	0.9107	0.9097	0.9140	0.8759	0.9100	0.9082	0.0133
Combining with left and right RSVP	HDCA	0.9477	0.9434	0.9461	0.9448	0.9351	0.9381	0.9466	0.9656	0.9459	0.0091
	SWLD	0.9381	0.9469	0.9460	0.9552	0.9257	0.9228	0.9199	0.9361	0.9363	0.0127
Combining with left, right, and bottom RSVP	HDCA	**0.9572**	**0.9514**	**0.9520**	**0.9482**	**0.9465**	**0.9401**	**0.9520**	**0.9701**	**0.9522**	0.0088
	SWLD	**0.9580**	**0.9542**	**0.9518**	**0.9538**	**0.9448**	**0.9429**	**0.9364**	**0.9458**	**0.9485**	0.0072

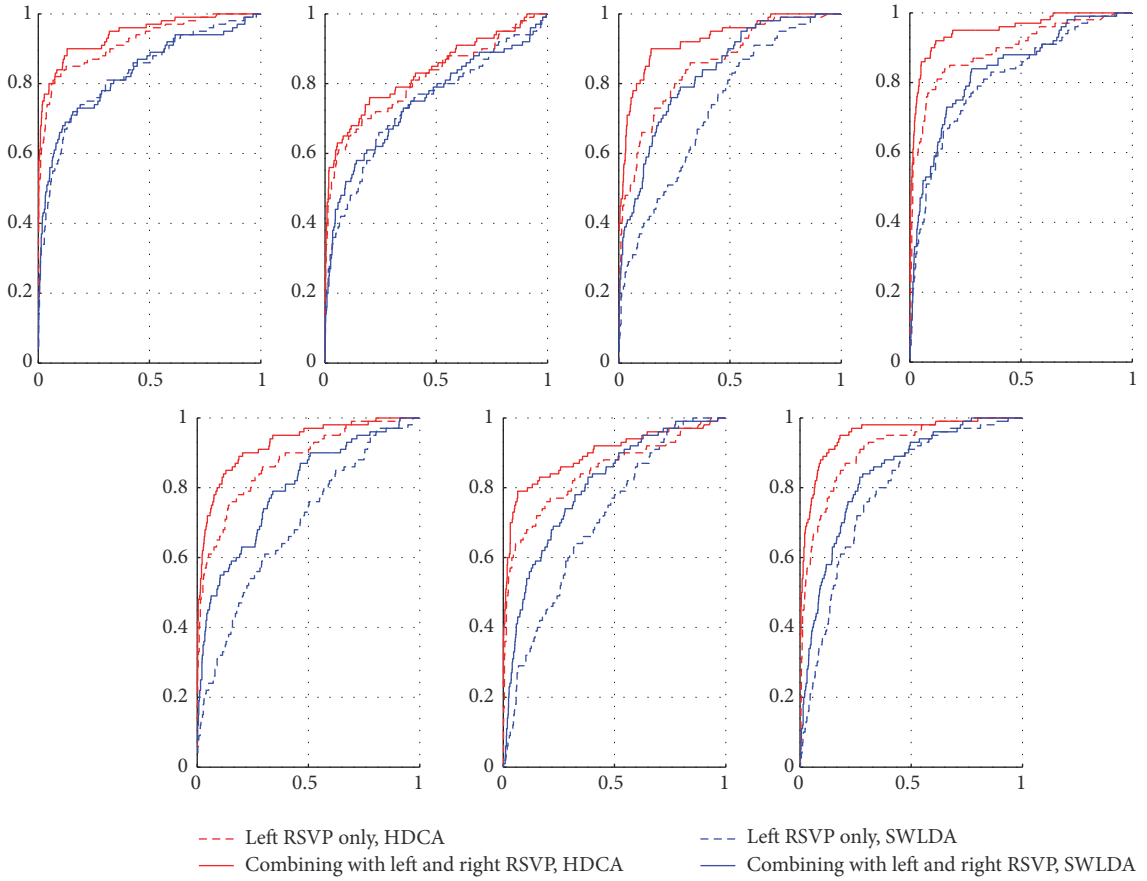

Figure 7: All subjects ROC curve in dual-RSVP paradigm. The red and blue line are the results of HDCA and SWLDA, respectively. The dotted line represents the ROC curve of the left image sequence EEG score. And the solid line represents the ROC curve of combination of the EEG scores from the left image sequence and right image sequences.

0.936–0.957 (mean: 0.948; std: 0.032). The Wilcoxon signed rank test results are $p < 0.05$.

We further plot the ROC curves of all subjects (Figures 7 and 8) in different paradigms (dual-RSVP and triple-RSVP paradigms) and used different P300 detection algorithms (HDCA and SWLDA). We divided the data into two parts, one for training the classifier and one for testing. Figures 7 and 8 show the ROC curves for the test section. Figure 7 is the ROC curve in dual-RSVP paradigm; the red and blue lines are the results of HDCA and SWLDA, respectively. The results of the combined left and right RSVP sequences are better than those of the left RSVP sequence alone. Analogously, Figure 8 shows the ROC curves for all subjects in triple-RSVP paradigm. The results of the combination of the left, right, and bottom RSVP sequences are better than those of the combination of the left and right RSVP sequences, whereas the combination of the left and right RSVP sequences is better than the left RSVP sequence alone.

4. Discussion

The multi-RSVP simultaneously presents multiple images (left side, right side, bottom side, or more of the screen). The right images are formed by delaying the left images for a short period of time, the bottom images are formed by delaying the right images for a period of time, and so on. The subject first looks at the left side, then at the right side, and lastly at the bottom side until the target image appears on each respective side. Finally, the subject focuses again to the left side. Thus, the participant views the target image for multiple times. Experimental results show that this framework effectively improves the accuracy of target recognition.

Obviously, presenting the target image for multiple times effectively improves the accuracy of P300 recognition. In the dual-RSVP paradigm or triple-RSVP paradigm, once the subject sees the target image, he/she naturally acknowledges that the target image will appear again in another sequence after an approximate time. In the cognition of the subject, the probability of the reappearance of the target image increases and thus reduces the induced P300 attribute. As shown in Figure 5(b), in the triple-RSVP paradigm, the peak of the third P300 component is smaller than that of the first and second, and the third P300 latency is longer. This finding indicates that detection of the third P300 component is more difficult than that of the first or second P300 component. Figure 8 and Table 3 show that the increased performance of

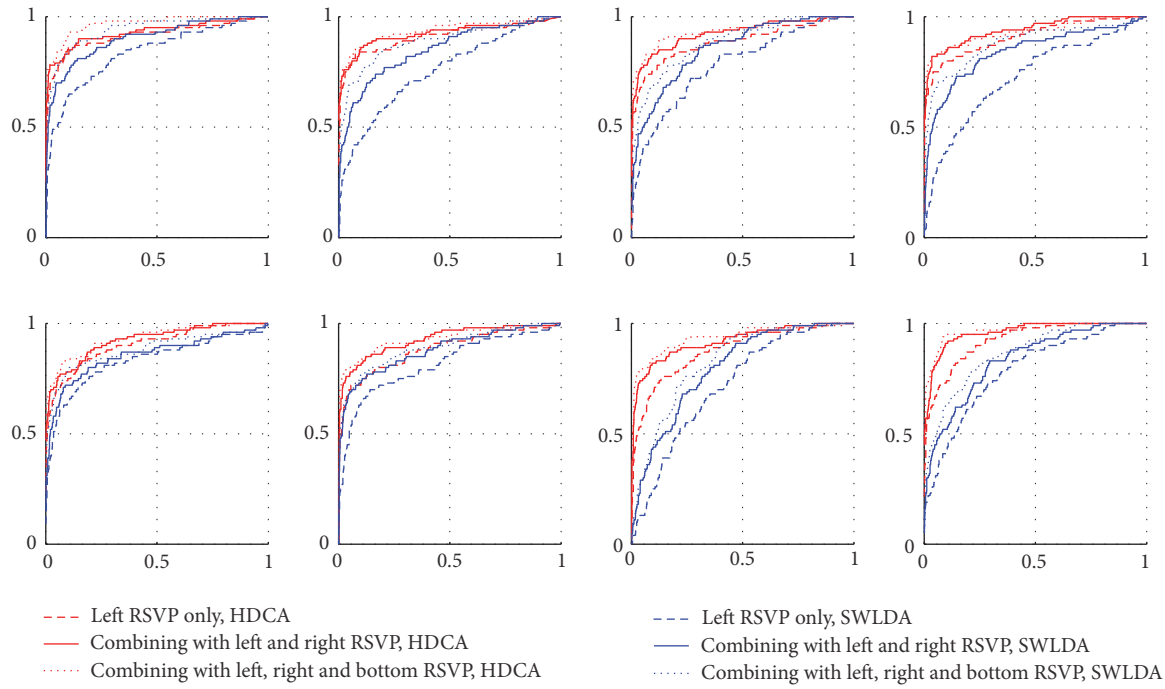

Figure 8: All subjects ROC curve in triple-RSVP paradigm. The red and blue lines are the results of HDCA and SWLDA, respectively. The dotted line represents the ROC curve of the left image sequence EEG score. The solid line represents the ROC curve of the combination of the EEG scores from the left and right image sequences. The small dotted line represents the ROC curve of the combination of the EEG scores from the left, right, and bottom image sequences.

the triple-RSVP compared with the dual-RSVP is lower than that of the dual-RSVP compared with the single-RSVP. This finding reveals that in the multi-RSVP framework, the ability of quadruple-RSVP (or higher) to increase the accuracy is limited, and the complexity of the operation should also be considered. One possible strategy to improve the multi-RSVP framework is to randomize the reappearance time interval of the target image in another image sequence. Hence, the subject cannot confirm the specific time when the target image reappears. This theory will be studied in a future research.

In practical applications, we need to consider the conditions where multi-RSVP (dual-, triple-, or more) is applicable. In the experiment, we assumed that the adjacent target image does not appear; however, this phenomenon can occur in practice. In this paper, the probability of appearance of target image is 0.1. In the dual-RSVP paradigm, the subjects observe the same target twice at 1250 ms to 1500 ms, during which the subjects ignore the original image sequence (5-6 images) after the target appears, during which the subjects ignore 5-6 images in the image sequence of the screen left side. Similarly, in the triple-RSVP paradigm, the subject misses 8-9 images. These missed images probably contain the target image. In the quadruple- (or more) RSVP paradigm, the probability of missing the target image is high. Therefore, the probability of target occurrence is an important factor in selecting the appropriate multi-RSVP (dual-, triple-, or more) paradigm. Figure 9 shows the relationship curve of the probabilities when the target appears and the target is missed. The target miss probability is calculated by

$$P_{\text{miss}} = 1 - \left(1 - P_{\text{target}}\right)^{N}, \tag{3}$$

where P_{miss} represents the target miss probability in the process of the subject transfer sight. N is the number of ignored images, and P_{target} is the target probability.

Thus, the multi-RSVP paradigm is valid only when the probability of target occurrence is low. This finding impedes the application of multi-RSVP paradigm. In practical applications, some scenes can satisfy this condition. For example, the probability of a particular target image (such as the threat image) is extremely low in the Cognitive Technology Threat Warning System [27, 28]. However, serious consequences likely occur when the threat of the target is undetected. Under these conditions, the multi-RSVP paradigm is an effective method. The target image then appears many times and thus ensures the high-precision identification of the target.

5. Conclusion

In this study, we verified the feasibility of the dual-RSVP paradigm [22] proposed by Cecotti in EEG data and further established a triple-RSVP paradigm. Multi-RSVP framework is effective for target detection. The multi-RSVP paradigm achieves higher recognition accuracy than the standard RSVP paradigm.

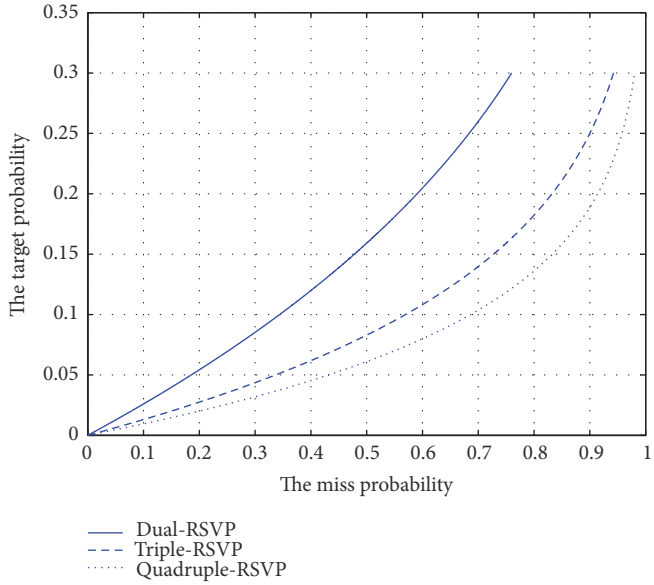

Figure 9: Target appearing probability and target miss probability in dual-, triple-, and quadruple-RSVP paradigms.

Conflicts of Interest

The authors declare that there are no conflicts of interest regarding the publication of this paper.

References

[1] Y. Huang, D. Erdogmus, M. Pavel, S. Mathan, and K. E. Hild, "A framework for rapid visual image search using single-trial brain evoked responses," *Neurocomputing*, vol. 74, no. 12-13, pp. 2041–2051, 2011.

[2] J. Touryan, L. Gibson, J. Horne, and P. Weber, "Real-time classification of neural signals corresponding to the detection of targets in video imagery," in *Proceedings of the International Conference on Applied Human Factors and Ergonomics*, 2010, p. 60.

[3] J. Polich, "Updating P300: an integrative theory of P3a and P3b," *Clinical Neurophysiology*, vol. 118, no. 10, pp. 2128–2148, 2007.

[4] S. Sutton, M. Braren, and J. Zubin, "Evoked-potential correlates of stimulus uncertainty," *Science*, vol. 150, no. 3700, pp. 1187-1188, 1965.

[5] P. Sajda, A. Gerson, and L. Parra, "High-throughput image search via single-trial event detection in a rapid serial visual presentation task," in *Proceedings of the 1st International IEEE EMBS Conference on Neural Engineering*, pp. 7–10, ita, March 2003.

[6] L. A. Farwell and E. Donchin, "Talking off the top of your head: Toward a mental prosthesis utilizing event-related brain potentials," *Electroencephalography and Clinical Neurophysiology*, vol. 70, no. 6, pp. 510–523, 1988.

[7] D. J. Krusienski, E. W. Sellers, F. Cabestaing et al., "A comparison of classification techniques for the P300 Speller," *Journal of Neural Engineering*, vol. 3, no. 4, article 007, pp. 299–305, 2006.

[8] C. J. Gonsalvez and J. Polich, "P300 amplitude is determined by target-to-target interval," *Psychophysiology*, vol. 39, no. 3, pp. 388–396, 2002.

[9] H. Ramoser, J. Müller-Gerking, and G. Pfurtscheller, "Optimal spatial filtering of single trial EEG during imagined hand movement," *IEEE Transactions on Rehabilitation Engineering*, vol. 8, no. 4, pp. 441–446, 2000.

[10] B. Rivet, H. Cecotti, A. Souloumiac, E. Maby, and J. Mattout, "Theoretical analysis of XDAWN algorithm: Application to an efficient sensor selection in a P300 BCI," in *Proceedings of the 19th European Signal Processing Conference, EUSIPCO 2011*, pp. 1382–1386, esp, September 2011.

[11] B. Rivet, A. Souloumiac, V. Attina, and G. Gibert, "xDAWN algorithm to enhance evoked potentials: application to brain-computer interface," *IEEE Transactions on Biomedical Engineering*, vol. 56, no. 8, pp. 2035–2043, 2009.

[12] N. Bigdely-Shamlo, A. Vankov, R. R. Ramirez, and S. Makeig, "Brain activity-based image classification from rapid serial visual presentation," *IEEE Transactions on Neural Systems and Rehabilitation Engineering*, vol. 16, no. 5, pp. 432–441, 2008.

[13] A. D. Gerson, L. C. Parra, and P. Sajda, "Cortically coupled computer vision for rapid image search," *IEEE Transactions on Neural Systems and Rehabilitation Engineering*, vol. 14, no. 2, pp. 174–179, 2006.

[14] L. C. Parra, C. Christoforou, A. D. Gerson et al., "Spatiotemporal linear decoding of brain state," *IEEE Signal Processing Magazine*, vol. 25, no. 1, pp. 107–115, 2008.

[15] P. Sajda, E. Pohlmeyer, J. Wang et al., "In a blink of an eye and a switch of a transistor: Cortically coupled computer vision," *Proceedings of the IEEE*, vol. 98, no. 3, pp. 462–478, 2010.

[16] E. A. Pohlmeyer, J. Wang, D. C. Jangraw, B. Lou, S.-F. Chang, and P. Sajda, "Closing the loop in cortically-coupled computer vision: A brain-computer interface for searching image databases," *Journal of Neural Engineering*, vol. 8, no. 3, Article ID 036025, 2011.

[17] G. F. Alpert, R. Manor, A. B. Spanier, L. Y. Deouell, and A. B. Geva, "Spatiotemporal representations of rapid visual target detection: A single-trial EEG classification algorithm," *IEEE Transactions on Biomedical Engineering*, vol. 61, no. 8, pp. 2290–2303, 2014.

[18] A. R. Marathe, A. J. Ries, and K. McDowell, "A novel method for single-trial classification in the face of temporal variability," *Lecture Notes in Computer Science (including subseries Lecture Notes in Artificial Intelligence and Lecture Notes in Bioinformatics)*, vol. 8027, pp. 345–352, 2013.

[19] A. R. Marathe, A. J. Ries, and K. McDowell, "Sliding HDCA: Single-trial eeg classification to overcome and quantify temporal variability," *IEEE Transactions on Neural Systems and Rehabilitation Engineering*, vol. 22, no. 2, pp. 201–211, 2014.

[20] H. Cecotti, M. P. Eckstein, and B. Giesbrecht, "Single-trial classification of event-related potentials in rapid serial visual presentation tasks using supervised spatial filtering," *IEEE Transactions on Neural Networks and Learning Systems*, vol. 25, no. 11, pp. 2030–2042, 2014.

[21] A. Rakotomamonjy and V. Guigue, "BCI competition III: dataset II-ensemble of SVMs for BCI P300 speller," *IEEE Transactions on Biomedical Engineering*, vol. 55, no. 3, pp. 1147–1154, 2008.

[22] H. Cecotti, "Single-trial detection with magnetoencephalography during a dual-rapid serial visual presentation task," *IEEE Transactions on Biomedical Engineering*, vol. 63, no. 1, pp. 220–227, 2016.

[23] O. Russakovsky, J. Deng, H. Su et al., "ImageNet large scale visual recognition challenge," *International Journal of Computer Vision*, vol. 115, no. 3, pp. 211–252, 2015.

[24] C. Zhang, L. Tong, Y. Zeng et al., "Automatic Artifact Removal from Electroencephalogram Data Based on A Priori Artifact Information," *BioMed Research International*, vol. 2015, Article ID 720450, 2015.

[25] C. Zhang, H.-B. Bu, Y. Zeng, J.-F. Jiang, B. Yan, and J.-X. Li, "Prior artifact information based automatic artifact removal from EEG data," in *Proceedings of the 7th International IEEE/EMBS Conference on Neural Engineering, NER 2015*, pp. 1108–1111, fra, April 2015.

[26] C. Cortes, "AUC optimization vs. Error rate minimization," *Advances in Neural Information Processing Systems*, pp. 313–320, 2004.

[27] U. Visser, "Human-Centered Robotics," *KI - Künstliche Intelligenz*, vol. 27, no. 2, pp. 173–177, 2013.

[28] C. Sagers Herzog, "Brain-in-the-loop integration: CT2WS enters a new phase," *Diplomatic Courier*, 2012.

Hindawi
BioMed Research International
Volume 2017, Article ID 1463512, 13 pages
https://doi.org/10.1155/2017/1463512

Research Article

Virtual and Actual Humanoid Robot Control with Four-Class Motor-Imagery-Based Optical Brain-Computer Interface

Alyssa M. Batula,[1] Youngmoo E. Kim,[1] and Hasan Ayaz[2,3,4]

[1]*Department of Electrical and Computer Engineering, Drexel University, 3141 Chestnut Street, Philadelphia, PA 19104, USA*
[2]*School of Biomedical Engineering, Science and Health Systems, Drexel University, 3141 Chestnut Street, Philadelphia, PA 19104, USA*
[3]*Department of Family and Community Health, University of Pennsylvania, 3737 Market Street, Philadelphia, PA 19104, USA*
[4]*Division of General Pediatrics, Children's Hospital of Philadelphia, 3401 Civic Center Blvd, Philadelphia, PA 19104, USA*

Correspondence should be addressed to Hasan Ayaz; hasan.ayaz@drexel.edu

Received 1 April 2017; Accepted 6 June 2017; Published 18 July 2017

Academic Editor: Pedro P. R. Filho

Motor-imagery tasks are a popular input method for controlling brain-computer interfaces (BCIs), partially due to their similarities to naturally produced motor signals. The use of functional near-infrared spectroscopy (fNIRS) in BCIs is still emerging and has shown potential as a supplement or replacement for electroencephalography. However, studies often use only two or three motor-imagery tasks, limiting the number of available commands. In this work, we present the results of the first four-class motor-imagery-based online fNIRS-BCI for robot control. Thirteen participants utilized upper- and lower-limb motor-imagery tasks (left hand, right hand, left foot, and right foot) that were mapped to four high-level commands (turn left, turn right, move forward, and move backward) to control the navigation of a simulated or real robot. A significant improvement in classification accuracy was found between the virtual-robot-based BCI (control of a virtual robot) and the physical-robot BCI (control of the DARwIn-OP humanoid robot). Differences were also found in the oxygenated hemoglobin activation patterns of the four tasks between the first and second BCI. These results corroborate previous findings that motor imagery can be improved with feedback and imply that a four-class motor-imagery-based fNIRS-BCI could be feasible with sufficient subject training.

1. Introduction

The ability to direct a robot using only human thoughts could provide a powerful mechanism for human-robot interaction with a wide range of potential applications, from medical to search-and-rescue to industrial manufacturing. As robots become more integrated into our everyday lives, from robotic vacuums to self-driving cars, it will also become more important for humans to be able to reliably communicate with and control them. Current robots are difficult to control, often requiring a large degree of autonomy (which is still an area of active research) or a complex series of commands entered through button presses or a computer terminal. Using thoughts to direct a robot's actions via a brain-computer interface (BCI) could provide a more intuitive way to issue instructions to a robot. This could augment current efforts to develop semiautonomous robots capable of working in environments unsafe for humans, which was the focus of a recent DARPA robotics challenge [1]. A brain-controlled robot could also be a valuable assistive tool for restoring communication or movement in patients with a neuromuscular injury or disease [2].

The ideal, field-deployable BCI system should be non-invasive, safe, intuitive, and practical to use. Many previous studies have focused on electroencephalography (EEG) and, to a lesser extent, functional magnetic resonance imaging (fMRI). Using these traditional neuroimaging tools, various proof-of-concept BCIs have been built to control the navigation of humanoid (i.e., human-like) robots [3–9], wheeled robots [10–12], flying robots [13, 14], robotic wheelchairs [15], and assistive exoskeletons [16]. More recently functional near-infrared spectroscopy (fNIRS) has emerged as a good

candidate for next generation BCIs, as fNIRS measures the hemodynamic response similar to fMRI [17, 18] but with miniaturized sensors that can be used in field settings and even outdoors [19, 20]. It also provides a balanced trade-off between temporal and spatial resolution, compared to fMRI and EEG, that sets it apart and presents unique opportunities for investigating new approaches, mental tasks, information content, and signal processing for the development of new BCIs [21]. Several fNIRS-based BCI systems have already been investigated for use in robot control [22–27].

Motor imagery, or the act of imagining moving the body while keeping the muscles still, has been a popular choice for use in BCI studies [3, 11, 13, 22, 23, 28–37]. It is a naturalistic task, highly related to actual movements, which could make it a good choice for a BCI input. While motor-execution tasks produce activation levels that are easier to detect, motor imagery is often preferred as issues with possible proprioceptive feedback can be avoided [38]. EEG BCIs have shown success with up to four classes, typically right hand, left hand, feet, and tongue [11, 28, 29]. Other studies have shown potential for EEG to detect difference between right and left foot or leg motor imagery [39, 40] and even individual fingers [41]. Studies have also used fNIRS to detect motor-imagery tasks, with many focusing on a single hand versus resting state [30], left hand versus right hand [31, 32], or three motor-imagery tasks and rest [33]. Shin and Jeong used fNIRS to detect left and right leg movement tasks in a four-class BCI [42], and in prior studies we presented preliminary offline classification results using left and right foot tasks separately in a four-class motor-imagery-based fNIRS-BCI [22, 23]. fNIRS has also been used to examine differences in motor imagery due to force of hand clenching or speed of tapping [34].

Many factors can affect the quality of recorded motor-imagery data. Kinesthetic motor imagery (i.e., imagining the feeling of the movement) has shown higher activation levels in the motor cortex than visual motor imagery (i.e., visualizing the movement) [43, 44]. Additionally, individual participants have varying levels of motor-imagery skill, which also affects the quality of the BCI [45–47]. In some participants, the use of feedback during motor-imagery training can increase the brain activation levels produced during motor imagery [48, 49].

Incorporating robot control into a BCI provides visual feedback and can increase subject motivation. Improved motivation and feedback, both visual and auditory, have demonstrated promise for reducing subject training time and improving BCI accuracy [50, 51]. The realism of feedback provided by a BCI may also have an effect on subject performance during motor imagery. For example, Alimardani et al. found a difference in subject performance in a follow-up session after receiving feedback from viewing a robotic gripper versus a lifelike android arm [52].

In this study, we report the first online results of a four-class motor-imagery-based fNIRS-BCI used to control both a virtual and physical robot. The four tasks used were imagined movement of upper and lower limbs: the left hand, left foot, right foot, and right hand. To the best of our knowledge, this is the first online four-class motor-imagery-based fNIRS-BCI, as well as the first online fNIRS-BCI to use left and right foot as separate tasks. We also examine the differences in oxygenated hemoglobin (HbO) activation between the virtual and physical-robot BCIs in an offline analysis.

2. Materials and Methods

Participants attended two training sessions, to collect data to train an online classifier for the BCI, followed by a third session in which they used the BCI to control the navigation of both a virtual and actual robot. This section outlines the methods used for data collection, the design of the BCI, and offline analysis of the collected data following the completion of the BCI experiment.

2.1. Participants. Thirteen healthy participants volunteered to take part in this experiment. Subjects were aged 18–35, right-handed, English-speaking, and with vision correctable to 20/20. No subjects reported any physical or neurological disorders or were on medication. The experiment was approved by the Drexel University Institutional Review Board, and participants were informed of the experimental procedure and provided written consent prior to participating.

2.2. Data Acquisition. Data were recorded using fNIRS as described in our previous study [53]. fNIRS is a noninvasive, relatively low-cost, portable, and potentially wireless optical brain imaging technique [19]. Near-infrared light is used to measure changes in HbO and HbR (deoxygenated hemoglobin) levels due to the rapid delivery of oxygenated blood to active cortical areas through neurovascular coupling, known as the hemodynamic response [54].

Participants sat in a desk chair facing a computer monitor. They were instructed to sit with their feet flat on the floor and their hands in their lap or on chair arm rests with palms facing upwards. Twenty-four optodes (measurement locations) over the primary and supplementary motor cortices were recorded using a Hitachi ETG-4000 optical topography system, as shown in Figure 1. Each location recorded HbO and HbR levels at a 10 Hz sampling rate.

2.3. Experiment Protocol. Motor-imagery and motor-execution data were recorded in three one-hour-long sessions on three separate days. The first two sessions were training days, used to collect initial data to train a classifier, and the third day used this classifier in a BCI to navigate both a virtual and physical robot to the goal location in a series of rooms. The two robots are described below in Section 2.3.3 Robot Control. The training session protocol included five tasks: a "rest" task and tapping of the right hand, left hand, right foot, and left foot. This protocol expands on a preliminary study reported previously [22, 23]. Data collection for the two training days has been described previously [53].

2.3.1. Tasks. Subjects performed all five tasks during the two training days (rest, along with the (actual or imagined) tapping of the right hand, left hand, right foot, and left foot).

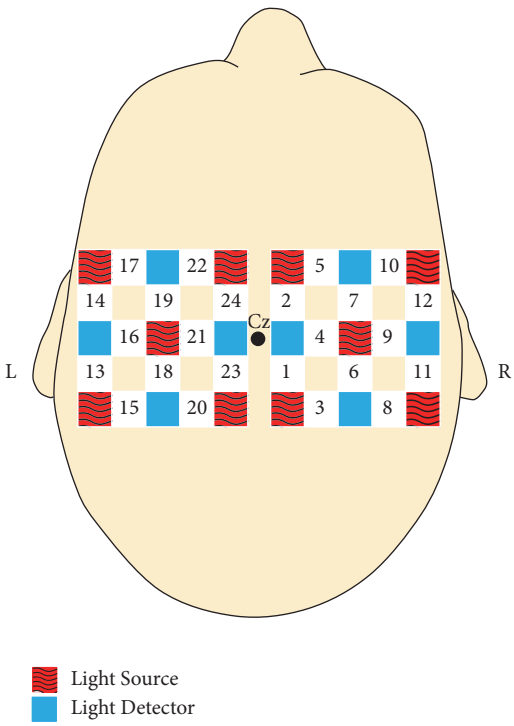

Figure 1: fNIRS sensor layout of light sources (red squares) and detectors (blue squares). Adjacent sources and detectors are 3 cm apart and create 24 optodes (numbered 1–24).

During the third session, only the four motor-imagery tasks were used to control the BCI.

Participants were instructed to self-pace their real or imagined movements at once per second for the duration of the trial. The hand-tapping task was curling and uncurling their fingers towards their palm as if squeezing an imaginary ball, while the foot-tapping task involved raising and lowering the toes while keeping the heel on the floor. While resting, subjects were instructed to relax their mind and refrain from moving. During motor-imagery tasks, subjects were instructed to refrain from moving and use kinesthetic imagery (i.e., imagine the feelings and sensations of the movement).

Each trial consisted of 9 seconds of rest, a 2-second cue indicating the type of upcoming task, and a 15-second task period. During the two training sessions the cue text indicated a specific task (e.g., "Left Foot"), while, during the robot-control task, it read "Free Choice," indicating the subject should choose the task corresponding to the desired action of the robot. Trials during the training days ended with a 4-second display indicating that the task period had ended. During the robot-control session, the task was followed by a reporting period so that the subject could indicate which task they had performed. The BCI then predicted which task the user had performed and sent the corresponding command to the robot, which took the corresponding action. The timings for training and robot-control days are shown in Figure 2.

2.3.2. Session Organization. In total, 60 motor-execution and 150 motor-imagery trials were collected during the training days, and an additional 60 subject-selected motor-imagery trials were recorded during the robot-control portion. The two training days were split into two runs, one for motor execution and one for motor imagery, which were repeated three times as shown in Figure 3. The protocol alternated between a run of 10 motor-execution trials and a run of 25 motor-imagery trials in order to reduce subject fatigue and improve their ability to perform motor imagery [55]. Each run had an equal number of the five tasks (rest and motor execution or motor imagery of the right hand, left hand, right foot, and left foot) in a randomized order. The third day (robot control) had two runs of 30 motor-imagery tasks, chosen by the user, which were used to control the BCI. The rest and motor-execution tasks were collected for offline analysis and were not used in the online BCI.

2.3.3. Robot Control. The robot-control session had two parts, beginning with control of a virtual robot using the MazeSuite program (http://www.mazesuite.com) [56, 57] and followed by control of the DARwIn-OP (Dynamic Anthropomorphic Robot with Intelligence-Open Platform) robot [58]. The objective in both scenarios was to use the BCI to navigate through a series of three room designs (shown in Figure 4), in which there was a single goal location (a green cube) and an obstacle (a red cube). A room was successfully completed if the user navigated the robot to the green cube, and it failed if the robot touched the red cube. After completion or failure of a room, the subject would advance to the next room. The sequence was designed such that the robot started closer to the obstacle in each successive room to increase the difficulty as the subject progressed. The run ended if the subject completed (or failed) all three rooms or reached the maximum of 30 trials. Each room could be completed in 5 or fewer movements, assuming perfect accuracy from the BCI.

To control the BCI, subjects selected a motor-imagery task corresponding to the desired action of the (virtual or physical) robot. The task-to-command mappings were as follows: left foot/walk forward, left hand/turn left 90°, right hand/turn right 90°, and right foot/walk backward. These four tasks were chosen to emulate a common arrow-pad setup, so that each action had a corresponding opposite action that could undo a movement. During BCI control, the original experiment display showed a reminder of the mapping between the motor-imagery tasks and the robot commands. A second monitor to the left of the experiment display showed a first-person view of the experiment room for either the virtual or physical robot. The experiment setup and example display screens are shown in Figure 5.

The virtual robot was controlled using the built-in control functions of the MazeSuite program [56, 57]. The virtual environment and movements of the virtual robot were designed to replicate as closely as possible the physical room and movements of the DARwIn-OP, allowing the participants to acquaint themselves with the new robot-control paradigm before adding the complexities inherent in using a real robot. The virtual robot could make perfect 90° turns in place, and the forward and backward distance was adjusted to match the relative distance traveled by the DARwIn-OP robot as closely as possible. The goal and obstacle were shown as floating

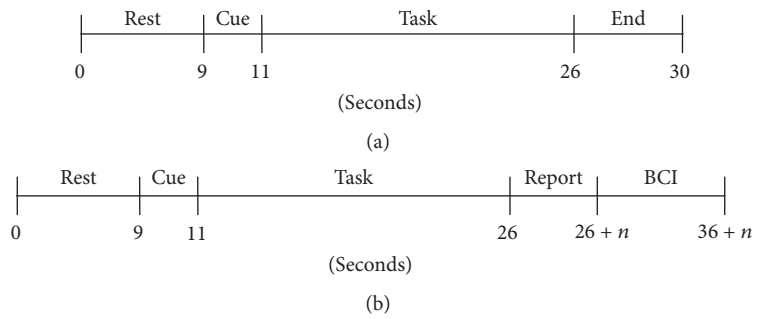

Figure 2: Trial timing diagrams for training sessions (a) and robot-control session (b).

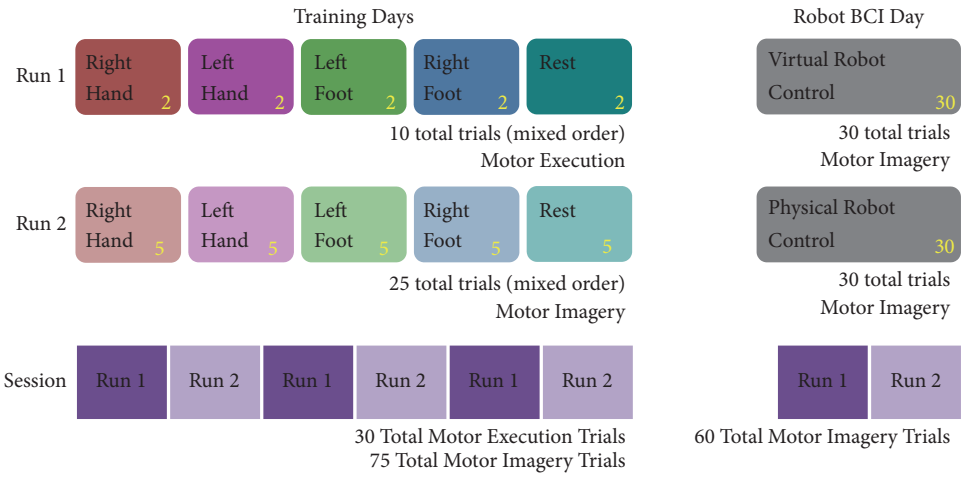

Figure 3: Trial organization protocol for the two training days and single robot-control day of the experiment.

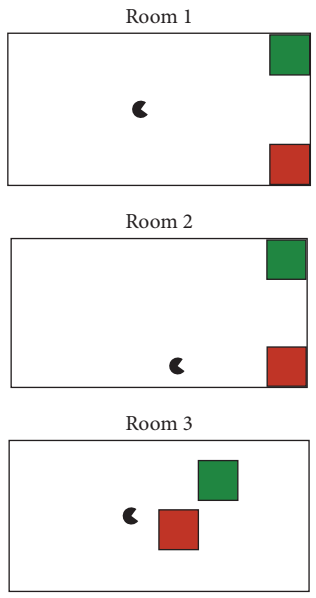

Figure 4: The three room layouts used during robot control.

green and red cubes, respectively, that would trigger a success or failure state on contact with the virtual robot.

During the second run, the user controlled the DARwIn-OP in an enclosed area with a green box and red box marking the location of the goal and obstacle, respectively. Success or failure was determined by an experimenter watching the robot during the experiment. The DARwIn-OP is a small humanoid robot that stands 0.455 m tall, has 20 degrees of freedom, and walks on two legs in a similar manner to humans [58]. The robot received high-level commands from the primary experiment computer using TCP/IP over a wireless connection. Control of the DARwIn-OP was handled via a custom-built C++ class that called the robot's built-in standing and walking functions using prespecified parameters to control the movements at a high level. This class was then wrapped in a Python class for ease of communication with the experiment computer. The head position was lowered from the standard walking pose, in order to give a better view of the goal and obstacle. In order to turn as closely to 90° in place as possible, the robot used a step size of zero for approximately 3 seconds with a step angle of approximately 25° or −25°. When moving forward or backward, the DARwIn-OP used a step size of approximately 1 cm for 2 or 3 seconds, respectively. The exact values were empirically chosen for this particular robot.

2.4. Data Analysis. In addition to the evaluation of the classifier performance during the online BCI, a secondary

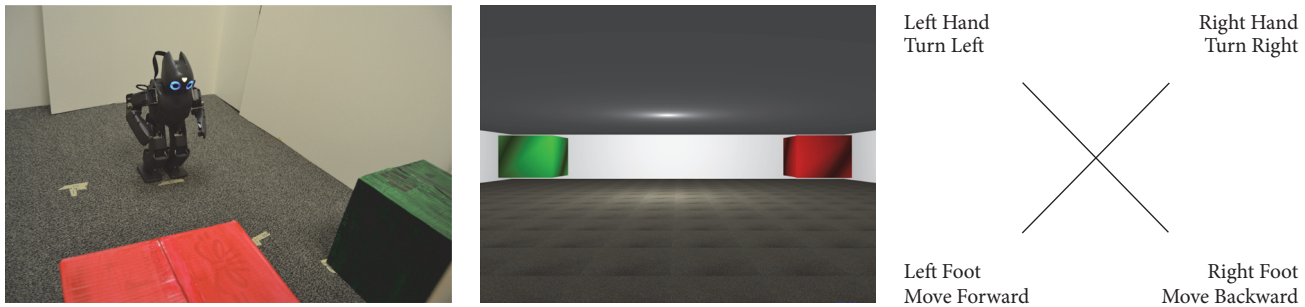

Figure 5: The DARwIn-OP robot standing at the starting location of the first room (a), the first-person display of the virtual room (b), and the experiment display showing the mappings between motor-imagery tasks and robot commands (c).

offline analysis of the data was performed to further compare the two robot BCIs.

2.4.1. Online Processing. Motor-imagery data from the two training days were used to train a subject-specific classifier to control the BCI during the third day. The rest and motor-execution trials were excluded from the training set, as the BCI only used the four motor-imagery tasks. All data recordings from the training days for HbO, HbR, and HbT (total hemoglobin) were filtered using a 20th-order FIR filter with a 0.1 Hz cutoff. Artifacts and optodes with poor signal quality were noted and removed by the researcher. One subject was excluded from the online results due to insufficient data quality.

In addition to using only the low-pass filter, a variety of preprocessing methods were evaluated: correlation-based signal improvement (CBSI), common average referencing (CAR), task-related component analysis (TRCA), or both CAR and TRCA. CBSI uses the typically strong negative correlation between HbO and HbR to reduce head motion noise [59]. CAR is a simple method, commonly used in EEG, in which the average value of all optodes at each time point is used as a common reference (i.e., that value is subtracted from each optode at that time point). This enhances changes in small sets of optodes while removing global spatial trends from the data. TRCA creates signal components from a weighted sum of the recorded data signals [60]. It attempts to find components that maximize the covariance between instances of the same task while minimizing the covariance between instances of different tasks.

Individual task periods were extracted and baseline corrected, using the first 2 seconds of each task as the baseline level. Figure 6 shows an example of how preprocessing methods affect the recorded HbO and HbR for a single optode during one task period. Comparing Figures 6(a) and 6(b) shows how filtering removes a significant quantity of high-frequency noise from the signal. Figure 6(c) shows the change in the signal after applying CAR and baseline correction.

Four different types of features were calculated individually on each optode for HbO, HbR, and HbT. The features used were as follows: mean (average value of the last 10 seconds of the task), median (median of the last 10 seconds of the task), max (maximum value of the last 10 seconds of the task), and slope (slope of the line of best fit of the first 7 seconds of the task). Datasets were created using features calculated on HbO, HbT, or both HbO and HbR. Each feature set was reduced to between 4 and 8 features using recursive feature elimination. If both HbO and HbR were used, the specified number of features was selected for each chromophore. This resulted in 300 possible datasets (5 preprocessing methods, 3 chromophore combinations, 4 types of features, and 5 levels of feature reduction). Features in each dataset were normalized to have zero mean and unit variance.

Prior to the BCI session, a linear discriminant analysis (LDA) classifier was trained on the data from the two training days, following the flow chart shown in Figure 7 [61]. LDA is one of the simplest classification methods commonly used in BCIs [38], requiring no parameter tuning, which reduces the number of possible choices when selecting a classifier. LDA was implemented using the Scikit-learn toolkit [62].

To select an online classifier, an LDA classifier was trained on one training day (60 motor-imagery trials) and tested on the other for each of the 300 feature sets. This was repeated with the two days reversed, and the feature set with the highest average accuracy was selected. The classifier was then retrained on both training days (120 motor-imagery trials) using the selected feature set and was used as the online classifier for both robot-control BCIs.

Results are reported as accuracy (average number of correct classifications), precision (positive prediction value), recall (sensitivity or true positive rate), F-score (the balance between precision and recall), and the area under the ROC curve (AUC). The F-score is calculated as $F\text{-Score} = 2 \times (\text{precision} \times \text{recall})/(\text{precision} + \text{recall})$.

2.4.2. Offline Processing. For the offline analysis, an automatic data-quality analysis was used on the BCI session data to determine which optodes and trials should be removed due to poor quality. This was done separately for the virtual and DARwIn-OP runs using a modified version of the method described by Takizawa et al. for fNIRS data [63]. Any optodes with a very high (near maximum) digital or analog gain

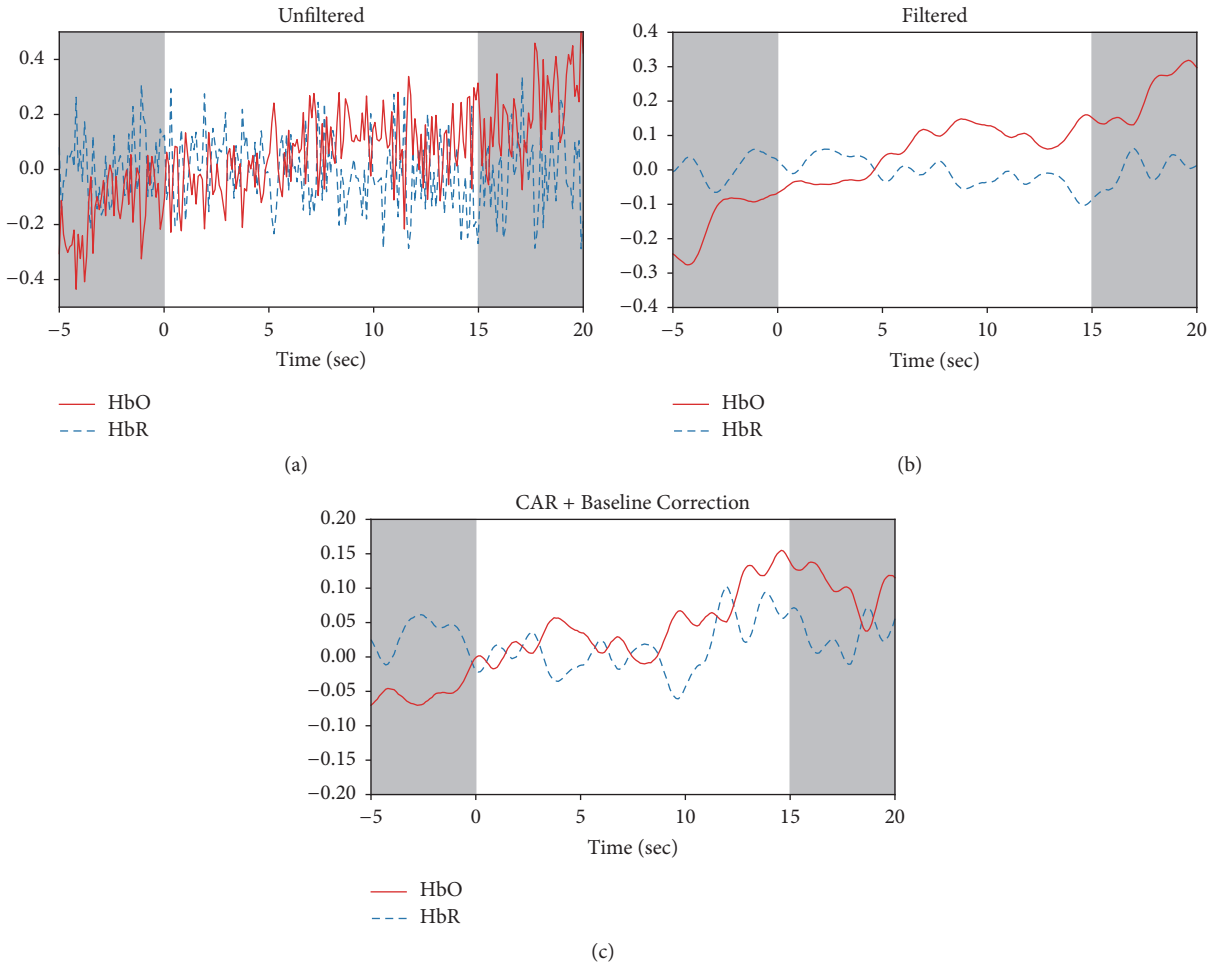

FIGURE 6: Example of data analysis for a representative trial. Data from a single optode showing the original HbO and HbR signals (a), the data after filtering (b), and after applying CAR and baseline correction (c). Resting periods before and after the task are shown by gray boxes.

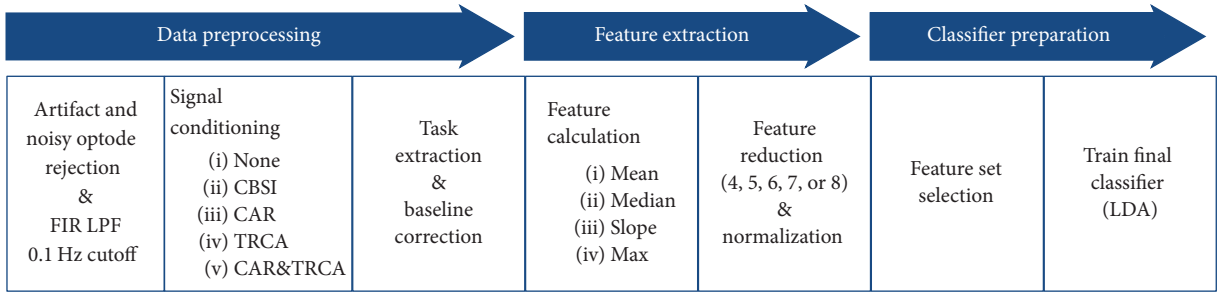

FIGURE 7: Flow chart outlining the creation of the online classifier.

were removed, as these were likely contaminated by noise. Areas with a standard deviation of 0 in a 2-second window of the raw light-intensity data were considered to have been saturated, and artifacts were determined to be areas with a change of 0.15 [mM] during a 2-second period on HbO and HbR data after application of the low-pass filter. Optodes that had at least 20 (of the original 30) artifact- and saturation-free trials were kept, with the remaining optodes being removed. Then, any trials with artifacts or saturated areas in any remaining good optodes were removed. An additional 5 subjects were excluded from the offline analysis due to insufficient data quality.

CAR was used for all offline analysis, followed by task data extraction and baseline correction as in the online analysis. Offline analysis examined the average HbO activation levels during the first and last second of each trial. Statistical

Table 1: Effects and interactions of task, optode, and robot type for the BCI control session.

	F-value	p value
Task	0.011	0.998
Optode	10.982	**0.000**
Robot type	0.043	0.835
Optode ∗ task	1.393	**0.018**
Task ∗ robot type	0.008	0.999
Optode ∗ robot type	2.155	**0.001**
Optode ∗ task ∗ robot type	1.147	0.192

analysis was done using linear mixed models, with multiple tests being corrected using false discovery rate (FDR).

3. Results

Offline analysis found that optode (24 levels), the interaction of optode and task (4 levels: right hand, left hand, right foot, and left foot), and the interaction of optode and robot type (2 levels: virtual and DARwIn-OP) had a significant effect on the average HbO activation during the last second of each trial. A post hoc analysis run individually for each optode found no significant effect for task, robot type, or task ∗ robot type interaction. F-values and p values for the main effects are shown in Table 1, with the post hoc analysis available in Table S1 in Supplementary Material available online at https://doi.org/10.1155/2017/1463512.

A second post hoc analysis, run individually for each optode under each task condition separately, showed that robot type had a significant effect on at least one optode under each task condition ($p < 0.05$, FDR corrected). The effect was found for two optodes (14 and 16) for the left hand task, one optode (14) for left foot, 6 optodes (4, 9, 16, 18, 20, and 23) for right foot, and one optode (6) for right hand. The full table of p values is available in Table S2 in Supplementary Material.

A comparison of topographic HbO activation levels demonstrated differences between individual tasks as well as the two BCIs. Left hand showed a much more contralateral activation pattern with the DARwIn-OP robot, with two optodes on the ipsilateral side showing a significant decrease in HbO levels between the first and last second of the task, whereas, during control of the virtual robot, it had a more ipsilateral activation pattern and no optodes with statistically significant changes in activation over the course of the task. Right hand, however, became strongly ipsilateral, with one ipsilateral optode showing significant activation, during the DARwIn-OP BCI.

Right foot activation became more contralateral, with stronger activation being closer to C_z on the contralateral side and a significant decrease in activation on the ipsilateral side. Left foot changed from a centralized bilateral activation near C_z when controlling the virtual robot to a more diffuse and ipsilateral activation pattern during DARwIn-OP control. It did, however, show an optode with significant decrease in HbO activation on the ipsilateral side during DARwIn-OP control.

Table 2: Online BCI results.

	Accuracy	Precision	Recall	F-Score	AUC
S1	30.00	0.31	0.29	0.30	0.50
S2	27.12	0.32	0.29	0.30	0.50
S3	25.00	0.19	0.25	0.22	0.47
S4	21.67	0.30	0.26	0.28	0.50
S5	30.00	0.28	0.28	0.28	0.54
S6	26.67	0.37	0.28	0.32	0.50
S7	35.00	0.36	0.37	0.37	0.59
S8	36.67	0.34	0.32	0.33	0.53
S9	18.33	0.22	0.21	0.21	0.54
S10	20.00	0.20	0.21	0.20	0.45
S11	31.67	0.22	0.25	0.24	0.49
S12	23.33	0.23	0.23	0.23	0.52
Avg.	27.12	0.28	0.27	0.27	0.51

Topographic plots of the average HbO activation during the last second of each task across all subjects are shown in Figure 8. Optodes showing a significant difference in average HbO level between the first and last second of the task are circled ($p < 0.05$, FDR corrected).

While controlling the online four-class BCI, participants achieved an average accuracy of 27.12% for the entire session. Five participants (S1, S5, S7, S8, and S11) achieved an accuracy of 30% or higher, reaching 36.67% accuracy (S8). The online accuracy, precision, recall, F-Score, and AUC for each subject are detailed in Table 2.

There was a significant increase in classification accuracy during DARwIn-OP control as compared to virtual robot control (one-sided paired t-test, $t(11) = 2.077$, $p = 0.031$), with the average accuracy increasing by 5.21 +/− 2.51% (mean +/− standard error). All but one subject achieved the same or better performance in the second run while controlling the DARwIn-OP compared to during the first run with the virtual robot, and two subjects achieved 40% accuracy. The online accuracy, precision, recall, F-Score, and AUC for each subject for each BCI individually are detailed in Table 3. One subject (S5) did not use the left hand task during the virtual robot run, and therefore no AUC value is listed.

This improvement in performance appears to be reflected in the number of goals reached by the participants. While controlling the virtual robot, subject S11 was the only participant to run into an obstacle, and they were also the only participant to reach a goal. During control of the DARwIn-OP robot, two subjects (S2 and S5) reached two of the goals, and two others (S1 and S11) reached a single goal. Two subjects (S1 and S7) collided with an obstacle while navigating the DARwIn-OP.

Subjects S1 and S6, who showed the largest improvement between the virtual and DARwIn-OP BCIs, have confusion matrices that indicate differing methods used to increase accuracy. The confusion matrix of online classification results for subject S1 shows a strong diagonal pattern when controlling the DARwIn-OP, as expected for a well-performing classifier. Interestingly, left foot and right foot are never

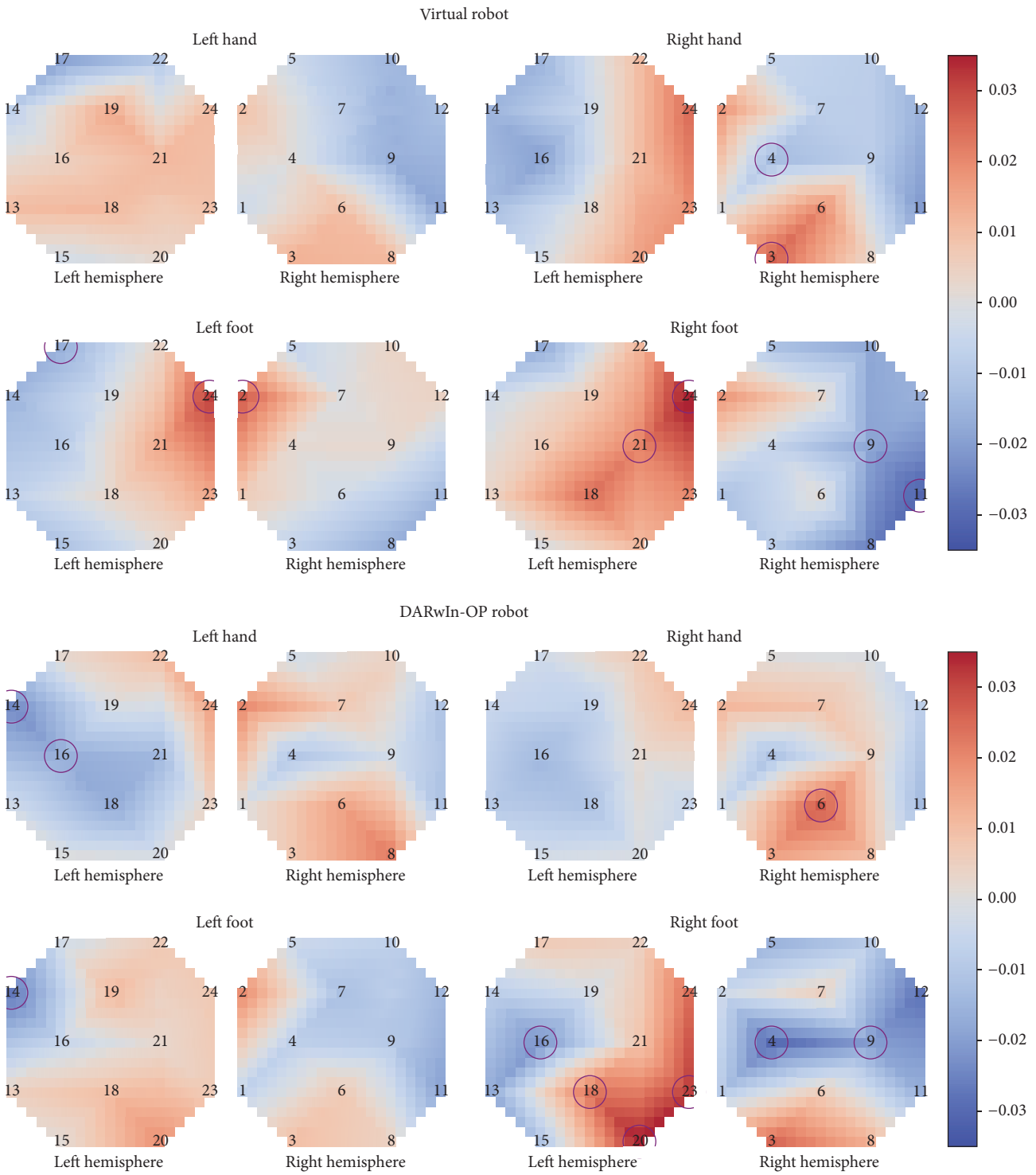

FIGURE 8: Average HbO activation for each task during virtual and DARwIn-OP robot BCIs. Optodes with significant differences in HbO activation levels between the first and last second of the task are circled ($p < 0.05$, FDR corrected).

misclassified as the opposite foot, as might be expected based on their close proximity in homuncular organization, even though such misclassifications were present when controlling the virtual robot. Left hand was the most frequently misclassified task, commonly confused with left foot and right hand. Left foot tasks were also misclassified as left hand tasks but were correctly classified much more often. Subject S6, on the other hand, achieved higher accuracy when controlling the DARwIn-OP by primarily classifying the two hand tasks correctly. This subject's classifier had a strong tendency to

Table 3: Online BCI results for virtual and DARwIn-OP BCIs individually.

	Virtual robot					DARwIn-OP robot				
	Accuracy	Precision	Recall	*F*-Score	AUC	Accuracy	Precision	Recall	*F*-Score	AUC
S1	23.33	0.27	0.28	0.27	0.51	36.67	0.36	0.38	0.37	0.53
S2	24.14	0.24	0.23	0.23	0.40	30.00	0.44	0.34	0.38	0.63
S3	23.33	0.16	0.25	0.19	0.55	26.67	0.20	0.23	0.21	0.43
S4	26.67	0.36	0.44	0.40	0.59	16.67	0.17	0.18	0.18	0.47
S5	30.00	0.29	0.23	0.25	N/A	30.00	0.35	0.31	0.33	0.57
S6	13.33	0.21	0.14	0.17	0.42	40.00	0.55	0.52	0.53	0.65
S7	33.33	0.35	0.34	0.35	0.59	36.67	0.46	0.39	0.42	0.57
S8	33.33	0.29	0.30	0.29	0.53	40.00	0.40	0.35	0.38	0.54
S9	16.67	0.16	0.22	0.18	0.52	20.00	0.25	0.20	0.22	0.55
S10	20.00	0.17	0.22	0.20	0.42	20.00	0.20	0.17	0.18	0.48
S11	30.00	0.23	0.25	0.24	0.44	33.33	0.19	0.27	0.22	0.54
S12	20.00	0.21	0.19	0.20	0.50	26.67	0.26	0.30	0.28	0.58
Avg.	24.51	0.24	0.26	0.25	0.50	29.72	0.32	0.30	0.31	0.54

predict right hand tasks during both BCIs, although actual right hand tasks were often misclassified during virtual robot control. The two foot tasks in both scenarios were frequently misclassified, typically as right hand. The confusion matrices are shown in Figure 9.

4. Discussion

In this work, we present the results of a four-class motor-imagery-based BCI used to control a virtual and physical robot. There were significant differences in performance between controlling the virtual robot and the physical DARwIn-OP robot with the BCI. Subjects had significantly higher accuracy when controlling the DARwIn-OP than when controlling the virtual robot (29.72% versus 24.51% accuracy, resp.). An offline analysis showed that the interaction between optode and robot type had a significant effect on HbO levels, indicating that this increase in accuracy may be at least partially due to changes in HbO activation patterns during the tasks. Topographic plots of HbO activation also show changes in activation pattern between the virtual and DARwIn-OP BCIs, with left hand and right foot tasks moving to a more contralateral activation pattern while right hand and left foot became more ipsilateral in the second BCI.

These changes could be due to the participants adapting their mental strategy based on the BCI's classifier while controlling the virtual robot, thereby modifying their motor-imagery activation patterns. Confusion matrices of the online BCI classifiers show different patterns of correct and incorrect classification between subjects and between control of the virtual and physical robot. Such changes could reflect differences in the activation patterns generated during motor imagery, potentially showing differences in mental strategy developed by the participants while using the BCIs. This is in line with previous findings that feedback, especially from a BCI, can improve motor-imagery activation [49, 52, 64, 65]. Participants could also have improved as they became more familiar with the BCI experiment protocol, increasing their confidence in using the BCI, which has also been shown to have an effect on motor-imagery ability [45].

It is also possible that the differences between the virtual and DARwIn-OP robots themselves contributed to differences in subject performance. The more realistic visuals when using the DARwIn-OP could have had an effect, similar to the results found by Alimardani et al. [52]. There has been limited study on this topic, and further experiments would be needed in order to determine if this was a factor in subject performance.

There was a large difference between the accuracy of the highest-accuracy and lowest-accuracy subjects (40% versus 16% accuracy), in line with previous findings that people have different motor-imagery abilities [45–47]. Future studies could be improved by screening participants for motor-imagery abilities, as suggested by Marchesotti et al. [46], and potentially using feedback to improve the performance of participants identified as low motor-imagery ability [48]. As Bauer et al. found that the use of a robot BCI could improve motor-imagery performance, longer or additional BCI sessions could be incorporated in order to improve motor-imagery performance [49].

In this work, we adapted the preprocessing pipeline for each subject based on classifier performance on the two training days. While this allows one more element of customization for each subject-specific classifier, it also increases the likelihood of overfitting on the training data, which can result in poor performance on the online BCI. Future work could compare the different preprocessing methods and select a single method that performs best across subjects. Additionally, the ability to distinguish between four motor-imagery tasks with simple descriptive features and classifiers may be limited. Future work could employ more intelligent feature reduction methods (e.g., Sequential Floating Forward Selection) or explore more powerful feature design methods using deep neural networks or autoencoders. Support vector machines with nonlinear kernels may be able to achieve higher classification accuracy than LDA classifiers. The more

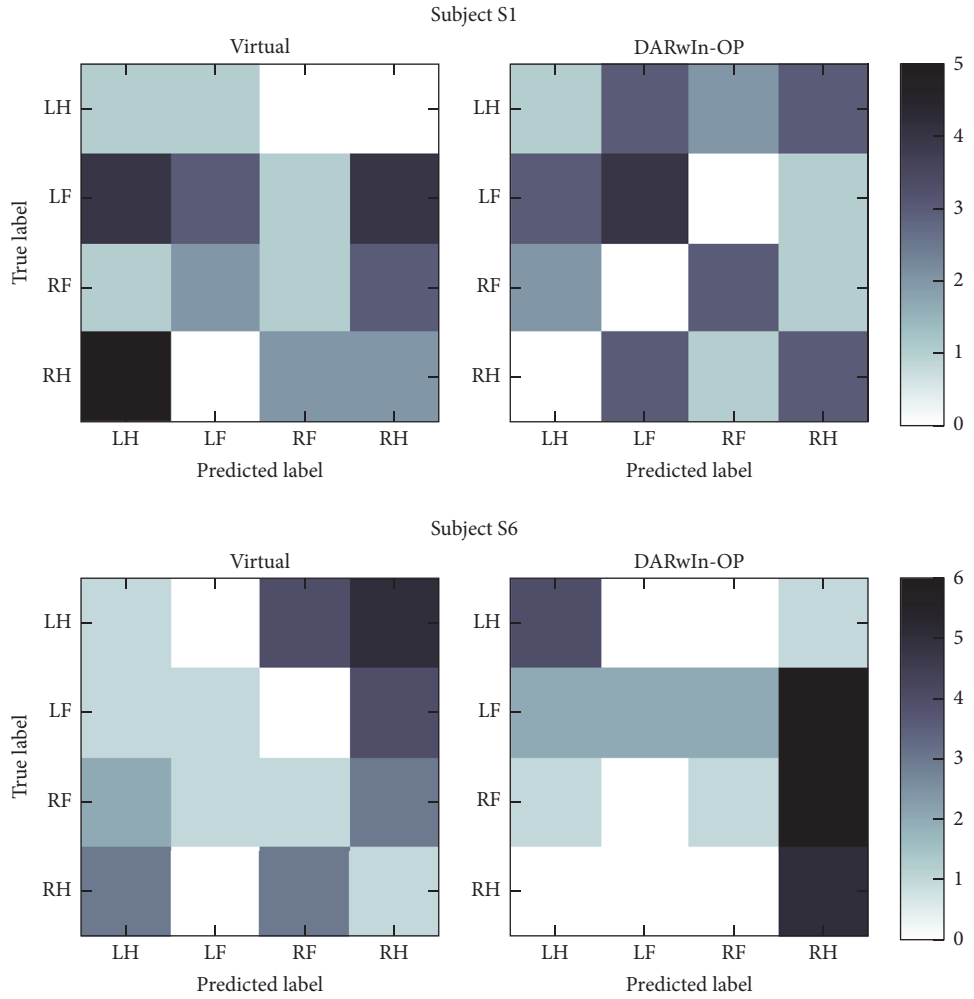

Figure 9: Confusion matrices for the two subjects showing the most improvement between the virtual and DARwIn-OP online BCI results. The confusion matrices indicate different strategies for improving accuracy during DARwIn-OP control: S1 shows a mostly diagonal pattern while S6 shows a focus on correct classification of the two hand tasks.

powerful classification abilities of neural networks may also prove beneficial for improving BCI performance, as has been explored recently with EEG-based BCIs [66–69].

5. Conclusions

This study reports the first online results of a motor-imagery-based fNIRS-BCI to control robot navigation using four motor-imagery tasks. Subjects used the BCI to control first a virtual avatar and then a DARwIn-OP humanoid robot to navigate to goal locations within a series of three rooms. Classification accuracy was significantly greater during the DARwIn-OP BCI, and an offline analysis found a significant interaction between optode and both task and robot type on HbO activation levels. These findings corroborate previous studies that show feedback, including feedback from controlling a robot BCI, can improve motor-imagery performance. It is also possible that the use of a physical, as opposed to virtual, robot had an effect on the results, but future study would be needed to assess that. Furthermore, the activation patterns for left hand and right foot change to show a more strongly contralateral activation pattern during the second BCI, becoming more in line with the expected activation patterns based on the cortical homunculus layout of the motor cortex.

These findings indicate that future studies could benefit from additional focus on feedback during training and in particular additional training periods spent controlling the actual BCI. There was also a large discrepancy between the accuracy of the highest-accuracy and lowest-accuracy subject, indicating that future studies could be improved by screening potential subjects for BCI abilities and potentially providing these subjects with extra feedback training.

Conflicts of Interest

fNIR Devices, LLC, manufactures optical brain imaging instruments and licensed IP and know-how from Drexel University. Dr. Ayaz was involved in the technology development and thus offered a minor share in the new startup

firm fNIR Devices, LLC. The authors declare that the research was conducted in the absence of any commercial or financial relationships that could be construed as potential conflicts of interest.

Acknowledgments

This work was supported in part by the National Science Foundation Graduate Research Fellowship under Grant no. DGE-1002809. Work reported here was run on hardware supported by Drexel's University Research Computing Facility.

References

[1] E. Guizzo and E. Ackerman, "The hard lessons of DARPA's robotics challenge," *IEEE Spectrum*, vol. 52, no. 8, pp. 11–13, 2015.

[2] J. R. Wolpaw, N. Birbaumer, D. J. McFarland, G. Pfurtscheller, and T. M. Vaughan, "Brain-computer interfaces for communication and control," *Clinical Neurophysiology*, vol. 113, no. 6, pp. 767–791, 2002.

[3] Y. Chae, J. Jeong, and S. Jo, "Toward brain-actuated humanoid robots: asynchronous direct control using an EEG-Based BCI," *IEEE Transactions on Robotics*, vol. 28, no. 5, pp. 1131–1144, 2012.

[4] W. Li, M. Li, and J. Zhao, "Control of humanoid robot via motion-onset visual evoked potentials," *Frontiers in Systems Neuroscience*, vol. 8, 2015.

[5] B. J. Choi and S. H. Jo, "A low-cost EEG system-based hybrid brain-computer interface for humanoid robot navigation and recognition," *PLoS ONE*, vol. 8, no. 9, article e74583, 2013.

[6] A. Guneysu and L. H. Akin, "An SSVEP based BCI to control a humanoid robot by using portable EEG device," in *Proceedings of the 35th Annual International Conference of the IEEE Engineering in Medicine and Biology Society (EMBC '13)*, pp. 6905–6908, Osaka, Japan, July 2013.

[7] O. Cohen, S. Druon, S. Lengagne et al., "fMRI-Based robotic embodiment: controlling a humanoid robot by thought using real-time fMRI," *Presence: Teleoperators and Virtual Environments*, vol. 23, no. 3, pp. 229–241, 2014.

[8] M. Bryan, J. Green, M. Chung et al., "An adaptive brain-computer interface for humanoid robot control," in *Proceedings of the 2011 11th IEEE-RAS International Conference on Humanoid Robots, HUMANOIDS 2011*, pp. 199–204, svn, October 2011.

[9] C. J. Bell, P. Shenoy, R. Chalodhorn, and R. P. N. Rao, "Control of a humanoid robot by a noninvasive brain-computer interface in humans," *Journal of Neural Engineering*, vol. 5, no. 2, pp. 214–220, 2008.

[10] C. Escolano, J. M. Antelis, and J. Minguez, "A telepresence mobile robot controlled with a noninvasive brain-computer interface," *IEEE Transactions on Systems, Man, and Cybernetics, Part B: Cybernetics*, vol. 42, no. 3, pp. 793–804, 2012.

[11] A. O. G. Barbosa, D. R. Achanccaray, and M. A. Meggiolaro, "Activation of a mobile robot through a brain computer interface," in *Proceedings of the IEEE International Conference on Robotics and Automation (ICRA '10)*, pp. 4815–4821, May 2010.

[12] J. D. R. Millán, F. Renkens, J. Mouriño, and W. Gerstner, "Noninvasive brain-actuated control of a mobile robot by human EEG," *IEEE Transactions on Biomedical Engineering*, vol. 51, no. 6, pp. 1026–1033, 2004.

[13] K. Lafleur, K. Cassady, A. Doud, K. Shades, E. Rogin, and B. He, "Quadcopter control in three-dimensional space using a noninvasive motor imagery-based brain-computer interface," *Journal of Neural Engineering*, vol. 10, no. 4, pp. 711–726, 2013.

[14] A. Akce, M. Johnson, O. Dantsker, and T. Bretl, "A brain-machine interface to navigate a mobile robot in a planar workspace: enabling humans to fly simulated aircraft with EEG," *IEEE Transactions on Neural Systems and Rehabilitation Engineering*, vol. 21, no. 2, pp. 306–318, 2013.

[15] R. Leeb, D. Friedman, G. R. Müller-Putz, R. Scherer, M. Slater, and G. Pfurtscheller, "Self-paced (asynchronous) BCI control of a wheelchair in virtual environments: a case study with a tetraplegic," *Computational Intelligence and Neuroscience*, vol. 2007, Article ID 79642, 8 pages, 2007.

[16] E. López-Larraz, F. Trincado-Alonso, V. Rajasekaran et al., "Control of an ambulatory exoskeleton with a brain-machine interface for spinal cord injury gait rehabilitation," *Frontiers in Neuroscience*, vol. 10, 2016.

[17] X. Cui, S. Bray, D. M. Bryant, G. H. Glover, and A. L. Reiss, "A quantitative comparison of NIRS and fMRI across multiple cognitive tasks," *NeuroImage*, vol. 54, no. 4, pp. 2808–2821, 2011.

[18] Y. Liu, E. A. Piazza, E. Simony et al., "Measuring speaker-listener neural coupling with functional near infrared spectroscopy," *Scientific Reports*, vol. 7, article 43293, 2017.

[19] H. Ayaz, B. Onaral, K. Izzetoglu, P. A. Shewokis, R. Mckendrick, and R. Parasuraman, "Continuous monitoring of brain dynamics with functional near infrared spectroscopy as a tool for neuroergonomic research: empirical examples and a technological development," *Frontiers in Human Neuroscience*, vol. 7, no. 871, 2013.

[20] R. McKendrick, R. Mehta, H. Ayaz, M. Scheldrup, and R. Parasuraman, "Prefrontal hemodynamics of physical activity and environmental complexity during cognitive work," *Human Factors*, vol. 59, no. 1, pp. 147–162, 2017.

[21] K. Gramann, S. H. Fairclough, T. O. Zander, and H. Ayaz, "Editorial: trends in neuroergonomics," *Frontiers in Human Neuroscience*, vol. 11, article 165, 2017.

[22] A. M. Batula, H. Ayaz, and Y. E. Kim, "Evaluating a four-class motor-imagery-based optical brain-computer interface," in *Proceedings of the 36th Annual International Conference of the IEEE Engineering in Medicine and Biology Society (EMBC '14)*, pp. 2000–2003, Chicago, Ill, USA, August 2014.

[23] A. M. Batula, J. Mark, Y. E. Kim, and H. Ayaz, "Developing an optical brain-computer interface for humanoid robot control," in *Lecture Notes in Computer Science (including subseries Lecture Notes in Artificial Intelligence and Lecture Notes in Bioinformatics)*, D. D. Schmorrow and M. C. Fidopiastis, Eds., vol. 9743, pp. 3–13, Springer International Publishing, Toronto, Canda, 2016.

[24] C. Canning and M. Scheutz, "Functional near-infrared spectroscopy in human-robot interaction," *Journal of Human-Robot Interaction*, vol. 2, no. 3, pp. 62–84, 2013.

[25] S. Kishi, Z. Luo, A. Nagano, M. Okumura, Y. Nagano, and Y. Yamanaka, "On NIRS-based BRI for a human-interactive robot RI-MAN," in *Proceedings of the in Joint 4th International Conference on Soft Computing and Intelligent Systems and 9th International Symposium on Advanced Intelligent Systems (SCIS & ISIS)*, pp. 124–129, 2008.

[26] K. Takahashi, S. Maekawa, and M. Hashimoto, "Remarks on fuzzy reasoning-based brain activity recognition with a compact near infrared spectroscopy device and its application to robot control interface," in *Proceedings of the 2014 International Conference on Control, Decision and Information Technologies, CoDIT 2014*, pp. 615–620, fra, November 2014.

[27] K. Tumanov, R. Goebel, R. Möckel, B. Sorger, and G. Weiss, "FNIRS-based BCI for robot control (demonstration)," in *Proceedings of the 14th International Conference on Autonomous Agents and Multiagent Systems, AAMAS 2015*, pp. 1953-1954, tur, May 2015.

[28] A. J. Doud, J. P. Lucas, M. T. Pisansky, and B. He, "Continuous three-dimensional control of a virtual helicopter using a motor imagery based brain-computer interface," *PLoS ONE*, vol. 6, no. 10, article e26322, 2011.

[29] S. Ge, R. Wang, and D. Yu, "Classification of four-class motor imagery employing single-channel electroencephalography," *PLoS ONE*, vol. 9, no. 6, article e98019, 2014.

[30] S. M. Coyle, T. E. Ward, and C. M. Markham, "Brain-computer interface using a simplified functional near-infrared spectroscopy system," *Journal of Neural Engineering*, vol. 4, no. 3, pp. 219–226, 2007.

[31] N. Naseer and K.-S. Hong, "Classification of functional near-infrared spectroscopy signals corresponding to the right- and left-wrist motor imagery for development of a brain-computer interface," *Neuroscience Letters*, vol. 553, pp. 84–89, 2013.

[32] R. Sitaram, H. Zhang, C. Guan et al., "Temporal classification of multichannel near-infrared spectroscopy signals of motor imagery for developing a brain-computer interface," *NeuroImage*, vol. 34, no. 4, pp. 1416–1427, 2007.

[33] T. Ito, H. Akiyama, and T. Hirano, "Brain machine interface using portable near-InfraRed spectroscopy—improvement of classification performance based on ICA analysis and self-proliferating LVQ," in *Proceedings of the 26th IEEE/RSJ International Conference on Intelligent Robots and Systems: New Horizon (IROS '13)*, pp. 851–858, 2013.

[34] X. Yin, B. Xu, C. Jiang et al., "Classification of hemodynamic responses associated with force and speed imagery for a brain-computer interface," *Journal of Medical Systems*, vol. 39, no. 5, 53 pages, 2015.

[35] L. Acqualagna, L. Botrel, C. Vidaurre, A. Kübler, and B. Blankertz, "Large-scale assessment of a fully automatic co-adaptive motor imagery-based brain computer interface," *PLoS ONE*, vol. 11, no. 2, article e0148886, 2016.

[36] B. Koo, H.-G. Lee, Y. Nam et al., "A hybrid NIRS-EEG system for self-paced brain computer interface with online motor imagery," *Journal of Neuroscience Methods*, vol. 244, no. 1, pp. 26–32, 2015.

[37] W. Yi, L. Zhang, K. Wang et al., "Evaluation and comparison of effective connectivity during simple and compound limb motor imagery," in *Proceedings of the 36th Annual International Conference of the IEEE Engineering in Medicine and Biology Society (EMBC '14)*, pp. 4892–4895, Chicago, Ill, USA, August 2014.

[38] N. Naseer and K. Hong, "fNIRS-based brain-computer interfaces: a review," *Frontiers in Human Neuroscience*, vol. 9, pp. 1–15, 2015.

[39] Y. Hashimoto and J. Ushiba, "EEG-based classification of imaginary left and right foot movements using beta rebound," *Clinical Neurophysiology*, vol. 124, no. 11, pp. 2153–2160, 2013.

[40] W.-C. Hsu, L.-F. Lin, C.-W. Chou, Y.-T. Hsiao, and Y.-H. Liu, "EEG classification of imaginary lower LIMb stepping movements based on fuzzy SUPport vector MAChine with Kernel-INDuced MEMbership FUNction," *International Journal of Fuzzy Systems*, vol. 19, no. 2, pp. 566–579, 2017.

[41] L. Stankevich and K. Sonkin, "Human-robot interaction using brain-computer interface based on eeg signal decoding," in *Proceedings of the Interactive Collaborative Robotics (ICR)*, A. Ronzhin, G. Rigoll, and R. Meshcheryakov, Eds., vol. 9812, pp. 99–106, Springer International Publishing.

[42] J. Shin and J. Jeong, "Multiclass classification of hemodynamic responses for performance improvement of functional near-infrared spectroscopy-based brain-computer interface," *Journal of Biomedical Optics*, vol. 19, no. 6, article 067009, 2014.

[43] M. Lotze and U. Halsband, "Motor imagery," *Journal of Physiology Paris*, vol. 99, no. 4–6, pp. 386–395, 2006.

[44] A. Guillot, C. Collet, V. A. Nguyen, F. Malouin, C. Richards, and J. Doyon, "Brain activity during visual versus kinesthetic imagery: an fMRI study," *Human Brain Mapping*, vol. 30, no. 7, pp. 2157–2172, 2009.

[45] C. Jeunet, B. N'Kaoua, and F. Lotte, "Advances in user-training for mental-imagery-based BCI control: pychological and cognitive factors and their neural correlates," *Progress in Brain Research*, vol. 228, pp. 3–35, 2016.

[46] S. Marchesotti, M. Bassolino, A. Serino, H. Bleuler, and O. Blanke, "Quantifying the role of motor imagery in brain-machine interfaces," *Scientific Reports*, vol. 6, article 24076, 2016.

[47] F. Lebon, W. D. Byblow, C. Collet, A. Guillot, and C. M. Stinear, "The modulation of motor cortex excitability during motor imagery depends on imagery quality," *European Journal of Neuroscience*, vol. 35, no. 2, pp. 323–331, 2012.

[48] K. J. Miller, G. Schalk, E. E. Fetz, M. Den Nijs, J. G. Ojemann, and R. P. N. Rao, "Cortical activity during motor execution, motor imagery, and imagery-based online feedback," *Proceedings of the National Academy of Sciences of the United States of America*, vol. 107, no. 9, pp. 4430–4435, 2010.

[49] R. Bauer, M. Fels, M. Vukelić, U. Ziemann, and A. Gharabaghi, "Bridging the gap between motor imagery and motor execution with a brain-robot interface," *NeuroImage*, vol. 108, pp. 319–327, 2015.

[50] M. Ahn and S. C. Jun, "Performance variation in motor imagery brain-computer interface: a brief review," *Journal of Neuroscience Methods*, vol. 243, pp. 103–110, 2015.

[51] E. Tidoni, P. Gergondet, A. Kheddar, and S. M. Aglioti, "Audio-visual feedback improves the BCI performance in the navigational control of a humanoid robot," *Frontiers in Neurorobotics*, vol. 8, 2014.

[52] M. Alimardani, S. Nishio, and H. Ishiguro, "The importance of visual feedback design in BCIs; from embodiment to motor imagery learning," *PLoS ONE*, vol. 11, no. 9, 2016.

[53] A. M. Batula, J. A. Mark, Y. E. Kim, and H. Ayaz, "Comparison of brain activation during motor imagery and motor movement using fNIRS," *Computational Intelligence and Neuroscience*, vol. 2017, Article ID 5491296, 12 pages, 2017.

[54] A. Villringer and B. Chance, "Non-invasive optical spectroscopy and imaging of human brain function," *Trends in Neurosciences*, vol. 20, no. 10, pp. 435–442, 1997.

[55] V. Rozand, F. Lebon, P. J. Stapley, C. Papaxanthis, and R. Lepers, "A prolonged motor imagery session alter imagined and actual movement durations: potential implications for neurorehabilitation," *Behavioural Brain Research*, vol. 297, pp. 67–75, 2016.

[56] H. Ayaz, S. L. Allen, S. M. Platek, and B. Onaral, "Maze Suite 1.0: a complete set of tools to prepare, present, and analyze navigational and spatial cognitive neuroscience experiments," *Behavior Research Methods*, vol. 40, no. 1, pp. 353–359, 2008.

[57] H. Ayaz, P. A. Shewokis, A. Curtin, M. Izzetoglu, K. Izzetoglu, and B. Onaral, "Using MazeSuite and functional near infrared

spectroscopy to study learning in spatial navigation," *Journal of Visualized Experiments*, no. 56, article 3443, 2011.

[58] I. Ha, Y. Tamura, H. Asama, J. Han, and D. W. Hong, "Development of open humanoid platform DARwIn-OP," in *Proceedings of the SICE Annual Conference 2011*, pp. 2178–2181, 2011.

[59] X. Cui, S. Bray, and A. L. Reiss, "Functional near infrared spectroscopy (NIRS) signal improvement based on negative correlation between oxygenated and deoxygenated hemoglobin dynamics," *NeuroImage*, vol. 49, no. 4, pp. 3039–3046, 2010.

[60] H. Tanaka, T. Katura, and H. Sato, "Task-related component analysis for functional neuroimaging and application to near-infrared spectroscopy data," *NeuroImage*, vol. 64, no. 1, pp. 308–327, 2013.

[61] C. M. Bishop, *Pattern Recognition and Machine Learning*, Springer, 2006.

[62] F. Pedregosa, G. Varoquaux, and A. Gramfort, "Scikit-learn: machine learning in Python," *Journal of Machine Learning Research*, vol. 12, pp. 2825–2830, 2011.

[63] R. Takizawa, K. Kasai, Y. Kawakubo et al., "Reduced frontopolar activation during verbal fluency task in schizophrenia: a multi-channel near-infrared spectroscopy study," *Schizophrenia Research*, vol. 99, no. 1–3, pp. 250–262, 2008.

[64] C. L. Friesen, T. Bardouille, H. F. Neyedli, and S. G. Boe, "Combined action observation and motor imagery neurofeedback for modulation of brain activity," *Frontiers in Human Neuroscience*, vol. 10, 2017.

[65] A. Vourvopoulos and S. Bermúdezi Badia, "Motor priming in virtual reality can augment motor-imagery training efficacy in restorative brain-computer interaction: a within-subject analysis," *Journal of NeuroEngineering and Rehabilitation*, vol. 13, no. 1, article 69, 2016.

[66] A. Yuksel and T. Olmez, "A neural network-based optimal spatial filter design method for motor imagery classification," *PLoS ONE*, vol. 10, no. 5, articel e0125039, 2015.

[67] N. Lu, T. Li, X. Ren, and H. Miao, "A deep learning scheme for motor imagery classification based on restricted boltzmann machines," *IEEE Transactions on Neural Systems and Rehabilitation Engineering*, vol. PP, no. 99, 1 page, 2016.

[68] Y. R. Tabar and U. Halici, "A novel deep learning approach for classification of EEG motor imagery signals," *Journal of Neural Engineering*, vol. 14, no. 1, article 016003, 2017.

[69] Z. Tang, C. Li, and S. Sun, "Single-trial EEG classification of motor imagery using deep convolutional neural networks," *Optik - International Journal for Light and Electron Optics*, vol. 130, pp. 11–18, 2017.

Hindawi
BioMed Research International
Volume 2017, Article ID 8316485, 8 pages
https://doi.org/10.1155/2017/8316485

Research Article

Noninvasive Electroencephalogram Based Control of a Robotic Arm for Writing Task Using Hybrid BCI System

Qiang Gao,[1] Lixiang Dou,[1] Abdelkader Nasreddine Belkacem,[2] and Chao Chen[1]

[1]*Key Laboratory of Complex System Control Theory and Application, Tianjin University of Technology, Tianjin 300384, China*
[2]*Endowed Research Department of Clinical Neuroengineering, Global Center for Medical Engineering and Informatics, Osaka University, Osaka 565-0871, Japan*

Correspondence should be addressed to Chao Chen; cccovb@hotmail.com

Received 31 March 2017; Accepted 10 May 2017; Published 1 June 2017

Academic Editor: Victor H. C. de Albuquerque

A novel hybrid brain-computer interface (BCI) based on the electroencephalogram (EEG) signal which consists of a motor imagery-(MI-) based online interactive brain-controlled switch, "teeth clenching" state detector, and a steady-state visual evoked potential-(SSVEP-) based BCI was proposed to provide multidimensional BCI control. MI-based BCI was used as single-pole double throw brain switch (SPDTBS). By combining the SPDTBS with 4-class SSEVP-based BCI, movement of robotic arm was controlled in three-dimensional (3D) space. In addition, muscle artifact (EMG) of "teeth clenching" condition recorded from EEG signal was detected and employed as interrupter, which can initialize the statement of SPDTBS. Real-time writing task was implemented to verify the reliability of the proposed noninvasive hybrid EEG-EMG-BCI. Eight subjects participated in this study and succeeded to manipulate a robotic arm in 3D space to write some English letters. The mean decoding accuracy of writing task was 0.93 ± 0.03. Four subjects achieved the optimal criteria of writing the word "HI" which is the minimum movement of robotic arm directions (15 steps). Other subjects had needed to take from 2 to 4 additional steps to finish the whole process. These results suggested that our proposed hybrid noninvasive EEG-EMG-BCI was robust and efficient for real-time multidimensional robotic arm control.

1. Introduction

Brain-computer interface (BCI) offers a direct communication channel between the brain and external devices without relying on the brain normal output pathways of peripheral nerves and muscles [1]. According to different signal acquisition methods, BCI systems can be divided into two main categories, invasive and noninvasive BCI systems [2–5]. Although invasive BCI systems seem suitable for some clinical applications because of their high signal-to-noise ratio (SNR) and the information transfer rates (ITR), they still suffer from potential surgical risks and postoperative immune response. Noninvasive BCIs might be more suitable for daily life applications for many socioeconomic reasons such as the user's safety and a relatively low cost. Electroencephalography (EEG) is a popular electrophysiological monitoring method to record brain activity and is widely used in noninvasive BCI researches and applications since Berger's discovery [6] and Vidal's first BCI prototype [7].

Nowadays, there are huge opportunity and necessity for helping handicapped people to enhance or increase their abilities to interact with complex environment, such as rehabilitation training sessions, mind-controlled prosthetic arm applications [8, 9], and augmentative and alternative communication systems [10]. However BCIs can also benefit healthy people for entertainment and increasing their independency, especially for elderly persons [11–13]. For decades, several EEG-based typical BCI systems have been proposed based on slow cortical potential (SCP) [14], motor imagery (MI) [15], steady-state visual evoked potential (SSVEP) [16], and the P300 wave of the human event-related potential [10, 17]. Each type of these BCI systems has its unique advantages and some disadvantages. For example, the SSVEP-based BCI system has many advantages such as less training and higher SNR and ITR. MI-based BCI has the advantage of fast response but is limited by the number of tasks. Therefore, there has been increasing interest in solving dimensionality issue by using hybrid BCI which has to be composed of two

BCI modalities' combination (e.g., motor imagery with P300, motor imagery with SSVEP, and P300 with SSVEP) or it can be also a combination of brain and nonbrain activity such as eye movements (EOG), muscles activity (EMG), and heart electrical activity (ECG) to improve the overall performances of BCI systems [18–22]. The electrical activity of muscles can easily interfere with EEG signal considering the anatomical locations of facial or masticatory muscles surrounding the skull. This myogenic contamination of the EEG can constitute a serious problem in BCI applications and it can be useful information in the same time for developing hybrid BCIs. Pfurtscheller et al. proposed an online system using SSVEP-based BCI and a type of ERD BCI, called a "brain switch" [19]. Lately, Punsawad et al. controlled practical machine through hybrid EEG-EOG brain-computer interface system [23]. Then Wang et al. controlled wheelchair directions through unilateral hand imagination and a wheelchair speed through P300 and EOG [24].

Controlling a robotic arm with noninvasive hybrid BCIs surely provides a desirable alternative, but prior to this study it has not been shown that such hybrid systems could achieve multidimensional control of robotic arm in three-dimensional (3D) space. These systems offer a potentially effective control for complex and naturalistic environment through the combination of brain- and nonbrain-based multifunctional BCI. They can reduce user fatigue by switching from a modality to another and increase the degree of freedom for augmentative and alternative BCI systems. The aim of this study is to improve the performance of BCI system by design a new hybrid EEG-EMG-BCI system (i.e., combination of brain activity (MI and SSVEP) with muscles activity such as teeth clenching). In this paper, a hybrid BCI system was described, including motor imagery-based brain switch, "teeth clenching" state detector, and a steady-state visual evoked potential- (SSVEP-) based BCI. In our proposed hybrid BCI, motor imagery decoding was used as a single-pole double throw brain switch (SPDTBS) which can complete multitasks, combined with 4-class SSVEP-based BCI system. In addition, "stop" command was executed by recognizing facial action by recording EMG artifact from EEG signals. For real-time application, a writing task was implemented to verify the performances of our proposed hybrid system. Healthy subjects succeed to write an English word though our proposed hybrid noninvasive BCI system. In the following sections, we describe our proposed system in detail and its real-time writing application to enhance the user's abilities to interact with a complex environment.

2. Methods

2.1. Experimental Paradigm. Our proposed hybrid noninvasive EEG-EMG-BCI system mainly consists of three hardware components which are a portable EEG acquisition device (Emotiv EPOC), a host computer, and a robotic arm (see Figure 1). The EEG signals were recorded and transmitted to the host computer with an USB transceiver dongle. Then, EEG signals were processed and decoded in the host computer. Based on this proposed BCI architecture, the intension of subjects was transformed to multidimensional control commands and sent to operate the Dobot (robotic arm) via the wireless module in real time.

The hybrid BCI consists of MI-, EMG-, and SSVEP-based BCI systems. As shown in Figure 2, the subject imagines the left hand or right hand movement for 4 s as the first step. Once the imagined movements' type (e.g., left hand and right hand movements) was confirmed, the system will enter the second hybrid BCI phase. In the second phase, SSVEP and "teeth clenching" were decoded. The presence of "teeth clenching" was detected during the second phase. Once "teeth clenching" state is confirmed, the program will execute stop command of SSVEP modality and go back to the first motor imagery modality. For SSVEP paradigm, four white blocks (with different frequencies: 6 Hz, 7.5 Hz, 8.57 Hz, and 10 Hz) of stimuli flicker were presented at the top, bottom, left, and right positions in black board.

According to each unilateral movement (right or left hand imagination), the SPDTBS was designed. The SPDTBS was combined with four tasks of SSVEP-based BCI modality to provide more commands (i.e., to achieve multidimensional BCI control) for the robotic arm movements such as the forward, backward, left, right, upward, and downward movements (see Figure 3). All these commands were shown in Table 1.

Eight healthy subjects participated in the experiment (age 23.62 ± 1.06 years (mean ± standard deviation "SD"); one female and seven males). All of them were undergraduate students, without any experience with BCI system. The subjects were seated in a comfortable chair, 50 cm away from the computer screen. The robot arm was placed on the table, about 45° in the left front of the subject. Each subject was able to look at both the monitor and the movement of the robot arm. The subjects were requested to write the word "HI" and the essential steps were shown in Figure 4. It takes at least 15 steps to complete the writing of BCI; each step represents a horizontal or vertical line. The subjects can choose the order of writing, and each step can be written repeatedly.

The following points are used to evaluate the performance of the hybrid BCI system:

(1) Time: time required to complete a task.

(2) Step count: the number of steps to complete the task in paper.

(3) Obvious errors: number of obvious errors. For example, if the writing task is O letter but the result is Q, this result is defined as obvious error.

(4) Information transfer rate, which is defined as

$$\mathrm{ITR} = \frac{60}{T} \times \left[\log_2 N + P\log_2 P + (1-P)\log_2\left(\frac{1-P}{N-1}\right)\right], \quad (1)$$

where N is the number of targets, P is the accuracy rate, and T is the time window length.

The EEG data were sampled at a frequency of 2048 Hz and then downsampled to 128 Hz for signal processing. The

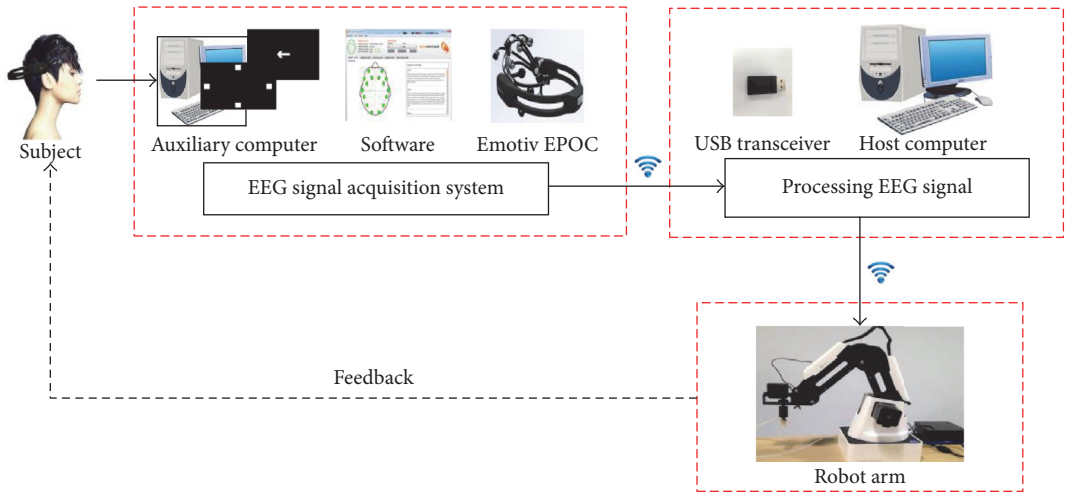

Figure 1: Schematic architecture of the experimental setup for the real-time hybrid BCI-controlled robotic arm.

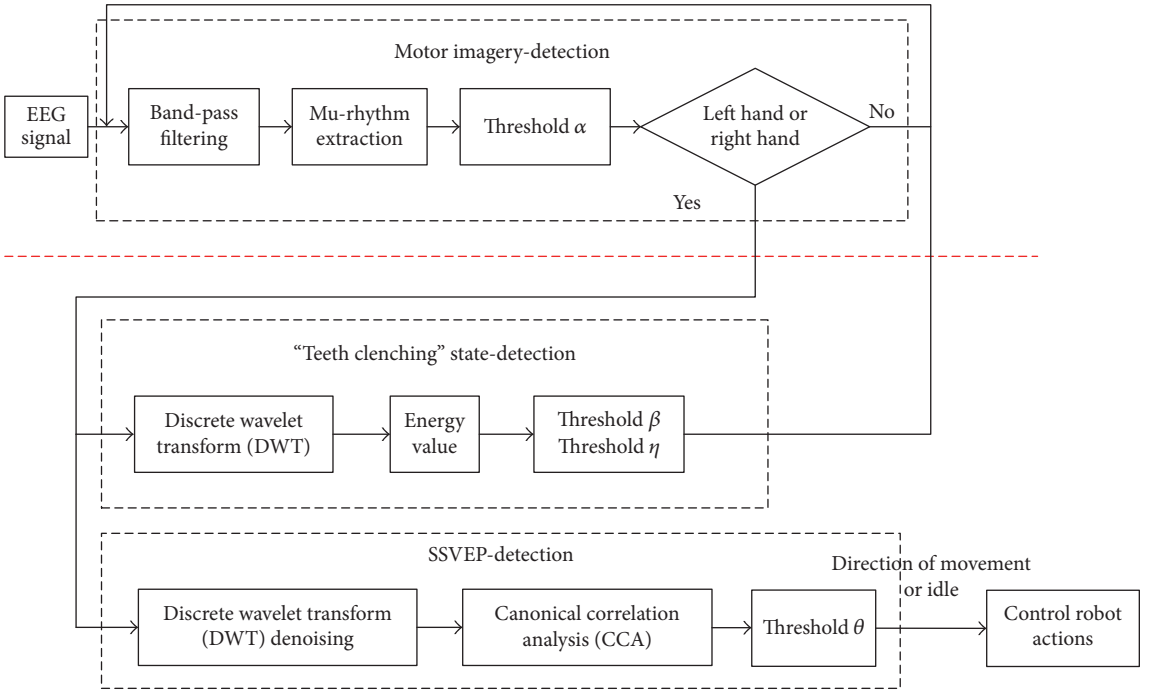

Figure 2: Flowchart of the proposed algorithm for hybrid EEG-EMG-BCI system.

(a) (b) (c)

Figure 3: The six possible directions of the robotic arm. (a) Upward and downward movements. (b) Left and right movements. (c) Forward and backward movements.

Table 1: The control commands of hybrid BCI.

	SPDTBS	SSVEP-based BCI frequency	Control command
Brain activity based on imagined unilateral hand movements (motor imagery) and SSVEP	Left hand imagination	6 Hz	Forward
		7.5 Hz	Backward
		8.57 Hz	Left
		10 Hz	Right
		Idle	No command
	Right hand imagination	6 Hz	No function
		7.5 Hz	No function
		8.57 Hz	Upward
		10 Hz	Downward
		Idle	No command
Muscles activity (EMG artifacts)	"Teeth clenching" state		Stop

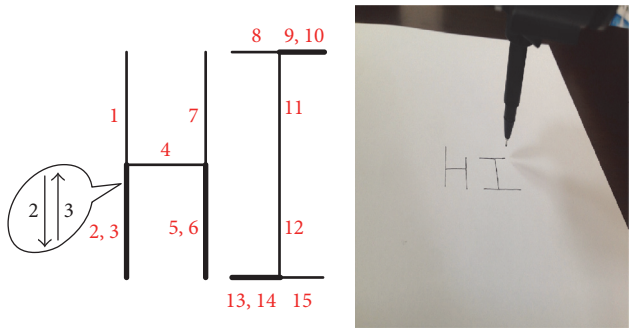

Figure 4: Essential steps for the robotic arm to write the word "HI" with the writing result of the robotic arm controlled by our proposed hybrid BCI in the right side.

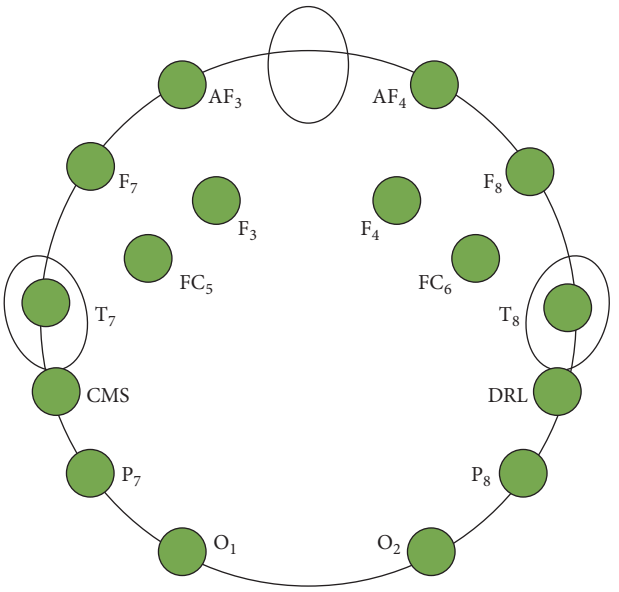

Figure 5: Position of EEG electrodes used in this study for recording brain and nonbrain signals.

electrodes were placed at 10-20 system locations, AF3, F7, F3, FC5, T7, P7, O1, O2, P8, T8, FC6, F4, F8, and AF4, as well as two reference electrodes located above the ears of the subject (i.e., either CMS and DRL or left/right mastoids). Electrodes P7, P8, O1, and O2 were selected to collect SSVEP-based EEG signal. Electrode FC5 and FC6 were used to capture EEG signals in MI. The signals during "teeth clenching" state were collected mainly by electrodes F7 and F8 (see Figure 5).

2.2. Processing Methods for SSVEP-Based BCI. To reduce the effect of signal-to-noise ratio (SNR), discrete wavelet transform (DWT) was employed for preprocessing of EEG signals. Assuming that $x(n)$ is the EEG signal, the DWT of $x(n)$ is defined as

$$C_{j,k} = 2^{-j/2} \sum_{n=-\infty}^{\infty} x(n)\, \overline{\varphi}_{j,k}\left(2^{-j}n - k\right) = \left\langle x(n), \varphi_{j,k} \right\rangle, \quad j,k \in Z, \tag{2}$$

where $\varphi(n)$ is the wavelet basis function, j is the resolution of the frequency, and k is the amount of time translation.

EEG signals were decomposed in different layers (5 layers) by using Daubechies wavelet (db4) function and reconstructed by removing frequency components (0–2 Hz).

The Canonical Correlation Analysis (CCA) is a multivariable statistical method, which was used to analyze the potential correlation between two sets of data [25]. CCA method has been widely used in SSVEP-based BCI system [16, 26].

Suppose two multidimensional random variables X, Y; that is, $X \in R^{H\times J}, Y \in R^{I\times J}$. CCA finds a pair of weight vectors $w_X \in R^{H\times 1}$ and $w_Y \in R^{I\times 1}$, respectively, which maximize the correlation between linear combinations $x = {w_X}^T X$ and $y = {w_Y}^T Y$. It is defined as

$$\max_{w_X, w_Y} \rho(x, y) = \frac{E\left[xy^T\right]}{\sqrt{E\left[xx^T\right] E\left[yy^T\right]}} = \frac{E\left[{w_X}^T XY^T w_Y\right]}{\sqrt{E\left[{w_X}^T XX^T w_X\right] E\left[{w_Y}^T YY^T w_Y\right]}}, \tag{3}$$

Table 2: The results of canonical correlation analysis coefficients for different SSVEP states.

SSVEP state	Mean ± SD
6 Hz	0.4238 ± 0.1060
7.5 Hz	0.4621 ± 0.0857
8.57 Hz	0.4985 ± 0.1000
10 Hz	0.5105 ± 0.0381
Idle	0.1542 ± 0.0397

where the maximum of ρ is the maximum canonical correlation. x and y are projected onto w_X and w_Y.

The reference signals Y_i are set as

$$Y_i = \begin{pmatrix} \sin(2\pi f_i t) \\ \cos(2\pi f_i t) \\ \vdots \\ \sin(2\pi N_h f_i t) \\ \cos(2\pi N_h f_i t) \end{pmatrix}, \quad t = \frac{1}{S}, \frac{2}{S}, \ldots, \frac{N}{S}, \tag{4}$$

where N is the number of sampling points, S is the sampling frequency, and N_h is the number of harmonics.

The control command K is recognized as

$$K = \max_i \rho_i, \quad i = 1, 2, 3, 4, \tag{5}$$

where ρ_i are the CCA coefficients obtained from the four reference signals.

Each subject has different thresholds θ, so threshold θ was defined in training phase. To calculate the threshold θ in CCA, 20 offline experiments were held for each subject. The results were shown in Table 2. The average correlation coefficient of idle state is 0.1542 ± 0.0397 (mean ± SD). So, the threshold θ was defined to be 0.22.

2.3. Processing Methods for MI-Based BCI and "Teeth Clenching" State Detector. The motor imagery classification based on mu frequency power has been widely used for processing event-related synchronization (ERS) and event-related desynchronization (ERD) [15, 27–29]. The second-order moment energy algorithm was employed to classify the left hand with low computational complexity and simple principle [30]. So, these algorithms could be suitable for achieving online BCI systems.

Assuming a signal of length N, the second-order moment is estimated by

$$E_2 = E\left[x^2(n)\right] \approx \frac{1}{N}\sum_{n=1}^{N} x^2(n). \tag{6}$$

In MI-based BCI experiment, while imagining the left hand or right hand movement, the EEG signals are collected with band-pass filtering (0–32 Hz), mu rhythm energy change of FC5 and FC6 was computed, and the energy difference between FC5 and FC6 channels is used to calculate the threshold α for classification. Mu rhythm energy change of FC5 and FC6 is denoted as E.

$$\hat{e} = \begin{cases} +1 & \text{if } E > \alpha \\ 0 & \text{otherwise} \\ -1 & \text{if } E < -\alpha. \end{cases} \tag{7}$$

When $\hat{e} = 1$, which indicates the subject is imagining left hand motor imagery, the first path is closed in SPDTBS. When $\hat{e} = -1$, which indicates the subject is imagining right hand motor imagery, then the second path is closed in SPDTBS. When $\hat{e} = 0$, which indicates the subject is in an idle state, no command will be given to the system, and the SPDTBS is opened.

Accuracy of detecting "teeth clenching" state is higher than other facial states in EEG-based BCI system [31]. Thus, "teeth clenching" state was detected to work as interrupt system, which can confirm motor imagery result and improve the performance of whole system.

According to the characteristics of different states ("natural" versus "teeth clenching"), the threshold β of standard deviation and threshold η of the peak distance (the absolute value of the difference between the maximum and the minimum) of the EEG signals were calculated, respectively. In online experiment, to detect the "teeth clenching" state, standard deviation S_s and peak distance S_p were computed and compared with thresholds β and η.

$$\hat{s} = \begin{cases} 1 & \text{if } S_s > \beta,\ S_p > \eta \\ 0 & \text{otherwise,} \end{cases} \tag{8}$$

where $\hat{s} = 1$ indicates that the subject is in "teeth clenching" state and, otherwise, $\hat{s} = 0$ means that the subject is in "natural" state.

3. Results of Brain-Control Tasks

In the first stage, an offline experiment was held for MI-based BCI and SSVEP-based BCI and "teeth clenching" state detector, respectively. As shown in Figure 6, the average accuracy of eight subjects in MI-based BCI and SSVEP-based BCI is 0.73 ± 0.05 and 0.93 ± 0.03, respectively. The ITR of SSVEP-based BCI is 18.43 ± 1.63 (Figure 7). For "teeth clenching" state detector, all subjects achieved accuracy near 1.

Eight subjects joined the writing task using a robotic arm. The results were shown in Figures 4, 6, and 7. All of subjects were successful in writing the word "HI." Eight subjects completed the writing task in 297.37 ± 57.96 seconds on average. As shown in Figure 7, four subjects took 15 steps (optimal number of steps) to finish writing, three subjects took 17 steps, and one subject took 19 steps. Only one subject has 1 significant error. The average accuracy was obtained as 0.92 ± 0.03.

4. Discussion

In this paper, a novel multichannel hybrid BCI system was proposed for multidimensional control purpose, which was composed of a motor-imagery-based brain switch, "teeth

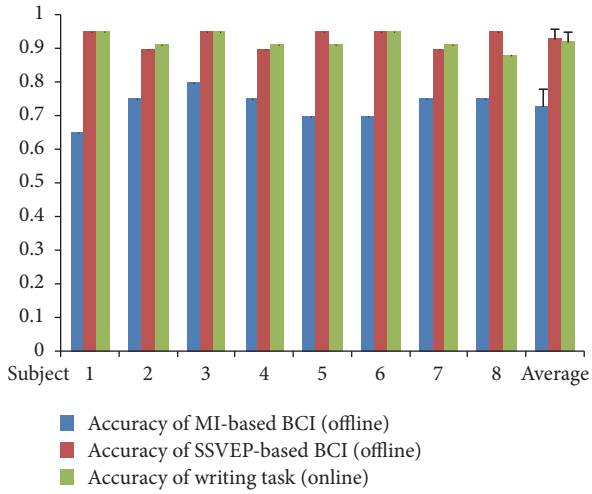

Figure 6: Decoding accuracy of the hybrid BCI system.

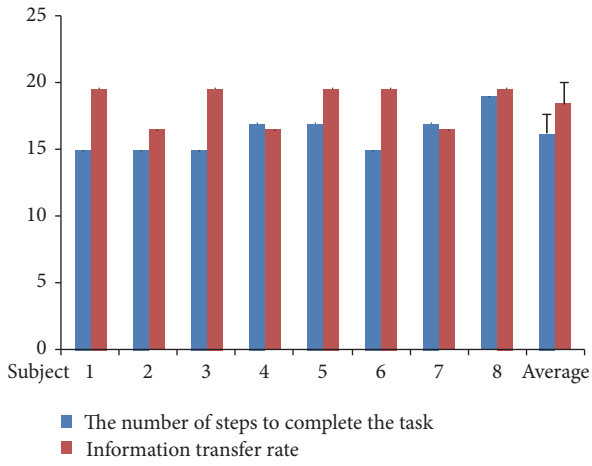

Figure 7: Performances of writing task.

clenching" state detector, and SSVEP-based BCI. For achieving a multidimensional control of robotic arm, seven commands which can be up to nine were designed for real-time BCI application. Writing task was held to evaluate the performances of the proposed hybrid system. Eight subjects completed the movement tasks of the robotic arm to write the word "HI."

Pfurtscheller et al. [19] used MI-based brain switch to turn on/off an SSVEP BCI for reducing the errors in resting periods, while, in this present work, MI-based brain switch was used as single-pole double throw brain switch (SPDTBS) to extend the number of commands which robotic arm needs to be fully controlled and manipulated to achieve a naturalistic hand pathway of writing a simple word. In addition, a "teeth clenching" state detector was design to initialize the statement of SPDTBS. Because of the relative lower accuracy of motor imagery BCI, the "teeth clenching" state detector can confirm the result of MI-based BCI, which can improve the accuracy of hybrid BCI system significantly. Thus, the accuracy of proposed system is almost the same as previous work [19], which can lead us to conclude that the proposed system is efficient and robust for real-time multifunctional BCI systems. Compared with the current BCI systems [32–34], the proposed hybrid BCI system shows higher accuracy with high degree of freedom. Moreover, wireless manner was used to build a stable and suitable connection for online experiment, which is meaningful for portable noninvasive BCI products for real-life use.

In this study, we found that a group of healthy subjects could willingly use brain and nonbrain activity to control a robotic arm with high accuracy for performing writing tasks requiring human intention, error feedback, and multiple degrees of freedom by combination of MI, SSVEP, and EMG activity (see Supplementary video in Supplementary Material available online at https://doi.org/10.1155/2017/8316485). The robotic arm could only move and write horizontal and vertical lines using our proposed BCI paradigm. There are still two commands, "no function," in the proposed system, which can be used for writing slanted lines. This option will be added in the near future to achieve naturalistic hand writing. Thus, the users will be able to write any intended complex word in real time, which not only can be used as communication tool for the disable people, but also can be applied for education purposes for children and students using e-learning aspect which could be an innovative way to practice using teleoperation to remotely access a robotic arm using their brain activity.

5. Conclusions

This paper presented a combination of synchronous and asynchronous control using a novel hybrid EEG-EMG-based BCI which consists of motor imagery, muscle artifacts, and SSVEP to provide a multidimensional control. The synchronous control is based on SSVEP paradigm which requires the user to focus on the screen and the asynchronous control is based on the motor imagery which does not need any synchronization between the user and the screen because it is based on the imagination of the unilateral movements. Users were able to write an English word using our robust real-time control of a robotic arm through the proposed hybrid BCI. This proposed BCI was designed for multiclass control in a complex environment. Results of the study indicated that successful multidimensional control is possible using suitable combination of BCI modalities to detect and classify brain activity in different situations.

In the near future, for rehabilitation, e-learning, and entertainment, we would like to design low cost, portable, noninvasive, and hybrid EEG-EMG-based robotic arm using minimum number of wearable wireless sensors.

Conflicts of Interest

The authors declare that there are no conflicts of interest regarding the publication of this paper.

Acknowledgments

This work was financially supported by Natural Science Foundation of Tianjin City (15JCYBJC51800), Tianjin Key

Laboratory Foundation of Complex System Control Theory and Application (TJKL-CTACS-201702), and Young and Middle-Aged Innovation Talents Cultivation Plan of Higher Institutions in Tianjin (Grant no. 20130830).

References

[1] J. R. Wolpaw, N. Birbaumer, D. J. McFarland, G. Pfurtscheller, and T. M. Vaughan, "Brain-computer interfaces for communication and control," *Clinical Neurophysiology*, vol. 113, no. 6, pp. 767–791, 2002.

[2] N. Birbaumer, C. Weber, C. Neuper, E. Buch, K. Haapen, and L. Cohen, "Physiological regulation of thinking: brain-computer interface (BCI) research," *Progress in Brain Research*, vol. 159, pp. 369–391, 2006.

[3] L. R. Hochberg and J. P. Donoghue, "Sensors for brain-computer interfaces: Options for turning thought into action," *IEEE Engineering in Medicine and Biology Magazine*, vol. 25, no. 5, pp. 32–38, 2006.

[4] G. Schalk, P. Brunner, L. A. Gerhardt, H. Bischof, and J. R. Wolpaw, "Brain-computer interfaces (BCIs): detection instead of classification," *Journal of Neuroscience Methods*, vol. 167, no. 1, pp. 51–62, 2008.

[5] S. G. Mason, A. Bashashati, M. Fatourechi, K. F. Navarro, and G. E. Birch, "A comprehensive survey of brain interface technology designs," *Annals of Biomedical Engineering*, vol. 35, no. 2, pp. 137–169, 2007.

[6] H. Berger, "Uber das elektrenkephalogramm des menschen," *European Archives of Psychiatry and Clinical Neuroscience*, vol. 87, no. 1, pp. 527–570, 1929.

[7] J. J. Vidal, "Toward direct brain-computer communication," *Annual Review of Biophysics and Bioengineering*, vol. 2, pp. 157–180, 1973.

[8] G. Pfurtscheller and C. Neuper, "Motor imagery and direct brain-computer communication," *Proceedings of the IEEE*, vol. 89, no. 7, pp. 1123–1134, 2001.

[9] C. Wang, S. P. Kok, K. A. Kai et al., "A feasibility study of non-invasive motor-imagery BCI-based robotic rehabilitation for stroke patients," in *Proceedings of the 4th International IEEE/EMBS Conference on Neural Engineering*, pp. 271–274, May 2009.

[10] L. A. Farwell and E. Donchin, "Talking off the top of your head: toward a mental prosthesis utilizing event-related brain potentials," *Electroencephalography and Clinical Neurophysiology*, vol. 70, no. 6, pp. 510–523, 1988.

[11] A. Finke, A. Lenhardt, and H. Ritter, "The Mindgame: a P300-based brain-computer interface game," *Neural Networks*, vol. 22, no. 9, pp. 1329–1333, 2009.

[12] J. A. Pineda, D. S. Silverman, A. Vankov, and J. Hestenes, "Learning to control brain rhythms: making a brain-computer interface possible," *IEEE Transactions on Neural Systems and Rehabilitation Engineering*, vol. 11, no. 2, pp. 181–184, 2003.

[13] T. M. Nunes, A. L. V. Coelho, C. A. M. Lima, J. P. Papa, and V. H. C. de Albuquerque, "EEG signal classification for epilepsy diagnosis via optimum path forest—a systematic assessment," *Neurocomputing*, vol. 136, pp. 103–123, 2014.

[14] N. Birbaumer, N. Ghanayim, T. Hinterberger et al., "A spelling device for the paralysed," *Nature*, vol. 398, no. 6725, pp. 297-298, 1999.

[15] G. Pfurtscheller and F. H. L. da Silva, "Event-related EEG/MEG synchronization and desynchronization: basic principles," *Clinical Neurophysiology*, vol. 110, no. 11, pp. 1842–1857, 1999.

[16] Z. Lin, C. Zhang, W. Wu, and X. Gao, "Frequency recognition based on canonical correlation analysis for SSVEP-based BCIs," *IEEE Transactions on Biomedical Engineering*, vol. 53, no. 12, pp. 2610–2614, 2006.

[17] S. Sutton, M. Braren, and J. Zubin, "Evoked-potential correlates of stimulus uncertainty," *Science*, vol. 150, no. 3700, pp. 1187-1188, 1965.

[18] G. Pfurtscheller, B. Z. Allison, C. Brunner et al., "The hybrid BCI," *Frontiers in Neuroscience*, vol. 4, article 30, 2010.

[19] G. Pfurtscheller, T. Solis-Escalante, R. Ortner, P. Linortner, and G. R. Muller-Putz, "Self-paced operation of an SSVEP-based orthosis with and without an imagery-based "brain switch": a feasibility study towards a hybrid BCI," *IEEE Transactions on Neural Systems and Rehabilitation Engineering*, vol. 18, no. 4, pp. 409–414, 2010.

[20] Y. Li, J. Pan, F. Wang, and Z. Yu, "A hybrid BCI system combining P300 and SSVEP and its application to wheelchair control," *IEEE Transactions on Biomedical Engineering*, vol. 60, no. 11, pp. 3156–3166, 2013.

[21] B. Rebsamen, E. Burdet, Q. Zeng et al., "Hybrid P300 and Mu-Beta brain computer interfaceto operate a brain controlled wheelchair," *Assistive Technol*, pp. 51–55, 2008.

[22] A. N. Belkacem, S. Saetia, K. Zintus-Art et al., "Real-time control of a video game using eye movements and two temporal EEG sensors," *Computational Intelligence and Neuroscience*, vol. 2015, Article ID 653639, 10 pages, 2015.

[23] Y. Punsawad, Y. Wongsawat, and M. Parnichkun, "Hybrid EEG-EOG brain-computer interface system for practical machine control," in *Proceedings of the 2010 32nd Annual International Conference of the IEEE Engineering in Medicine and Biology Society (EMBC 2010)*, pp. 1360–1363, Buenos Aires, August 2010.

[24] H. Wang, Y. Li, J. Long, T. Yu, and Z. Gu, "An asynchronous wheelchair control by hybrid EEG-EOG brain-computer interface," *Cognitive Neurodynamics*, vol. 8, no. 5, pp. 399–409, 2014.

[25] H. Hotelling, "Relations Between Two Sets of Variates," *Biometrika*, vol. 28, no. 3/4, p. 321, 1936.

[26] G. Bin, X. Gao, Z. Yan, B. Hong, and S. Gao, "An online multi-channel SSVEP-based brain-computer interface using a canonical correlation analysis method," *Journal of Neural Engineering*, vol. 6, no. 4, Article ID 046002, 2009.

[27] G. Pfurtscheller, G. R. Müller-Putz, A. Schlögl et al., "15 years of BCI research at graz university of technology: current projects," *IEEE Transactions on Neural Systems and Rehabilitation Engineering*, vol. 14, no. 2, pp. 205–210, 2006.

[28] G. Pfurtscheller, G. R. Müller-Putz, A. Schlögl et al., "15 years of BCI research at graz university of technology: current projects," *IEEE Transactions on Neural Systems and Rehabilitation Engineering*, vol. 14, no. 2, pp. 205–210, 2006.

[29] E. Dong, C. Li, L. Li et al., "Classification of multi-class motor imagery with a novel hierarchical svm algorithm for brain computer interfaces," *Medical Biological Engineering & Computing*, pp. 10–1007, 2017.

[30] G. Pfurtscheller, C. Neuper, C. Andrew, and G. Edlinger, "Foot and hand area mu rhythms," *International Journal of Psychophysiology*, vol. 26, no. 1-3, pp. 121–135, 1997.

[31] J. Lin and Z. Y. Jiang, "An EEG-based BCI system to facial action recognition," *Wireless Personal Communications*, pp. 1–16, 2016.

[32] I. Martišius and R. Damaševičius, "A prototype SSVEP based real time bci gaming system," *Computational Intelligence & Neuroscience*, vol. 2016, no. 3, Article ID 3861425, 15 pages, 2016.

[33] K. Holewa and A. Nawrocka, "Emotiv EPOC neuroheadset in brain—computer interface," in *Proceedings of the 15th International Carpathian Control Conference (ICCC '14)*, pp. 149–152, IEEE, Velke Karlovice, Czech Republic, May 2014.

[34] Y. Liu, X. Jiang, T. Cao et al., "Implementation of SSVEP based BCI with Emotiv EPOC," in *Proceedings of the 10th IEEE International Conference on Virtual Environments, Human-Computer Interfaces, and Measurement Systems (VECIMS '12)*, pp. 34–37, Tianjin, China, July 2012.

Hindawi
BioMed Research International
Volume 2017, Article ID 7395385, 10 pages
https://doi.org/10.1155/2017/7395385

Research Article

A MISO-ARX-Based Method for Single-Trial Evoked Potential Extraction

Nannan Yu,[1] Lingling Wu,[1] Dexuan Zou,[1] Ying Chen,[1] and Hanbing Lu[2]

[1]*School of Electrical Engineering and Automation, Jiangsu Normal University, Xuzhou 221116, China*
[2]*Department of Internal Neurology, Xuzhou Central Hospital, Xuzhou 221116, China*

Correspondence should be addressed to Hanbing Lu; luhanbing111@126.com

Received 15 November 2016; Accepted 9 January 2017; Published 8 February 2017

Academic Editor: Victor H. C. de Albuquerque

In this paper, we propose a novel method for solving the single-trial evoked potential (EP) estimation problem. In this method, the single-trial EP is considered as a complex containing many components, which may originate from different functional brain sites; these components can be distinguished according to their respective latencies and amplitudes and are extracted simultaneously by multiple-input single-output autoregressive modeling with exogenous input (MISO-ARX). The extraction process is performed in three stages: first, we use a reference EP as a template and decompose it into a set of components, which serve as subtemplates for the remaining steps. Then, a dictionary is constructed with these subtemplates, and EPs are preliminarily extracted by sparse coding in order to roughly estimate the latency of each component. Finally, the single-trial measurement is parametrically modeled by MISO-ARX while characterizing spontaneous electroencephalographic activity as an autoregression model driven by white noise and with each component of the EP modeled by autoregressive-moving-average filtering of the subtemplates. Once optimized, all components of the EP can be extracted. Compared with ARX, our method has greater tracking capabilities of specific components of the EP complex as each component is modeled individually in MISO-ARX. We provide exhaustive experimental results to show the effectiveness and feasibility of our method.

1. Introduction

Evoked potentials (EPs) are localized potential changes generated by the central nervous system when stimulated by well-defined external stimuli (such as electrical, light, sound, and other stimuli) [1]. Thus, EPs can be categorized as auditory evoked potentials (AEPs), visual evoked potentials (VEPs), somatosensory evoked potentials (SEPs), and motor evoked potentials (MEPs) according to the modality of stimulation. Depending on the experimental paradigm, EPs may include a complex of partially overlapping components [2], reflecting different processing stages along the neural pathways. The latency variations of specific components can objectively reflect changes in the underlying state of the neural pathways, which is very meaningful in cognitive science research and clinical applications [3]. Many single-trial EP extracting methods have been proposed in order to enhance the ability to track latency variations.

Parametric modeling using autoregression with exogenous inputs (ARX) is a commonly used method for extracting single-trial EPs over the conventional moving time average [4]. ARX modeling for single-trial EP estimation was first proposed by Cerutti et al. [5]. In ARX, the electroencephalogram (EEG) can be viewed as an autoregression (AR) model driven by white noise, and the EP can be accurately modeled by an autoregressive-moving-average (ARMA) filter with a known signal [6]. The known signal is typically the average of the reference EPs (AREP). The order and parameters of the AR and ARMA models can be estimated by utilizing various optimization techniques, such as the final prediction error (FPE) [5] and the least-squares (LS) method [7]. The EPs can then be reconstructed by ARMA filtering with the AREP. ARX modeling has been widely adopted by researchers to rapidly extract middle latency AEPs, VEPs, and SEPs. For example, Mainardi et al. [8] used the ARX model to quantify changes in auditory N100 for

the monitoring of sedation in cardiac surgery patients. Rossi et al. [9] extracted single-trial SEPs with ARX filtering for monitoring the functional integrity of the spinal cord during surgery. Lange and Inbar [10] further extended the ARX estimator to make the single-trial estimation process resistant to noise present in the system using a robust evoked potential estimator (REPE). However, Cerutti et al. [5] recently found, by systemic experimentation, that EP extraction using ARX modeling is completely invalid when latency varies greatly compared with the AREP. We carried out a further study on the single-trial extracting experiments made by De Silva et al. [11]. We found that they always assumed temporal lag between the input and the output of the ARX model equaled zero, which causes significant error when latency varies greatly. In addition, they limited the ARX method to yield a waveform similar to the average response, differing only in global latency. Thus, their procedure cannot demonstrate the method's tracking capabilities of specific components of the EPs. An EP complex may contain components that originated from different functional brain sites [12]. The summation of these components results in component overlap, which may cause partial occlusion of the desired component's features. Because of this, the tracking of latency variations of specific components is very difficult.

In this paper, we present a novel single-trial evoked potential estimation method based on multiple-input single-output ARX (MISO-ARX). In MISO-ARX, each component of the EP is individually modeled by an ARMA filter with a reference signal to avoid different components interfering with each other as in ARX. In addition, all parameters are calculated synchronously to guarantee that the estimated EP is optimal overall. Moreover, as EPs have been proven (in our previous paper) to have strong sparsity over an appropriate dictionary, we first roughly estimate the temporal lag of specific components with sparse coding before calculating the parameters of MISO-ARX in order to improve robustness against great latency variations. A series of experiments carried out on simulated and human test responses confirmed the superior performance of our MISO-ARX method for tracking latency variations even in situations of extremely low SNR. The rest of this paper is organized as follows. Section 2 gives a detailed description of our single-trial estimation algorithm. Section 3 contains our experimental results obtained by using the MISO-ARX method and a comparison with ARX and REPE methods. Section 4 presents our conclusions.

2. Single-Trial Evoked Potential Extraction with MISO-ARX

EPs are always embedded in the ongoing spontaneous EEG background, and the SNR is extremely low (below 0 dB). The main parts of our method consist of removing the EEG $e(t)$ from the measurement $y(t)$ and then reconstructing the single-trial EP $s(t)$ [13]. The measurement $y(t)$ is

$$y(t) = s(t) + e(t). \tag{1}$$

2.1. The EP Signal. The single-trial EP is considered as a complex containing many components; these components may originate from different functional brain sites and can be distinguished according to their respective latencies and amplitudes. The EP waveform $s(t)$ is assumed to be a superposition of Q components:

$$s(t) = \sum_{q=1}^{Q} k_i v_q\left(t - \tau_q\right), \tag{2}$$

where $v_q(t)$ is the basic shape of the qth component, τ_q is the component's latency, and k_q indicates the component's amplitude.

In MISO-ARX, each component $v_q(t)$ is derived by filtering the reference $u_q(t)$ using the ARMA model parameters, as shown in

$$v_q(t) = \frac{B_q\left(z^{-1}\right)}{A_q\left(z^{-1}\right)} u_q(t), \tag{3}$$

where $A_q(z^{-1}) = 1 - \sum_{i=1}^{n^q} a_i^q z^{-i}$ and $B_q(z^{-1}) = z^{-d^q} \sum_{j=0}^{m^q-1} b_j^q z^{-j}$. Thus, (2) can be rewritten as

$$s(t) = \sum_{q=1}^{Q} k_q v_q\left(t - \tau_q\right) = \sum_{q=1}^{Q} k_q \frac{B_q\left(z^{-1}\right) u_q\left(t - \tau_q\right)}{A_q\left(z^{-1}\right)}. \tag{4}$$

In (4), $k_q B_q(z^{-1}) u_q(t - \tau_q)$ can be parameterized as

$$\begin{aligned} k_q B_q\left(z^{-1}\right) u_q\left(t - \tau_q\right) &= k_q \sum_{j=0}^{m^q-1} b_j^q u_q\left(t - j - d^q - \tau_q\right) \\ &= \sum_{j=0}^{m^q-1} \left(b_j^q k_q\right) u_q\left[t - j - \left(d^q + \tau_q\right)\right]. \end{aligned} \tag{5}$$

Then, we assume $\overline{b}_j^q = b_j^q k_q$ and $\overline{d}^q = d^q + \tau_q$, which yields

$$\begin{aligned} &k_q B_q\left(z^{-1}\right) u_q\left(t - \tau_q\right) \\ &\quad = \sum_{j=0}^{m^q-1} \left(b_j^q k_q\right) u_q\left[t - j - \left(d^q + \tau_q\right)\right] \\ &\quad = \sum_{j=0}^{m^q-1} \overline{b}_j^q u_q\left(t - j - \overline{d}^q\right). \end{aligned} \tag{6}$$

Thus, $k_q B_q(z^{-1}) u_q(t - \tau_q) = \overline{B}_q(z^{-1}) u_q(t)$, and we obtain

$$s(t) = \sum_{q=1}^{Q} k_q v_q\left(t - \tau_q\right) = \sum_{q=1}^{Q} \frac{\overline{B}_q\left(z^{-1}\right) u_q(t)}{A_q\left(z^{-1}\right)}. \tag{7}$$

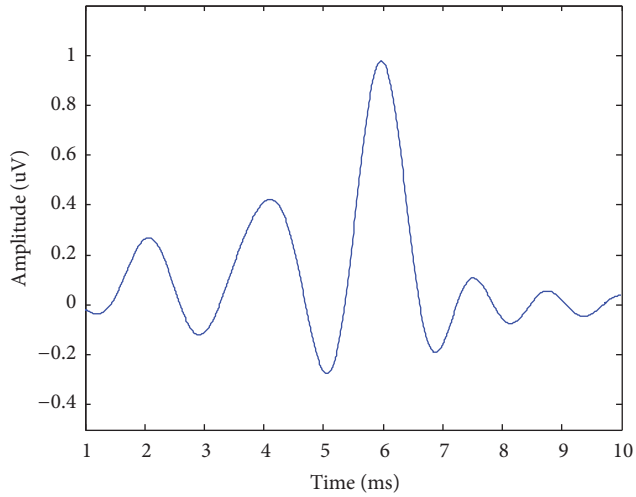

Figure 1: The reference signal extracted from the AREP.

2.2. Reference Signal for Each Component. The selection of reference signals, which directly affects the accuracy of EP extraction, is a very important process. In MISO-ARX, we extract the reference signal $u_q(t)$ for each component from the AREP using a specific filtering window function, such as the Hamming window or the Blackman window. The central location and width of the window are determined by the location and width of the peak, respectively. An example of a simulated decomposition is provided in Figure 1. It can be seen that the simulated waveform consists of three underlying components, which were extracted using a Hamming window.

2.3. The EEG Signal. In this paper, the EEG signal $e(t)$ is viewed as an AR model driven by white noise $w(t)$, defined as

$$e(t) = \frac{1}{A_e\left(z^{-1}\right)} w(t), \tag{8}$$

where $A_e(z^{-1}) = 1 - \sum_{i=1}^{n^e} a_i^e z^{-i}$.

2.4. Estimation of Temporal Lag. In ARX, most researchers assume that temporal lag d between the input and output of the model is equal to zero before estimating the model orders m and n. This assumption is not in accordance with practice. In this study, we used sparse coding to roughly estimate the value of d. Sparse coding has had significant success in signal denoising and separation. In addition, in our previous paper, EPs were proven to have strong sparsity over an appropriate dictionary [14]. Assuming D and θ are the dictionary and the sparse coefficients, respectively, $s(t)$ can be expressed as $s(t) = D\theta$ [15]. Thus, $y(t)$ is

$$y(t) = s(t) + e(t) = D\theta + e(t). \tag{9}$$

The estimator for θ is calculated by solving

$$\begin{aligned} \widehat{\theta} = \arg\min_{\theta} \quad & \|\theta\|_0 \\ \text{s.t.} \quad & \left\| y(t) - D \cdot \theta \right\|_2 \le \varepsilon_0, \end{aligned} \tag{10}$$

where ε_0 is determined by the variance of the EEG. Equation (10) can be solved by using optimization methods, such as basis pursuit [16], orthonormal matching pursuit [17], and Lasso [18]. Since the atoms of D are constructed by left or right translation of the basic components of EPs, we use the location of nonzero values in θ to estimate the temporal lag d.

2.5. Single-Trial Extraction. By replacing (7) and (8) in (1), we get

$$\begin{aligned} y(t) &= s(t) + e(t) \\ &= \sum_{q=1}^{Q} \frac{\overline{B}_q\left(z^{-1}\right) u_q(t)}{A_q\left(z^{-1}\right)} + \frac{1}{A_e\left(z^{-1}\right)} w(t). \end{aligned} \tag{11}$$

In order to simplify this model, we assume $A_q(z^{-1}) = A_e(z^{-1}) = A(z^{-1})$. This implies a partial loss of generality with respect to the AR model for the noise and the ARMA model for the signal, completely independent of each other. Nevertheless, the MISO-ARX model requires more complex algorithms to be characterized. In this paper, this MISO system is characterized with the global separable nonlinear multi-innovation recursive least-squares-identification method [19]. Then, parameters $A(z^{-1})$ and $\overline{B}_q(z^{-1})$ are estimated. The EP can be reconstructed as

$$s(t) = \sum_{q=1}^{Q} s_q(t) = \sum_{q=1}^{Q} \frac{\overline{B}_q\left(z^{-1}\right) u_q(t)}{A\left(z^{-1}\right)}. \tag{12}$$

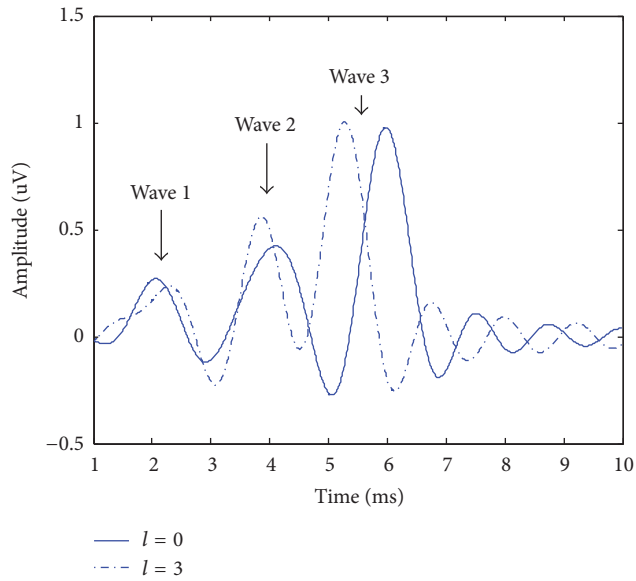

Figure 2: The waves of the reference signals in $l = 0$ and $l = 3$.

3. Experimental Results

3.1. Simulation Experiment. A computer simulation was conducted to verify the performance of our MISO-ARX method for EP signal estimation. Three single-trial-estimation methods for EP signals, namely, ARX, REPE, and SP, were compared in the following simulations. In order to measure the performance of each of the methods, we measured the SNR of the estimated EPs and the accuracy of the latencies for different SNRs to evaluate the quality of these methods. All experiments were implemented in Matlab R2006b on a Pentium 2.7 GHz PC with 4 GB RAM.

The reference signals $v_i(k)$ were simulated by the superimposition of three basic components, which can be represent by the Gaussian distribution function [20]; thus

$$\begin{aligned} u(t) &= 0.25\,\mathrm{sinc}\left[0.13\pi\left(4t-8\right)\right] \\ &\quad + 0.5\,\mathrm{sinc}\left[0.13\pi\left(4t-16\right)\right] \\ &\quad + \mathrm{sinc}\left[0.13\pi\left(4t-24+l\right)\right]. \end{aligned} \tag{13}$$

The synthetic reference signals ($l = 0$ and $l = 3$) are shown in Figure 2.

From Figure 2, it can be seen that all three components have changed and the latency of the third wave varies significantly. In this study, we used an EP with $l = 0$ as the reference signal. The background EEG superimposed on the EP signal was simulated by an autoregressive process [21], as shown in the following equation:

$$\begin{aligned} q(t) &= 1.5084q(t-1) - 0.1587q(t-2) \\ &\quad - 0.3109q(t-3) - 0.0510q(t-4) + w(t), \end{aligned} \tag{14}$$

where $w(t)$ is Gaussian white noise. During the process of estimation, the SNR of the observations may change over time due to the nonstationary characteristics of the EEG. Therefore, in this experiment, the performance of the four different methods was examined under various SNR conditions. The SNRs of the observations were changed from 0 dB to −10 dB, and l was changed from −5 to 5. For each SNR value, 100 pairs of observations were generated. The average results for different SNR and l values in 100 independent runs are shown in Figure 3.

It is clear that, with the decrease of the value of the SNR, estimation performance declines. However, in MISO-ARX, the changes in l had hardly any impact on the estimation results. This illustrates that our method is apt for tracking latency variation of EPs. Since the SNR is defined by the complete signal and not by a specific feature of it, we measured the MISO-ARX method's ability of tracking latency variations. We compared ARX and MISO-ARX in the case of three different SNR values (0 dB, −5 dB, and −10 dB) and four different latencies (4.17 ms ($l = 7$), 5.29 ms ($l = 3$), 6.26 ms ($l = -1$), and 7.24 ms ($l = -5$)). Results are shown in Figure 4. We can see from Figures 4(a) and 4(b) that, for high SNR values (0 dB and −5 dB), our method had strong tracking capability for all latencies. Figure 4(c) indicates a deterioration of latency tracking performance when the SNR decreased, but the MISO-ARX method's accuracy rate still exceeded 70%. With ARX, even for high SNR values, for $l = -5$ and $l = 7$ the estimations were totally wrong, suggesting that tracking such variations is not possible.

3.2. Real Data. For further evaluation of the performance of our method, VEPs were collected from six eyes belonging to three human subjects during pattern reversal VEP experiments. This study was conducted with the approval of the local ethics committee, and all experiments with human

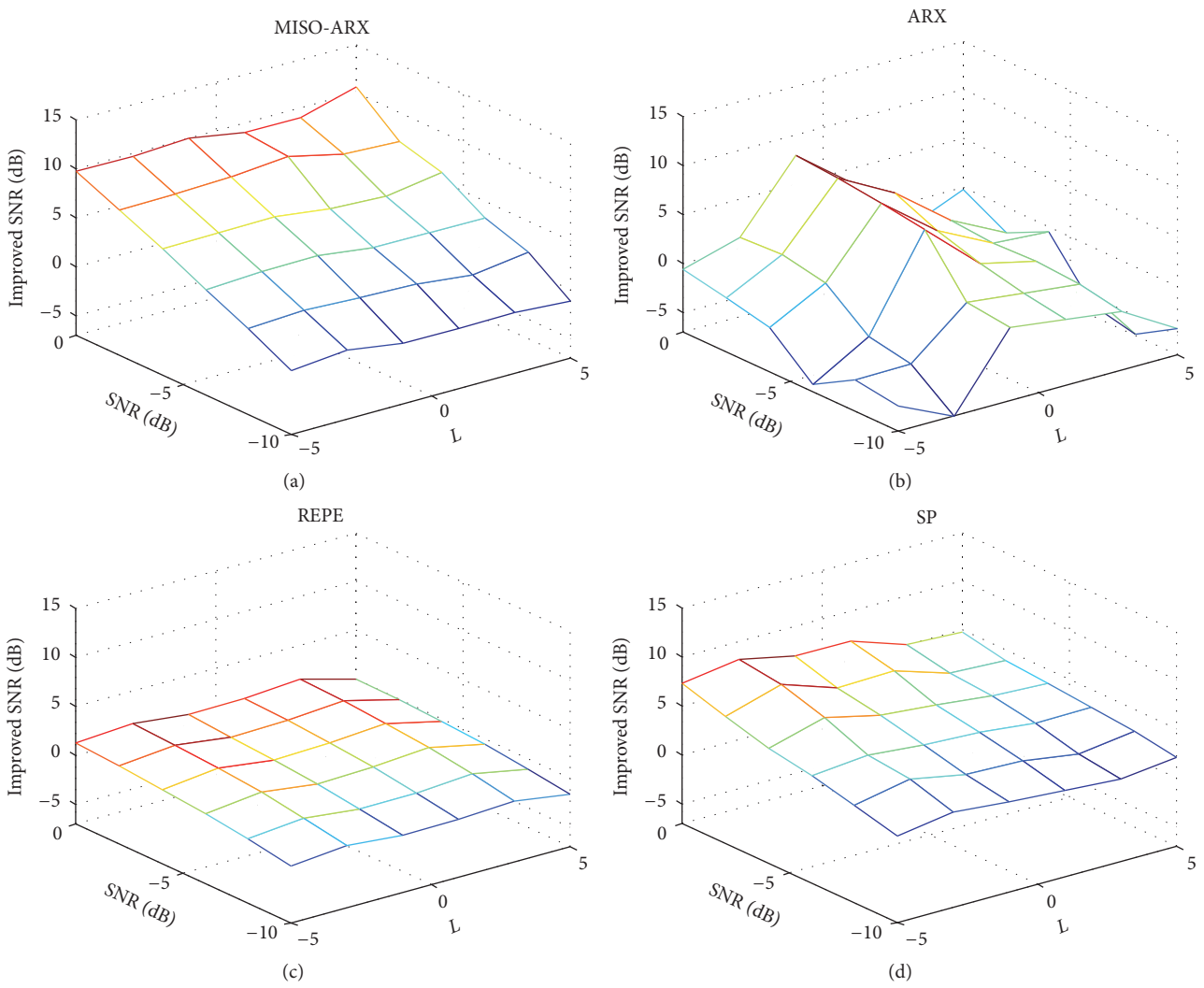

Figure 3: Performance evaluation of four methods with different SNR and l values.

participants were performed according to the National Institutes of Health Guidelines. VEP signals were recorded via a surface electrode placed on the occipital region of the scalp (Oz), using the right earlobe as a reference, with the forehead grounded. Subjects were required to gaze at a cross on the stimulus screen. The stimulus pattern was a conventional black-and-white checkerboard, which was reversed every half a second. Recordings were made using a digital EEG recording system (NuAmps EEG Amplifier, NeuroScan, USA) with a sampling rate of 1000 Hz and stored on a computer. Signals were bandpass filtered in the range of 0.05–450 Hz.

In the VEP signal, critical responses were located at approximately 100 ms after stimulation, where the positive peak (P100) occurred. With the stimulus being delivered at 0 ms, we processed each VEP trial from 0 ms to 200 ms. We used data from the first 50 pairs of trials to perform the experiment, from six eyes belonging to three subjects, as shown in Figure 5. As shown in the figure, it is clear that most estimated VEPs have a peak at around 100 ms.

For each eye, we used data from the first 50 pairs of trials to calculate the average of the estimated VEPs. The results are shown in Figure 6. The estimates using MISO-ARX are indicated by solid line, and the averages of the measurements are indicated by dashed-dotted line. Clearly, as shown in Figure 6, the average of the estimated results for each eye is very similar to the average of the measurements.

Then, we estimated the latency of the P100 for each trial, as shown in Figure 7. The estimates are indicated by dots, the averages of the estimates are indicated by solid line, and the P100 latencies of the average of the measurements are indicated by dashed-dotted line. We can see that the trial-to-trial variation in the latencies of P100 is large. However, the averages of the estimates are close to the results of the average of the measurements.

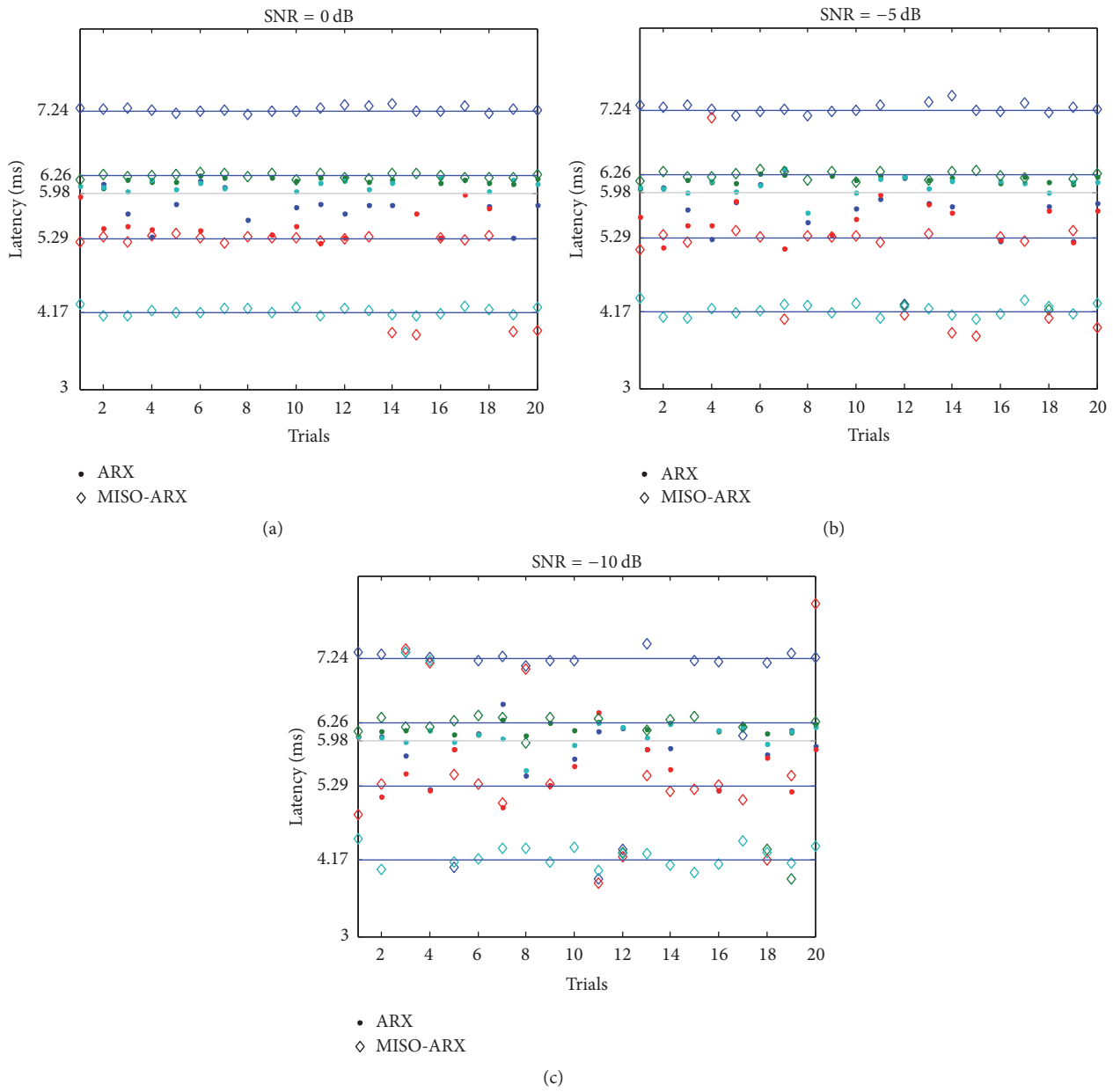

Figure 4: Latency tracking of the third wave using ARX and MISO-ARX.

4. Conclusion

In this paper, we presented a novel single-trial EP extraction method based on MISO-ARX. This method considers the single-trial EP as a complex containing many components, and each component can be modeled by ARMA. In addition, in order to improve the accuracy of the model parameters estimation, we used sparse coding to roughly estimate temporal lag. Since each component is modeled individually, our method has greater tracking capabilities of specific components of the EP complex. We conducted a series of experiments on synthetic and real data, and the results were evaluated using waveform observations and several metrics. From point of view of the experimental results, our method achieved a better and more favorable estimation performance than other currently used state-of-the-art methods in single-trial EP estimations.

Competing Interests

The authors declare that they have no financial and personal relationships with other people or organizations that can inappropriately influence their work; there are no professional or other personal interests of any nature or kind in any product, service, and/or company that could be construed as influencing the position presented in, or the review of, this

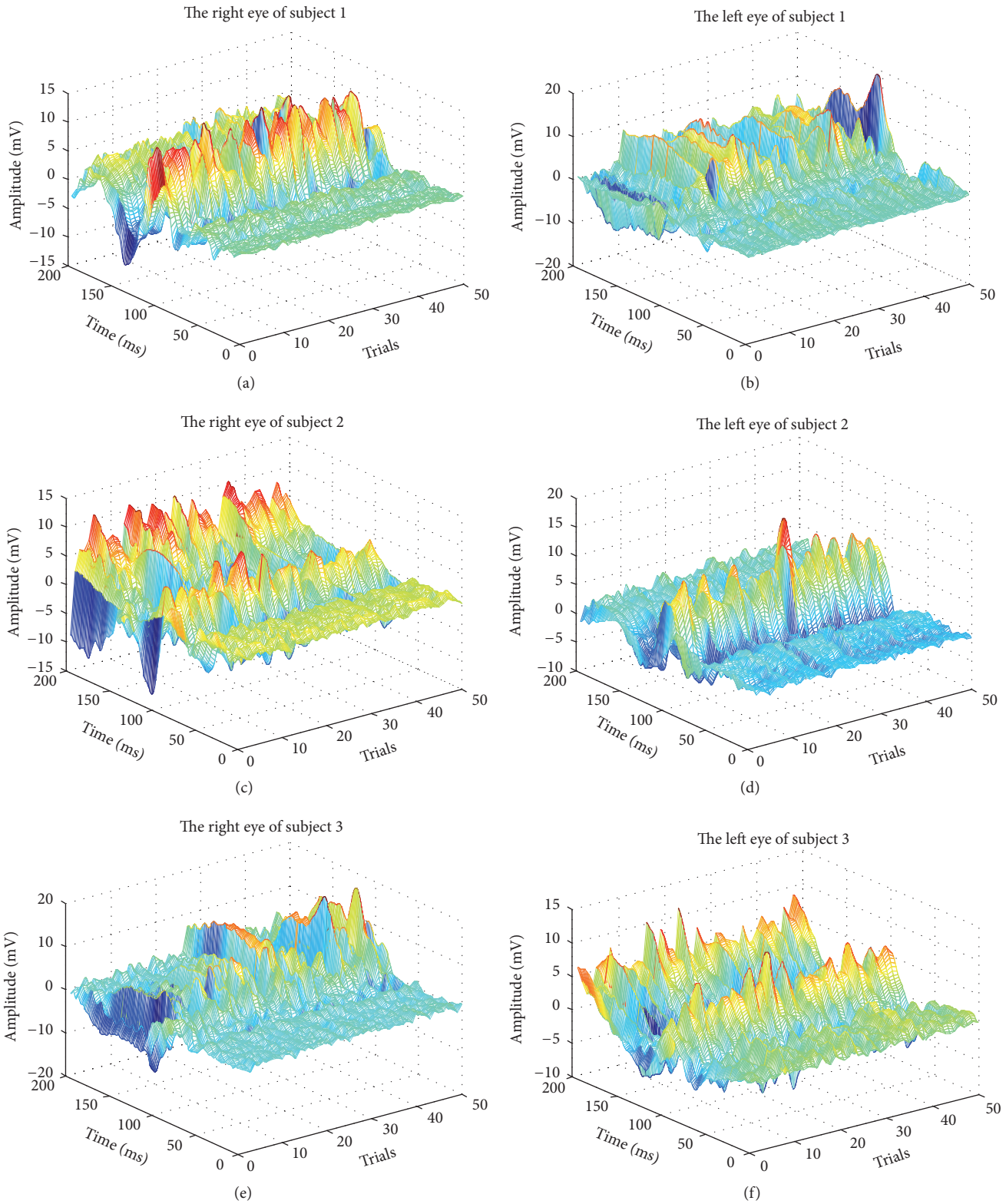

Figure 5: Estimation performance.

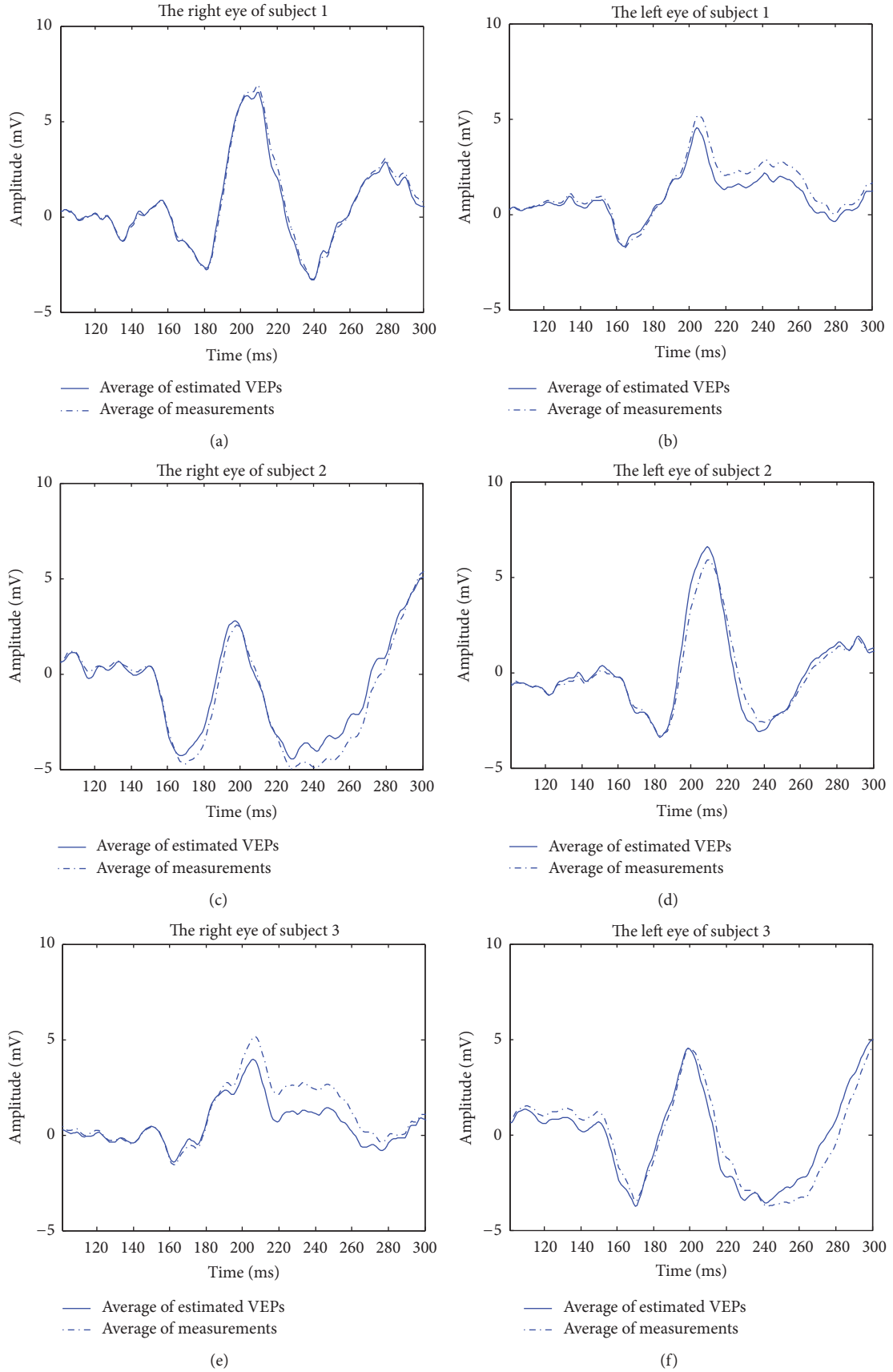

Figure 6: Average of the estimated VEPs and the average of the measurements.

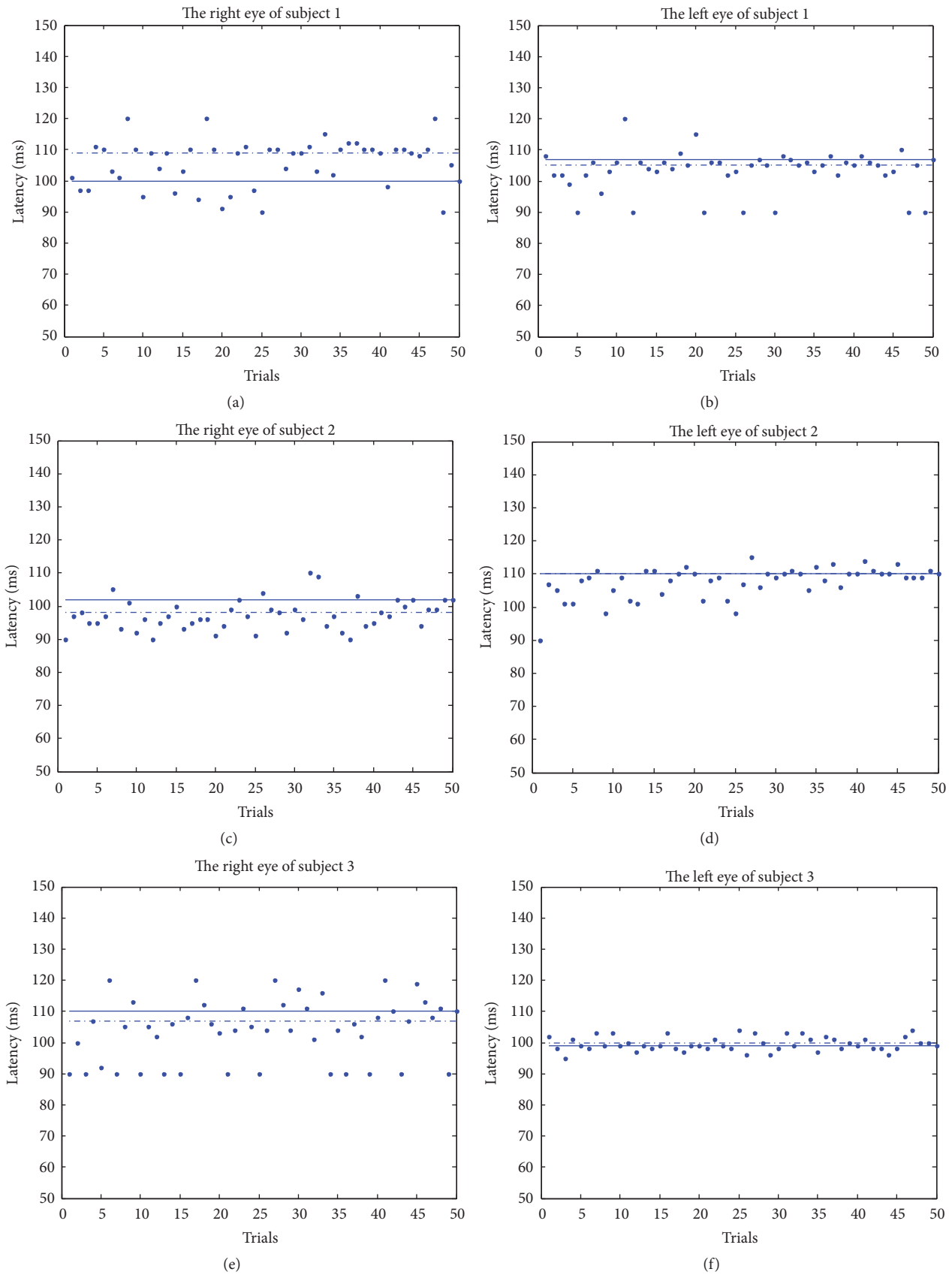

Figure 7: Estimation of latencies of P100 by MISO-ARX.

manuscript. And the funding in "Acknowledgments" would not lead to any conflict of interests regarding the publication of this manuscript.

Acknowledgments

This work was supported by the Nature Science Foundation of China (Grant no. 61401181) and Nature Science Foundation of China (Grant no. 61403174).

References

[1] Q. Wang, Y. Wu, W. Liu, and L. Gao, "Dominant eye and visual evoked potential of patients with myopic anisometropia," *BioMed Research International*, vol. 2016, Article ID 5064892, 6 pages, 2016.

[2] A. S. Gevins, "Analysis of the electromagnetic signals of the human brain: milestones, obstacles, and goals," *IEEE Transactions on Biomedical Engineering*, vol. 31, no. 12, pp. 833–850, 1984.

[3] M. H. Costa, "Estimation of the noise autocorrelation function in auditory evoked potential applications," *Biomedical Signal Processing & Control*, vol. 7, no. 5, pp. 542–548, 2012.

[4] S. F. Regaçone, D. D. B. D. Lima, V. E. Valenti, and A. C. F. Frizzo, "Resting heart rate and auditory evoked potential," *BioMed Research International*, vol. 2015, Article ID 847506, 6 pages, 2015.

[5] S. Cerutti, G. Baselli, D. Liberati, and G. Pavesi, "Single sweep analysis of visual evoked potentials through a model of parametric identification," *Biological Cybernetics*, vol. 56, no. 2, pp. 111–120, 1987.

[6] B. Berger, T. Minarik, G. Liuzzi, F. C. Hummel, and P. Sauseng, "EEG oscillatory phase-dependent markers of corticospinal excitability in the resting brain," *BioMed Research International*, vol. 2014, Article ID 936096, 8 pages, 2014.

[7] H. Kumru, D. Soler, J. Vidal, J. M. Tormos, A. Pascual-Leone, and J. Valls-Sole, "Evoked potentials and quantitative thermal testing in spinal cord injury patients with chronic neuropathic pain," *Clinical Neurophysiology*, vol. 123, no. 3, pp. 598–604, 2012.

[8] L. T. Mainardi, J. Kupila, K. Nieminen et al., "Single sweep analysis of event related auditory potentials for the monitoring of sedation in cardiac surgery patients," *Computer Methods & Programs in Biomedicine*, vol. 63, no. 3, pp. 219–227, 2000.

[9] L. Rossi, A. M. Bianchi, A. Merzagora, A. Gaggiani, S. Cerutti, and F. Bracchi, "Single trial somatosensory evoked potential extraction with ARX filtering for a combined spinal cord intraoperative neuromonitoring technique," *BioMedical Engineering Online*, vol. 6, article no. 2, 2007.

[10] D. H. Lange and G. F. Inbar, "A robust parametric estimator for single-trial movement related brain potentials," *IEEE Transactions on Biomedical Engineering*, vol. 43, no. 4, pp. 341–347, 1996.

[11] A. C. De Silva, N. C. Sinclair, and D. T. J. Liley, "Limitations in the rapid extraction of evoked potentials using parametric modeling," *IEEE Transactions on Biomedical Engineering*, vol. 59, no. 5, pp. 1462–1471, 2012.

[12] D. H. Lange, H. Pratt, and G. F. Inbar, "Modeling and estimation of single evoked brain potential components," *IEEE Transactions on Biomedical Engineering*, vol. 44, no. 9, pp. 791–799, 1997.

[13] J. L. K. Kramer, J. Haefeli, A. Curt, and J. D. Steeves, "Increased baseline temperature improves the acquisition of contact heat evoked potentials after spinal cord injury," *Clinical Neurophysiology*, vol. 123, no. 3, pp. 582–589, 2012.

[14] N. Yu, H. Liu, X. Wang, and H. Lu, "A joint sparse representation-based method for double-trial evoked potentials estimation," *Computers in Biology & Medicine*, vol. 43, no. 12, pp. 2071–2078, 2013.

[15] N. Yu, F. Hu, D. Zou, Q. Ding, and H. Lu, "Single-trial sparse representation-based approach for VEP extraction," *BioMed Research International*, vol. 2016, Article ID 8569129, 9 pages, 2016.

[16] O. Shental, "Sparse representation of white Gaussian noise with application to L0-norm decoding in noisy compressed sensing," in *Proceedings of the Qualcomm Technology Forum (QTECH '11)*, San Diego, Calif, USA, June 2011.

[17] S. S. Chen, D. L. Donoho, and M. A. Saunders, "Atomic decomposition by basis pursuit," *SIAM Review*, vol. 43, no. 1, pp. 129–159, 2001.

[18] Y. C. Pati, R. Rezaiifar, and P. S. Krishnaprasad, "Orthogonal matching pursuit: recursive function approximation with applications to wavelet decomposition," in *Proceedings of the 27th Asilomar Conference on Signals, Systems and Computers*, vol. 1, pp. 40–44, Pacific Grove, Calif, USA, November 1993.

[19] J. H. Wang, D. B. Wang, and Z. S. Wang, "Recursive identification of MISO systems with multiple unknown time delays," *Control and Decision*, vol. 25, no. 1, pp. 93–98, 2010.

[20] D. L. Jewett and J. S. Williston, "Auditory-evoked far fields averaged from the scalp of humans," *Brain*, vol. 94, no. 4, pp. 681–696, 1971.

[21] N. Kamel, M. Z. Yusoff, and A. F. M. Hani, "Single-trial subspace-based approach for VEP extraction," *IEEE Transactions on Biomedical Engineering*, vol. 58, no. 5, pp. 1383–1393, 2011.